Pedestrian-Induced Lateral Excitation of Footbridges

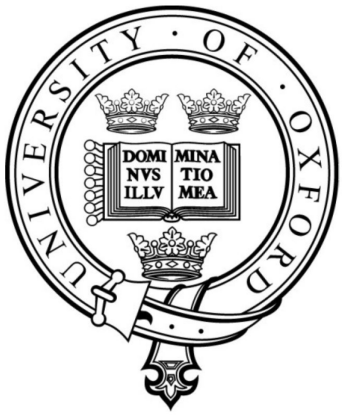

Daniel E. Claff
Keble College
University of Oxford

A thesis submitted for the degree of
Doctor of Philosophy

Michaelmas Term 2015

Abstract

This thesis investigates human-structure interactions between pedestrians and oscillating footbridges via experimental kinematic and kinetic tests. The first aspect was to improve and validate a simple frontal plane gait model, the Inverted Pendulum Model (IPM), based on kinematic and kinetic gait data for stable ground walking. Next, test subjects were recorded while crossing a laterally swaying footbridge in order to examine kinematic and kinetic walking patterns and assess the model's accuracy at predicting unstable gait.

Participants were recorded walking over force plates in a gait laboratory so their normal ground forces could be compared to each other and the IPM. High inter-subject variability and low intra-subject variability were observed. The IPM did not reproduce transient components of the ground forces. An analysis of the IPM's inherent assumptions revealed that some were inappropriate. A Modified Inverted Pendulum Model (MIPM) is proposed, eliminating some of the IPM's assumptions. For all samples examined, the correlation between the real ground forces and the MIPM was higher than that of the IPM.

Custom-designed force plates were installed into a novel laboratory footbridge rig. The footbridge was excited naturally by the participants' walking and the participants responded naturally to the swaying of the bridge. The participants' step widths could be predicted by the phase of the structure at the previous heel strike. At high structural amplitudes, CoP and ground force patterns were dominated by the motion of the structure. Centre of Mass (CoM) motion was found to be 'fixed-in-space' with patterns dissimilar to those anticipated by the IPM. The MIPM was typically better than the IPM at predicting ground forces on the moving base.

Finally, a spherical model was compared to the two-dimensional MIPM. The model exhibited few discrepancies to the spherical kinematic data, but the predicted medial-lateral ground forces were significantly different to the force plate data.

To my mother and father

For their enduring love and encouragement

And for inspiring in me a passion for learning.

Acknowledgements

I would venture that if you are reading this, you are in one of two groups. Those in the first group are academics and students whom have likely already written a thesis or are undertaking one themselves. Thank you for taking the time to delve into my research. I hope you will find the work as interesting as I have, and that its results may prove useful in your own investigation. Otherwise those in the second group have been family, friends, and mentors who have directly and indirectly supported and encouraged me. Thank you for the countless moments that have seen me through this DPhil. I hope you enjoy seeing the data that you have literally and figuratively produced.

They say it takes a village to raise a child, and I think the same should be said of writing a doctoral thesis. I am indebted to my supervisors, Prof. Martin Williams and Prof. Tony Blakeborough, for their time, patience, and encouragement throughout the project. For the Nuffield Orthopaedic Centre tests, I am very thankful for Dr Julie Stebbins and the Oxford Gait Laboratory team, who showed me how to use the lab and assisted with my tests, in addition to Meredith Newman for lending us their Tekscan software and pressure tracking insoles. For the Jenkin tests, I am deeply grateful to Clive for his incredible expertise helping to assemble my force plates and getting my testing off the ground. I am also grateful to Dr Vito Racic from Sheffield University for lending me their CODA motion tracking equipment. Finally, many thanks to Alison for all her administrative assistance and keeping me on track.

A large number of my peers have also been directly instrumental in my thesis work. I am particularly grateful to the 25 individuals who volunteered to walk *a lot* in the name of science: AK, AL, BZ, CA, CV, DB, EH, EJ, EM, GWC, HD, HH, IH, JB, JQ, JS, LG, LM, LT, RG, RL, SC, SS, WB, and ZW. In addition, the testing would not have transpired without the direct and indirect contributions of my fellow DPhil students in Jenkin Room 11 and the Civils group post-docs. To Chris, Christelle, and Susannah, I especially appreciate surviving our doctorates together.

I have been very fortunate to be surrounded by an amazing community in Oxford. I could not have asked for better housemates than Ellie, Liam, Dave, Sam, Rebecca, and Bea, who have not only supported my scientific endeavours but challenged my world views and helped me develop as a person. I am grateful for the many friends from my Keble cohort as well as the coaches, dancers, and my amazing dance partners from the Oxford University Dancesport Club. The friendships formed in these groups have been dynamic, thought-provoking, and fun, and more than any other factor they have given me the patience and perseverance to complete this thesis.

I would be remiss if I did not acknowledge my friends, mentors, and family, who facilitated my admission into Oxford. To my parents and family for their unwavering support; to Tyler, Rachael, Kalli, Dr Janice Odom, Dr Ross Bassett, Dr Randy Foy, and Dr Roy Borden for encouraging me to explore my full potential; and to Matt, Tony, Tom, Harrison, Joseph, Paul, Josh, Dianne, Kaleigh, and their families for always encouraging the best in me, I am forever grateful.

Finally, I also gratefully acknowledge the financial support of the Clarendon Scholars and Oxford University Press, who provided the means by which I could undertake this doctorate.

Contents

Nomenclature

A_i	Amplitudes for exploratory parametric MIPM (mm).
$\vec{\mathbf{a}}_\mathbf{s}$, $\vec{\mathbf{v}}_\mathbf{s}$, $\vec{\mathbf{d}}_\mathbf{s}$	Acceleration (m s^{-2}), velocity (m s^{-1}), and displacement (m) of a point in spherical coordinates.
$\vec{\mathbf{a}}$	Acceleration of a point, Cartesian coordinates (m s^{-2}).
a_x	M-L Acceleration (m s^{-2}).
b_{min}	Margin of Stability (m).
C	Structural coefficient of damping (N s^2 m^{-1}).
c_p	Equivalent added damping by pedestrians (N s^2 m^{-1}).
D_i	Dynamic Amplification Factor (-).
d_p	Pedestrian M-L Displacement (m).
E	Young's Modulus of Elasticity (mild steel: 2.10×10^5 MPa).
$\vec{\mathbf{F}}$	External force applied to pedestrian (N).
F_A, F_B, F_C	Dynamic Load Factors (DLFs) (-).
F_{ped}	Simulated applied pedestrian force on SDOF oscillator (N).
F_{st}	Equivalent pedestrian M-L static force (N).
F_x	M-L pedestrian ground force (N).
F'_x	Body weight normalised M-L pedestrian ground force (-).
F_{xa}, F_{xv}	M-L pedestrian ground force in phase with acceleration or velocity (N).
$\bar{F}_{xa}$, $\bar{F}_{xv}$	Mean M-L pedestrian ground force in phase with acceleration or velocity (N).
F_y	A-P pedestrian ground force (N).
F_z	Vertical pedestrian ground force (N).
f	Frequency (Hz).
f_b	Structural natural frequency (Hz).
f_p	Gait cycle frequency (Hz).
GF	Gauge factor of a strain gauge (-).
g	Acceleration due to gravity (9.81 m s^{-2}).

$\vec{\mathbf{H}}$	Total angular momentum (kg m^2/s).
h_{ASI}	Height of the anterior superior iliac spine (m).
$\bar{h}_{CoM}$	Mean height of the CoM, exploratory parametric model (mm).
h_p	Pedestrian height (m).
h_t	Height of the greater trochanter (m).
$\hat{\mathbf{i}}$, $\hat{\mathbf{j}}$, $\hat{\mathbf{k}}$	Orthogonal unit vectors.
I	Second moment of area (m^4).
K	Structural stiffness (N s m^{-1}).
k_{fp}	Spring element stiffness in force plates (N s m^{-1}).
k_{ss}	Superstructure stiffness (N s m^{-1}).
L	Inverted pendulum length (m).
L_b	Bridge length (m).
l	Bernoulli-Euler beam length (mm).
M	Torque, moment of force (Nm).
M_A, M_B	Bernoulli-Euler reaction moments (Nmm).
M_o	Moments about Cartesian origin (Nm).
m_b, m_{bi}	Structural mass, total or i^{th} mode (kg).
m_p	Pedestrian mass (kg).
N_c	Critical number of pedestrians (-).
n	Number of footsteps (-).
n_h	Fourier domain harmonic number (-).
n_p	Number of pedestrians on structure (-).
n_t	Number of three-step trials (-).
$p(\tau)\,\mathrm{d}\tau$	Duhamel integral impulse function.
q	Generalised coordinate for structural displacement (-).
R	Electrical resistance of a load (e.g. strain gauge) (Ω).
R_A	Bernoulli-Euler reaction force (N).
R_{ASI}	Ratio of ASI height to total pedestrian height (-).
$\hat{\mathbf{r}}$, $\hat{\boldsymbol{\theta}}$, $\hat{\boldsymbol{\phi}}$	Unit vectors in spherical coordinates.
r, θ, ϕ	Dimensions in spherical coordinates (distance from origin (m), angle from z-axis ($^\circ$), angle from $-y$-axis in $x-y$ plane ($^\circ$)).
r	Pearson's correlation coefficient (-).
r^2	Coefficient of Determination (-).
r_{xy}	Projection of spherical inverted pendulum in xy-plane (m).
S	Parameter measuring pedestrian sensitivity to base motion (m^{-1}s^{-1}).

$[T]$, $[P]$	θ and ϕ state spaces, spherical coordinates.
T	Gait cycle period (s).
t	Time (s).
t'	Normalised time (-).
t_0	Initial time (s).
u	Inverted pendulum model M-L Centre of Pressure position (m).
V_{ex}	Excitation voltage (V).
V_s	Output (signal) voltage (V).
v_p	Pedestrian walking velocity (m s^{-1}).
W	Bernoulli-Euler applied force (N).
X	Structural M-L oscillation amplitude (m).
$\bar{X}$	Coefficient of structural oscillation amplitude (m).
$\hat{\mathbf{x}}$, $\hat{\mathbf{y}}$, $\hat{\mathbf{z}}$	Unit vectors in cartesian coordinates.
x, y, z	Dimensions in Cartesian coordinates (lateral, forward, vertical).
x_{CoM}, x_{toe}, x_{CoP}	M-L position of the Centre of Mass, toe, and Centre of Pressure (m).
x	Structural M-L displacement (m).
x_l	Location along Bernoulli-Euler beam (mm).
$\ddot{x}_{si}$	M-L acceleration of body segment i (m s^{-2}).
y	Inverted pendulum model M-L Centre of Mass position (m).
y_0	Inverted pendulum model M-L Centre of Mass position at heel-strike (m).
y_{NA}	Bernoulli-Euler neutral axis depth (mm).
z_{CoM}, z_{toe}, z_{CoP}	Height of the Centre of Mass, toe, and Centre of Pressure (m).
α	Body angular acceleration (rad s^{-2}).
α_0, α_1, α_2, α_3	Experimentally determined optimised coefficients for (varying units).
β	Frequency ratio, ω_p/ω_b (-).
γ	Inverted pendulum to leg angle (°).
ΔE	Internal energy exerted by a pedestrian to maintain continuous walking (J).
ΔR	Change of electrical resistance (Ω).
ΔT	Period of integration (s).
Δl	Bernoulli-Euler beam deflection (mm).
Δt	Change of time (s).
$\Delta\Phi_b$	Change of bridge phase (rad).

δ, δ_I, δ_N	Step width: general, instantaneous, and net (mm).
ε	Mechanical strain (-).
ζ	Stochastic parameter (-).
η	Coefficient for determining critical number (-).
θ	Inverted pendulum angle (rad).
θ_1, θ_2, θ_3	Equal Angle Model anatomic angles (rad).
κ	CoM-CoP separation (mm).
λ_a	Ratio of pedestrian to structural motion (-).
λ_l	Fraction of locked-in pedestrians (-).
λ_m	Segment mass to body mass ratio (-).
λ_s	Fraction of synchronised pedestrians (-).
ξ_b	Structural damping ratio (-).
ξ_p	Pedestrian damping ratio (-).
ξ_{tot}	Composite damping ratio for a bridge-pedestrian system (-).
ρ	Pendulum length, spherical coordinates (m).
ϱ_p	Equivalent added mass per pedestrian (kg).
σ	Mechanical bending stress (MPa).
τ	Phase, Phase lag (s).
Φ_b	Phase of structural oscillation (rad).
Φ_l	Phase lag by Strogatz *et al.* [1] (rad).
Φ_p	Gait cycle phase (rad).
ϕ_{qi}	Structural mode shape (-).
Ψ	Optimised body segment mass coefficient (-).
Ω_p	Inverted pendulum frequency $\sqrt{g/L}$ (rad).
ω_b	Structural natural frequency (rad).
ω_p	Gait cycle frequency (rad).

Chapter 1

Introduction

When one considers great feats of engineering, a wide variety of structures comes to mind. Many of these famous structures are likely to be bridges: the Golden Gate Bridge, the Brooklyn Bridge, London's Tower Bridge, the Millau Viaduct, the Sutong Bridge, the Akashi Kaikyō Bridge, the Sydney Harbour Bridge, and so on (Figure 1.1). These structures are noteworthy because they are old, prominent, high-capacity, historic, cutting-edge, or aesthetically unique. But all of these famous bridges – these global landmarks – also solve a common and ancient problem of how to connect people. Throughout history humans have always needed to span impasses, be it crossing a ravine to gain access to fundamental food supplies or traversing a busy highway to allow the movement of goods. Bridges are valuable assets to any civilisation.

In nations that can afford such monumental landmarks as the bridges listed above, the biggest bridges are often designated for high-occupancy, multi-purpose traffic. They span the longest distances because technology and funding have allowed them to do so. They carry vehicles, trains, and even boats, allowing for the movement of people and goods from one place to another. These bridges, be they shiny or rustic, are all glamorous in their function. Yet such magnificent structures can all trace their roots to much humbler beginnings: footbridges.

Arguably a footbridge is the most simple form of structure. Putting a log across a ditch constitutes the most rudimentary of footbridges. Thus, these 'structures' are

Figure 1.1: Some famous bridges. [2, 3, 4, 5, 6, 7]

likely as old as civilisation. Yet through the ages footbridges have taken different shapes and forms according to different design and technological limitations, developing with advancements in materials and construction. In modern times the range of forms and functions for footbridges is immense. Seemingly basic cable and wood-plank footbridges provide essential access to education, food, clean water, and medical attention for communities in developing countries [8, 9]. These rural structures can span immense distances using relatively simple materials. On the other end of the spectrum, footbridges reflect the current state-of-the-art both aesthetically and technologically – even incorporating amusing concepts such as London's Rolling Bridge [10] or the Ferris wheel-laden Yong-Le Bridge [11], Figure 1.2.

The diversity of structural forms for twenty-first century footbridges reveals a complex world of design implications. Despite cheap and effective 'flimsy' rope, cable, and wooden (etc.) bridges in the developing world, the culture of modern developed society (or, arguably, post-Industrial Revolution city life) has ushered in expectations of comfort, convenience, and safety. In general, scientific advancements in the last

Figure 1.2: Footbridges from essential to eccentric. [8, 12, 13, 10]

two centuries and the emergence of design codes have allowed these expectations to be met via the construction of overly-redundant structures. In the last few decades however, the cultural value of aesthetically pleasing architecture has increased. With less redundancy and a move towards urban regeneration footbridges are increasingly slender and sleek, allowing them to blend into or enhance their environment, be it urban, suburban, or rural. They beneficially minimise adverse environmental and aesthetic impacts while subtly or overtly adding value to a user's journey. An unintended consequence of creating these slender footbridges is that some have proven prone to unwanted pedestrian-induced motion.

In light of the fact that design guidelines (e.g. [14, 15, 16, 17]) have little to offer regarding pedestrian-induced lateral vibrations in footbridges, this thesis investigates the biomechanics of lateral ground force with respect to laterally oscillating footbridges. The first aim is to gain a better understanding of how humans develop lateral ground forces to maintain their balance during normal walking on a stable surface. This is done by analysing and improving an existing biomechanical model, the Inverted Pendulum Model. Then the research explains how pedestrians react to unanticipated lateral ground motion, as might be expected from crossing a long-span footbridge. A custom-designed laboratory suspension footbridge allows subjects to naturally react to lateral oscillations while recording their body movements and ground forces. Most of the

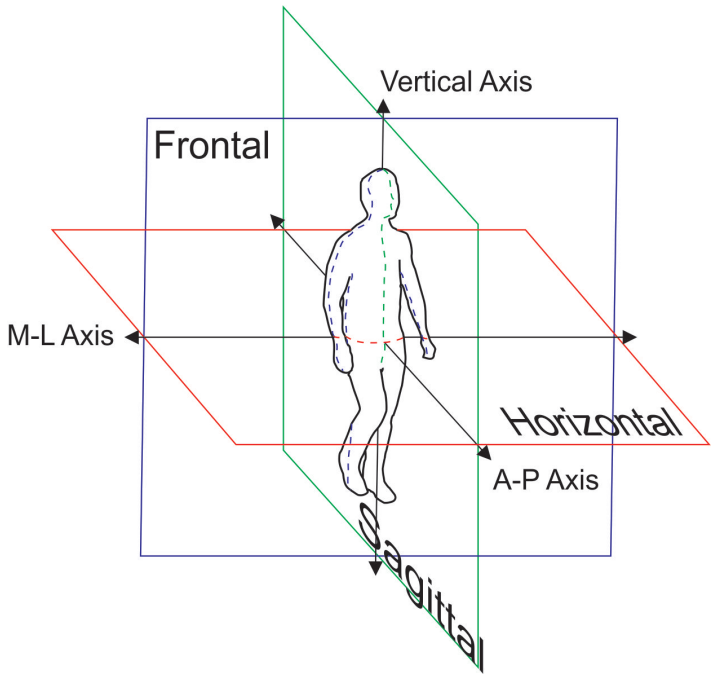

Figure 1.3: The three anatomic planes (Frontal, Sagittal, and Horizontal) along with their Cartesian axes (medial-lateral, antero-posterior, and vertical).

studied kinematics and kinetics are due to the phase and amplitude of the structure, which can be predicted.

The subsequent sections in the Introduction first present a review of the literature before examining the Inverted Pendulum Model (IPM) and stable ground gait kinematics in greater detail. In order to provide a succinct Literature Review, many terms are only defined in subsequent sections or chapters where they become of benefit to the thesis research. To aid the reader, a comprehensive glossary has been provided at the end of the text. In addition, Figure 1.3 depicts the anatomic planes and axes which will be used throughout the thesis. In Chapter 2 the four experimental regimes undertaken during the study are presented, distinguishing between stable and unstable ground tests. This concludes the introductory portion of the thesis.

Chapters 3 to 5 investigate the IPM with respect to experimentally recorded ground forces on stable surfaces. First, Chapter 3 analyses individual footsteps across a sample population in an attempt to characterise representative lateral force patterns. These

patterns are compared with the IPM, revealing significant differences. Chapter 4 correlates the motion of the head, trunk, and pelvis to lateral ground force samples as a possible alternative to using the IPM. In Chapter 5 attention is returned to the theory of the IPM, challenging assumptions made by the model and suggesting improvements.

Chapters 6 and 7 present experimentation on the laterally oscillating laboratory bridge. The former explains the design, construction, and calibration of the custom-designed force plates used in the bridge before Chapter 7 examines the kinematics and kinetics of pedestrians crossing the bridge. Finally, Chapter 8 wraps up the thesis by presenting a novel adaptation of the Inverted Pendulum Model in spherical coordinates. This adaptation nominally allows for a more precise kinematic representation of body movement both in stable ground and moving base situations.

The portions of the content for several of the chapters have been presented in prior works. These papers by Claff *et al.* contribute to Chapter 3 [18], Chapter 4 [19], and Chapter 6 [20]. In addition, the content in Chapter 5 has been submitted to a structural engineering journal for review.

Several conclusions are drawn from the work conducted for this thesis. First, the medial-lateral ground forces are found to be prone to significant inter-subject variability but low intra-subject variability. Correlations between ground forces and body segment motion are moderately good, but not enough to create an accurate model. The Inverted Pendulum Model is found to not be a good predictor of medial-lateral ground forces, failing to predict the amplitude or frequency content of the data. Alterations to the IPM, however, produce significant improvements to these predictions. Using bespoke force plates with other instrumentation on a swinging footbridge, it was found that participants' kinematics and kinetics are highly dependent on bridge phase. Finally, the spherical model shows very good correlation between theoretical and experimental spherical kinematics but poor results when used to predict ground forces.

The major benefits of this research are twofold. The research provides kinetic

and kinematic data of adaptive walkers on an adaptive footbridge for the first time. It also provides recommendations for gait model improvements such that a simple yet more accurate model can be used in bridge design and analysis. Future work, therefore, should focus on advancing the quantitative relationships observed here, which could lead to a human-structure interaction (HSI) model solely dependent on structural motion.

1.1 Literature Review

An overview of the literature shows the breadth and lack of depth of conclusive research in the fields pertaining to pedestrian-induced lateral bridge excitation. But first, to introduce the challenges, consider a tree. If a group of 15 friends walking down the street comes across a 10 m tall plant with a trunk, branches, and leaves, it is likely that all 15 people would identify the plant as a tree. It has these defining qualities. Yet if those same 15 were sitting in a room and asked to draw or describe a tree, it is possible they would produce 15 unique trees. Some are short or tall, some have light or dark green leaves (or needles!), some might be bushy with fruit while others might have few branches at all. Generally speaking, it is easy to look at a tree and say it is such, but developing a botanically accurate definition of a tree is much more difficult. As it happens, people and bridges are like trees. When one sees a person moving down the street, it is easy to identify walking as opposed to running or skipping, yet most people walk with a unique, distinctive gait. Sometimes one can identify a person from a distance simply because of how they are walking. Similarly all 15 friends could look at any one of the photos in Figure 1.1 and agree that it is undoubtedly a bridge – but when asked to draw a bridge the group would conjure up 15 unique designs. This challenge is the core difficulty in predicting pedestrian-induced lateral excitation of bridges. The research attempts to predict human-structure interactions when both pedestrian ground forces and bridge characteristics may be easily identified but difficult

or impossible to define in an all-encompassing yet precise manner.

The studies presented here focus on two fields. First is a review of literature discussing HSI. These primarily examine the mechanics of single or multi-modal bridge motion under the influence of some applied external force. This applied force can either be described in the time or frequency domain, pertain to a single pedestrian or a group, and may or may not include feedback elements. The second relevant field is the biomechanics of gait analysis. These studies focus on how a human maintains balance while walking through a stable or variable environment. They examine how an individual perceives their environment and alters the force they exert on the ground in order to avoid falling over, tripping, becoming disorientated, etc. They also examine such topics as gait stability and so-called 'social forces'.

A distinction may be drawn between the HSI literature and the biomechanics literature by assessing which entity is the receiver of forces. HSI research is typically undertaken by engineers seeking to understand how people affect bridge motion. In this context the pedestrian(s) exert the forces; the bridge is the receiver. Biomechanists, however, are more concerned with how people react to a moving environment, and as such the literature is often concerned with the adaptation of one or few individuals to specific alterations in environment.

While both engineers and biomechanists are interested in the interactions between a moving base and the individuals crossing that base, the foci tend to be dichotomised as indicated. Still, this has led to a fair amount of overlap between the fields (along with studies in robotics, which are primarily interested in adapting biomechanics and neuroscience into control theory) without much consensus on an overall human-structure interaction relationship. This lack of consensus is indicative of the complexity of the problem, which simultaneously requires scientists to model in a precise, comprehensive, yet simple fashion the unique characteristics of human walkers and unique bridges; both of which are subject to a great deal of variation.

As a matter of clarification, two terms must be explained at the outset: stability and synchronisation. In literature many authors fail to discriminate between gait stability and structural stability. Gait stability refers to the balance of a pedestrian, particularly on a moving surface. Some authors use the term 'margin of stability' to refer to the motion of a person's Centre of Mass (CoM) with respect to his/her feet. If the person loses balance, the margin of stability has been exceeded and the person stumbles or falls. This gait stability is not to be confused with structural stability. A bridge is said to be unstable if, particularly after exceeding a critical number of pedestrians, the displacement of the bridge increases rapidly and/or non-linearly. In cases of structural stability, authors typically discuss a bridge's 'stability criteria', indicating the conditions required for the bridge not to move excessively. These will be investigated in more detail, however the reader should be aware that both the human system and the structural system can become unstable and in some literature the author's meaning must be discerned from context.

The literature, and in particular early literature, sometimes uses the term 'synchronisation' loosely. Later works have identified that researchers must discern between pedestrian-structure synchronisation, now typically called 'lock-in', and pedestrian-pedestrian synchronisation, which is still referred to as simply synchronisation. This thesis will explicitly refer to the different phenomena as either lock-in or synchronisation, although readers should be aware that the terms may be used interchangeably in literature.

The HSI literature across engineering, biomechanics, and robotics is quite diverse, including studies of gyms, hospitals, grandstands, and many other structural and non-structural applications. As the scope of this thesis pertains to lateral motion of bridges due to walking, the following review is mostly limited to *walking* forces of *healthy* individuals exerting *lateral* ground forces. In fact, studies of lateral walking ground forces are far fewer in number than studies of vertical forces, running forces, and studies

of gait pathology for a number of reasons. Lateral walking ground forces have fewer clinical applications, are more difficult to measure, are more variable, and constitute a small fraction of the magnitude of vertical forces. Still they constitute an important aspect of the bridge-excitation problem.

1.1.1 HSI: Observation & Experimentation

From a human-structure interaction standpoint, several literature reviews have covered the field extensively. In 2005 Živanović *et al.* undertook the first major literature review for footbridge vibration serviceability [17]. They gave an overview of forcing patterns in the time domain but delved deeper into the body of work investigating dynamic load factors (DLFs) for Fourier decomposition-based load models. They then compared existing HSI models (including some lock-in and synchronisation models) but stated that the vast majority of prior research was based on vibrations in the vertical direction. In addition they also briefly discussed existing design codes but suggested that the use of outdated and limited data rendered the standards somewhat obsolete.

The review undertaken by Racic *et al.* discussed 270 sources relating to biomechanics (namely kinetics and kinematics of walking) and synchronisation, with an aim towards structural applications [21]. They examined at length the techniques used to record ground forces and body motion, aimed at developing lateral forcing models for structures. That said, the authors reported that the state of the field was fragmented and under-researched, calling particularly for the development of a large, coherent database of pedestrian ground force records and the creation of a probability-based pedestrian load model.

Over the next few years a variety of additional research was conducted leading to the review produced by Ingólfsson *et al.* [22]. This is the most complete recent review of HSI theory, combining investigations of early case studies, full-scale studies, laboratory research, and the development of linear and non-linear structural models. It did

not cover biomechanics-based experimentation but discussed a number of theoretical mathematical pedestrian and crowd models.

Structural Case Studies

Quite a number of observational and experimental studies have attempted to characterise HSI. The most relevant of these are identified here, beginning with field observations and full-scale studies. The modern age of pedestrian-induced bridge excitation research began with the unanticipated serviceability failures of the Pont de Solférino footbridge in Paris and the London Millennium Bridge a year apart at the turn of the century. Both structures were opened to the public and quickly discovered to exhibit significant lateral vibrations when crowded. Information about the Solférino bridge is scarce, although a book about the structure's architecture, design, and construction was written by Fromonot [23] and the primary scientific reports about the structure's closure, analysis, and retrofitting are by Dziuba *et al.* in French [24]. Tests with approximately 100 and 70 participants were undertaken on the bridge before and after the installation of dampers. The subjects ran, lunged, and walked with small and large steps, sometimes synchronised to a buzzer. The bridge was particularly susceptible to motion between 1.7 and 2.25 Hz and at 2.37 Hz, corresponding with typical pedestrian step rate. After installing 14 tuned mass dampers – six pendulum type and eight spring-mass type – the damping level increased from 0.5-2% to 2.5-4%.

Much more has been written about the London Millennium Bridge, which closed three days after opening due to significant lateral sway on the order of 70 mm at 0.95 Hz [25]. Video footage of the structure appears to show pedestrians rocking from side to side in synchronisation with each other, locked in to the frequency of the bridge. Subsequent testing by Arup led to several important findings that would define the next decade and a half (and counting) of pedestrian-structure interaction research. Dallard *et al.* found that long span slender structures are prone to 'synchronous lateral excitation' (SLE), a phenomenon that 'arises because it is more comfortable for pedestrians

to walk [locked-in] with the natural swaying of the bridge, even if the degree of swaying is initially very small' [26]. Based partially on supplementary laboratory work conducted at the University of Southampton and Imperial College London, theories were developed (1) to determine the critical number of pedestrians to ensure structural stability and (2) regarding the onset of pedestrian-induced negative lateral damping, which will be discussed later. Two aspects of this pair of serviceability failures led subsequent researchers to invest heavily in HSI research. The first, obviously, was the prominence of the structures and the fact that the failures were so visible. The second was the suggestion that the failures were caused by a previously unconsidered type of dynamic force – that of synchronisation.

Following these prominent cases, reports emerged of other footbridges exhibiting pedestrian-induced lateral excitation. Fujino *et al.* conducted a thorough analysis of the Toda Park Bridge in Japan after crowds caused the cable stayed bridge to sway laterally [27]. Video analysis showed that the heads of the pedestrians moved in a synchronised manner, suggesting that their walking was synchronised as well. Nakamura and Nakamura conducted field tests on the Toda Park Bridge, Maple Valley Bridge, and Water Village Bridge [28, 29]. They similarly concluded that pedestrians were likely to lock-in their stride with one or more modal frequencies of the bridge. Macdonald serendipitously recorded a mass exodus of pedestrians on the Clifton Suspension Bridge [30]. The pedestrians excited the bridge in two modes simultaneously, suggesting that lock-in must not be essential for structural instability to occur.

As designers and researchers became more aware that pedestrian-induced structural instability could occur, full-scale structural testing became more common. Two newly constructed bridges underwent full scale testing before being opened to the public. The bridges were the Changi Mezzanine Bridge in Singapore [31, 32] and the Ponte Pedro e Inês in Coimbra, Portugal [33]. Sure enough, both experiments revealed that pedestrians could excite lateral harmonics in the structures. Tuned mass dampers were

installed in both bridges to attenuate the oscillations. Full scale *in situ* pedestrian tests have also become more common. Most, however, focus on vertical rather than lateral loading [34, 35, 36, 37]. From a lateral excitation standpoint these tests are useful insofar as modal analyses inform researchers about potential autoparametric excitation. This phenomenon will be addressed in the next section.

A number of other structures have been observed to be lively but received less scientific attention than the above examples. These include bridges such as the Alexandra Bridge in Ottawa [38], the Queens Park Bridge in Chester, U.K. [38], a pedestrian bridge in Kiev [39], the Bosphorus Bridge in Istanbul [40], the Lardal Bridge in Norway [41], the Auckland Harbour Bridge [26], and the Weil-am-Rhein Bridge in Germany [42]. In addition the Golden Gate Bridge was opened exclusively to pedestrians during its 50th anniversary. Hundreds of thousands of people loaded the structure, which exceeded its design capacity [43]. Lateral winds caused the strained bridge to sway laterally and the dense crowds began to panic from claustrophobia. Amateur video footage (e.g. [44]) shows pedestrians swaying in a synchronised fashion similar to footage from the London Millennium Bridge. While it is difficult to assess whether pedestrians were locked in or contributed to the lateral motion of the deck, pockets of synchronisation certainly occurred.

The most important message to be taken away from these full scale observations and experiments is that pedestrian-induced lateral bridge excitation occurs in a wide variety of structures including suspension bridges, box girder designs, trusses, and arches of wood, steel, concrete, and composite construction. The structures tend to have a long (slender) span and most of the aforementioned authors report natural frequencies below 1.3 Hz, especially with pedestrian-excited harmonics around 0.9 Hz. The most complete observations and tests utilise accelerometers, metronomes, and video cameras to track the motion of the structure when loaded in different combinations. Cameras allow researchers to estimate crowd density and crowd velocity while the use of metronomes

attempts to develop synchronisation amongst the participants. Arguably, however, these methods are insufficient for accurately tracking the motion of individuals and their exact influence on the bridge. Limitations in recording technology make it essentially impossible to record ground forces or body motion of individuals in a crowd. Thus the few full scale data available reflect overall rather than discrete behaviour.

Laboratory Testing

In addition to full scale tests researchers have conducted a variety of HSI laboratory tests. Such testing falls into two categories: treadmill or moving platform experiments. Treadmill-based experimentation tends to be more widespread amongst the civil engineering community because it allows researchers to record long sequences of footsteps. Treadmill rigs for studying lateral HSI typically consist of a belt passing around a steel frame walking surface such as developed by Ricciardelli [45]. The frame may be mounted to a pair of tracks oriented in the lateral direction such that the frame can be excited by an actuator. Typically the frame is mounted on four tri-axial force transducers for the measurement of ground forces. Handrails and harnesses are often employed for safety.

Peters *et al.* asked participants to walk on a treadmill for 20 minutes in order to study stride time entrainment [46]. After steady state walking was established, sinusoidal perturbations were applied to the treadmill. They found that participants acclimated to the motion of the treadmill within 10 minutes and five out of 19 participants entrained their stride (i.e. locked in) to the perturbation frequency. They also found that perturbation frequency (either 0.2 or 0.3 Hz) did not significantly affect stride entrainment.

Ingólfsson *et al.* tested 71 participants over 55 km walking on the treadmill developed by Ricciardelli [45]. They observed that at low deck oscillation frequencies pedestrians add damping and stiffness to the treadmill whereas at high frequencies pedestrians remove damping and stiffness. That said, they report that these results

contradict the results of others and that very large inter-subject variability was observed. They also made the qualitative observation that individuals did not necessarily lock-in with the motion of the treadmill, even if their pace was close to the frequency of treadmill oscillations. In 2014 Ricciardelli *et al.* expanded on this work, reporting that the lateral force produced by a subject was relatively unaffected by low amplitudes of treadmill oscillation [47]. In contrast, when large amplitudes were applied to the treadmill, the net lateral force tended to correlate to frequency.

Research by Carroll *et al.* involved asking two and 10 male subjects to walk on a laterally oscillating treadmill moving at various frequencies and amplitudes [48, 49]. In the first study they observed a high correlation between head, trunk, and pelvis motion and lateral ground force over a 20 s period. They also reported that balance was primarily achieved through foot placement – a conclusion supported by many other researchers as well. The second study confirmed that foot placement is a primary determinant of balance and that stride width increases when treadmill oscillation is present.

While treadmill studies have some advantages for studying HSI, they do also have disadvantages. Physiologically there has been debate about whether subjects feel as comfortable on a treadmill as they do on normal ground [50]. Whether or not that is the case, HSI tests are reliant on participants maintaining a walking speed equal to the belt speed. In videos of the London Millennium Bridge, individuals are seen to stop or pause to regain stability; this is not possible on a treadmill. The cases examined above either impart a series of belt speeds or allow the participant to walk at a self-selected speed, but regardless speed remains constant throughout each test sample.

In contrast to treadmill studies, a few HSI studies have been undertaken on moving platforms. The first of these was done by Hobbs at Imperial College London as part of the follow-up research from the London Millennium Bridge incident [51]. The test involved walking across a 7.2 m long laterally driven platform. Dallard's summary of

the results suggests that dynamic load factor (i.e. lateral force normalised by body weight) increases with structural oscillation amplitude. They also state that the force applied by a pedestrian to the bridge is proportional to the probability of the pedestrian being locked-in [26]. McRobie *et al.* installed a treadmill on top of a laterally oscillating platform following the London Millennium Bridge failure, showing that with an increase in deck amplitude came an increase in step width [52, 22]. This accompanied an observation that lateral ground forces on a moving base can easily exceed 100 N (whereas in normal walking peak lateral forces are typically in the range of 20-50 N). Platform based tests were also conducted in the wake of the Solferino bridge incident suggesting that the lateral deck velocity did not correlate to the pedestrian ground force [53, 22]. Finally, as part of his doctoral thesis, Rönnquist undertook a set of experiments on a hanging platform, though he observes that such tests fail to replicate field-typical pedestrian-to-structure mass ratios [41, 54].

Beyond these HSI experiments and observations, a variety of treadmill and platform studies have been conducted which primarily focus on biomechanics of balance. Those will be discussed later in the literature review.

In spite of the diversity of HSI observations and experimentation that has been conducted so far, few conclusive observations have been made. The most important observation has been that structural motion increases step width. Oddsson *et al.* show that step width is proportional to structural motion but the results of Ricciardelli *et al.* suggest that maybe it is not so simple [55, 47]. Limitations in pedestrian motion-tracking technology make field observations of HSI challenging to obtain. Several authors have identified a significant dearth of *in situ* data, which are crucial for gaining a deeper understanding of the phenomenon and developing theoretical models [21]. Nonetheless, laboratory experimentation on treadmills and platforms has started to produce a body of data that can be used (with qualifying assumptions) to verify existing models, the topic of the next section.

1.1.2 HSI: Theoretical Models for Lateral Bridge Motion

Much work has been done to develop theoretical HSI models parallel to experimental and field studies. These models fall into a variety of forms depending how the developer chose to represent several parameters. The force can be modelled either as an individual person (e.g. inverted pendulum models, random narrow band processes, dynamic load factor models), a collection of individual people (discrete elements), or as a single signal representing the entire crowd. Application of the force (moving, stationary, mode shapes) depends on the configuration of the structure being modelled (SDOF oscillator, SDOF beam, MDOF beam, multi-modal finite element model). In addition, many models incorporate some characterisation of the synchronisation and lock-in phenomena (critical number models), autoparametric (self-excited) forces, and/or the concepts of equivalent added damping and mass. Finally, models exist both in the time and frequency domains. The diversity of models is immense, so some of the models exhibiting the greatest potential are discussed here. For some additional models, readers should consult Venuti *et al.* [56], Piccardo and Tubino [57], and Ricciardelli [58].

Before discussing the models, however, some attention must be given to the issues of synchronisation and lock-in. Fujino *et al.* determined that the effective lateral force produced by a densely packed partially synchronised crowd of n_p pedestrians is equal to the force produced by a perfectly synchronised crowd of size $\sqrt{n_p}$ pedestrians [27]. Following the Millennium Bridge incident authors such as Dallard *et al.* [26] and Newland [59] identify synchronisation and lock-in as important parameters for understanding bridge excitation. The former determine a critical number of synchronised pedestrians that are necessary to destabilise a structure in synchronous lateral excitation. As time progressed, some results (e.g. Macdonald [30] and Carroll *et al.* [60]) showed that neither synchronisation nor lock-in was necessary to significantly excite a structure. Ricciardelli and Pizzimenti produced a flow chart identifying multiple causes of lateral bridge excitation [61], some of which only required general vibrations

to destabilise a structure. Even still, no consensus has been reached whether (a) synchronisation is due to either lock-in or attaining a critical pedestrian density, (b) lock-in results as a function of synchronisation, or (c) whether (or to what extent) synchronisation and lock-in are related at all. In spite of the debate, researchers since Dallard *et al.* have produced a variety of critical number models, some of which depend on pedestrian synchronisation or lock-in while others do not. These models are reviewed presently.

Critical Number Models and Other Stability Criteria

Ultimately HSI models are closely tied to *stability criteria*. A structural (as opposed to biomechanical) stability criterion establishes a threshold beyond which some structural parameter, such as displacement, becomes divergent. Dallard *et al.*, Strogatz *et al.*, Roberts, and Ricciardelli *et al.* have proposed different stability criteria whereby if a critical number of pedestrians on the bridge is exceeded, the amplitude of bridge motion will suddenly increase rapidly. Due to the spotlight on the Millennium Bridge, the model by Dallard *et al.* has probably received the most attention. They describe the critical number of synchronised and locked-in pedestrians as [26]

$$N_c = \frac{8\pi\xi_b f_b m_b}{c_p} \tag{1.1}$$

where ξ_b is the critical damping ratio, f_b is the structural natural frequency, m_b is the structural modal mass, and c_p is a structure-specific, empirically determined damping coefficient related to the walking force. For the Millennium Bridge c_p was estimated at 300 Ns m^{-1} based on full scale walking tests. This model has been used as the gold standard for subsequent models and testing, which have sought – and to some measure succeeded – to validate its prediction.

Where Dallard *et al.* arrive at their critical number by assuming proportionality between ground force and structural motion, Strogatz *et al.* apply a sinusoidal walking

force to a more traditional equation of motion [1].

$$m_b \frac{\mathrm{d}^2 x}{\mathrm{d}t^2} + C\frac{\mathrm{d}x}{\mathrm{d}t} + Kx = F_x \sum_{i=1}^{N} \sin \Phi_{pi} \tag{1.2}$$

where m_b, C, and K are the modal mass, damping, and stiffness respectively, x is the structural displacement, F_x is the peak lateral force, and Φ_{pi} corresponds to the gait cycle phase per pedestrian. Assuming an individual's gait cycle is governed by the equation

$$\frac{\mathrm{d}\Phi_{pi}}{\mathrm{d}t} = \omega_{pi} + SX \sin(\Phi_b - \Phi_{pi} + \Phi_l), \tag{1.3}$$

which is based on a formula for other biological oscillators, then the critical number of pedestrians can be determined as

$$N_c = \frac{4\xi_b}{\pi}\left(\frac{K}{F_x SP(f_{d0})}\right), \tag{1.4}$$

where S is an empirical parameter describing a pedestrian's sensitivity to base motion, $X(t)$ and Φ_b are the amplitude and phase of that motion, and ω_p is the gait frequency centred around $\omega_{p0} = \sqrt{K/m_b}$. Φ_l describes a phase lag and $\xi_b = C/\sqrt{4m_b K}$. S is estimated to be 16 $\mathrm{m^{-1}s^{-1}}$ based on Millennium Bridge tests. When the critical number is exceeded, synchronisation and lock-in are said to occur simultaneously.

Roberts also utilises a basic spring-mass-damper system as the basis for his motion equation [62]. To this he applies the pedestrian lateral force

$$F_x(t) = -m_p d_p \omega_p^2 \sin\left(\omega_p(t+\tau)\right) \tag{1.5}$$

where m_p is the mass of a pedestrian, d_p is its lateral displacement amplitude, ω_p is the angular walking frequency (synchronised with other pedestrians), and τ is a phase lag. Unfortunately the author does not make it clear what is meant by the pedestrian's lateral displacement amplitude – step width, Centre of Mass motion, head motion, or something else. Nonetheless, he assumes that a critical condition occurs when the bridge motion equals the pedestrian motion, making the critical number

$$N_c = \frac{m_{bi} L_b}{m_{pi} \beta_i^2 D_i} \tag{1.6}$$

with m_{bi}/m_{pi} constituting the structural to pedestrian modal mass ratio, L_b the length of the bridge, β_i the frequency ratio, and D_i the dynamic amplification factor. Roberts observes that the $\beta_i^2 D_i$ term is extremely sensitive near resonance for structures with low damping ratios. He recommends using an average value for $0.8 < \beta_i^2 D_i < 1.2$, for which he provides a table. Curiously, in another work Roberts applies a pedestrian load based on Fourier coefficients to produce a different stability criterion. He states that 'synchronisation can occur with any number of pedestrians on the bridge, with the increase in lateral bridge amplitude being either stable or unstable' depending on which loading condition controls, either structural motion due to uncorrelated walking or due to partial synchronisation [63]. Collectively his work suggests that synchronisation is not dependent on pedestrian density and so bridge amplitude can increase in either a stable or unstable manner regardless of pedestrian density, but when synchronisation does occur the critical number for stability is according to Equation 1.6.

Here a couple of non-critical number stability criteria are worth mentioning. Piccardo and Tubino develop a stability criterion similar to the critical number methods mentioned above [57]. It states that the pedestrian to structure mass ratio must be less than a frequency term,

$$\frac{m_{pi}}{m_{bi}} < \frac{4\omega_{bi}^2 \xi_b}{g \lambda_s F_C} \tag{1.7}$$

where ω_{bi} and ξ_b correspond to the structural natural frequency (modal) and damping ratio respectively, λ_s is the fraction of synchronised pedestrians, and F_C is a dynamic load factor coefficient taken from the Imperial College tests [26]. Blekherman develops a stability criterion based on solving a double pendulum model (i.e. the bridge plus a person) using the perturbation method of multiple scales to determine the critical angular displacements [39, 64]. Newland also develops a stability criterion based on a spring-mass-damper system but instead of obtaining a critical number of pedestrians he arrives at the result [59, 65]

$$2\xi_b > \lambda_a \lambda_l m_p / m_b \tag{1.8}$$

for which ξ_b is the modal damping ratio, λ_a is the ratio of pedestrian Centre of Mass amplitude to base amplitude, and λ_l is the fraction of locked-in pedestrians. He relates this form to Scruton numbers from the study of vortex shedding and develops a so-called pedestrian Scruton number. At about the same time McRobie *et al.* also developed a pedestrian Scruton number, though theirs was for vertical excitation [52].

In 2014 Ricciardelli collated many of the stability criteria identified above and others, putting all of the criteria in terms of critical number [58]. He recognised that the equations were all of the form

$$N_c = \eta \frac{m_b \xi_b}{m_p} \tag{1.9}$$

where η is a coefficient unique to the model – sometimes a function of structural natural frequency, sometimes of dynamic load factor, sometimes of synchronisation proportion, and sometimes related to acceleration due to gravity. A comparison of suggested values for η revealed a range from 2.9 to 40.2 depending on the assumptions made. Clearly there is little consistency in these predictions. Where most of the aforementioned methods were predominantly theoretical, Ricciardelli used the results from an oscillating treadmill test (see Ingólfsson *et al.* [45]) to develop a stability criterion based on the equivalent added damping and mass contributed by the participants to the structure. A discussion about equivalent damping and mass will be presented below, but for now it shall suffice to say that Ricciardelli's critical number, based on applying the lateral force of an *uncorrelated* crowd (i.e. not locked in) to a spring-mass-damper system, is

$$N_c = -2 \frac{m_b \xi_b}{\xi_p m_p} \tag{1.10}$$

which includes the pedestrian damping ratio, ξ_p. Notably, this is the only stability criterion which explicitly describes the force produced by pedestrians not locked in with the structure, though it ignores the possibility of synchronisation entirely. Ricciardelli reports that using the same assumptions as for the other stability criteria, η $(= -2/\xi_p)$ is equal to 5, which matches well with Dallard's results from the Millennium Bridge.

A variety of theoretical structural stability criteria have been discussed. Many of these criteria are based on the premise that exceeding a critical number of pedestrians will cause a bridge to rapidly destabilise. In some cases the critical number assumes that some portion of the pedestrians will be synchronised or locked-in, whereas in other cases the pedestrians are uncorrelated until the critical number is exceeded. Most importantly, these criteria take a variety of forms with a fair amount of variation as observed by Ricciardelli [58]. This may be attributed to the lack of data associating structural stability to pedestrian motion.

Parametric Excitation: Equivalent Added Damping and Mass

Harmonically oscillating systems may be excited via a number of means: externally, parametrically, autoparametrically, or they may be self-excited. To illustrate this concept consider a girl on a swing [66]. External excitation occurs if the girl's parent stands behind the swing and pushes it. The pushes occur at a frequency equal to the resonant frequency, so the swing oscillates with ease; the force is applied from outside the system.

Parametric excitation occurs if the girl 'pushes' herself. The child is part of the system, so no external force is applied. As the girl alters the location of her Centre of Mass, the swing starts to oscillate. Eventually the girl can 'lock in' her mass shifts to twice the resonant frequency of the swing to attain a higher amplitude. Motion is a result of a change of system parameters, in this case the pendulum length.

Autoparametric excitation occurs when the girl, sitting motionless in the swing is disrupted by an eager boy in the swing next to her. As he starts swinging, energy is transferred through the (motionless) swing-set frame into the girl's swing. To her surprise, the girl finds her swing oscillating back and forth. This form of excitation is the result of a multi-component system in which the two components are quasi-independent, and often found in systems where the modal frequencies have a 2:1 relationship.

Lastly is self-excitation, for which the girl (once again swinging alone) observes that the frame of the swing-set lurches forward and backward during each cycle. The lurching – though disconcerting – contributes energy to her swinging, making it easier for her to gain amplitude. Another analogy of self-excitation is drawing a bow across the string of a musical instrument, such as a cello. The alternating stick-slip mechanism of the string against the bow causes the string to vibrate. This type of excitation is particularly observed when a system switches back and forth between two nearby resonant frequencies or stable states.

Unsurprisingly, models of the interaction between (synchronised/locked-in) pedestrians and bridges have taken all of these forms. Several of the critical number examples already examined constitute externally forced systems. Fujino *et al.* were the first to consider autoparametric excitation caused by pedestrians [27]. They recognised that the deck and cable stay frequencies in the Toda Park Bridge exhibited a 2:1:1 ratio. Blekherman also promotes an autoparametric model due to the fact that the Solferino Bridge, the Millennium Bridge, and the Kiev suspension bridge all exhibit vertical to horizontal deck frequency ratios of 2:1 [39, 64]. In his earlier work he develops a model based on a vertically-forced sprung pendulum while in the latter he analyses the motion of a double pendulum, both of which he ascribes to the bridge-pedestrian system.

Examples of parametrically-excited and self-excited systems will now be considered simultaneously. Even though the behaviours are different, the elementary example of the girl in the swing rightfully suggests that they are not mutually exclusive. The work produced by Dallard *et al.* suggests that a system (i.e. bridge) destabilises if its effective total damping becomes negative [26]. Thus, assuming that the damping supplied by the bridge is always positive, the critical number of pedestrians corresponds to some critical amount of negative damping for which the total system damping is zero. Also assuming a uniform distribution of pedestrians across the bridge, the critical damping is uniformly distributed amongst the pedestrians. This attributes to each pedestrian

equivalent added damping, which happens to be negative during synchronous lateral excitation. The force due to this equivalent added damping constitutes a source of parametric excitation which is proportional to the velocity of the structure.

Later Macdonald investigated the motion of an inverted pendulum walker on a moving base [67]. He discovered that the lateral force produced by the pendulum not only exhibited the frequency and harmonics of the pendulum, but self-excited forces pertaining to the base frequency as well. These harmonics were located at $n_h f_p \pm (f_b - f_p)$, where n_h is the odd harmonic number, f_p is the walking frequency and f_b is the base frequency. He then states that the total lateral force may be split into quadrature components in-phase with the structural acceleration and velocity:

$$F_{xv} = \frac{2}{\Delta T} \int_{t_0}^{t_0+\Delta T} F_x \cos[\omega_b(t-\tau)]\,\mathrm{d}t \tag{1.11a}$$

$$F_{xa} = \frac{-2}{\Delta T} \int_{t_0}^{t_0+\Delta T} F_x \sin[\omega_b(t-\tau)]\,\mathrm{d}t. \tag{1.11b}$$

Here, F_x represents lateral force with ΔT corresponding to an arbitrary duration of integration from time T_0. ω_b is the structural natural frequency and τ is the phase. Next Macdonald uses these to determine the equivalent added damping and mass per pedestrian,

$$c_p = \frac{-\bar{F}_{xv}}{X\omega_b} \tag{1.12a}$$

$$\varrho_p = \frac{-\bar{F}_{xa}}{X\omega_b^2}, \tag{1.12b}$$

where X is structural oscillation amplitude and the bar represents the average value. Macdonald clarifies that these calculations are valid only during steady state bridge oscillations and that transient vibrations may be subject to a significant amount of variation.

Ingólfsson *et al.* developed a model that incorporates both an equivalent 'static' pedestrian force and the parametric equivalent added damping and mass. The damping

and mass terms are of the form

$$c_p \text{ or } \varrho_p = \alpha_0 + \alpha_1 X + \zeta \alpha_2 e^{\alpha_3 X} \tag{1.13}$$

where c_p and ϱ_p are the equivalent added damping or inertia per pedestrian as a function of normalised bridge frequency, the α_i terms are curve-fitted coefficients of the mean and standard deviation added damping or mass, determined experimentally, as a function of normalised bridge frequency, ζ is a stochastic variable, and X is the bridge displacement amplitude [68]. Based on a simply supported SDOF bridge with modal damping ratio ξ_b and natural frequency ω_b, the motion equation is

$$\ddot{q}(t) + 2\xi_b \omega_b \dot{q}(t) + \omega_b^2 q(t) = F_x'(t) \tag{1.14}$$

where q is a generalised displacement coordinate for the given mode in the time domain and the mass-normalised applied load F_x' is such that

$$F_x'(t) m_b = F_{st} \phi_q(v_p t) + (c_p \dot{q}(t) + m_p \varrho_p \ddot{q}(t))[\phi_q(v_p t)]^2 \tag{1.15}$$

with location-dependent mode shape ϕ_q and equivalent static force F_{st}. Notice that the final two terms in Equation 1.15 are proportional to the structural velocity and acceleration, and are therefore parametric (i.e. non-external) forces. The equivalent static force F_{st} is produced by fitting separate Gaussian distributions to each of the first five normalised load harmonics of a population of power spectral density (PSD) plots [47]. That is, the PSD was obtained for each sample of a population of walking trials. For the first harmonic the PSD of each sample was normalised by the gait cycle frequency and then a Gaussian curve fitted to the data. This was repeated for the second to fifth harmonics. These best-fit 'means' are accompanied by standard deviations, allowing the authors to produce a quasi-random time series for the equivalent static force. Over a number of different loading scenarios, the authors found reasonably good agreement between the simulation and the Millennium Bridge, both in terms of

vibration amplitude and in terms of the critical number of pedestrians to effect negative damping.

In 2012 Bocian *et al.* continued the work done by Macdonald by developing a set of simultaneous equations defining a structure's stability limit based on equivalent damping and mass [69]. They coupled a 'high volume' of inverted pendulum based walkers to a 2DOF structural model based on the Clifton Suspension Bridge and found that the two lateral modes were prone to significant excitation after 210 and 400 walkers were applied. This led to further work by the same group whereby a probabilistic stability criterion was developed [70]. Unlike the stochastic model developed by Ingólfsson *et al.* the model by Bocian *et al.* is entirely in the time domain and based on the premise that the total damping – the constant structural damping plus the probabilistic equivalent added damping – must be greater than zero. It requires the user to predict the distribution and walking velocity of the crowd on the structure, which make a significant difference to the resulting stability.

The research by Carroll *et al.* provide experimental evidence supporting the theory of self-excited forces [49]. The motion of pedestrians on a laterally oscillating treadmill appears to be amplitude modulated whereby the dominant excitation frequencies occur at $n_h f_b$ with side bands around $n_h f_b \pm f_p$, for odd harmonics $n_h = 1,\ 3,\ 5$, etc.

McRobie *et al.* explore the long term impacts of Macdonald's parametric model [71]. Using complex mathematics, they generalise Macdonald's formulae for equivalent added damping and mass and investigate the cases of perfect tuning and phase of lock-in. They determine that perfect tuning can lead to particularly high added damping values but the phase between the walker(s) and the structure matters significantly. Most importantly, they identify a three-way discrepancy between: the full scale tests on the Millennium Bridge [26], Clifton Suspension Bridge [30], and Changi Mezzanine Bridge [31]; the experimental results produced by Ingólfsson *et al.* [45]; and the theoretical models produced by himself, Macdonald [67], and Ingólfsson *et al.* [68]. They

show that the full scale predictions of equivalent added damping tend to be much higher than the theoretical predictions but states that the dearth of field data (and possibly, the inappropriateness of single-pedestrian lab tests) make it difficult to tune theoretical models. Still, he suggests such analytical parametric studies allow researchers to investigate various new theories.

Finally, the most recent parametric model was proposed by Ricciardelli, who determined his aforementioned critical number via a simple deterministic calculation for the motion of the footbridge [58]:

$$(m_b + \varrho_p m_p)\ddot{x}(t) + (C + c_p)\dot{x}(t) + Kx(t) = F_x(t), \tag{1.16}$$

where ϱ_p is the non-dimensional added mass coefficient. He then identifies the total damping ratio as

$$\xi_{tot} = \frac{C + c_p}{2\omega_b(m_b + \varrho_p m_p)} = \frac{\xi_b + m_p\xi_p/m_b}{\sqrt{1 + m_p\varrho_p/m_b}}, \tag{1.17}$$

recognising that the numerator of the right-most expression must be greater than zero for the bridge to remain stable. For a bridge of constant cross section and uniform pedestrian load with a single sinusoidal mode shape, the stability criterion $\xi_b + m_p\xi_p/m_b > 0$ can be rearranged to find the critical number in Equation 1.10.

Some other models

Beyond the models that have already been presented, a variety of others exist. Some of these are identified here as a representative sample of the diversity of different representations of HSI. Erlicher writes that models can be characterised as either micro-scale models or macro-scale models depending on whether they focus on the individual pedestrian or the collective, a classification that will be adopted presently [72].

Micro scale models examine the behaviour of an individual with respect to their environment. Qin *et al.* developed a model whereby stick figure individuals with compliant sprung and damped legs cross a simply supported beam 'bridge' [73]. It is interesting because it derives motion equations from the use of Lagrangian equations

with kinetic and potential energy summations and principles of virtual work. After developing a feedback mechanism based on the energy required to cause horizontal work in the bridge (though the horizontal direction is ambiguous), the system is solved using a state-space method and a time-stepping routine. In the work by Morbiato *et al.* a walker is considered to be an upright pendulum subjected to 'ring dynamics' with an excitation torque $M(\Delta E)$, a moment produced by the expenditure of internal energy [74]. To also facilitate the use of Lagrangians, they characterise the pendulum-structure system in terms of kinetic and potential energy. In several simulations, they find that pendula settle into beforehand quadrature lock-in depending on the initial frequency ratio. In a quite different study, Carroll *et al.* model the Clifton Suspension Bridge coupled to discrete element inverted pendulum-based walkers [60]. The walkers move across the bridge according to several *social force* rules, whereby their pace and orientation are determined by attractive and repellent 'forces' to their destination and obstacles (e.g. the railing, other pedestrians) respectively. Importantly, the model allows for participants in dense crowds to slow down and speed up, which in turn means they can lock in with the structure. The authors found that the predictions – which were reasonably good – did not require synchronisation to achieve structural instability.

As far as macro scale models, here only two more are presented. Venuti *et al.* develop a crowd-sized lateral force function which can be applied to a structural model [75]. The force produced by a crowd is equal to the sum of the force produced by locked-in pedestrians, the force produced by synchronised pedestrians, and the force produced by uncorrelated pedestrians. Though simulated conditions on the Toda Park Bridge and Millennium Bridge match reasonably well, the authors state that the model only presents an initial framework for future development due to inadequate supporting data. Finally, in the most complex model thus far examined, Caprani sought to develop a model that accounts for significant inter- and intra-subject varia-

tions [76]. Coupling the pseudo-excitation method with the modal precise integration method, a power spectral density plot for walking is applied, over a time series, across the length of a simply supported beam bridge. While it claims to be faster and more accurate than Monte Carlo (stochastic) methods, its application to a real multi-modal structural design could be quite complicated.

In this section a wide variety of HSI theories have been introduced. The breadth of the types of models is very wide and unfortunately few comprehensive data exist by which the models can be verified. With the exception of the critical number models and the parametric excitation models, none of the other models have been explored more broadly. Even the critical number models and parametric excitation models are based on the initial post-Millennium Bridge study by Dallard *et al.*, which are founded on a single incident. Much more work needs to be done to explore how humans interact with moving structures and whether existing models are accurate enough to be used for design and analysis.

Moreover, many of the models explored thus far have either represented the biomechanics of walking in quite simplistic means or expressed footfall forces in terms of (simplifying) Fourier coefficients. Both renderings of walking have their limitations, either in establishing an anatomically incorrect representation of gait on a moving surface, or imparting a perfectly periodic, steady-state frequency domain model to a situation that requires an understanding of transient biomechanics.

And so attention is now turned away from the structural aspect of HSI to focus on the human side. The next two sections of this literature review examine theories of biomechanics on stationary and moving surfaces and the experimental studies which have been done to assess the nature of lateral ground forces.

1.1.3 Biomechanics of Gait: Experimental Observations

The biomechanical side of human-structure interaction has a number of important aspects. Firstly, one must understand gait stability, or balance, on rigid ground. While

research has been conducted to characterise the kinematics and kinetics of gait [77, 78], surprisingly few detailed quantifications of gait cycle timings and force magnitudes have been reported in the biomechanics literature. Quantifying gait characteristics is challenging because there is variability from person to person ('inter-subject variability') and from step to step of one person ('intra-subject variability'). In addition, much of the research into human kinematics and kinetics has been purposed for clinical applications such as diagnosing and treating a wide variety of genetic, developmental, circumstantial, and neurological pathologies. In these applications the exact quantity of the ground force, the Centre of Mass displacement, joint angles, etc. is not as important as the overall pattern. Thus, a qualitative understanding of gait is usually sufficient for clinical purposes. When trying to determine how much force a crowd of synchronised pedestrians exerts on a bridge, however, this generality is not sufficient.

Secondly, supposing a sufficiently accurate reproduction of ground forces can be produced, engineers need to understand how stable ground walking translates to walking on a moving surface. How is gait affected by monotonic ground displacements, an oscillating base of some amplitude and frequency, or the movement of one's visual frame of reference? There are many variables to consider including pedestrian stature, gait to structure phase lag, gait frequency, walking speed, step length and width, and structural properties such as displacement, acceleration, velocity, and frequency (e.g. Archbold and Mullarney [79]). These could even be compounded by cultural effects such as shoe type, emotions, and purpose of journey. Complicating matters, as a base motion becomes more familiar one is likely to adapt his or her gait to make walking as comfortable (least energy costly) as possible. Clearly the mechanisms behind gait stability are challenging to identify, and are likely to be situation specific.

With an understanding of how an individual reacts to base motion, the last question is how the pedestrian deals with the base motion in the non-structural environment. How is the individual's gait affected by walking in a crowd late at night after an event

versus walking on a sparsely populated bridge on a sunny day 20 m over a river? The environment and circumstances may make a significant difference to one's reaction to structural motion. Some reports show evidence of crowds becoming panicked while in other cases people deliberately oscillate a structure, technically known as 'vandal loading' [17].

This section presents experimental studies of walking biomechanics. The first major topic is the overall characterisation of ground forces on stable ground. Force plate and treadmill studies are discussed and compared before discussion turns to studies of biomechanics on unstable surfaces. Lastly a few studies are described that investigate pedestrian-pedestrian interactions.

Characterisation of Ground Forces

Scientific investigations of gait kinematics and kinetics are far from novel. Only in the last half century, however, have developments in technology allowed researchers to accurately record ground forces while walking. In 1967 Murray published a landmark kinematic study analysing joint rotation during walking [80]. The study investigated the kinematics of 30 healthy adult walkers, characterising parameters such as stride length, swing and double stance duration, cadence, and segment rotations. He used interrupted light technique to track the motions of various body parts through space in the sagittal (forward-vertical) plane. He also compared the movement of these 30 healthy individuals to the kinematics of several types of locomotive pathologies. While recognising the importance of understanding normal gait, his aim was directed at clinical purposes. Given that this study did not use force plates and was geared toward clinical diagnoses, it is easy to understand why subsequent use of more advanced technology has primarily produced knowledge for clinical applications. Nonetheless Murray's study, which among other things defines the gait cycle and reveals a relationship between walking speed and other gait parameters, was fundamental for subsequent HSI research.

Since humans walk in the sagittal plane, interrupted (and continuous) light technique was used extensively for recording vertical and forward motion. Though technology for recording shear ground forces has improved and three-dimensional motion tracking cameras have replaced interrupted light techniques, much more vertical kinematic and kinetic research has been conducted than in the lateral direction. Two studies of vertical ground forces are of particular relevance. In the first, Galbraith and Barton measured vertical ground forces of subjects wearing different shoes walking on different surfaces [81]. They determined that the walking speed affected the shape of the ground force as well as the duration of double stance, but neither the footwear nor the surface had any significant influence. Ebrahimpour *et al.* built a stationary 14 x 2 m platform with force plates that allowed him to record the forces of individuals, side-by-side pairs, and 2 x 2 foursomes [82]. Not only did they find that the double stance duration and gait period varied inversely with walking speed, but that the ratio of the two remained relatively constant regardless of speed. They also developed dynamic load factors for different speeds of simulated crowds based on the frequency response of small groups of walkers. Even though these tests were conducted for vertical ground forces, they show that the walking speed is of immense importance for understanding the characteristics of ground force in general.

One of the most comprehensive texts about the biomechanics of human motion is the sum of two decades of research by Winter [83]. He identifies that the first force plates were used in the 1930s (e.g. Elftman [84]) but says very little about what defines lateral ground forces. His text is mostly concerned with sagittal plane forces amongst a variety of other biomechanically related topics, including instrumentation, data analysis, and kinematic modelling of joint motion.

Schneider and Chao undertook a study in which 26 subjects crossed a force plate while wearing footswitches [85]. They determined the 'essential number' of Fourier harmonics needed to reproduce a force plate signal to 75%, 90%, or 95% accuracy

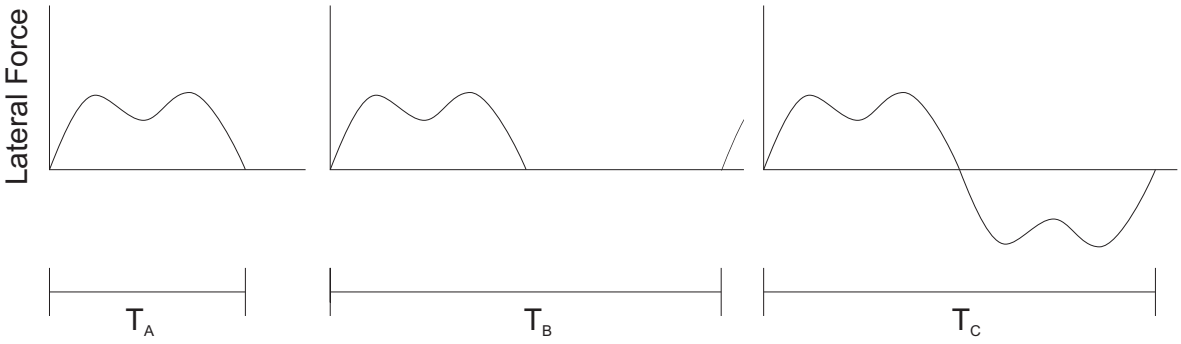

Figure 1.4: Period definitions as identified by Schneider and Chao [85].

Table 1.1: Number of essential Fourier harmonics to reproduce components of ground force to varying levels of accuracy. See text for period definitions [85].

Force Component	Accuracy Level	Nr Essential Harmonics by Period Definition		
		Def A	Def B	Def C
Vertical	0.75	3	3	3
	0.90	11	10	9
	0.95	14	20	26
Fore-aft	0.75	6	8	10
	0.90	13	20	28
	0.95	23	36	45
Med-lat	0.75	8	11	12
	0.90	17	24	29
	0.95	28	43	52

level. Using only one plate strike per person, a period was defined as either the stance phase length, twice the stance phase length, or twice the stance phase length with the first stance phase repeated and inverted, Figure 1.4. The resulting number of essential harmonics was in general quite high. For every accuracy level and period definition, the number was higher for lateral force than forward or vertical force (Table 1.1). As a result of their study, they published the first twelve even and odd Fourier coefficients for normal ground walking.

Giakas and Baltzopoulos undertook the first (and to the author's knowledge, only) fully time-domain characterisation of ground forces in 1997 [86]. Using standard gait analysis techniques, they asked 10 healthy males to walk a 15 m track until 20 clean force plate strikes were recorded for each subject. The authors identified key landmarks in the vertical, forward, and lateral force time histories which are shown in Figure 1.5 and Table 1.2. The lateral forces are of significantly lower magnitude than the vertical

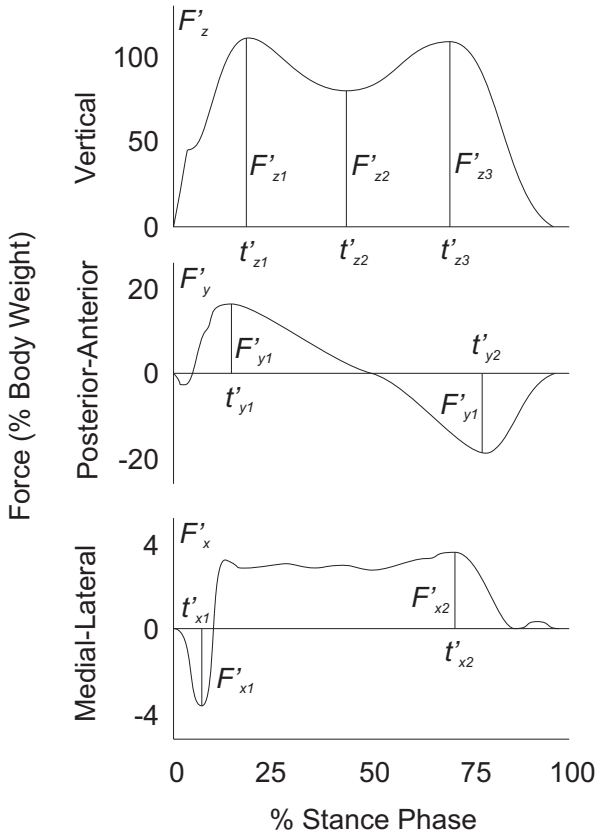

Figure 1.5: Time-domain characterisation of ground reaction forces based on Giakas and Baltzopoulos [86]. See Table 1.2.

Table 1.2: Ground force amplitudes (normalised to body weight) and times (normalised to total stance) averaged across 10 male subjects [86].

Parameter	Left side		Right side	
	Mean (%)	S.D.(%)	Mean (%)	S.D.(%)
F'_{z1}	117.79	8.2	117.10	9.8
t'_{z1}	22.85	2.1	21.97	1.4
F'_{z2}	76.47	5.4	74.58	6.9
t'_{z2}	48.14	4.2	74.58	2.7
F'_{z3}	106.60	4.2	111.69	6.3
t'_{z3}	16.32	2.1	111.69	2.9
F'_{y1}	18.61	2.9	19.36	3.3
t'_{y1}	17.15	1.8	16.94	1.1
F'_{y2}	22.24	2.9	1.21	2.9
t'_{y2}	86.24	0.9	86.14	1.7
F'_{x1}	4.85	0.8	5.31	1.3
t'_{x1}	4.76	0.5	4.84	0.4
F'_{x2}	4.11	1.3	4.09	0.8
t'_{x2}	39.35	12.4	48.62	17.59

Table 1.3: Spatial-temporal gait parameters as determined by Stolze (mean ± SD) [87].

Gait parameter	Adults		Children	
	Overground walking	Treadmill walking	Overground walking	Treadmill walking
Gait velocity (m s^{-1})	1.5 ± 0.2	1.5 ± 0.2	1.1 ± 0.2	1.1 ± 0.2
Stride length (cm)	162.6 ± 16.0	155.7 ± 14.7	109.3 ± 13.3	97.9 ± 11.5
Step length related to leg length	0.9 ± 0.1	0.8 ± 0.1	0.9 ± 0.1	0.8 ± 0.1
Step length related to body height	0.5 ± 0.03	0.5 ± 0.03	0.4 ± 0.04	0.4 ± 0.03
Cadence (steps min^{-1})	113.1 ± 11.1	120.7 ± 5.2	120.2 ± 11.4	133.3 ± 11.2
Step width (mm)	81.2 ± 19.6	104.3 ± 17.6	81.0 ± 22.2	105.5 ± 23.2
Foot angle (degrees)	9.1 ± 4.4	11.3 ± 3.8	5.8 ± 4.9	9.4 ± 4.8
Stance phase (ms)	630.2 ± 43.6	587.0 ± 29.2	605.9 ± 49.0	530.7 ± 44.3
Swing phase (ms)	406.6 ± 27.3	426.2 ± 26.5	394.4 ± 40.6	383.5 ± 46.0
Double limb support (ms)	111.7 ± 17.4	81.1 ± 11.2	106.5 ± 11.7	74.6 ± 20.8
Cycle duration (ms)	1036.8 ± 65.6	1013.2 ± 51.0	1000.3 ± 86.5	914.2 ± 79.8

or forward forces and, notably, the time of the second lateral landmark is subject to a great deal of variation. The studies by Schneider and Chao and Giakas and Baltzopoulos represent opposite ends of the experimental spectrum. The former presents a purely Fourier domain characterisation of ground force while the latter applies a purely time-domain method.

In research by Stolze *et al.* adults and children completed both a force plate test and a treadmill test [87]. They published a table of 11 different gait parameters including walking speed, stride length and width, cadence, and different gait phase durations (Table 1.3). These *spatial-temporal* parameters – similar to those measured by Murray – are easy to identify and generally assumed to define human motion. The most important findings of this study, however, were that the participants (1) acclimatised to treadmill walking over the first 10 minutes but (2) the gait parameters were still different to overground walking even after the adjustment period. They state that while their findings are corroborated by some studies and opposed by others, theirs is unique for maintaining the same walking speed between the overground and treadmill tests. A later study by Rosenblatt and Grabiner agree with Stolze *et al.*, stating that self-selected walking speed, step width, and step width variability are statistically significantly different between overground and treadmill walking [88]. They also state that while treadmill walking might be able to reflect overground walking in the sagittal plane, the study by Stolze *et al.* is the only one of which they are aware to investigate frontal plane differences.

The data of two other tests are also worth mentioning. In 2011 Archbold and Mullarney published the walking records of 14 men and 13 women who walked across a force plate [89]. In addition to the parameters indicated above, they recorded the subjects' *foot landing position*, which they defined as the angle of turnout from the direction of walking to the centreline of the foot. The mean turnout was 6.03 degrees with a standard deviation of 4.71 degrees and ranged from -6.5 degrees (i.e. 6.5 degrees turn-in) to 14.8 degrees. They found the step width to be 79 ± 30 mm and the cadence to be 112.8 ± 7.8 steps min^{-1}, which both match well with Stolze. The other dataset was collected by Dang and Živanović in 2015 [90]. This data sought to characterise inter- and intra-subject variation in the explicit context of footbridge design and modelling. They collected data on seven parameters as a function of walking speed, while also asking participants to characterise each of 11 test speeds as slow, normal, or fast. The variables included pacing rate, step length and width, angle of attack and egress, trunk angle, and dynamic load factor. Each variable appeared to correlate to walking speed except for step width, which exhibited a wide scatter at all speeds. This correlates with the aforementioned tests by Ingólfsson *et al.*, who observed slight correlations between walking speed and walking frequency, and between pedestrian weight and the root mean squared (RMS) lateral force [45].

Two cadaver studies have sought to characterise the anthropometric measurements of the human body. The first was done by Zatsiorsky and Seluyanov [91], which initially provided body segment masses and CoM locations. Thirteen years later, de Leva adjusted these anthropometric values, defining body segment lengths from joint centres instead of bony landmarks [92]. These anthropometric values have been widely used across fields since then.

Force Plate and Treadmill Studies for Assessing Gait Stability

Where works in the previous section sought to characterise ground forces and gait parameters, the studies identified in this section focus on the kinematics and kinetics

of body parts relative to each other. They examine various aspects of how the body moves through space while walking on a stable surface.

In Mackinnon and Winter's research four men were asked to complete 10 walking trials each while wearing motion tracking markers and crossing a pair of force plates [93]. They compared the moments of force about both the hip and the standing ankle with experimentally determined values of the whole-body inertial torque $I\alpha$. They stated that foot placement was the most important aspect of gait stability and showed that fine tuning could occur through adjustments by the ankle and hip moments. They also show that pelvic tilt plays an important role in assisting the hip abductors to stabilise the upper body during double stance. Pandy *et al.* calculated the contributions of various lower body muscles during gait [94]. They found that abduction in the standing hip (i.e. raising the pelvis) plays a primary role in gait stability, even revealing the characteristic shape of the lateral ground force pattern. Contrary to the findings of Mackinnon and Winter however, these findings show that the hip abductors cause the Centre of Mass to move medially. The authors also show that muscles whose dominant function is to propel the body forward (e.g. quadriceps and calves) play a role in stabilising the Centre of Mass laterally. These results are supported by Jansen *et al.* and John *et al.*, the latter of which stated that 92% of lateral ground forces are attributable to internal muscle activity [95, 96].

In addition to the importance of hip abduction Mackinnon and Winter discuss the role of the ankle in gait stability. Hoogvliet *et al.* and King and Zatsiorsky also undertook tests to examine the role of the ankle joint in maintaining stability [97, 98]. The former showed that lateral motion of the body over the ankle is similar to an inverted pendulum over a rocker. King and Zatsiorsky show that ankle movement not only plays a role in lateral force production but also the location of the Centre of Pressure. They stated that foot rocking is a technique used for maintaining balance both through moment generation and shear (lateral) force development. The aforementioned work

of Pandy *et al.* corroborates these findings, as evidenced by the moment contribution of the subtalar muscles.

Several treadmill studies are also of importance to this thesis. The study by Hof *et al.* of normal and above-knee amputees produced a set of data comparing mean values of various gait determinants, including stride time and width, margin of stability, and gait phase durations [99]. The tests were undertaken to compare healthy and impaired walking and to examine the margin of stability in absolute terms. In 2008 Bruijn *et al.* undertook a detailed study of angular momentum during walking, finding that the angular momentum of the whole body was tightly controlled throughout the gait cycle over a range of walking speeds [100]. Interestingly, they observed that where the upper trunk (thorax) was always out of phase with the swing leg, the phase of the pelvis relative to the swing leg depended on the speed of walking. At low speeds, the pelvis was somewhat out of phase and at high speeds became in phase. Tesio *et al.* analysed the motion of the pelvis at different walking speeds and found that where the pelvis traced a figure eight pattern at slow speeds, the pattern became more narrow and U-shaped at higher speeds [101]. These tests show that walking speed not only makes a difference to gait parameters and ground forces, but to kinematics as well. The human body appears to inherently adopt different means of locomotion in order to move at different speeds. Like a continuously variable transmission, the kinematic and kinetic alterations happen seamlessly.

Lastly, a study by Herr and Popović established a parameter called the centroidal moment pivot (CMP) [102]. This point is at ground level, located such that a force parallel to the ground reaction force from this point would develop no moment about the CoM. Thus, if the ground reaction force is aimed from the Centre of Pressure to the Centre of Mass, the CMP is located at the Centre of Pressure. Herr and Popović found that the CMP almost always remained within the Base of Support, though it varied from the CoP. Moreover, the authors find that a simple inverted pendulum –

without a varying CoP or CMP – would be insufficient for modelling lateral ground force.

Studies of Gait Stability on Moving Surfaces

Beyond the studies that have been conducted on stable ground, a number of studies have also been conducted on laterally oscillating surfaces. These tests again fall into two categories: moving treadmill tests and oscillating platform tests. As a reminder, the previous moving base tests examined HSI as a complete system; the following tests, in contrast, are predominantly concerned with the biomechanics of stability.

A few moving platform tests are of particular importance. In the tests by Oddsson *et al.*, participants crossed an actuated platform [55]. The platform gave a single monotonic perturbation 180-200 ms after right foot heel-strike. The perturbation was either 5 or 10 cm in amplitude and either 45 degrees front right or 45 degrees back left compared to the direction of walking. They found that the horizontal separation between the standing leg and the sternum increased linearly with perturbation amplitude and that the subsequent left step usually reflected the same qualitative response. Though the participants followed a metronome (100 steps min^{-1}) and the perturbation was monotonically applied at the same point in the gait cycle for every test, this study provides valuable information about how people react to sudden base motion.

Another study, conducted by Brady *et al.*, involved putting a treadmill on a laterally oscillating platform of constant amplitude to see how participants responded to prolonged sinusoidal perturbations [103]. The authors found that walkers adopted a combination of two strategies to cope with base movement. One strategy was to fix their Centre of Mass to the room, allowing their feet to oscillate laterally beneath them ('fixed-in-space'). The second strategy was to keep their CoM moving with the oscillations of the treadmill ('fixed-to-base'). While most of the participants adopted one strategy or the other, some switched strategies during the test. A follow-up study by Peters *et al.* studied stride entrainment (lock-in) during the aforementioned test [46].

They showed that during the 20 minute test only a quarter of the participants maintained structural lock-in for an extended period. That said, all participants were able to walk comfortably within 10 minutes, showing that although participants did require time to adapt, adaptation occurred relatively quickly.

While not a moving platform test, Rietdyk *et al.* conducted important tests on stationary standing subjects [104]. Their subjects were asked to keep one foot on each of two force plates while lateral perturbations were applied to either their shoulder or their hip. They found that the contralateral (abducting) hip provided the greatest moment response to the perturbations. In addition, they found that the participants' Centre of Pressure moved laterally in the same direction as the perturbation. They observe a compound pendulum nature for maintaining balance but affirm that a single inverted pendulum model is sufficient for modelling purposes.

Sari and Griffin conducted a treadmill test whereby pedestrians were subjected to different frequencies of lateral base motion [105]. During the first set of trials the velocity was kept constant for each frequency; during the second set the acceleration remained constant. Across all combinations, they found that an increase in perturbation displacement resulted in an increased perception of fall likelihood. For acceleration-constant tests, low oscillation frequencies resulted in higher fall-perception than high frequencies. Velocity-constant tests, on the other hand, were frequency-independent; the frequency did not influence fall-perception.

Hof *et al.* also conducted a treadmill test in which participants were laterally perturbed via a waist-mounted belt and rod attached to a motor [106]. The treadmill speed was fixed proportionally to each participant's leg length. Perturbations of varying amplitudes were applied every eight to 12 gait cycles at various times within the chosen gait cycle. The study confirms the presence of a stepping strategy and an ankle-roll strategy as simultaneous means for establishing and maintaining balance. In addition they partially verify a 'constant margin hypothesis' whereby the distance between the

Extrapolated Centre of Mass (XCoM) and the Centre of Pressure remained constant, even immediately after perturbation.

Pedestrian-Pedestrian Interaction

Finally, a number of pedestrian-pedestrian interaction studies are relevant to the question of synchronisation during walking. While these tests do not concern biomechanics in the strictest sense, their independence from structural analysis means they pertain more to biomechanics than HSI.

Several studies examine the interactions of paired subjects walking side by side. Zivotofsky and Hausdorff observed students walking side by side down a 15 m corridor with four different types of feedback: visual-only, auditory-only, tactile-only (holding hands), and no feedback [107]. Overall 26 out of 56 trials resulted in synchronised walking, of which 14 were in phase with each other and 12 were out of phase. Of those trials, however, only tactile-only feedback resulted in significantly different synchronisation (50% of couples) than no feedback (7%). Despite the small sample size, this suggests that some amount of incidental synchronisation is likely to occur regardless of feedback, and that synchronisation is more likely if subjects are in physical contact with each other.

Nessler and Gilliland published a pair of similar studies whereby walkers were asked to walk with a variety of different feedback cues [108, 109]. They found evidence that visual and auditory cues in addition to tactile cues contributed to the likelihood of synchronising with a partner, perhaps even in phase. That said, they also found that forced entrainment (i.e. participants instructed to synchronise) may cause people to alter their gait. Unlike these treadmill tests, a follow-up test by Nessler *et al.* required instrumented subjects to walk around outside [110]. The subjects either walked solo, side by side in pairs, or side by side and forced to synchronise. In these tests the stride times for paired walking were not statistically different to solo walking, but the stride times for forced walking were statistically longer than both paired and solo conditions.

The aforementioned platform tests by Ebrahimpour *et al.* agreed that subjects walking to a metronome or in a group tend to synchronise their steps [82].

A brief acknowledgement should also be given to so-called 'social forces'. Helbing and Molnar proposed a set of equations describing how an individual moves within an environment given competing 'forces' which implicitly cause a pedestrian to move towards or away from something [111]. One equation represents an attractive vector to drive the individual in a straight line towards their destination at a desired speed. Other equations represent repulsive vectors to avoid contact with strangers or physical obstacles and an attractive vector is also described that models a pedestrian's propensity to gravitate towards friends or interesting distractions (e.g. artists, store fronts). The model can account for the formation of friendship groups, movement in a dense crowd (e.g. over a bridge), or through a narrow gap such as a door. A subsequent study by Moussaïd *et al.* studied group size and shape in two populations of pedestrians [112]. They found that while pairs tended to walk side by side, groups of three tended to take a 'V' formation and groups of four took a 'U' formation. They extended the social force model to include a group force, which encompasses visual, attraction, and repulsion terms specific to the group. The width of the field-observed formations were dependent on crowd density; at a certain density the group formations collapsed into a stream of walkers. These observations were supported by the model. The social force models identified here formed the basis of the HSI model developed by Carroll *et al.*, which has already been discussed [60].

1.1.4 Biomechanics of Gait: Theory

When it comes to transforming experimental data into theoretical models it has already been shown that a wide variety of variables must be considered. Many of the existing applicable walking models are variations on so-called *inverted pendulum models*, which are beneficial for their simplicity and physical resemblance to a walking person. As the primary focus of this thesis their development and application will be discussed

at length. First, however, other biomechanical forcing models are presented that have been used in the study of human structure interaction.

Non-Inverted Pendulum Walking Models

To date, most non-inverted pendulum models are based on *dynamic load factors* or DLFs. These empirically derived coefficients are determined by dividing the Fourier amplitude of a particular walking force harmonic by an individual's body weight. Thus the lateral force exerted by an individual takes the form of a Fourier series [61, 85]:

$$F_x(t) = F_{A0} + \sum_{n_h=1}^{N} (F_{An} \cos n_h \omega_p t + F_{Bn} \sin n_h \omega_p t), \tag{1.18}$$

where for every harmonic n_h at walking frequency ω_p the even and odd DLFs are F_{An} and F_{Bn}. For the case of symmetric gait, the offset F_{A0} and the even terms F_{An} must be zero. Van Nimmen *et al.* recorded test subjects walking on a treadmill, from which they determined the subjects' DLFs [34]. They compared the forcing function developed from the DLFs with the original ground force from the treadmill. In spite of imperfectly periodic walking, manifested in the bandwidth of the dominant harmonics, they found the simulation reproduced the original signal well. Studies undertaken by Bachmann and Amman [113], Ricciardelli and Pizzimenti [61], Ingólfsson *et al.* [68], and Archbold and Mullarney [89] among others determine the vertical and lateral dynamic load factors for individuals walking on a stable surface. Many of the previously identified HSI studies have utilised these factors.

While some researchers are willing to assume gait is perfectly periodic (using, e.g. Equation 1.18), others have tried to account for the real non-periodicity of walking. Ricciardelli *et al.* recorded walkers on a treadmill as well [61]. They discussed three methods for representing lateral ground forces: deterministic periodic, deterministic non-periodic, and stochastic. The use of deterministic DLFs as in Equation 1.18 constitutes a deterministic periodic load model, but the researchers show that this would not account for the non-periodicity of walking. A deterministic non-periodic model

would take into account the bandwidth of the dominant harmonics. Doing so, they found that the probability density function (PDF) of lateral ground forces is somewhere 'between' the PDF of a (deterministic periodic) sine wave and a (deterministic non-periodic) Gaussian process, suggesting a stochastic phenomenon. Thus, normalising the power spectral density plots for the first five harmonics of a population – described by Ingólfsson [114] – they developed a population-specific stochastic model.

Ricciardelli and Pizzimenti described human walking as a *narrow-band random process* from which they developed their stochastic load model [61]. A narrow-band random process $F(t)$ is a system in which the PSD is non-zero only in the range of $f_1 \pm f_2$ where f_2 is small compared to the fundamental frequency f_1 [115]. Suppose a pedestrian walks to the beat of a metronome which beeps at f_1. If the individual walks perfectly to the beat and higher harmonics are neglected, the PSD would be a single spike at f_1. In reality, however, the individual will sometimes step slightly ahead of the beat and sometimes slightly later. This means that some variation occurs about the target frequency. Over a large number of steps, the PSD will present the narrow band of frequencies $f_1 \pm f_2$.

Several studies at the University of Sheffield have proposed gait models based upon narrow-band random processes. Živanović *et al.* accounted for inter- and intra-subject variability by fitting curves to the normalised dynamic load factors around each of five harmonics and subharmonics [116]. These fitted curves are functions of gait cycle frequency, DLF amplitude, and step length, which the researchers obtained from probability density functions. The overall vertical force produced by a pedestrian thus accounts for all frequencies within a bandwith of each of the (sub)harmonics. Racic and Brownjohn later produced different models for vertical [50] and lateral [117] near-periodic forces. In their model, a time series of the force is decomposed into n one-cycle periods. These nominally identical chunks of the force record are then 'averaged' into a representative one-cycle period of duration T using dynamic time warping. A sum-

mation of Gaussian curves – stepping each peak's centre over T – is optimised to fit the data of the representative curve. This summation is thus the equation of a single narrow-band footfall. Finally synthetic series of n period lengths and n impulses (i.e. the integral of force over one period) are created based on the original record of n periods. These synthetic values are applied to the Gaussian equation in order to create a new force record of quasi-identical frequency spectrum to the original. Ultimately all of these methods are useful for representing walking on a stable surface, but they cannot capture the transient corrective motions needed when crossing an oscillating surface.

Inverted Pendulum Models

Inverted pendulum models come in a variety of forms. The most simple of these – utilised by Macdonald – is the basis for the work presented in this thesis, and will be presented independently in the next section. In this section a number of variants are discussed along with their merits.

One of the oldest prominent sets of experiments was described by Saunders *et al.* who identified six *determinants of gait* [118]. These determinants are pelvic rotation, pelvic tilt, knee and hip flexion in stance, ankle mechanisms, knee mechanisms, and lateral pelvic displacement. Though only described qualitatively, the research formed the backbone for most of the experimental and theoretical studies that have been conducted since. In the paper and the subsequent book by Inman *et al.* the determinants were described with the aid of a nine-segment lower body stick model [77], comprising of two thighs, two shins, two feet, two toe panels, and a pelvis with a mass. All joints were modelled as hinges except for the ball-and-socket hips. The six determinants of gait have been researched extensively; the nine segment model has influenced the development of a number of complex multi-segment musculoskeletal computer simulators, such as OpenSim [119] and AnyBody [120].

Following the model by Saunders *et al.*, Townsend developed a six segment whole body model consisting of two rigid arms, two rigid legs, head with upper trunk, and lower trunk [121]. His work studied the dominant translational and angular motions of the six body segments, with a particular focus on the upper and lower torso. This original model was three-dimensional, although it was primarily used to study motion in the sagittal (vertical-forward) plane. The use of deterministic anatomic values allowed Townsend to make numerical estimates of the segments' kinematics. In his subsequent work, he focused more on gait stability by expanding his model to include a foot placement control law and a (small angle) moment arm between the CoM and foot [122].

Winter and colleagues studied gait and the IPM extensively [83, 93, 123, 124], producing a variant of the model based on hip and ankle joint moments [83, 93]. The authors equate the sum of three moments to an inertial torque. The three moments include an applied moment due to the hip abductors (or ankle inverters), a gravity moment from the CoM, and an applied lateral force at the height of the CoM. Moments about the hip constitute a double inverted pendulum, while a summation of moments about the ankle reflects the behaviour of a single inverted pendulum.

Zijlstra and Hof conducted an analysis of pelvis motion in each of the three orthogonal planes [125]. In the frontal plane they assume that stability requires the ground reaction force to be aimed from the CoP towards the CoM. Hof *et al.* adopted Townsend's model and established the *Extrapolated Centre of Mass* (XCoM), a function of lateral CoM velocity and position [126],

$$XCoM = y + \frac{\dot{y}}{\Omega_p}, \tag{1.19}$$

where y is the CoM position, and Ω_p is the pendulum frequency of the body (noting that this is different from the gait cycle frequency). The authors suggested that it is insufficient for gait stability for the CoM to remain between the left and right foot Centres of Pressure: the XCoM must do so as well. This led to the establishment of

the *margin of stability*,

$$b_{min} = y + \frac{\dot{y}}{\omega} - u \tag{1.20}$$

where b_{min} is the margin of stability (a constant) and u is the location of the CoP. Following the London Millennium Bridge incident in 2000 [25], a greater interest was taken in the inverted pendulum model from the civil engineering perspective, especially as it applies to lateral ground forces. Macdonald *et al.* analytically applied an inverted pendulum model to walking on a laterally moving base [67, 69]. Bruijn *et al.* compare several stability models including the XCoM model by Hof *et al.* [127]. While the authors suggest that other methods derived from dynamical systems theory might be better for assessing unperturbed gait, the XCoM model is the most valid and most used biomechanically-based model, and it is the best overall model for assessing perturbed gait, lending it credibility.

A 2007 study by Kuo compared the six determinants of gait versus an inverted pendulum model in the sagittal plane [128]. He showed that a flat CoM trajectory – as advanced by the six determinants – is actually more energy costly than an inverted pendulum model. On the other hand, inverted pendula require costly energy expenditure to overcome the impulse of landing for each step. Thus, neither model is ideal; he proposes refining the models by using a 'dynamic walking approach', which focuses on the exchange of positive and negative work rather than the kinematics and kinetics of real gait.

Unlike the simple inverted pendulum models which have rigid stick support legs, a number of researchers have investigated compliant legged inverted pendulum models. Alexander produced an early compliant model for motion in the sagittal plane with a number of limitations that did not consider ground forces [129]. Geyer *et al.* examined compliant leg behaviour over one step of a sprung inverted pendulum model [130]. They showed that fundamental trajectories and ground reaction forces of walkers and runners can be qualitatively reproduced using body mass, leg stiffness and length, and angle

of attack as parameters. Hong *et al.* collected data of young and elderly participants walking in a laboratory at controlled speeds and pacing frequencies [131]. Ground reaction forces and kinematics were recorded. A model was developed based on a sprung and damped inverted pendulum model with rocker feet. Determining the leg stiffness and damping by minimising the least squares error between the motion equation and data, a reasonably good match was found between the model and experimental ground reaction forces over three steps. Finally, in the most sophisticated compliant-leg model to date, Yang *et al.* also developed a sprung and damped inverted pendulum walker, producing records of lateral ground force, Centre of Mass motion, and other parameters over representative three-second intervals [132]. The authors state that the model suffered from lateral instability so they applied a stabilising ankle moment in order to keep the Centre of Mass within the Base of Support.

With regard to pendulum motion, a few researchers have proposed that aspects of gait more closely resemble the motion of an upright rather than inverted pendulum. Lee *et al.* studied the kinematics of balancing a stick on one's fingertip [133]. They state that where others have modelled the stick's motion as an inverted pendulum, they believe the motion is much more similar to an upright pendulum. They show that different pendulum types are identified by where the pivot point lies with respect to the stick (i.e. at the base for an inverted pendulum; at or above the top of the stick for an upright pendulum). In a normal pendulum, a fast lateral movement of the point of contact – such as transferring weight from one step to another – keeps the top of the stick relatively stable. Milton *et al.* also conduct a stick balancing test, but relate it more directly to 'human postural sway', suggesting the Centre of Pressure oscillates around the Centre of Mass in order to maintain stability [134]. In gait, upright pendulum motion has also been observed by biomechanists such as Kuo [128].

1.2 The Inverted Pendulum Model

The simple frontal plane Inverted Pendulum Model (IPM) proposed by Macdonald and discussed throughout the thesis consists of a point mass positioned on top of two rigid, massless, stick supports, as seen in Figure 1.6 [67]. In order to develop a simple mathematical solution for the more complex biomechanical system of a walking person, seven assumptions about body movement during the gait cycle are applied.

1. The mass of a person can be estimated as a point mass acting at the person's CoM.
2. The legs are rigid; neither hip, knee, nor ankle motion/moments contribute to lateral ground force.
3. The upper body (specifically its angular momentum) does not contribute to lateral ground force.
4. There is no double stance phase; transition between feet is instantaneous and continuous.
5. The CoP remains fixed at a single point for each footstep.
6. The pendulum length L is assumed to equal $1.34h_t$, where h_t is the greater trochanter height [135, 126].
7. The angle between the pendulum and the vertical is approximately zero.

The mass alternately rotates about each CoP as one stick support after the other contacts the ground, representing alternating single stance phases of the gait cycle. With a metronomic motion path the mass moves at a constant radius from the CoP. The mass sweeps through less than 10 degrees per footstep, decelerating as one stick support approaches vertical (mid-stance) and accelerating when falling away from vertical (towards double stance). In normal gait the support never reaches vertical, promoting the so-called margin of stability described by Hof *et al.* [126]. Conversely, double stance

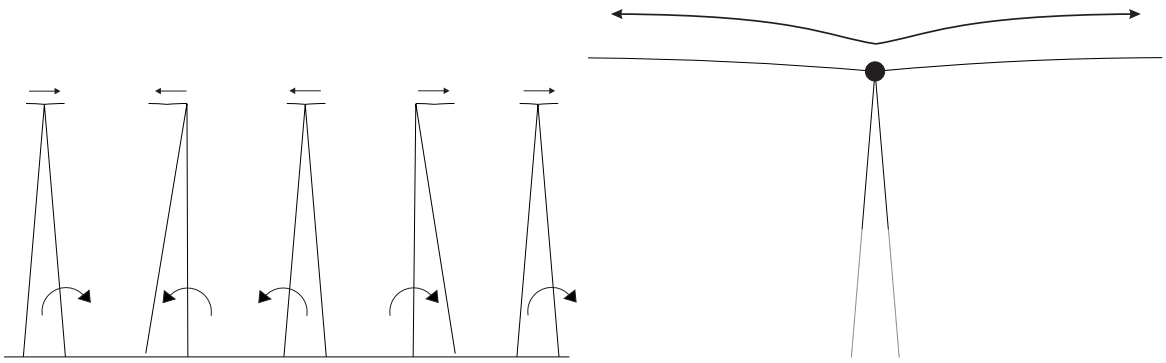

Figure 1.6: Motion of the Inverted Pendulum Model in the frontal plane and detail of Centre of Mass trajectory.

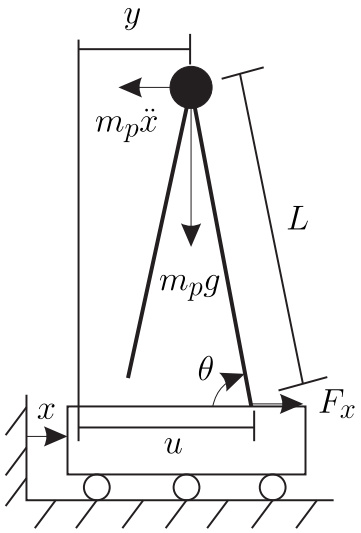

Figure 1.7: Inverted Pendulum Model in the frontal plane based on Macdonald [67]. Note that F_x is the ground force, the force exerted by the pedestrian on the ground.

occurs instantaneously when both stick supports contact the ground. The mass, at its minimum height, is transferred from the first to the second support.

Figure 1.7 depicts the model parameters. x is the lateral motion of the walking surface with the double dot representing the second derivative with respect to time; y is the lateral location of the CoM relative to an arbitrary datum in space; u is the lateral location of the CoP, which remains constant and is also relative to the arbitrary datum; F_x is the lateral ground force exerted by the walker on the walking surface; L is the leg length; and m_p is the mass.

A summation of the moments about the CoP gives Equation 1.21 [67]:

$$-m_p L^2 \ddot{\theta} = m_p g L \cos\theta + m_p \ddot{x} L \sin\theta \tag{1.21}$$

By taking θ to be approximately $90\,^\circ$, the small-angle approximations can be made:

$$\begin{aligned} L\cos\theta &\approx u - y \\ L\sin\theta &\approx L \\ L\ddot{\theta} &\approx \ddot{y} \end{aligned} \tag{1.22}$$

With $\Omega_p = \sqrt{g/L}$, the lateral CoM position and ground force are then given by

$$\ddot{y} + \Omega_p^2 (u - y) = -\ddot{x} \tag{1.23}$$

$$F_x = -m_p(\ddot{x} + \ddot{y}) = m_p \Omega_p^2 (u - y) \tag{1.24}$$

noting that F_x is the force exerted on the ground, not the ground reaction force. The function governing the model is time-piecewise, depending on which is the standing leg. The model assumes that double stance is instantaneous so heel-strike and toe-off of opposite feet coincide. Therefore at heel-strike u immediately switches to the new foot and the lateral difference $u-y$ usually switches sign. Macdonald shows the special case whereby if there is no base motion and a walker's gait is symmetric, the lateral ground force is [126, 67]

$$F_x = m_p u \Omega_p^2 \{\cosh[\Omega_p(t - t_0)] - \tanh(\Omega_p/(4f_p)) \sinh[\Omega_p(t - t_0)]\} \tag{1.25}$$

where f_p is the gait cycle frequency in Hertz. Macdonald assumes that lateral bridge motion is a sinusoidal function of the form $x = X \sin[\omega_b(t-\tau)]$ where X is the amplitude and ω_b is the angular frequency of the bridge. τ is the time lag between heel-strike and the start of the subsequent bridge oscillation. This leads to the general solution for Equation 1.23 [67]:

$$\begin{aligned} y =& u + \{y_0 - u + \bar{X} \sin[\omega_b(t_0 - \tau)]\} \cosh[\Omega_p(t - t_0)] \\ &+ \left\{ \frac{v_0}{\Omega_p} + \frac{\omega_b}{\Omega_p} \bar{X} \cos[\omega_b(t_0 - \tau)] \right\} \sinh[\Omega_p(t - t_0)] - \bar{X} \sin[\omega_b(t - \tau)], \end{aligned} \tag{1.26}$$

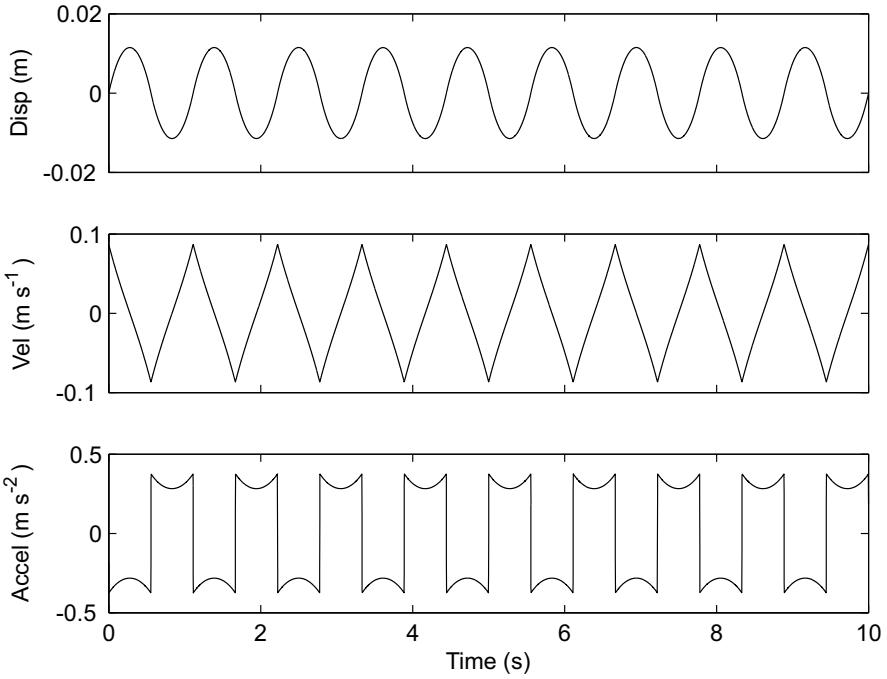

Figure 1.8: Motion of the IPM Centre of Mass (Based on Macdonald [67]).

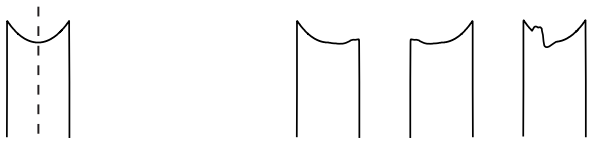

Figure 1.9: Left: Identical loading and unloading implied by IPM. Right: Three examples of irregular acceleration patterns the normal IPM might not reproduce well.

with $\bar{X} = X/[1 + (\Omega_p/\omega_b)^2]$. With no bridge motion, the typical pattern of the CoM's lateral displacement and acceleration are observed in Figure 1.8. The CoM appears to move in a smooth quasi-sinusoidal fashion whereas the velocity and acceleration plots more clearly exhibit the piecewise nature. The velocity is nearly linear during each footstep with a small amount of concavity; the acceleration during each footstep is not constant but slightly bowed. The implication of the acceleration pattern in Figure 1.8 is that the greatest acceleration (ergo, force) occurs at heel-strike and toe-off with a slight dip in between. Moreover, one would expect to see a jump discontinuity in the lateral acceleration for every footstep. Finally, the IPM implies identical loading and unloading during each step with no oscillations or deviations, as seen in Figure 1.9.

While the prevalence of the IPM is indicative of its ease of application and its reasonable representation of limited data, the model will be seen to have a number of shortcomings. Macdonald and other authors use the IPM as a jumping off point for frequency domain analyses, but the present research identifies a need to better understand the relationship between ground forces (via gait kinematics) and bridge motion, a time-domain analysis. This thesis seeks to break down the IPM compared to both stable ground and moving bridge tests, analyse its inadequacies, and make recommendations for more accurate predictions of lateral ground forces.

1.3 Kinematics of Human Walking

Walking is perhaps the most basic of voluntary human motions after breathing and talking, yet saying it is basic is comparable to saying that cooking is merely applying heat to ingredients. The skeletal and muscular composition of the body has been well documented, but understanding how the hundreds of components work together from a physical perspective is immensely complicated. Evolutionarily this only makes sense given that almost all terrestrial vertebrates have had hips, knees, and ankles since the first tetrapods developed from fish 400 to 350 million years ago (e.g. [136, 137]). Over the ages humans have had to conquer complex habitats from mountain terrain to swamps. They have had to chase down a kill over hundreds of miles and they have had to climb trees to hide or gain an element of surprise. The body is well adapted to the myriad challenges conjured up by the natural world. Yet all human locomotion starts with walking. The foundational need to walk efficiently is both the cause and the effect of the complexity of walking. We learn to walk before we can talk, yet it is the basis for a wide variety of nuanced human movement.

The full scope of the kinematics of human walking is thus a book-worthy topic in its own right (e.g. Inman *et al.* [77]), beyond the scope of this thesis. Nonetheless, an understanding of basic walking kinematics will contextualise the models discussed

throughout the thesis. This section provides an overview of locomotion in three dimensions, which, while difficult to visualise, should help the reader to understand planar motion. Next, sagittal plane motion is examined, predominantly showing how the legs, feet, and pelvis move vertically over a gait cycle. Finally, a discussion of motion in the frontal plane, the most important plane of motion for the thesis, shows how the Centre of Mass moves during the gait cycle to produce lateral ground force. Throughout this section, refer to Figure 1.10.

1.3.1 Walking in Three Dimensions

It is easy to take walking for granted but the sequence of walking kinematics is, as already stated, quite complex. While three-dimensional motion is difficult to visualise, it will prove valuable when considering planar motion in subsequent sections. Moreover, a discussion of three-dimensional motion will help to transition the reader from a holistic understanding of overall body motion to a nuanced description of the motion of specific body parts.

Throughout these sections, reference will be made to the exchange of kinetic and potential energy. Readers should be aware that these are not conserved systems. Muscles burn chemical energy to create kinetic and potential energy in the body. This is in addition to any mechanical exchange made by the body from kinetic to potential or vice versa. Still, the overall idea is beneficial for comprehending the general kinematics of walking.

The *gait cycle* will be referred to frequently throughout the thesis, so first it is useful to divide the gait cycle into its constituent components. The gait cycle for one leg can be divided into two phases: the stance phase (approx. 60%) and swing phase (approx. 40%). Stance is initiated by heel-strike, when the arriving foot contacts the ground. As the walker moves forward, his or her Centre of Pressure moves from heel to toes, where stance phase ends with toe-off. This point is also the beginning of the swing phase. Mid-stance occurs when the swing foot is even with the standing leg. The

Figure 1.10: Components of the gait cycle as seen in isometric view, sagittal plane, and frontal plane. RHS – right heel-strike, LTO – left toe-off, RMS – right mid-stance, LHS – left heel-strike, RTO – right toe-off, LMS – left mid-stance.

swing phase then ends with the swing foot touching ground for heel-strike. With the two feet alternating between stance and swing phases, an overlap occurs where both feet are in stance; this is called the double stance phase. When one foot is in swing phase it is also called single stance. Therefore, the gait cycle for an individual consists of two double stance phases and two single stance phases.

The first landmark of the gait cycle is heel-strike. The arriving foot – for the sake of clarity call it the right foot – is extended in front of the body on a nearly straight leg. The trailing (left) foot is just behind the body with the heel slightly lifted but the leg straight. The pelvis is level with the ground but angled to the left of the direction of travel. Compared to the lower body, the trunk and head remain relatively square to the direction of travel, but slightly turned to the right. The left arm leads and the right arm trails behind the body.

As the body progresses through the first double stance, it shifts from left to right with the centreline of the body crossing the midpoint between the feet. The left heel lifts off the ground, a motion permitted by flexion of the left knee. As the body moves towards the right leg, the right knee flexes slightly as the right toe touches the ground. The pelvis and upper body are at their lowest elevation just after heel-strike, but start to gain elevation beginning with the right hip, followed by the left. The forward velocity of the left hip is slightly greater than the right hip in preparation for the swing phase. The upper body and arms begin rotating leftward, though still angled to the right of the direction of travel.

At toe-off, the left leg raises off the ground and the ankle reaches its maximum elevation. This is matched by the pelvis attaining its maximum leftward tilt. The left hip remains behind the right hip but with a greater forward velocity.

The swing phase may be divided into two components, separated by mid-stance. Notably, at mid-stance the body is square to the direction of travel. The arms and legs are aligned with the body. The pelvis is level to the ground and at its maximum

elevation with the swing leg aligned with the stance leg. The body is also at its rightmost point of excursion. Thus, in the first half of the swing phase the pelvis rises up and to the right over the standing leg. The left hip sweeps through a greater arc in order to make up the elevation difference beneath and lag behind the right hip. This allows the swing leg to extend slightly, providing some of the kinetic energy needed to swing the leg forward in preparation for the next step. The right knee, while slightly flexed, must be straight enough to accommodate the swing of the left foot.

The forward velocity generated by the swing of the left leg is carried into the second half of the swing phase. The pelvis loses elevation, converting potential energy to kinetic energy. It rotates to the right but remains level, allowing the left leg to drift forward before heel-strike. Both legs straighten, with the right heel starting to leave the ground and the left ankle dorsiflexing. This allows the left toes to reach their highest elevation. Meanwhile, the body drifts very slightly to the left, with the upper body also rotating slightly left. This extends the right arm forward and the left arm backward.

After the left foot drifts forward, heel-strike occurs and the process is repeated for the contralateral (i.e. the opposite side) leg. Observing that double stance is approximately half the duration of single stance, the gait cycle can be divided into six periods with the following landmarks:

1. right heel-strike; body at lowest elevation; pelvis at maximum left rotation, level
2. left toe-off; pelvis at maximum leftward tilt
3. right mid-stance; body square to line of travel, at highest elevation; pelvis level
4. left heel-strike; body at lowest elevation; pelvis at maximum right rotation, level
5. right toe-off; pelvis at maximum rightward tilt
6. left mid-stance; body square to line of travel, at highest elevation; pelvis level

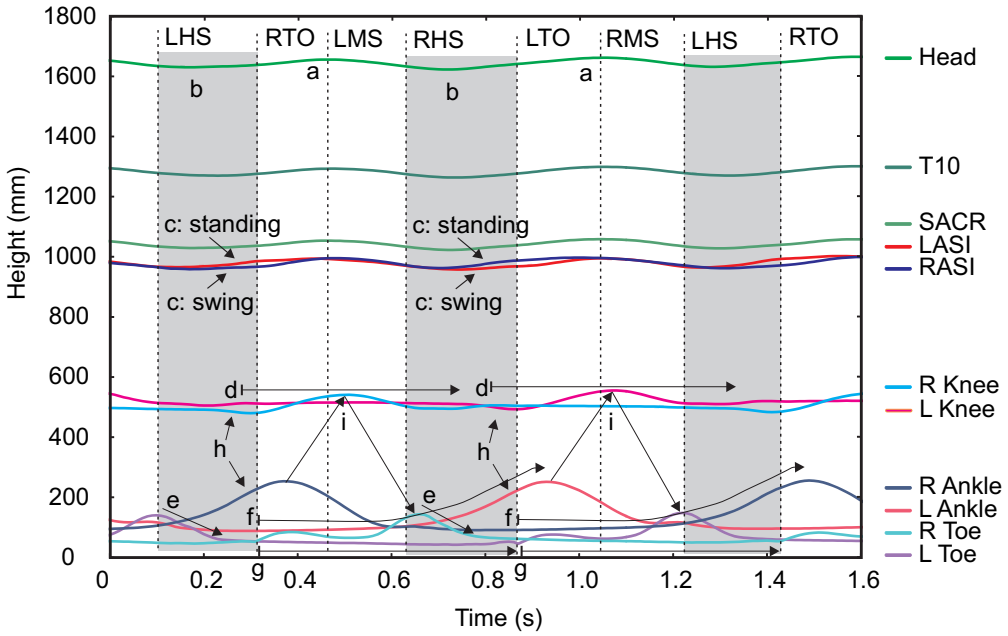

Figure 1.11: Sagittal plane motion of a female (ht=1.69 m, mass 63.8 kg) over multiple steps. Double stance shaded in grey. See text for label descriptions.

Special attention should be given to the kinematics and kinetics of the pelvis and hips during the gait cycle and the fact that transitioning between the six periods is smooth and continuous. This will be discussed in greater detail later.

1.3.2 Sagittal Plane Motion

In gait analysis it is beneficial to be able to visualise kinematics in each of the dominant planes of motion in addition to three-dimensionally. This is because most kinetic analyses pertain to motion in the sagittal or frontal planes. From a structural standpoint, sagittal and frontal plane kinematics correspond conveniently to longitudinal and transverse axes respectively, the primary axes of structural design and analysis.

Between frontal and sagittal plane kinematics, motion in the sagittal plane is easier to understand, primarily because forward displacement is comparable to motion over time (Figure 1.11). Moreover, the profile view of the body makes comparisons of the height of left and right body markers extremely straightforward.

The first observations pertain to the head and torso, which move together through-

out the gait cycle. They move in a sinusoidal fashion at a rate of one cycle per stride. The peak height is at mid-stance (a) and the minimum height is just after each heel-strike (b). The pelvis moves in a similar fashion although the standing hip is higher than the swing hip from mid-double stance to the following mid-single-leg stance (c). The total vertical excursion of the head, torso, and pelvis elevation is approximately 50 mm with little intra-subject variability in normal gait.

In the stance leg, stability is key. The stance knee stabilises just after heel-strike and maintains a constant elevation throughout the stance phase (d). While the knee is stabilising, the toes land on the ground (e), beginning a brief period (approx. 10% of stance) in which the whole foot contacts the ground. From the moment of contralateral toe-off, the standing heel begins to lift off the ground very gradually (f). This smooth and gradual elevation increase will continue through the entire swing phase, double stance, and past ipsilateral (i.e. the same side) toe-off. Meanwhile, the toes simply remain planted throughout stance until the elevated heel is nearly directly above them at the end of double stance (g).

In contrast to the stability of the stance leg and upper body, the swing leg undergoes a great deal of motion. During double stance, the 'swing' leg prepares with a small drop in knee elevation and a significant rise in heel elevation (h). At the moment of toe-off, the swing knee is at its lowest elevation, but significantly farther forward than the shin and foot. This allows the foot to easily lift off the ground. Then the heel, knee, and toe gain and lose elevation in quick succession through the swing phase (i). First the heel reaches its peak elevation, 200-300 mm above the ground. This constitutes the greatest rise and fall of any body part during the gait cycle. At this moment, the swing knee is even with the standing leg; the rise of the swing hip and the forward motion of the knee cause a rotational motion of the thigh in order to bring the trailing foot through. At, or just after, mid-stance the knee is at its highest elevation. This is at a level 40-60 mm above the stance knee and 60-70 mm total amplitude. The heel,

meanwhile, swings down and forward behind the toe. Finally, as the swing leg extends forward in preparation for heel-strike the toe rises to its peak elevation, approximately 150 mm above ground.

It should be noted that the head, trunk, pelvis, swing knee, and swing ankle all convert potential energy to kinetic energy between mid-stance and heel-strike. Only the swing toe gains potential energy, presumably as a protective measure to minimise the risk of tripping over the toes. The rest of the body is propelled down and forward into the next step.

1.3.3 Frontal Plane Motion

Unlike vertical and forward motion, frontal plane motion must be considered over a full gait cycle. This is because vertical and sagittal motion are repeated from step to step regardless of which is the standing foot, but frontal plane motion utilises the opposition of left and right stance. Here it is assumed that humans walk in a perfectly symmetric manner, but in reality even healthy individuals do not exhibit this trait [86]. Such asymmetry can be genetic, epigenetic, learned, or a product of injury/pathology. In subsequent chapters, left and right feet will be considered essentially as separate individuals but presently let it suffice to assume a symmetric gait.

One important aspect of lateral kinematics is stabilisation of the head, Figure 1.12 [138]. Keeping the head and trunk stable has two major benefits. Foremost, the individual's frame of reference is minimally disturbed, so it is easier for the central nervous system to maintain balance and affect movement through the environment. Secondly, any lateral motion of the upper body must be offset in subsequent strides. If motion does not directly benefit forward progression (or, more broadly, the desired locomotion) then the body expends energy unnecessarily. Keeping the upper body laterally stable minimises energy expenditure. As a result the abdomen acts as a hinge [94]. Lateral excursion of the pelvis is mirrored in the horizontal plane by a lateral excursion of the upper body, caused by compression of muscles on the swing

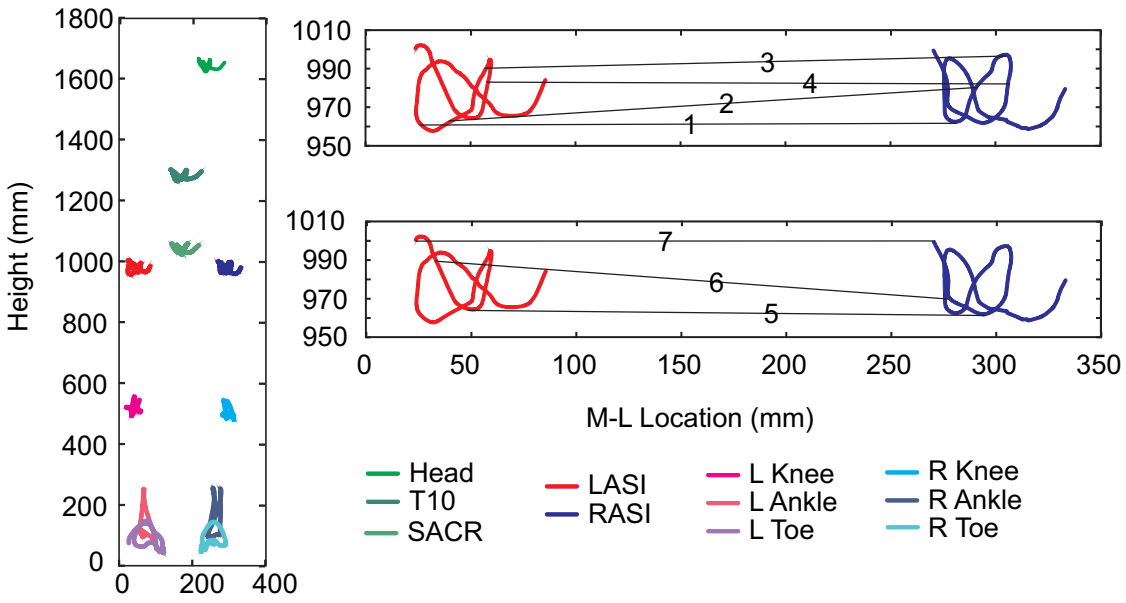

Figure 1.12: Frontal plane motion of the same female (ht=1.69 m, mass 63.8 kg) as seen from behind over the same time period. Most frontal plane motion occurs in feet. (Left) Motion of all pertinent markers. (Right top and bottom) LASI and RASI trajectories. Black lines show pelvic tilt over one gait cycle with lines 1 and 5 approximately corresponding to right and left heel-strike respectively. Lines 2 and 6 show left and right toe-off, respectively. Lines 3 and 7 for mid-stance. Line 4 shows late left foot swing phase.

side of the body. In this manner the upper body acts like an upright pendulum so that the head remains still.

The pelvis-legs assembly may be considered to be a seven-link chain including both feet, shanks, thighs, and the pelvis (Figure 1.12). As previously indicated, however, the knees remain relatively straight during stance, bending predominantly in swing phase in order to allow the foot to clear the ground (Figure 1.11). While the knees and ankles make a moment contribution to lateral stability [94], the feet themselves make a negligible contribution to lateral kinematics. Thus the relevant kinematics of the lower body can be reduced to a three-link chain consisting of the pelvis and two legs. The distance between the feet is less than the width of the pelvis. During walking, the Centre of Mass typically remains between the two feet while each foot remains medial of its corresponding hip.

In the present study of pedestrian-induced ground forces, acute attention must be

given to the motion of the pelvis during the gait cycle. Lateral ground forces are related to the motion of the body's Centre of Mass. It has been shown that the Centre of Mass is near to where the spinal cord meets the pelvis [125]. Thus, the kinematics of the pelvis will provide an approximation for Centre of Mass motion.

Over one gait cycle, the pelvis sweeps through an infinity sign or figure eight-shaped projection in the frontal plane. The most dominant lateral motion of the pelvis during the gait cycle occurs in double stance. When the pelvis is at its minimum height, muscles called *hip abductors* and *hip adductors* cause the pelvis to shift contralaterally from the trailing foot to the leading foot. This constitutes the 'cross' of the figure eight. During this time, the leading hip gains elevation relative to the trailing hip such that the pelvis is tilted up to 10° at or just after toe-off. The combination of lateral and upward motions gives the pelvis enough kinetic energy to level out by mid-stance; its maximum elevation. It is recalled that this is also the point of maximum lateral excursion. Next as the level pelvis drops in elevation (the 'loop' of the figure eight), it moves slightly medially, ending the half cycle. This pattern is mirrored for the second side with the pelvis going from bottom diagonally up and across the middle during double stance, up to peak by mid-stance, and dropping almost vertically before heel-strike.

During each step the stance leg rotates about the ankle in both sagittal and frontal planes. The frontal plane rotation of the CoM about the ankle gives rise to the two-dimensional Inverted Pendulum Model. In reality, however, the frontal plane projection of the stance leg in the early single stance phase becomes longer as the CoM rotates forward (i.e. in the sagittal plane) about the ankle. After mid-stance, the projection of the leg length becomes shorter as the CoM lowers in preparation for double stance. Thus the real motion of the Centre of Mass – as a function of three-dimensional kinematics – is more nuanced than a simple inverted pendulum describes.

1.4 Summary and Motivation for Research

Gait is a complicated phenomenon even though on first glance it is quite easy to identify and characterise. Every person walks with a unique gait, but with broadly similar characteristics. Applying a crowd of generally similar pedestrians to a slender footbridge leads to the possibility of the structure becoming laterally unstable. This human-structure interaction is little understood, due in part to the variability of human gait, the variability of structures, the possible effects of synchronisation or lock-in, and the difficulties of recording individual pedestrians in a crowded bridge excitation scenario. Though a wide variety of structural experiments have been conducted and a number of theories produced, little consensus has been reached because of the lack of available data. In the biomechanics community minimal research has been conducted regarding lateral ground forces – especially on oscillating surfaces – even though several researchers have developed gait stability models, such as the Inverted Pendulum Model.

The motivation for this research, therefore, is to examine the IPM in detail and provide novel walking data of men and women crossing a laterally oscillating bridge. The thesis analyses the fundamental assumptions of the IPM in the context of stable ground walking and compares the IPM with the motion of pedestrians on a naturally-oscillating 'bridge' platform. The research yields recommendations for the improvement of the Inverted Pendulum Model, including the incorporation of a non-static Centre of Pressure component and a novel three-dimensional application of the model in spherical coordinates.

Chapter 2

Experimental Methods

The data presented in this thesis has been compiled from four experimental regimes. The first set of data (NOC I) was collected at the Nuffield Orthopaedic Centre by their resident clinical research staff. The testing consisted of 21 healthy adult women and 17 healthy adult men walking in a gait laboratory. This 'stock' data was made available by the Gait Lab for initial analyses, which are presented in Chapter 3. The second set of data (NOC II) was also collected at the Nuffield Orthopaedic Centre, this time by the present author. This experimentation tested 10 women and 9 men, all healthy young adults. While these tests were similar to the previous set, it was hoped that many of the test subjects would be able to also undertake subsequent testing on a moving – rather than stable – surface.

The third and fourth sets of tests were undertaken in the Engineering Science Department on a laterally oscillating footbridge. Participants were asked to repeatedly cross a swinging bridge at a self-selected speed. Data from the third test (Jenkin I) has been largely omitted from the thesis for two reasons. First and foremost, the Jenkin I tests only recorded the lateral force exerted by the individual on the bridge, which proved insufficient for a thorough analysis of human-structure interactions. Furthermore, the bridge proved too stiff for the subjects to excite. After modifications were made, the final set of tests (Jenkin II) utilised a more intricate experimental set-up with altered structural properties.

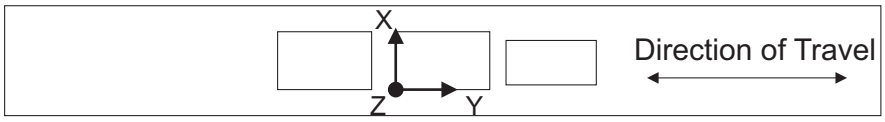

Figure 2.1: Nuffield Orthopaedic Centre Gait Lab track schematic. Inner rectangles show orientation of force plates with respect to track and global coordinate system.

2.1 NOC I Methods

Data for analysis were provided by the Oxford Gait Laboratory of the Nuffield Orthopaedic Centre, Oxford University Hospitals NHS Trust (NOC). The gait lab facility consists of three AMTI (Advanced Mechanical Technology Inc; Watertown, MA, USA; www.amti.biz) OR6 force plates aligned longitudinally on a 10 m indoor track, although only two of the plates were used for these tests. The force plates, measuring 508 x 463 mm, are installed flush with the gait lab floor with a 70 mm gap between them (Figure 2.1). Surrounding the track are 12 Vicon (Vicon Motion Systems Ltd; Oxford, UK; www.vicon.com) MX passive infrared motion tracking cameras. When combined, the system can capture ground reaction forces in three dimensions, the Centre of Pressure (CoP) locations across each force plate, and the three-dimensional locations of individual body segments, correlating the data from each instrument with respect to time. A frontal plane and a sagittal plane video camera have also been installed to record the general motion of each person when walking across the plates.

Over 20 healthy males and 20 healthy females were instrumented with reflective motion tracking markers and asked to repeatedly walk the length of the track from both ends while barefoot. The participants were not advised explicitly to step on each force plate, and so the participants were asked to walk the track until approximately six trials of exactly one foot per plate were completed. The data sampling rates for the tests were 1 kHz for the force plates and 100 Hz for the infrared motion tracking cameras. Following the lab tests, the data were imported into Vicon Nexus software v. 1.8.4 for initial processing. This testing was conducted by the NOC prior to the initiation of this thesis in order for the NOC to build a database of healthy adult

Table 2.1: Sample Population Statistics, NOC I Tests.

	Women	Men	Total
Number of People	21	17	38
Total Trials	97	61	158
Total Steps	194	122	316
Mass (kg)	61.4 ± 8.22	72.2 ± 14.6	66.1 ± 12.5
Height (m)	1.67 ± 0.0722	1.79 ± 0.0659	1.72 ± 0.0925
Age (years)*	24.7 ± 3.29	28.0 ± 7.69	26.2 ± 5.77

*Age statistics available for only 14 women and 12 men.

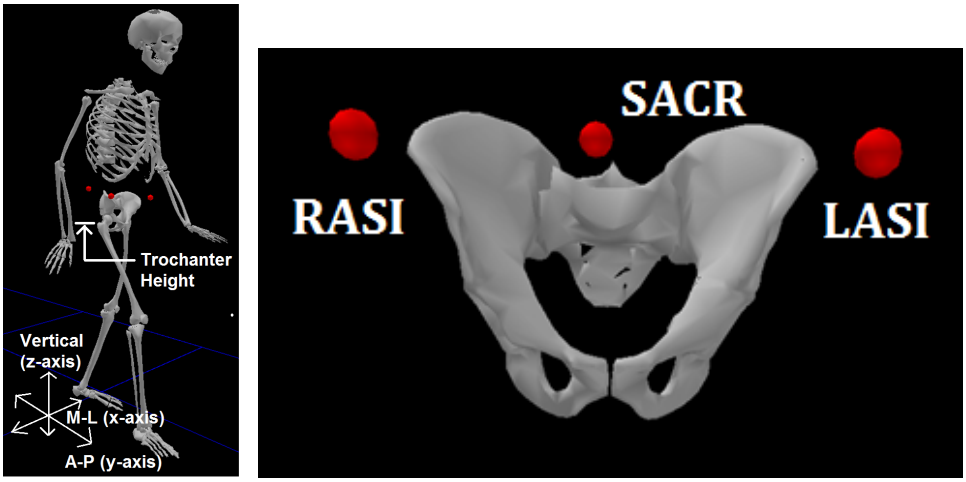

(a) (b)

Figure 2.2: (a) Identification of coordinate plane and trochanter height. (b) Positioning of pelvic body markers (Vicon Nexus).

walking samples for their own clinical and research purposes. Using a combination of video inspection and wire frame analysis, the present author omitted any trial in which the heel or toes of either foot extended off the force plate. The resulting population consisted of 21 women and 17 men, totalling 316 footsteps (Table 2.1).

For each trial, Vicon Nexus exported a .csv file consisting of the time step; the x (Medial-Lateral, or M-L) and y (Antero-Posterior, or A-P) Centre of Pressure location; the x, y, and z ground force; and the x, y, and z ground reaction moment for both force plates (Figure 2.2(a)). In addition, a separate .txt file was also exported consisting of the time step and the x, y, and z location of three motion tracking markers: the sacrum (SACR) and the left and right anterior superior iliac spine (LASI / RASI). These three points describe the motion of the pelvis, Figure 2.2(b).

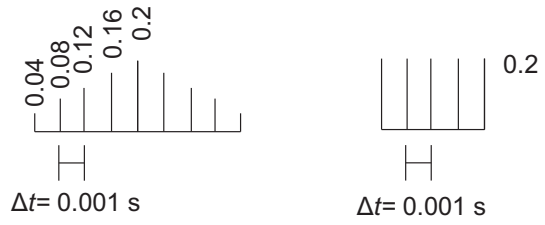

Figure 2.3: The pulse shapes used to filter the NOC I data. Each point of the pulse is multiplied by a point in the raw signal. These are then summed to create one data point in the filtered signal. The pulse shape is then moved one time step along the raw signal and the process is repeated to determine the next filtered point. The sum of the impulse amplitudes across each pulse shape equals one.

Since the participants walked from both ends of the track many of the resulting CoP, ground force, and CoM data needed to be rotated and translated about the lab coordinate axes to collate the subjects' respective first and second steps. A program was written in MATLAB to manipulate and reorganise the data.

In addition to collating the data, the data were normalised by time and force. The time for most participants to take one step ranged from approximately 0.4 s to 0.6 s. Thus, in order to compare the features of the footstep data, each time record was normalized by the duration of stance. The force data – normalised by body weight, according to Giakas [86] – could then be expressed as a function of the fraction of the stance elapsed, from zero to one.

Finally, a low-pass filter was applied to the M-L force data. To filter the lateral forces, each signal was convolved using built-in MATLAB `filter` functions with a pair of user-defined pulse shapes. Each signal was first passed through a triangular pulse shape in the forward direction, inducing a phase shift. To eliminate the phase shift, the signal was then passed through a rectangular pulse shape in the reverse direction. The shapes are shown in Figure 2.3. The width of the pulse shapes was determined by trial and error until the phase shift was minimised. The triangular shape width was 0.009 s wide, formed by convolving a five-sample ones vector with itself. The rectangular filter was formed by dividing a five-sample ones vector by the number of samples (five). The effects of the residual phase shift were minimal because the shift

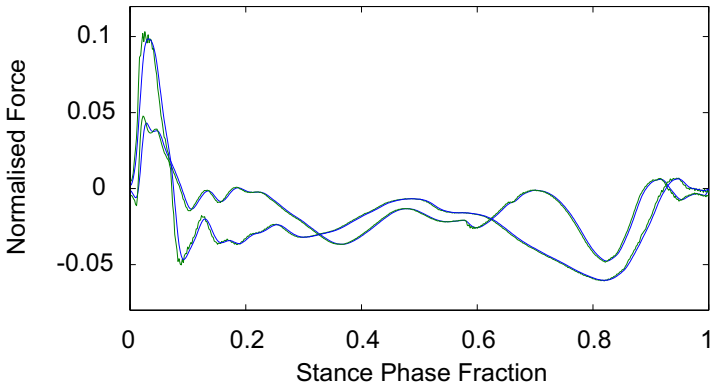

Figure 2.4: For two footsteps shown, a comparison of filtered (blue) and raw (green) NOC I ground force data.

was only approximately 2.5 ms; half the rectangular filter width (Figure 2.4).

Using MATLAB, the data were organized, analysed, and plotted according to various classifications. The force plate data were decimated from 1 kHz to correspond with the motion tracking data sampled at 100 Hz. Filtering and decimation affect the ground forces minimally between 20% and 80% of a stance phase but more so near the beginnings and ends of stance where rapid fluctuations in force occur. Thus observations concerning the beginning and ending 10% of the stance phase are made with caution.

As previously discussed, the strides of the participants were of unique durations, so the samples were normalised by stance phase duration. By normalising the times, the force samples can be plotted from $t' = 0$ at heel-strike to $t' = 1$ at toe-lift. This method allows for qualitative comparisons to be made across samples. A complicating factor for quantitative comparison, however, is that each sample consists of a unique number of data points: in one sample, $t = 0.200$ s might correspond to the 25% time, whereas in another sample the same time might correspond to the 50% time. Because of this, quantitative analysis could not rely on comparing the n^{th} datum point in each sample. To overcome this, the data means and standard deviations were calculated and compared at every 10% of the normalised stance phase duration, a convention used with the NOC I tests in Chapter 3. In subsequent experimental regimes where

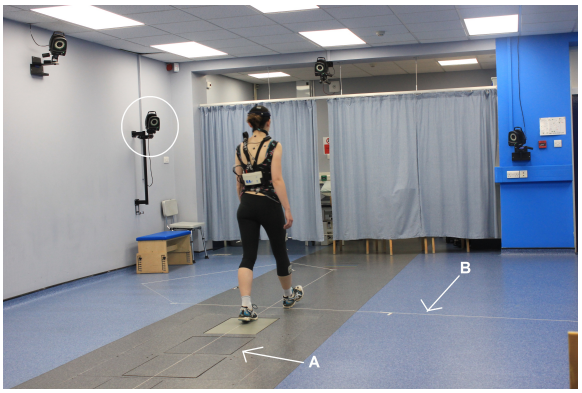

Figure 2.5: Participant crossing force plates (A) in Oxford Gait Laboratory wearing K4b2 breath analysis kit and passive motion tracking markers. Four Vicon motion tracking cameras (e.g. circled) are shown. Participants were asked to follow the white string (B), laid in a figure eight pattern, to maintain continuous walking.

the data were not time-normalised this method was not used.

2.2 NOC II Methods

The second set of tests was also undertaken at the Nuffield Orthopaedic Centre. In these tests, instead of the participants crossing back and forth across the force plates, they were asked to follow a 20.5 m long string that was laid in a figure eight pattern (Figure 2.5). This allowed the participants to walk on a continuous path for approximately 10 minutes, while crossing the three force plates in the same direction for every trial.

Ten healthy females and nine healthy males participated in the test (Table 2.2). Each participant was asked to wear comfortably tight athletic clothing and bring comfortable trainers or walking shoes. Participants first had their relevant anthropometric data measured: height, leg lengths, hip width, knee widths, and ankle widths. Next, participants were instrumented with 27 reflective spheres (henceforth called motion tracking markers), which were applied to their head (four), trunk (six: C7, T5, and T10 vertebrae, right shoulder blade, jugular notch, and sternum tip), pelvis (three: sacrum, left and right anterior superior iliac spine), and legs (2x7=14: left and right

Table 2.2: Sample Population Statistics, NOC II Tests.

	Women	Men	Total
Number of People	10	9	19
Total Barefoot Steps	224	209	433
Total Shod Steps	220	157	377
Barefoot Three-Step Trials	39	29	68 (204 steps)
Shod Three-Step Trials	31	7	38 (114 steps)
Mass (kg)	64.8 ± 7.04	83.7 ± 19.28	73.7 ± 16.86
Height (m)	1.70 ± 0.0555	1.82 ± 0.0715	1.76 ± 0.0869
Age (years)	23.3 ± 1.25	25.6 ± 2.74	24.4 ± 2.34

Figure 2.6: Location of motion tracking markers on a test subject during NOC II tests. Hidden markers indicated in red.

thigh, knee joint, shank, heel, second metatarsal, and lateral and medial malleoli) (Figure 2.6). In addition, participants wore a heart rate monitor and a K4b2 breath analysis kit, although the breathing results will not be presented in this thesis. The data were recorded because the researcher intended to compare energy consumption walking on stable ground with energy consumption while balancing on a moving base, but the stable ground data were noisy and the Jenkin test set-up was not conducive to reliable breath analysis readings.

The participants conducted each test twice, once in shoes and once in bare feet. The order of tests was selected at random. Each person completed a static test to

ensure that the markers were picked up by the cameras and to obtain the subject's mass. Then, each participant was shown how to follow the figure eight path and told to walk at a 'comfortable, normal pace'. They were not told to step on the force plates but merely to follow the string. This ensured that the subjects would not aim for the force plates, but only land on them naturally. Participants walked continuously for five minutes or until recording at least five clean force plate strikes with each foot, whichever took longer. A clean force plate strike was defined as a footstep that landed wholly within the edges of the force plate with neither the preceding nor subsequent step contacting the edge of the plate. At the end of this test, each participant either put on or removed his or her shoes and socks. Another static test was conducted before the participants walked for an additional five minutes or five clean left and right strikes. The longest any person required to record five clean strikes with each foot was 13 minutes 40 seconds.

The data were recorded in Vicon Nexus software. Like the NOC I tests, the motion tracking data were recorded at 100 Hz and the force plate data were recorded at 1 kHz. Using Vicon, trials with three clean force plate strikes were identified. The force plate data and marker data were then exported to .csv and .txt formats, respectively, so they could be accessed and manipulated using MATLAB. The marker signals and force plate signals were filtered with a user-defined rectangular shape of duration 0.03 s in both forward and reverse directions to eliminate any phase shift. These pulse shapes were developed in the manner of Figure 2.3, using the time step width matching the signal to which the filter was applied.

Table 2.2 shows that although over 800 clean footsteps were recorded in total, there were relatively few clean, shod three-step recordings. This was primarily due to the size and spacing of the force plates, which at the NOC are installed primarily for toddler and child testing. The force plates were 508 mm long with only a 70 mm separation, so the men – who collectively averaged 12 cm taller than the women – recorded many

fewer consecutive clean three-step trials. Interestingly, the number of clean three-step trials for women versus men was much more balanced for barefoot walking than for shod walking, suggesting that men might shorten their stride more than women when walking without shoes.

2.3 Jenkin I Methods

Having undertaken two sets of testing on stable ground, testing was also undertaken on a laterally oscillating footbridge in the Engineering Science Department. The footbridge was constructed in 2010 by Kaye [139]. The bridge deck measures 7 m long by 1.2 m wide, Figures 2.7 and 2.8. The deck is suspended from a stationary steel frame in each of the four corners of the bridge via a bearing pin assembly. The assembly consists of three plates: two plates are welded vertically from the deck's superstructure and the third plate is sandwiched in between, welded to a circular hollow section pipe (which doubles as a handrail) passing through a rotational bearing housing on the stationary steel frame. A steel bearing pin is placed in one of four holes that have been drilled through all three plates at different heights, producing a pendulum. The compound pendulum formed by the four bearing assemblies and the deck causes the deck to remain level to the ground during excitation (Figure 2.9). The four settings of the bearing assembly allow the researcher to select a natural pendulum frequency of 0.5 to 1 Hz. The maximum amplitude of lateral bridge displacement is limited by the width of the stationary steel frame, a peak-to-peak amplitude of approximately 300 mm. During peak lateral oscillation the pendulum motion causes the deck to elevate by approximately 25 mm, depending on the chosen frequency setting.

The superstructure of the bridge consists of two 150 x 100 x 4 mm steel rectangular hollow section girders joined by 50 mm square hollow section joists spaced at approximately 330 mm (See Figure 2.8). This is topped by a two-layer plywood deck of total thickness 28 mm. Due to space and material constraints, the bridge was built in two

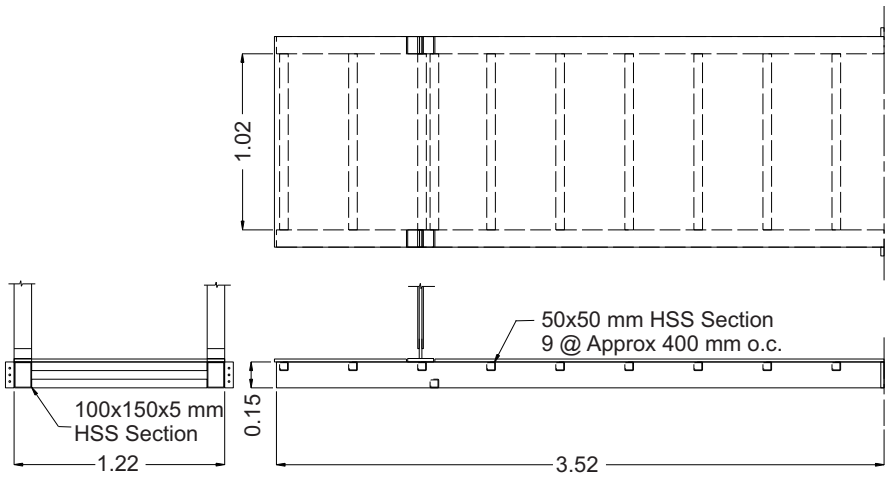

Figure 2.7: Section views of the as-built bridge superstructure in metres, before addition of force plates.

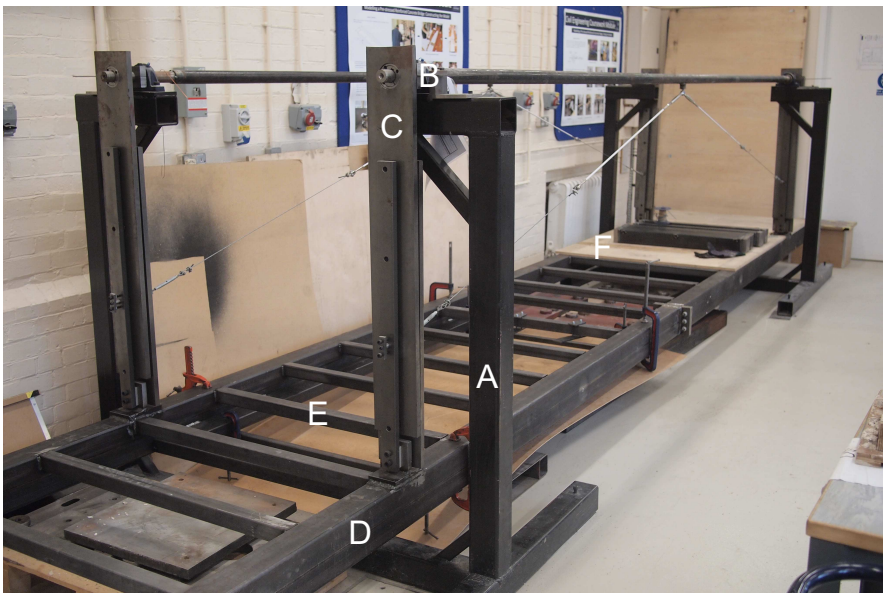

Figure 2.8: Configuration of the bridge before modification. (A) Structural support frame (B) Rotating bearing housing and circular handrail (C) Bearing pin assembly (D) Rectangular girders (E) Joists and (F) Plywood decking.

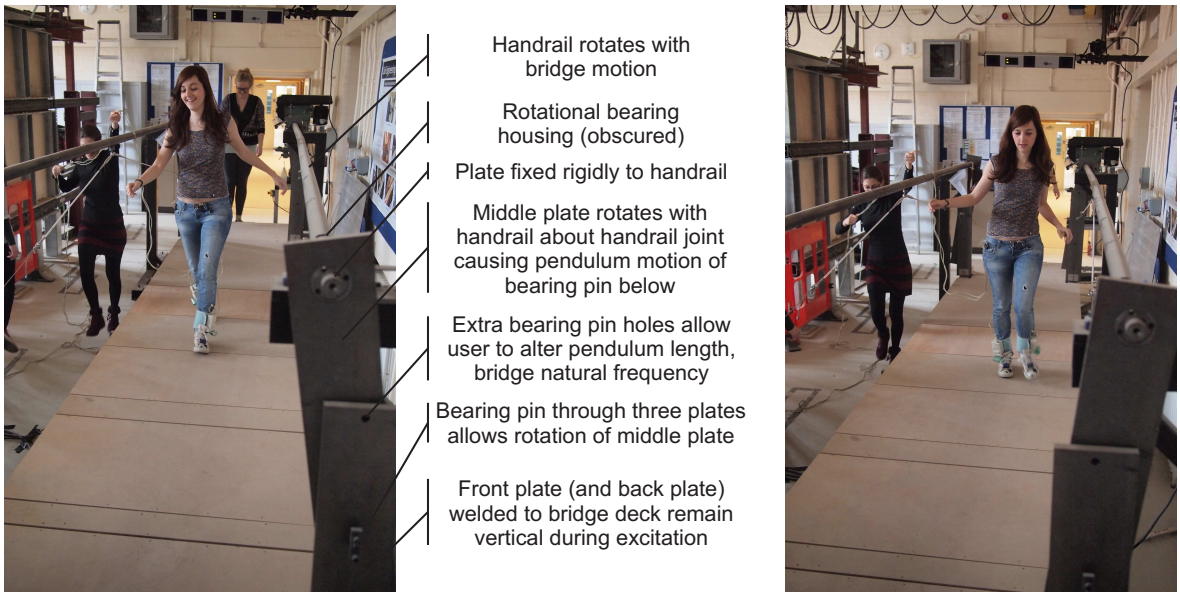

Figure 2.9: Motion of the bridge and bearing assembly during preliminary Jenkin II testing. Bridge swung to the right (left photo) and to the left (right photo).

half-lengths and bolted together at mid-span. The original structure was 678 kg. More information about Kaye's structure can be found in her Master's thesis [139].

Several modifications were made to the original bridge before the work conducted for this thesis. In 2011 Mather decreased the inherent frictional damping of the bridge by applying rotational bearings to the pin joints [140]. This reduced the damping factor to as low as 2.1%, a change which caused the deck to impact the supports at higher natural frequency settings. Mather also developed a means of determining which part(s) of the foot was in contact with the bridge by modifying a method developed by Nhleko [141]. He created a pair of shoe covers with two metal cleats each, connected to variable resistors and a potential-divided circuit. The bridge deck was covered in a grounded aluminium sheet. By tuning the resistances of the different cleats, a different potential would be recorded for each possible combination of cleat-deck contacts. This allowed Mather to track the heel-toe contact times of a walker on the bridge.

In 2012 Selley further modified the bridge [142]. She applied adjustable rotational stiffeners to the handrail pipe section which dramatically reduced the lateral excursion of the bridge. In addition to raising the stiffness, these elements also raised the damping

Table 2.3: Structural Characteristics, Jenkin I Tests.

Superstructure mass	1107	kg
Pendulum length	1.0	m
Natural frequency (lateral)	0.990	Hz
Natural frequency (torsion)	2.025	Hz
Damping ratio, ξ_b	1.78	%
Number of force plates	4	

slightly. The lateral natural frequency became closer to the longitudinal (i.e. axial) natural frequency, meaning that unwanted axial motion was sometimes observed during walking tests. To fix this problem, tension cables were applied in an 'A' configuration from the midpoint of the handrail to the bearing pins. This sought to raise the axial stiffness – and therefore raise the axial natural frequency above the lateral natural frequency.

Before the tests conducted for this thesis were undertaken, the author also altered the structure. The biggest shortcoming of the bridge was its inability to record lateral ground forces. Initially it was hoped that a ground force-recording shoe could be developed but this proved impractical for several reasons. In particular, it was practically impossible to install force transducers into shoes in a rigid enough manner to ensure a clean load path yet maintain enough flexibility in the shoe to promote normal walking. Thus it was decided to record lateral ground forces by using custom-designed lateral force plates. Design, construction, and calibration of the force plates will be discussed at length in Chapter 6 but for now it shall suffice to say that this alteration required removing Mather's heel-toe contact detection system. Additionally, accelerometers and strain potentiometers were oriented laterally on the bridge in order to record the bridge's motion.

The properties of the bridge at the time of testing can be found in Table 2.3. Participants from the NOC II tests were asked to participate in the swinging bridge tests in order to provide reliable comparison with the stable ground results, Table 2.4. Since not all participants of the NOC II tests could return, the testing consisted of six men and nine women. Participants were asked to undertake the test in random

Table 2.4: Sample Population Statistics, Jenkin I Tests.

	Women	Men	Total
Number of People	9	6	15
Total Passes (Bridge Locked)	169	120	289
Total Passes (Bridge Unlocked)	271	218	499
Three-Step Trials (Bridge Unlocked)	72	37	99 (297 steps)
Mass (kg)	63.7 ± 6.47	75.3 ± 15.84	68.3 ± 12.18
Height (m)	1.70 ± 0.0583	1.81 ± 0.0876	1.75 ± 0.0869
Age (years)	24.4 ± 1.24	25.7 ± 1.03	24.9 ± 1.28

groups of three. For each test, the participants were asked to cross the bridge 'in a casual manner, but as if they were going somewhere.' This instruction was intended to make the participants to walk slightly quicker than they might otherwise, in hopes they would excite the bridge laterally and avoid the axial natural frequency. The participants took turns crossing the bridge with one subject beginning to cross when the previous subject was approximately one metre from reaching the other end. When a participant finished crossing the bridge, he or she was to walk around to the start to prepare for his/her next crossing.

Each group of three participants undertook three tests of five to 10 minutes until each participant had crossed the bridge 18 to 30 times depending how many clean force plate strikes each subject recorded. In the first test the bridge was locked in place in order to emulate stable ground walking. This was done to familiarise the participants with crossing the bridge and to compare the results with the NOC II results. The second test was a free-swinging test in which the bridge was allowed to oscillate naturally. Finally, a test was undertaken with a metronome set to the lateral natural frequency of the bridge. The participants were asked to walk to the beat, but even with practice many participants struggled to synchronise with the beat consistently, a phenomenon observed in Nessler *et al.* [110], Nhleko [141], and Ebrahimpour and Fitts [143].

The force plate data was imported into and analysed in MATLAB. Each record consisted of the force plate strikes made by all three participants. The records therefore had to be divided into trial-sized sections that distinguished which participant was

Table 2.5: Structural Characteristics, Jenkin II Tests.

Superstructure mass	1123	kg
Pendulum length	0.5	m
Theoretical natural frequency (lateral)	0.705	Hz
Natural frequency (lateral)	0.674	Hz
Damping ratio, ξ_b	0.0057	%
Number of force plates	3	

crossing. This was completed using a custom MATLAB program and double checked manually.

The main finding from the Jenkin I tests was that under low-amplitude structural oscillation, walking was not significantly altered compared to stable ground walking. The lateral force patterns exhibited by the subjects were therefore very similar to the NOC tests. Thus, the need arose for a subsequent set of testing to take place to determine when walking would be affected.

2.4 Jenkin II Methods

The bridge structure and experimental set-up were modified before the second set of bridge-based testing. Structural modifications increased the natural frequency and reduced the damping of the bridge (Table 2.5). This allowed the structure to be excited more easily, meaning that the participants would be subjected to greater lateral oscillations. In addition, instrumentation was added in order to track the motion of the participants and their Centres of Pressure.

The natural frequency of the bridge was altered by changing the pendulum length of the bearing pin assembly. In the Jenkin I tests, the pendulum had been set for 1 m. The pins were changed to 0.5 m to increase the theoretical natural frequency to 0.705 Hz. As predicted by Mather [140], the real natural frequency at this pendulum length is very near to the theoretical pendulum frequency

$$\frac{1}{2\pi}\sqrt{g/L} = \frac{1}{2\pi}\sqrt{\frac{9.81\,\mathrm{m\ s^{-2}}}{0.5\,\mathrm{m}}} = 0.705\,\mathrm{Hz}. \tag{2.1}$$

In addition to increasing the natural frequency of the bridge, the stiffeners installed by Selley were removed. This decreased the damping ratio, allowing a high amplitude of motion to be maintained without continuous forcing. Additionally the bridge would continue oscillating even if damped by individual participants, meaning that a single participant could not stop the bridge during a single pass. In the Jenkin I tests subjects could easily cope with and even choose to dissipate the energy of the bridge, but in the Jenkin II tests the subjects were required to alter their gait significantly to maintain balance.

The experimental conditions were also modified with the addition of instrumentation. A portable CODA (Codamotion; Rothley, UK; www.codamotion.com) motion tracking system was utilised to record the movement of the subjects. Two portable CODA CX1 sensors were installed, one over each end of the bridge. Each sensor consists of three calibrated cameras. The sensors were installed at a height of approximately 2 m and were directed downwards at the force plates (Figure 2.9). This created a capture volume containing approximately 3 m of the length of the bridge.

The Vicon system used in the NOC tests is known as a passive motion tracking system because each marker is simply a sphere wrapped in reflective material. Each camera emits a high frequency blinking infrared 'light'. The cameras each take a photograph at every time step; the computer then runs an optimisation algorithm to determine the 3D location of each marker from the 2D photos. In processing, the user must establish the general spatial relationship between the markers so that the computer can distinguish between the markers from frame to frame.

In contrast the CODA system is an active infrared motion tracking system. Each marker is a battery-powered light emitting diode (LED) assigned to a unique channel based on the battery into which it is plugged. The LEDs pulse in rapid succession, one marker at a time, allowing the sensors to identify each marker automatically. Each time a marker blinks, the light passes through a mask in each sensor 'camera'. The mask

causes a pattern of shadows to be projected onto a linear array within the camera. By analysing the size and orientation of the so-called *masked linear array* in each camera, the computer can optimise for the location of the marker.

Each type of system has advantages and disadvantages [21, 78]. The passive system benefits from using markers that are extremely light and easy to attach whereas a full body active marker set could require the subject to wear 15 batteries with one or two marker cables attached to each. Both systems are prone to interference from other light sources. The passive system is susceptible to interference from reflective and fluorescent objects, which it mistakes as markers. The active system is less prone to interference from reflective objects but can still be blinded by ambient glare. On the other hand, the passive system simply records a map of reflective objects in each frame, so it can record the motion of many more markers than an active system, in which specific markers 'communicate' to the camera. From a processing standpoint, the preassigned channels of the active system markers make analysis very straightforward compared to the passive system, which requires the user to identify and verify marker assignments manually. Ultimately the passive system was used in the NOC tests because the permanent facility was available. In contrast, the Jenkin tests required a portable motion capture system to be set up in the laboratory where the bridge was located, for which only an active system was available.

In addition to the CODA system, a Tekscan Inc. (South Boston, MA; www.tekscan.com) F-scan insole system was also implemented. The F-scan system consists of a pair of insoles that detect the vertical pressure applied to their surfaces. The interchangeable insoles were tethered via PS/2 cables to a Magna DC power supply and analogue-to-digital (A/D) converter, which was in turn connected to PC via PCI Cardbus. Each insole consists of two thin polyester films bearing sensors printed in piezoresistive ink. On one layer is printed 60 rows of sensors while the other layer consists of 21 columns of sensors. The intersections of the rows and columns form a grid of 960 individual

nodes called *sensels*. An electrical signal is dispatched from the power supply to one film of the insole, across the piezoresistive sensors, and back through the opposite film to the power supply. As pressure is applied to a sensel, the resistivity of the ink decreases. The A/D converter changes the analogue currents from all the sensels to a digital signal, which it transmits to the computer. Tekscan's Foot Research software (v. 6.34) converts the signal into a raw linearised scale which can then be calibrated to show engineering units. The software can then produce data for vertical force, vertical pressure, and the location of the Centre of Pressure. See Tekscan's whitepaper for more information [144].

All tests were also video recorded using a Canon Rebel T2i DSLR camera mounted above the bridge.

The participants' height and weight were measured without shoes. Insoles were first cut to fit a participant's interior shoe size as closely as possible, Figure 2.10(a). The subject inserted one insole into each shoe. Putting on the shoe, the subject was asked to do their best to prevent the insole from wrinkling under their foot and to ensure the heel of the insole did not slide in the shoe. The insoles were clipped into the Tekscan cuff units, the detachable interface between the insoles and the PS/2 cables. The cuff units were attached above the subject's ankles via elastic Velcro bands (Figure 2.10(b)).

After calibrating the insoles in Tekscan's Foot Research v. 6.34 (which involved inputting the subject's weight and asking them to stand quietly on each foot), seven motion tracking markers were attached to the subject. One battery was taped to the top of each shoe with one marker mounted to the top of the heel (on the shoe, approximately where the Achilles tendon is located) and the other marker mounted to the shoe over the big toenail. While some potential existed for the toe to move relative to the marker during testing, this point was chosen over the second metatarsal (the 'toe' landmark in the NOC tests) because it could be easily identified through the shoe and because pressing down with the toe allowed for its easy identification in the

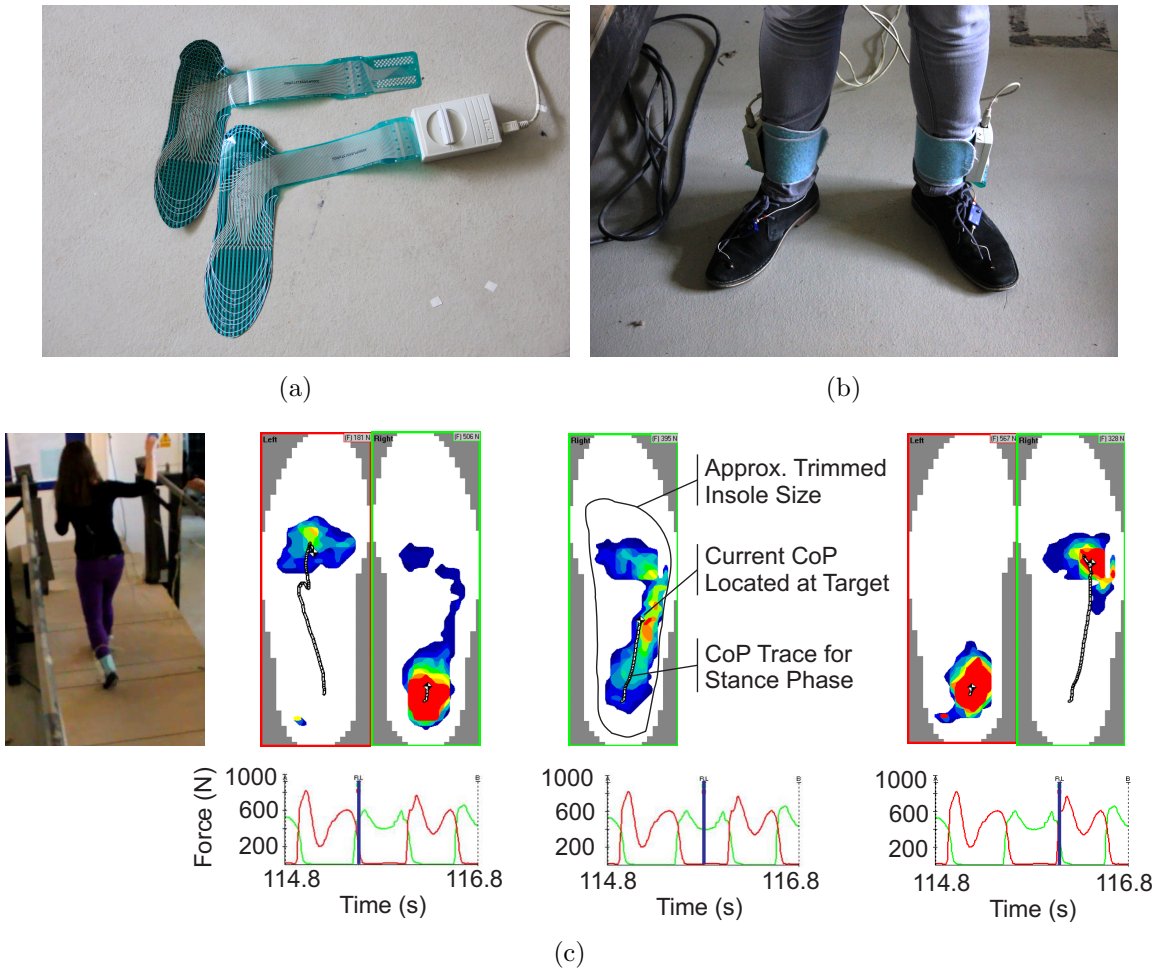

Figure 2.10: (a) Tekscan insoles cut to fit within a participant's shoes. Bottom insole connected to PS/2 interface. (b) Configuration of insoles and CODA markers before testing. (c) Example CoP trajectory and vertical force over the course of a right (green) footstep. Blue bar in force plots indicates time at which the above pressure maps were taken.

Tekscan Foot Research software. Matching the toe marker with the local coordinates of the insole was critical for post-processing. One battery was mounted to the subject's belt or stomach, with markers mounted to the left and right anterior superior iliac spine (LASI and RASI), and a battery was mounted to the shoulder blade with a marker mounted to the sacrum. The PS/2 cable was taped to the right side of the subject's leg or belt to minimise the tripping hazard. During the test, the free end of the cable was carried by a spotter to ensure it did not catch on the rig or any equipment. Finally, two markers were also mounted to the bridge, one at its midpoint and one at the base

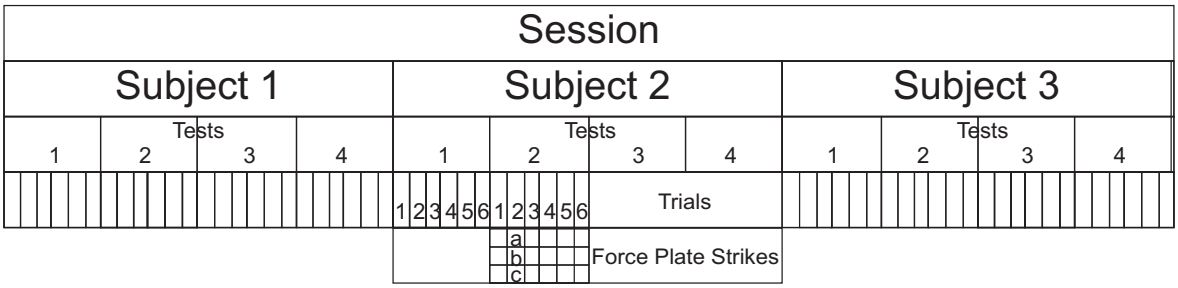

Figure 2.11: Schematic of the Jenkin II test regime.

of the bearing pin assembly. These captured the motion of the bridge on each end of the bridge section containing the force plates.

As with the Jenkin I tests, three participants were tested during each session. Unlike the earlier tests, however, the availability of only one set of insole equipment required each subject to be tested separately. Furthermore, RAM limitations of the Tekscan and CODA computers required tests to be no longer than approximately 115 s. As a result each subject undertook at least four tests while wearing the equipment with the other two participants simply crossing the bridge to impart energy into the structure. All Jenkin II tests were conducted on the freely swinging bridge without a metronome. Extra tests were sometimes carried out if a battery died mid-testing or a malfunction occurred with the insoles. Thus in a session each participant could expect to undertake 12-16 tests with each test consisting of six trials on average, Figure 2.11. Even though participants were allowed to acclimatise to the motion of the bridge before the start of the tests, several participants reported 'getting used to' the bridge motion or 'finding it easier' to cross the bridge as the session progressed. Since participants took turns being recorded, the third participant to be recorded in each session had significantly more opportunity to practice crossing the bridge than the first participant. Even so, where the goal of the testing was to understand how pedestrians interact with moving structures, the data are legitimate.

At the start of each test, the subject being recorded stamped on a force plate. The purpose of this was to provide a landmark in the three data samples that could be

Table 2.6: Sample Population Statistics, Jenkin II Tests.

	Women	Men	Total
Number of People	11	9	20
Number of Recorded Passes	312	253	566
Three-Step Trials	67	38	105 (315 steps)
Mass (kg)	63.5 ± 8.03	80.1 ± 21.06	71.0 ± 17.10
Height (m)	1.70 ± 0.0749	1.81 ± 0.0726	1.75 ± 0.0910
Age (years)	25.8 ± 2.32	26.1 ± 1.54	26.0 ± 1.96

easily aligned in post-processing, like a clapperboard in film production. The subject then crossed the bridge, succeeded by each of the other two participants. In this time, the instrumented subject had enough time to walk around the bridge and cross again. This was repeated until the CODA RAM ran out of memory. Between each test approximately two to three minutes were needed to save the data and set-up the next test. After a subject completed his or her tests approximately 20 minutes were needed to move the instruments to the next subject. It was observed that in some tests two minutes were sufficient to attain significant lateral bridge excitation without investigator interference. In some tests however, the researcher deliberately swung the bridge during crossings of the non-instrumented participants in order to acquire more data of walking across high-amplitude structural oscillations.

In total nine men and 11 women undertook the testing (See Table 2.6) completing a total of 93 tests consisting of 576 recorded trials. While 135 crossings consisted of three clean steps, 20 of those crossings consisted of incomplete data (due to faulty markers, dead batteries, etc.). The remaining 105 three-step crossings were undertaken by five men (38 crossings) and eight women (67 crossings) and consist of 74 left-right-left crossings to 31 right-left-right crossings.

Using audio, video, and the signal data of each test, the stamp times were set to zero and the records were trimmed. The force plate data were filtered using a fourth order Butterworth filter with cut-off frequency 10 Hz. The CODA and Tekscan data were filtered automatically within the programs. All the data samples for each test (i.e. force plates, Tekscan, and CODA) were then re-sampled at 200 Hz to produce signals

with equal numbers of samples. The prepared signals were then saved to MATLAB data files.

For each crossing the start and end times of each clean force plate strike were recorded manually. This allowed the insole and force plate data during a clean strike to be isolated from the ambient signal. In many cases determination of the precise moment of heel-strike and/or toe-off proved difficult to determine for various reasons. Most importantly, the application of the filter to the force plate data caused the force plate signal to spread slightly more than the other systems. In these situations a best estimate of the insole heel-strike and toe-off times was made, occasionally clipping one to five samples (less than 0.025 s) off the corresponding force plate heel-strike or toe-off. Since all records for each test were manually aligned, errors due to time shifts were negligible.

Finally the samples were analysed in MATLAB. By recording the start and end times of each clean step, any single trial (or indeed, step) could be called individually or as part of a batch (e.g. three-step samples, female samples, etc).

2.5 Ethics Approval

Where the NOC I tests were undertaken by the Nuffield Orthopaedic Centre, the data were provided and used in accordance with the Centre's clinical and research ethics practices and privacy policies. The NOC II tests were completed under the supervision and guidance of the Centre's research staff using their standard laboratory practices. Participants were provided a synopsis of the NOC and Jenkin test regimes and asked to fill out a medical questionnaire and provide informed written consent. The test regimen, information sheet, and questionnaire were approved by Oxford University's Central University Research Ethics Committee (CUREC) to cover testing undertaken both at the Nuffield Orthopaedic Centre and the Jenkin Engineering Science Laboratory.

2.6 Conclusion

This concludes the explanation of the methods undertaken during the four test regimes. While the terms NOC I, NOC II, Jenkin I, and Jenkin II will be used throughout the thesis, usage of the terms 'stable ground test' and 'moving/unstable bridge/ground test' will also be used to refer to the NOC and Jenkin tests respectively. This concludes the introductory section of the thesis.

Chapter 3

Medial-Lateral Ground Forces in Healthy Adult Walkers

As discussed by Ingólfsson *et al.* and McRobie, HSI research has focused on three areas – field observations, laboratory testing, and theoretical modelling – but little consensus has yet been achieved [68, 71]. In order to combine the theoretical and experimental aspects of HSI, a thorough study must first examine the lateral ground force patterns produced by healthy adults walking on stable ground.

Data for this examination was collected during the NOC I tests (Section 2.1) using two force plates and passive motion capture cameras. Participants completed the test barefoot. Force patterns are compared at the individual, group, and population level, providing perspective about how researchers should represent lateral ground forces. The kinematic and kinetic data from this test were then applied to the Inverted Pendulum Model to assess the model's ability to predict lateral ground forces. The overall aim of this test was to verify that the Inverted Pendulum Model accurately reproduced lateral ground forces. Instead the experimentation and analyses show that the model cannot produce a signal with the magnitude or variability of the real ground forces.

The results will be presented in three sections. The first section pertains to general characteristics of the medial-lateral force in the time domain, including data examining the whole participant population and comparisons of various subsets of the population. In the second section, the CoM and CoP data are input into the Inverted Pendulum

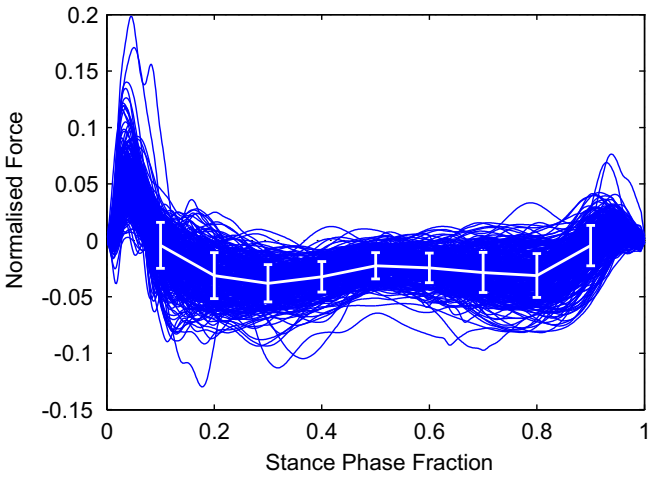

Figure 3.1: Population M-L force samples (as fraction of body weight) with means and standard deviation bars at increments of $t' = 0.1$ ($n = 316$).

Model and comparisons between the data and model are drawn. Finally, the CoP and CoM paths are analysed with respect to lateral ground force.

3.1 Medial-Lateral Force Patterns

M-L force variations must be investigated on several levels, including the population, population subsets, and individuals. Variations exhibited on these levels reveal systematic similarities and differences between groups or individuals, allowing conclusions to be drawn about inter- and intra-subject variability.

Figure 3.1 shows the plot of M-L ground force versus time for the entire 'population' of $n = 316$ footsteps. The force has been weight-normalised and the time has been unity-normalised. Positive values represent medial force, or force towards the centre of the body, whereas the negative values depict lateral, or outward, force. Thus, zero M-L force corresponds to a ground force vector in the sagittal plane with no M-L component. The M-L force curve is in the shape of a letter 'w', as described by previous studies [86, 21]. In the first 10% of the stance phase, there is a sharp medial peak centred at approximately $t' = 3.3\%$, which corresponds to the heel-strike. This part of the ground force pattern exhibits the highest variability with some peaks reaching

20% body weight while others remain just greater than zero. Some of the samples also exhibit a small laterally-oriented mini-peak before the dominant medial peak, although this could be an artefact of the leg wobbling, skin shifting under the heel as the foot contacts the ground, or foot pronation.

After the initial peak, the M-L force reverses to the lateral direction, where it persists for most of the stance phase duration. Most of the curves lie within the range of 10% lateral to 2.5% medial force between $t' = 0.1$ and $t' = 0.9$. This is significantly smaller than ground forces in the A-P or vertical directions. The M-L curves show a slight positive trend over the duration of the stance phase. It is important to observe that the ground force is not exclusively laterally-oriented, meaning that it can cross from lateral to medial and vice versa during a step. The implications of this behaviour will be examined in later chapters.

In the last 10% of the stance phase, the force returns to the medial direction, providing a smaller local maximum before tapering to zero at toe-off. This medial peak is typically less than 5% body weight, and once again some samples do not exhibit any late-stance medial peak at all. Patterns of force in the first and last 10% of the stance phase – during double stance – are affected by how an individual tracks his or her swing foot forward and the individual's step width during double stance.

The means $\pm$ one standard deviation are shown for every 10% of the stance phase. The maxima of the normalised lateral force means occur at $t' = 0.3$ (-0.038 ± 0.0165 normalised force) and $t' = 0.8$ (-0.0312 ± 0.0195). The lateral force minimum (-0.0225 ± 0.0116) occurs at mid-stance, which also corresponds to the time of the smallest standard deviation.

Four subsets of the population were compared to the overall population: women, men, left steps, and right steps. Figure 3.2 provides the female and male data samples overlaid with the population error bar from Figure 3.1 (grey) and the gender-specific error bar (red). The female mean follows the population mean closely, with a magnitude

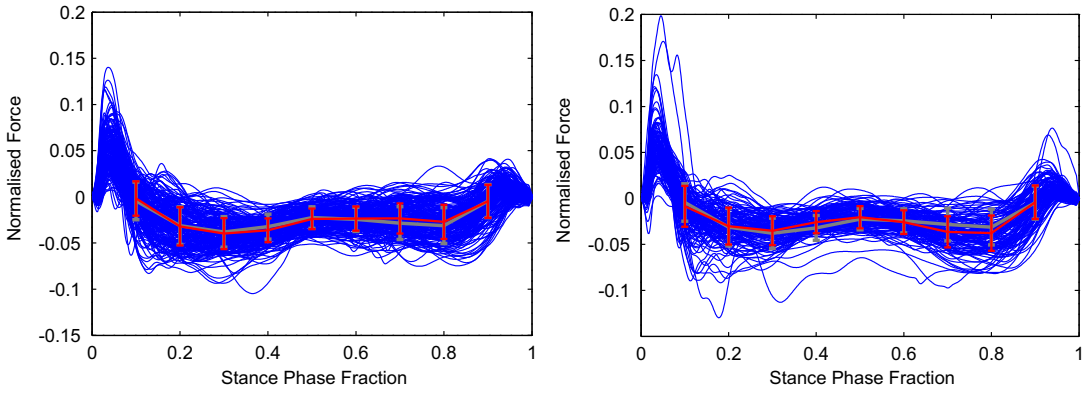

(a) (b)

Figure 3.2: (a) Female M-L force samples ($n = 194$) with population means (grey) and female means (red). (b) Male M-L force samples ($n = 122$) with population means (grey) and male means (red).

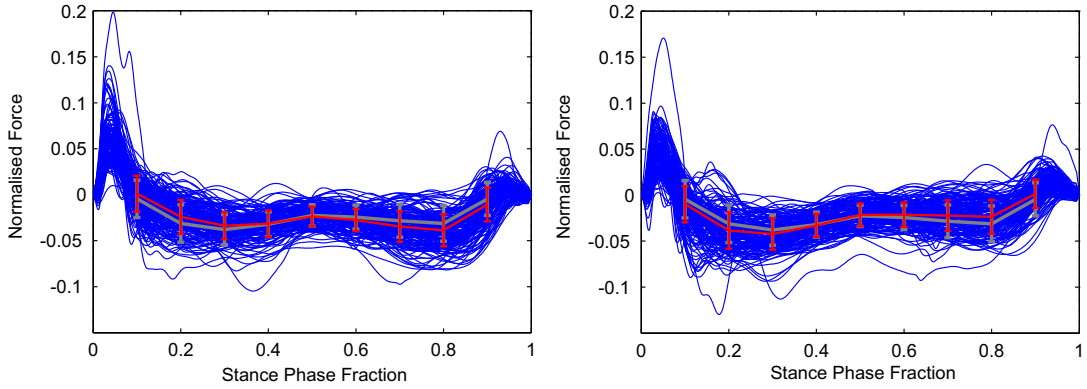

(a) (b)

Figure 3.3: (a) Left footsteps ($n = 158$) of entire population with population means (grey) and left foot means (red). (b) Right footsteps ($n = 158$) of entire population with population means (grey) and right foot means (red).

larger than that of the population for the first half of the stance. In the second half of the stance phase, however, the female lateral force does not peak a second time, but plateaus instead. The male lateral force means (Figure 3.2(b)) also follow closely to the overall mean through the first half of the stance phase. Unlike the second half of the female samples, however, the male samples exhibit a second peak instead of plateauing. Overall both subsets are always well within one standard deviation of the overall mean, so the difference between each gender and the population is negligible.

Left and right footsteps were also compared (Figure 3.3). Whereas one could plau-

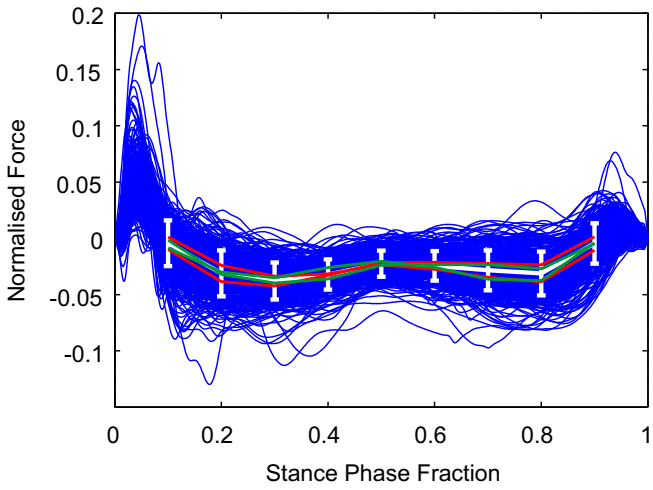

Figure 3.4: Comparison of female, male (green), left, and right (red) means to overall population mean (white). Each is well inside one standard deviation of the population mean.

sibly expect a difference between the force-time plots of women and men, a population of left feet should be the same as a population of right feet. The left feet exhibit the characteristic 'w' shape while the right feet follow a trough-and-plateau shape similar to the female plot. These differences are also small, however, so the left and right foot patterns are approximately the same as the population.

A comparison of the four subset means to the population mean (Figure 3.4) shows that overall the groups are very similar. The left and right foot means typically encompass the male and female means, showing that a slightly greater variation exists between the sides of body than between the genders. Nonetheless, since both the gender means and the left and right foot means fall well within the population standard deviation, the population mean represents the subsets well.

An examination of a variety of the individual M-L force patterns provides insight into whether the population and subset means are representative of specific participants. Figure 3.5 provides a sampling of individual plots, which have been analysed in terms of representativeness, repeatability, and intra-subject variability. In each plot, the red samples refer to a participant's left steps and the blue samples to his/her right steps. Each plot has also been overlaid with the population mean (black). In the quan-

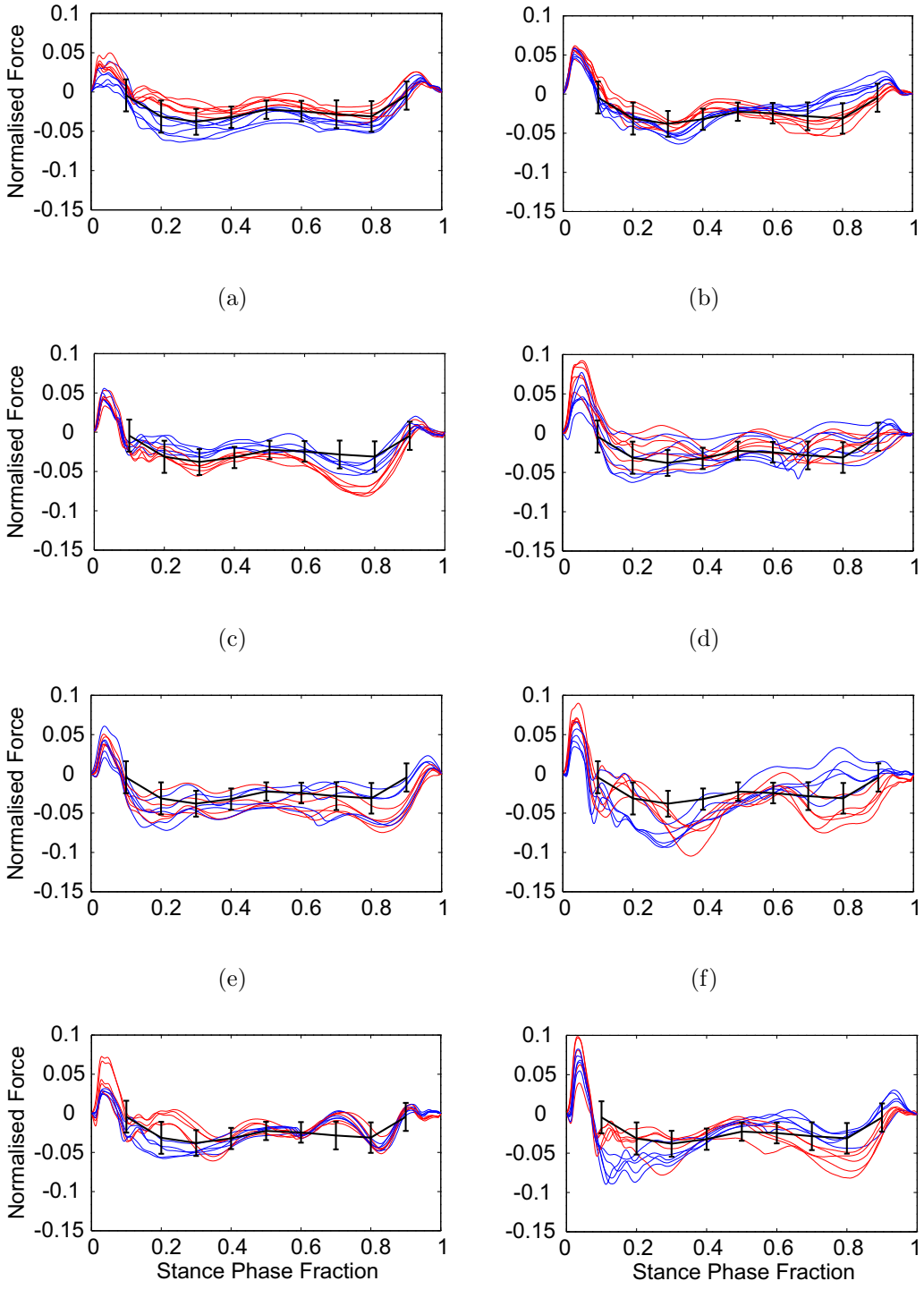

Figure 3.5: Several participant M-L force patterns. Left feet (red) and right feet (blue).

titative summaries that follow, participants with only one successful trial have been omitted.

The degree to which the population mean reflects an individual's M-L force pattern shall here be referred to as a participant's 'representability'. In this case, a step was considered representative if most of the samples fell within one standard deviation of the population mean. The participant depicted in Figure 3.5(a) is clearly the most representative since almost all of the samples of both feet fall within one standard deviation of the population mean. The left foot of the participant in Figure 3.5(b) and the right foot in Figure 3.5(c) are also very representative of the population. While perhaps both feet in Figures 3.5(d) and (e) are somewhat representative, the scatter of the repeated trials makes it difficult to discern whether the left and right steps are consistently so. Using the given criteria, only 29 of the 64 steps (i.e. 32 subjects, left and right) were represented by the shape of the population mean.

Whether or not a person's force patterns are representative of the population, they also have a degree of repeatability. A participant's 'repeatability' is defined as whether the force pattern of one footstep is the same or different from subsequent steps. Most participants exhibit a high degree of repeatability. The participant in Figure 3.5(g) exhibits the highest degree of repeatability. Each sample has almost the exact same shape as each of the other samples of the same foot. Even between $t' = 0.7$ and $t' = 0.9$ when there is rapid oscillation, the samples follow a tightly defined track, unique to that participant. To a slightly lesser extent, 3.5(a) through (c) also portray participants with a high degree of repeatability because the samples follow narrowly defined tracks with minimal variation, which are specific to the participant. The highly repeatable stepping strategy in these examples contrasts with those of Figures 3.5(d)-(f), whose samples vary greatly in amplitude and shape. The M-L forces for the participant in Figure 3.5(f) are particularly unique because they are neither representative nor repeatable. While almost two-thirds of the participants (20 out of 32) have a repeatable

M-L force strategy in at least one foot – unique, like a fingerprint – some steps, such as in Figure 3.5(f) are neither representative nor repeatable.

So far the concepts of representation and repeatability have revealed a high degree of inter-subject variability in participants' M-L force pattern. To investigate intra-subject variability the left and right force patterns for each subject are compared individually. The subjects with the lowest repeatability clearly exhibit high intra-subject variability because each sample is unique. The subject in Figure 3.5(d) exhibits a different force pattern for every right footstep; this person clearly has a variable walking pattern. Figures 3.5(c) and (g) show participants whose force patterns are repeatable in both feet. As a result, the variation they exhibit from gait cycle to gait cycle is minimal. A special case of this repeatability is symmetry, where both the left and right feet are identical. Figure 3.5(a) shows a participant whose gait is almost perfectly symmetric. Both feet are relatively precise and although the left step forces are of slightly less magnitude than the right the shape of both patterns is the same. Participants in Figures 3.5(b) and (g) are nearly symmetric except each has a short period during which the left force pattern differs from the right. Of the 32 participants analysed, only 11 exhibit near-symmetry. The remainder either have high variability or, like the subject in Figure 3.5(h), are harder to classify qualitatively.

3.2 Comparing Kinetic Data to the Inverted Pendulum Model

Consider Equation 1.24, Macdonald's Inverted Pendulum Model. On stable ground the motion of the walking surface, $\ddot{x}$, is zero. Normalising the M-L force by the weight of each participant, $m_p g$, leaves the non-dimensionalised force:

$$F'_x = (u - y)/L. \tag{3.1}$$

The data collected from the NOC I tests were used to verify the Inverted Pendulum Model using Equation 3.1. The CoP data (u) were collected directly from Vicon Nexus

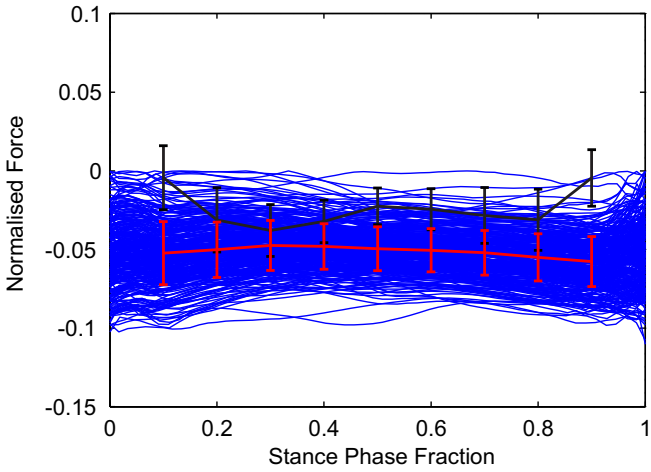

Figure 3.6: M-L forces calculated from IPM with mean and SD error bar (red). Original force plate data summarised by black mean and SD error bar.

and could be input directly. The CoM (y) was assumed to be located at the three-dimensional centroid of the LASI-RASI-SACR triangle and the pendulum length (L) assumed to be the height of the centroid.

Figure 3.6 shows that IPM predictions do not match the force plate data from the population. The red error bar provides the means and standard deviations of the underlying inverted pendulum data while the black error bar is for the force plate data given previously. The maxima occur at the first and last 10% of the stance phase (-0.0524 and -0.0577 normalised force) and the minimum is at $t' = 0.3$ (-0.0474). The shape of the model's error bar resembles the acceleration-time curve presented by Macdonald (Figure 1.8). The smallest difference between the model and force data occurs at $t' = 0.3$; the model over-predicts the data by approximately 1% of body weight. Across the remainder of the time period, the model over-predicts the data by as much as 5% of body weight. While in absolute terms this difference is small, the mean IPM pattern is approximately double the pattern of the force plate data throughout most of stance; only at $t' = 0.3$ is the IPM mean within one standard deviation of the real mean.

Some error is induced at the beginning and end of the step due to double stance. The theoretical IPM assumes an instantaneous transition between feet at $t' = 0$ and

$t' = 1$ [67] whereas the real data are affected by an initial and terminal double stance for up to 30% of each stance phase [145, 146], depending on the walking speed of the individual. Nonetheless, the IPM clearly does not reproduce the actual force pattern of the population during the single stance phase. The force plate data resembles the 'w' in shape, but the IPM is a smooth, concave-down curve that does not correlate well with the force data.

A wide variation of M-L force patterns has already been observed amongst different participants, so examining the Inverted Pendulum Model on the individual level should also produce a variety of results. Figure 3.7 gives the M-L force patterns for the same eight participants from Figure 3.5. In this set, the force plate data have been greyed and the Inverted Pendulum left and right feet are portrayed in red and blue, respectively. The most apparent trait of these plots is that the model fails to reflect acute oscillations in the real force data. The most significant cases are Figures 3.7(g) and (h), where peaks and troughs in the force plate data are entirely unrepresented by the model. Moreover the force plate data produce a unique 'fingerprint' for each individual, but the IPM patterns are not nearly as distinctive.

Examining Equation 3.1 helps to explain the shape of the plots. The pendulum length, L, remains almost constant, so the shape of the model must be attributed to the CoM-CoP separation, $u - y$. If the change in the numerator is small then the model will fail to reflect acute oscillations.

In Figures 3.7(b),(c),(e),(f), and (h), the model exhibits a high level of repeatability for at least one foot. The spacing between the CoM and CoP is therefore repeatable for each step of the same foot. In contrast, the splaying present in Figures 3.7(a),(d), and (g) shows that some participants' CoM-CoP separation varies from step to step.

For any given sample, a flatter pattern corresponds to less variation in the CoM-CoP separation. Some of the model patterns exhibit concavity at either the beginning or end of stance, but most of the patterns are flat at one or both ends. The absence of

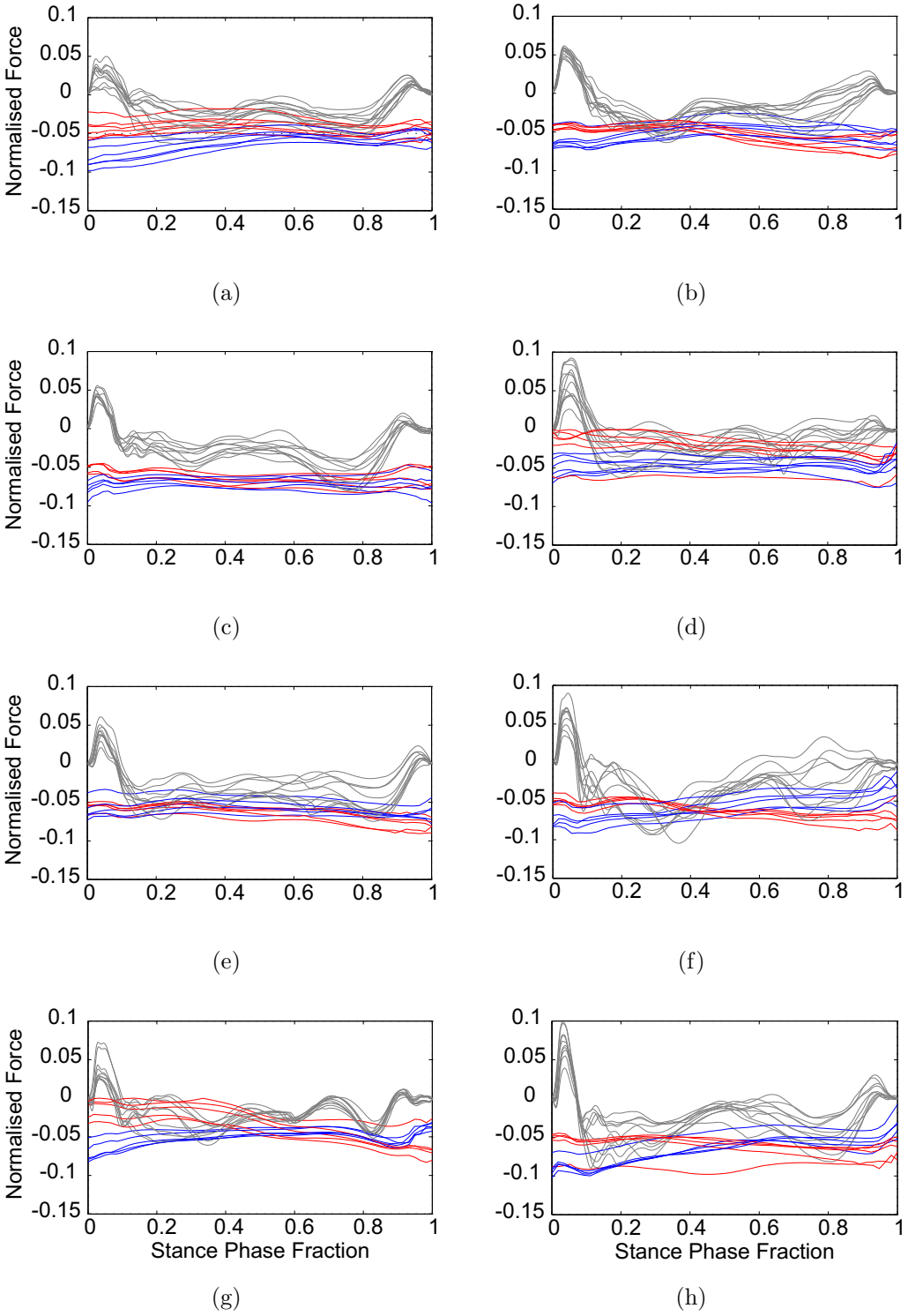

Figure 3.7: Individual Inverted Pendulum Models based on kinematic data: left foot (red) and right foot (blue) forces compared to real ground force data (grey).

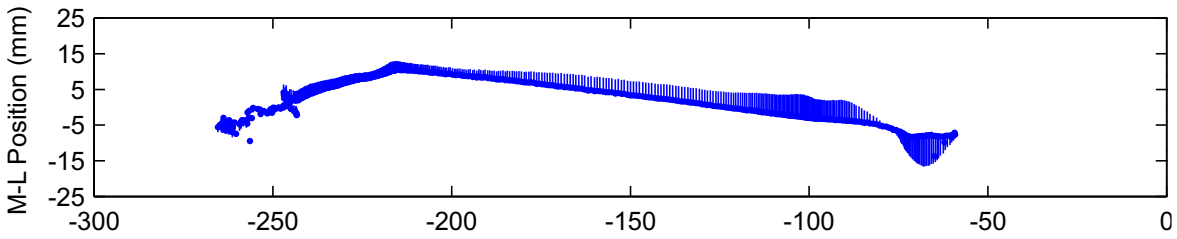

(a)

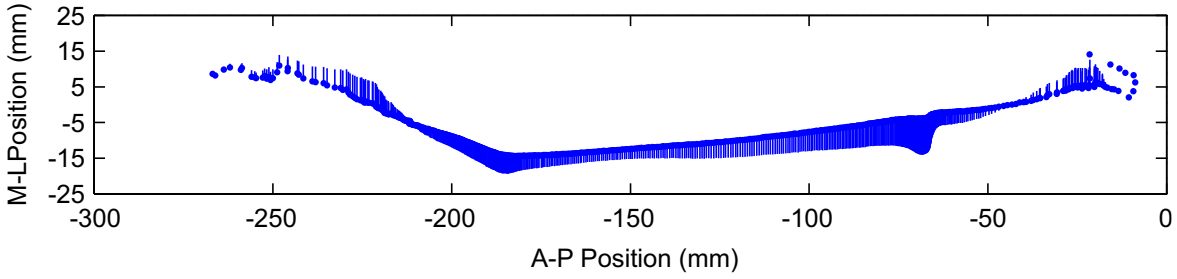

(b)

Figure 3.8: Relative M-L forces as a function of CoP location. Participants ((a) male R foot, 65.0kg, 1.71 m; (b) female L foot, 68.8kg, 1.74m) walking from right (heel-strike) to left (toe-lift) across the plot.

model oscillations suggests that the CoM-CoP separation may not fluctuate as much as the real ground force. This may be due to errors in measurement or a deficiency of the model.

3.3 Spatial Analysis of CoP and CoM Paths

Spatial analysis of participant stepping patterns could help to explain the discrepancy between the IPM and the data. Examining spatial patterns also provides insight on inter- and intra-participant step variability.

Figure 3.8 shows the Centre of Pressure paths of a right and left foot, respectively, from different participants. In both cases, the participant is 'walking' from right to left across the plot. The M-L force component has been extended from each CoP point. Following the paths from heel-strike to toe-off (right to left), the initial heel force is in the medial direction. As the CoP moves off the heel towards the outside of the foot, the

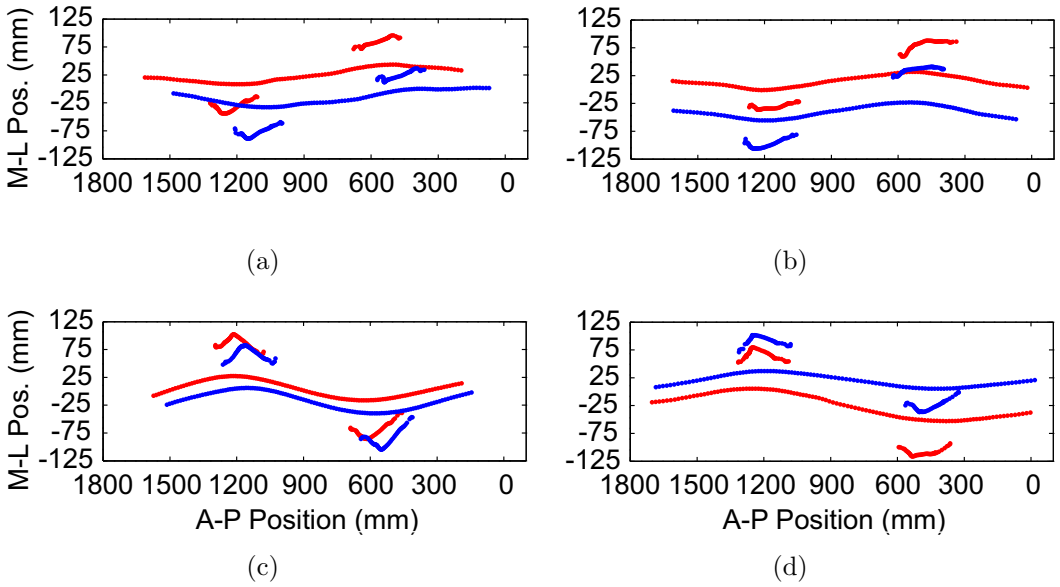

Figure 3.9: Two CoM-CoP displacement paths for each of four participants. Participants walking from right to left across the plot.

force changes to the lateral direction. Single stance occurs during this period, and the wider spacing of the CoP points (compared to the heel and toes) reveals that the speed of the CoP location has increased. When the CoP reaches the distal end of the fifth metatarsal, it tends to turn away from the edge of the foot in the shape of a backward (left foot) or normal (right foot) question mark ('?'), progressing across the foot before finally lifting off through the big toe. In some cases however, the CoP merely lifts off from what appears to be the middle or edge of the foot, leaving a straight CoP path instead of the '?' shape. Regardless, during this time, the CoP progression becomes much slower than during mid-stance; the body uses the double stance period to retain stability [123]. Finally, as the CoP reaches toe-lift, the force returns to the medial direction, although not as prominently as at heel-strike.

In Figure 3.9, one can gain a sense of the variation that occurs among participants in CoP and CoM paths. Again, the participants are 'walking' from right to left across the plot. Each of the plots also shows the projections of the CoM path for the two trials; the footsteps are easily distinguished by the distinctive '?' shape and on which

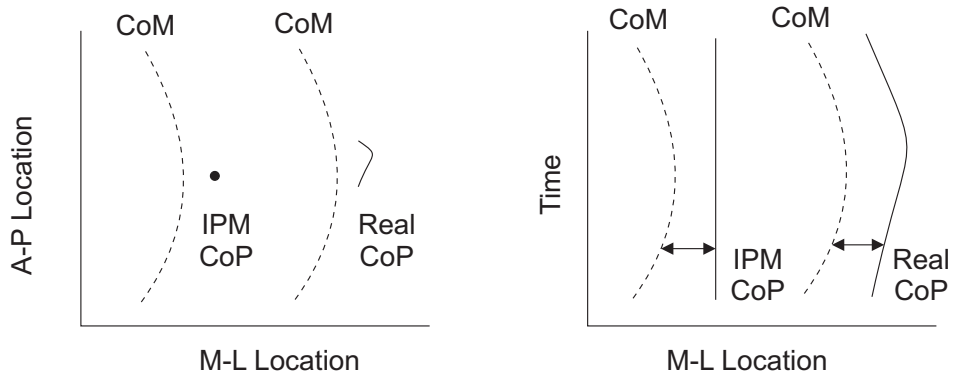

Figure 3.10: Depictions of the CoM (dashed) and CoP (solid) over one footstep. (Left) The spatial progression of the CoM against the CoP. The left pair shows that the IPM assumes the CoP remains fixed in place while the right pair shows the real CoP track. (Right) In the time domain the separation of the CoM and CoP is clearly wider for the case where the CoP is assumed fixed than the real track.

side of the CoM path they lie. Each figure shows that one CoM path in each plot is a near translation of the other, meaning that intra-participant variability of CoP and CoM paths is minimal. In contrast, the four participants vary their stride length, CoM displacement amplitude, step width, and step angle. While the two-step plots seem to be repeatable on a participant-by-participant basis, they do not appear to be repeatable universally.

One of the assumptions of the IPM is that the Centre of Pressure remains fixed throughout stance. In the preceding analysis, however, the real CoP has been used in the IPM instead of a fixed point. Figure 3.10 shows that this decreases the CoM-CoP separation throughout stance. The real CoP path is spatially located adjacent to the extreme location of the CoM path, but in the time domain the patterns are fairly concentric. Thus the M-L spacing between the CoM and CoP remains approximately constant and the IPM plots are relatively flat.

If a constant CoP location had been used in the IPM (an aspect that will be examined more in Chapter 5), the degree of concavity observed in the individual-level plots would be slightly increased. That said, the model patterns would still fail to reflect the oscillations of the real ground force patterns because the CoM trajectory

only appears to oscillate as a simple quasi-sinusoid (Figure 3.9) and, of course, the CoP would be constant. This results in a smooth CoM-CoP separation over time instead of exhibiting the higher frequency patterns seen in Figure 3.5.

3.4 Discussion & Conclusion

Results from the NOC I tests yielded new perspectives on (1) the correlation of M-L force data to population means and (2) the ability of the Inverted Pendulum Model to predict M-L ground force patterns. Comparing the population mean to the male, female, left foot, and right foot subsets, there was good correlation amongst the various groups, in spite of the fact that the female samples and right foot samples tended to level-off over the second half of stance instead of imitating the characteristic 'w' pattern. The fact that the variation between left and right feet was typically greater than the variation between genders showed that there was minimal difference between the force patterns produced by the different genders, and that a population was not perfectly symmetric.

Other factors (e.g. varying left and right leg lengths, body-mass index, left or right side dominance) could influence gait patterns, but the limited sample size made it difficult to separate systematic differences from normal inter-subject variation. In particular, the dependence of the (non-normalised) Inverted Pendulum Model on body mass suggests a linear relationship with ground force. It is possible, however, that an increase in body mass alters one's gait, which may be more or less like an inverted pendulum. This, of course, would not be manifested in the mass term of the IPM but rather in the kinematic term $u - y$.

The population means were compared to the patterns of individual participants. Most of the participants' patterns did not represent the population mean. This was particularly due to localised acute fluctuations in the M-L force which varied from participant to participant. A comparison of participant M-L force patterns showed

that they tended to be repeatable, indicating low intra-subject variability. When both feet exhibited the same strategy, the subject's gait was symmetric. While symmetry was rare, the force amplitude of one foot was often only slightly different than the other, whether at a point of local divergence or because one foot had a consistently higher force magnitude than – but identical shape to – the other.

The CoP and CoM data from the gait lab were input into the Inverted Pendulum Model in order to determine whether the model can effectively replicate the real M-L forces from the force plates. On a population level, the model was not representative of the data, overestimating the force plate data by 1-5% body weight. The means of the Inverted Pendulum Model created a concave down shape while the real population data resulted in a 'w' shape. On an individual level, the model and force plate data showed similar maximum amplitudes, but the model failed to represent any acute fluctuations in the force plate samples. Given the relatively flat model curves, very little variation occurred in the M-L separation between the CoP and the CoM.

This study proposes that deterministic models such as the Inverted Pendulum Model be used with caution in the case of lateral bridge excitation modelling. Individual pedestrians walk with unique loading patterns on stable ground, so their force patterns do not necessarily represent deterministic processes. The Inverted Pendulum Model is hindered both by its inability to model the double stance phase and by its failure to reflect acute changes in M-L force. These aspects are considered in greater detail later.

In the next chapter three kinematic methods are presented that aim to reproduce lateral ground forces, thereby avoiding the IPM altogether. Their successful application would have valuable benefits for field research, where recording the ground forces of an individual in a crowd is essentially impossible using present technology.

Chapter 4

Kinematic Predictions of Lateral Ground Force

Racic *et al.* highlighted the significant lack of data describing lateral ground force modelling [21]. In particular, they explain that while some data describe the vertical ground forces of runners and walkers, minimal research has analysed the lateral forces of either runners or walkers. Ideally researchers need to study the forces produced by individuals within a crowd on a bridge, but technological limitations make this difficult. Thus, establishing the relationship between body kinematics and ground force could be very useful. Fujino *et al.* sought to explain movement of the Toda Park Bridge by tracking the heads of individuals in a crowd [27]. Dallard *et al.* used similar techniques in both the review of the London Millennium Bridge oscillations and the verification of its subsequent damping modifications [26, 25]. These techniques were primarily used to assess structural motion, but they could perhaps be used to predict ground force if head motion is proved to be correlated.

Carroll *et al.* conducted experiments to reconstruct lateral forces by tracking a walking subject's kinematics on an instrumented treadmill [48]. These tests were carried out on two subjects for steady state walking. Over 20-second periods, they reported correlations of 0.94 and 0.95 between each subject's lateral ground force and the forces constructed from a Newtonian summation of body segment accelerations times their masses. The research proposes that if a subject is tracked on a stable

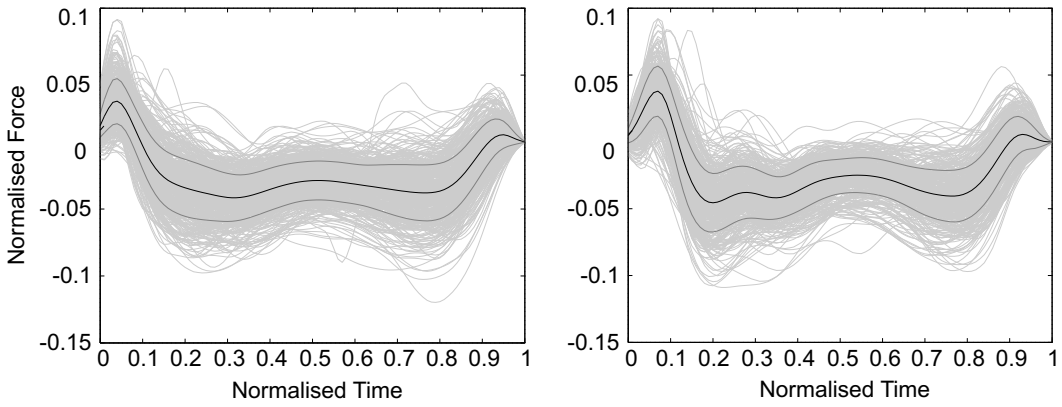

Figure 4.1: Medial-lateral force (body weight normalised) versus time for (a) 433 barefoot steps and (b) 377 shod steps. Mean (black) +/- SD (dark grey).

surface for 20 seconds or more, a summation of the head, trunk, and pelvis movements can accurately simulate the lateral ground force of the subject.

While tracking the full body of a subject over a long duration of steady state walking yields a high correlation with lateral ground force, it is likely that a field test of a crowded bridge will preclude the tracking of a whole body, or for steady state walking over such a long duration. Therefore, this chapter investigates the correlation between body segment motion and lateral ground force over sample durations of three footsteps.

4.1 Shod and Barefoot Walking

Results from the NOC I tests described in the previous chapter depict barefoot walkers traversing two force plates. Since barefoot walking may be different from normal shod walking – particularly over a bridge – the NOC II tests recorded participants walking both shod and barefoot in order to establish similarities and differences between the conditions. Figure 4.1 shows the lateral ground force for 477 barefoot steps against 377 shod steps.

The mean and standard deviation for the respective data sets is provided in Ta-

Table 4.1: Mean and SD normalised force for barefoot and shod walking.

	Barefoot ($n = 433$)		Shoes ($n = 377$)	
Time (t/t_{max})	Mean (N/N)	St Dev (N/N)	Mean (N/N)	St Dev (N/N)
0	0.0123	0.0088	0.0046	0.0054
0.03	0.0297	0.0167	0.0205	0.0142
0.07	0.018	0.0156	0.0379	0.0188
0.1	-0.0028	0.0175	0.0195	0.02
0.2	-0.0342	0.0213	-0.0456	0.0219
0.3	-0.0414	0.0179	-0.0387	0.0185
0.4	-0.0353	0.0157	-0.0367	0.0153
0.5	-0.0288	0.0145	-0.0259	0.0129
0.6	-0.0314	0.0149	-0.027	0.0135
0.7	-0.0361	0.0193	-0.0375	0.0172
0.8	-0.0366	0.0207	-0.0382	0.0195
0.9	-0.0057	0.0172	-0.0002	0.0169
1	0.0001	0.0002	0	0.0002

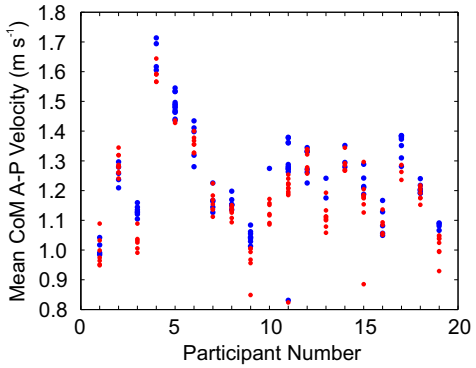

Figure 4.2: Mean walking velocity for all participants (females 1-10; males 11-19) while walking shod (blue) and barefoot (red).

ble 4.1. Even though minimal difference separates the descriptive statistics of the barefoot and shod trials, z-statistics show that large portions of the means are statistically different at a level of p <0.005 (assuming that the data is normally distributed). The largest difference between the means occurs at the heel-strike, where the mean peak lateral force in shod walkers is 0.7% of body weight higher than and $t' = 4\%$ later than that of barefoot walkers.

Walking velocity also plays a role in ground force development. Figure 4.2 compares walking velocities for the shod and barefoot trials, determined as the derivative of their A-P Centre of Mass position. The standard deviations for most trials ranged from 0.1-0.15 m s^{-1} while the means were typically within 1.0-1.5 m s^{-1}. Most participants'

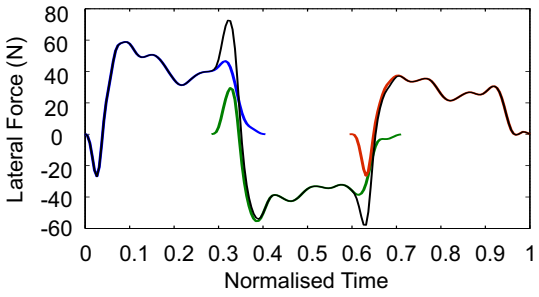

Figure 4.3: Individual records of three force plates (blue, green, red) and their sum for one trial (black).

barefoot trials are similar to but slower than their shod trials, which could affect their typical ground force pattern. Since shoes affect walking speed, and most bridge-crossers in the UK wear shoes anyway, only shod three-step trials are henceforth considered in this thesis.

Using three force plates for the NOC II tests, the ground force data is of the form shown in Figure 4.3. Positive force in the graph corresponds to ground force exerted to the left of the walker and negative force corresponds to force to the right. Thus zero M-L force does not infer zero ground force; A-P and vertical forces may still exist. Each force plate contributes the signal of one stance phase. The trial shown thus constitutes a left-right-left combination of footsteps. In periods of double stance, the time-domain signals of two force plates overlap. In the given trial the landmarks of each step are distinct, especially for the heel-strikes at $t' = 0.03$, 0.33, and 0.63 and the toe-off points at $t' = 0.40$, 0.71, and 1.0. Since this chapter is primarily concerned with the body's overall lateral forcing pattern over multiple steps, the forces in adjoining plates were summed to provide a total lateral ground force, shown by the black line in Figure 4.3. The double stance segments at the beginning and end of the three-step samples are not composites of the preceding toe-off or subsequent heel-strike. It is assumed that the influence of the missing components is negligible compared to the greater prominence of the oscillations throughout the rest of the three step signal.

Using MATLAB, the lateral motion of each body segment was estimated by aver-

aging the lateral displacement of all markers on the segment at every time step. Head motion is predicted by averaging the four head markers, pelvis motion is predicted by averaging the SACR, LASI, and RASI markers, and trunk motion is predicted by averaging the jugular notch, sternum, C7, and T10 markers. This approximation therefore assumes that each body segment is a rigid element and that markers placed on clothing or skin do not slip with respect to each other. Additionally this approximation assumes that over any time step, rotation in the frontal plane is negligible compared to translation in the same plane. Finally, it also assumes that the mean marker position is located on the body segment's axis of rotation, lest the segment's rotation contributes erroneously to the M-L acceleration. The velocities and accelerations of the segments were determined by applying a three-point central difference method to the displacements. For any three consecutive displacement data points, x_{i-1}, x_i, and x_{i+1}, the velocity $\dot{x}_i$ is approximated as

$$\dot{x}_i \approx \frac{x_{i+1} - x_{i-1}}{2\Delta t} \tag{4.1}$$

where Δt is the change in time between consecutive points. The acceleration $\ddot{x}_i$ is determined in the same manner using the velocity data.

Carroll *et al.* compared the lateral force from their instrumented treadmill with the reconstructed lateral force of head, trunk, and pelvis body segments, which they also determined by double differentiating the displacements of reflective markers [48]. Their samples - approximately 35 footsteps each – produced Pearson's correlation coefficient (r) values of 0.950 and 0.946, suggesting a strong correlation between body movement and lateral force. In the field, however, recording a pedestrian's motion for 20 seconds in a crowd may be impossible. Thus it is valuable to know whether a pedestrian's ground forces correlate to their body segment accelerations over a shorter sample period so that field recordings of body motion could be used to predict ground force.

In the present tests three methods were chosen in order to find the best correlation between the body markers and the force plate data. First, a direct comparison of the

Table 4.2: Body segment mass coefficients [92].

	Mass Fraction, λ_m (%)	
	Females	Males
Head	6.68	9.94
Upper Part of Trunk (UPT)	15.45	15.96
Middle Part of Trunk (MPT)	14.65	16.33
Lower Part of Trunk (LPT)	12.47	11.17

Newtonian forces was conducted. Second, an optimised parameter, Ψ, was introduced to allow for intra-body forces. Finally, the accelerations of the body segments were compared with the acceleration produced in the force plate.

4.2 Reconstructed Forces Versus Ground Forces

Based on Newtonian mechanics,

$$F_x = \sum_i \lambda_{mi} m_p \ddot{x}_{si} \tag{4.2}$$

where the force, F_x, recorded by the force plate for any given sample should be equal to the sum of the body segment masses times the lateral accelerations of their Centres of Mass, $\ddot{x}_s$. Here the segment masses are depicted as the product of the segment to body mass fraction, λ_m, times whole-body mass, m_p. The anthropometric body segment mass fractions were taken from de Leva [92], as utilized by Carroll [48]. De Leva provides the mass fractions, which are given in Table 4.2, for the body parts relevant to this discussion. Based on the marker set used in these experiments, the trunk is assumed to be the sum of the UPT and MPT components, while the LPT comprises the pelvis.

For each trial, the product of the components in Equation 4.2 leads to a family of plots like Figure 4.4(a). This figure shows the reconstructed lateral force from the head, trunk, and pelvis for one trial. The three steps are indicated by the most prominent positive-negative-positive trend, which corresponds to force to the subject's left, right, and left sides respectively. The trunk produces more lateral force than either the head or the pelvis and contributes a dramatic medial shift shortly after each heel-strike, as

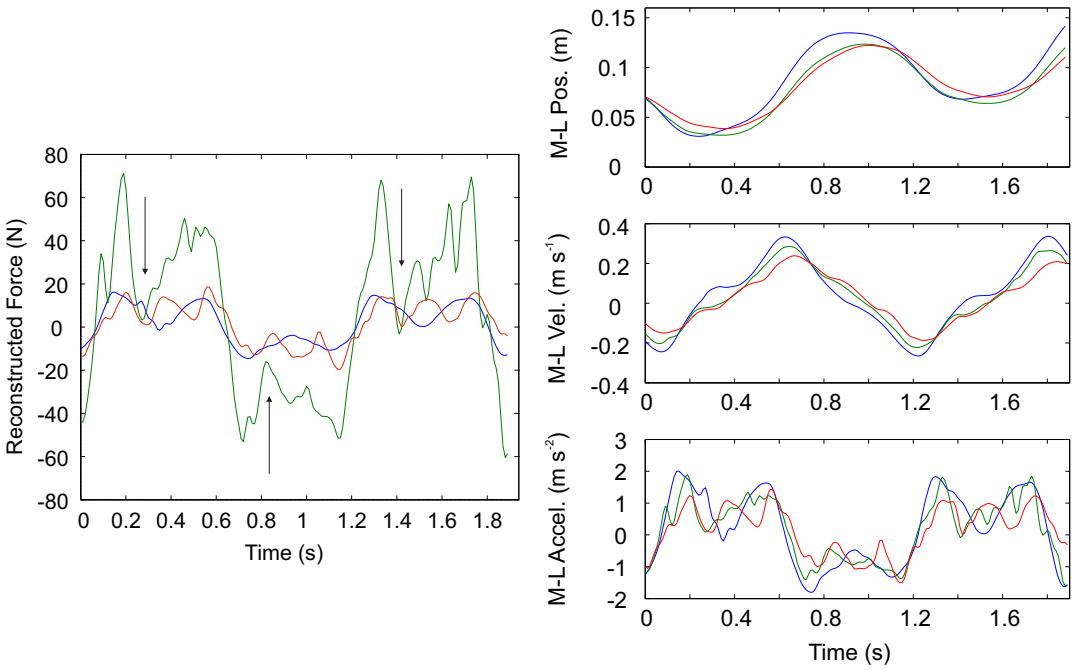

(a) (b)

Figure 4.4: (a) Reconstructed head, trunk, and pelvis force for one three-step trial. Head (blue), trunk (green), and pelvis (red). Arrows indicate medial spikes in reconstructed trunk force. (b) M-L position, velocity, and acceleration of each body segment.

indicated by arrows. As the heaviest part of the human body, the trunk has a higher inertia and will require more force to control than any other body segment. It then makes sense that any trunk acceleration will have a greater influence than other body segments.

The figure shows that the magnitude of the head and pelvis forces are approximately the same. The head force pattern is comparable to the lateral ground force 'w' in shape, but the pelvis force consists of a higher frequency content. A Fourier-domain analysis of head, trunk, and pelvis forces reveals that for most individuals the dominant frequency of the head and trunk forces is the gait cycle frequency. The pelvis force on the other hand is most often dominated by the fifth harmonic.

For reference, Figure 4.4(b) depicts the position, velocity, and acceleration of each of the body segments. Note that overall, the body segment positions and velocities

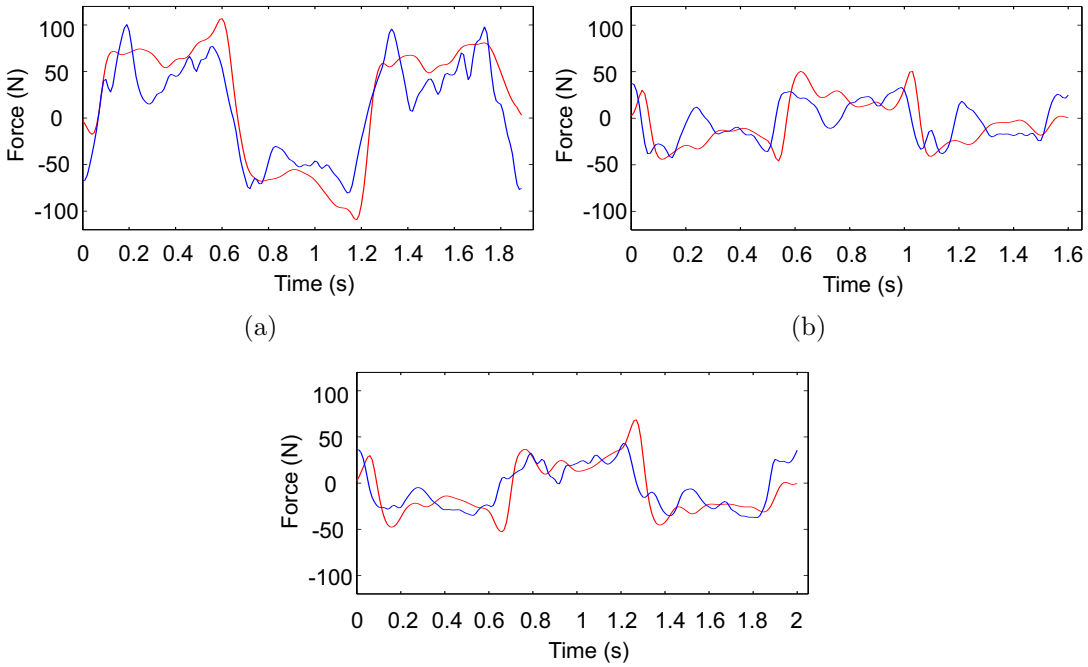

Figure 4.5: Comparison of reconstructed force (blue) to real ground force (red) with Pearson's correlation coefficients: (a) $r = 0.878$, (b) $r = 0.495$, (c) $r = 0.708$.

follow the same overall pattern as each other, which is similar to Macdonald's Inverted Pendulum Model (Figure 1.8). The acceleration plot reveals, however, that there are differences among the motion of the three body segments. This will be examined more in Section 4.4.

The head, trunk, and pelvis forces were summed for each trial and plotted against the real ground force. These two samples were compared by means of the Pearson's correlation coefficient, r. In the case of Figure 4.5(a), the force recorded by the force plate is similar to the reconstructed force; the resulting correlation coefficient is 0.878. Among the 38 trials, the correlation coefficient between the force plate force and the reconstructed force varied from 0.495 to 0.878 with a mean of 0.707. These are reflected in the two trials shown in Figures 4.5(b) and 4.5(c). Generally, the largest variation between the reconstructed force and the force plate force is in the amplitude level of the two signals during the medial shift of the trunk. A small amount of phase shift is also occasionally present between the two forces (e.g. in Figure 4.5(b)), which may

adversely affect the r value.

Like the composite reconstructed force, the head, trunk, and pelvis forces may also be compared to the ground force using Pearson's correlation coefficients. The mean reconstructed force to real force correlations among the 38 trials were 0.723, 0.645, and 0.455 for the head, trunk, and pelvis respectively. While the trunk represents the highest proportion of a person's weight and consequently the greatest reconstructed force, the head had a higher correlation to the M-L ground force than the trunk in 28 of the 38 three-step trials. The correlations show that a three-step sample is sufficient to imply a moderate relationship between the reconstructed marker-based force and the real ground force recorded by the force plates. While it might be possible to develop an empirical M-L force model based on head or head plus trunk data, the low correlation between the pelvis force and the ground force suggests that pelvis motion might contribute to something other than ground force, such as vertical or A-P stability.

4.3 Mass Coefficient Optimisation

One hypothesis for why the correlations are not higher could be that certain body segments contribute more to the M-L ground force than others due to isometric forces, internal losses, or other biomechanical reasons. This supplemental effort might not be represented in the lateral acceleration of a particular body segment, but might be manifested internally through the body into the feet. As an example, while standing with both feet separated and planted, a ground force can be created by contracting the hip adductors, producing a squeezing force without moving the legs. This isometric force would develop a ground force under each foot without producing any reconstructed body segment force. Alternatively, another hypothesis is that the mass coefficients supplied by de Leva could be incorrect for this group of participants if his subject group were of significantly different body shape. To test whether such factors negatively influence the reproduced ground force, each of the body segments was multiplied

by an arbitrary coefficient Ψ_i,

$$F_x = \sum_i \Psi_i \lambda_{mi} m_p \ddot{x}_{si}. \tag{4.3}$$

By optimising the coefficient, it is possible that the scaled reproduced segment forces produce a better correlation with the real ground force.

For each trial, MATLAB's `lsqnonlin` function minimised the sum of squared differences between the reconstructed force and the force plate force by optimising the unbounded coefficient Ψ. The optimisation was carried out with seven combinations of body segments in order to learn about the independent and interactive aspects of the coefficient optimisation. Table 4.3 shows the different body segment cases analysed, the mean coefficients Ψ_i that were produced, and the mean Pearson's correlation between the optimised reconstructed forces and the force plate sample. The table also provides the product of Ψ_i and the body mass fraction λ_{mi}, a weighted indicator of the importance of the optimised coefficient.

The head has the highest correlation to the ground force because it has the highest Ψ and $\Psi\lambda_m$ in every case where it is tested. The optimised head contribution is significantly greater than the trunk or pelvis contribution, reinforcing the conclusion of the previous section that it had the highest correlation of the three body segments. The trunk contributes the second highest $\Psi\lambda_m$ overall, although it should be noted that the trunk coefficient Ψ_t is approximately the same as that of the pelvis in cases where they are both applied. This indicates that the difference between the trunk force and the pelvis force is attributable largely to the mass fraction, not the optimised mass coefficient.

Most importantly, the table shows the correlation between the reconstructed force and the real ground force across different body segment combinations. Cases involving the head have the highest correlation coefficients, with the maximum being 0.797 for the head, trunk, and pelvis case. Physiologically the strong correlation between the head's optimised coefficient and the ground force is a bit surprising, given the implication that

Table 4.3: Mass coefficient optimisation cases.

		Head ($\lambda_{mh} = 0.0668$)		Trunk ($\lambda_{mt} = 0.3010$)		Pelvis ($\lambda_{mp} = 0.1247$)	
Case	r	Ψ_h	$\Psi_h\lambda_{mh}$	Ψ_t	$\Psi_t\lambda_{mt}$	Ψ_p	$\Psi_p\lambda_{mp}$
H,T,P	0.797	4.39	0.293	0.511	0.154	0.597	0.0745
H	0.724	5.84	0.390				
T	0.645			1.28	0.386		
P	0.455					1.92	0.239
H,T	0.788	4.44	0.296	0.657	0.198		
T,P	0.769			1.05	0.317	0.959	0.120
H,P	0.767	5.31	0.355			0.846	0.106

the head contributes non-kinematic, internal forces. The correlation for the H,T,P case is an increase of 0.090 over the comparison in Section 4.2, although this mean correlation is still approximately 0.15 points lower than the long-duration correlations reported by Carroll *et al.*

4.4 Marker Accelerations versus Normalised Force

De Leva's anthropometric mass coefficients assume that all subjects have approximately the same body type; college-aged athletes [92]. This was not the case for the NOC II tests, so it is possible that the body segment mass fractions are not representative of the participants in this study. Thus, a third set of comparisons avoided the use of de Leva's mass fractions by examining M-L accelerations instead of ground forces. The force plate samples were all divided by each subject's mass, $a_x = F_x/m_p$. The resulting family of plots compares accelerations instead of forces. Examples are shown in Figure 4.6. Figure 4.6(a) shows the same trial as Figures 4.1 and 4.3. Where the figures shown in Section 4.2 showed a dispersion of the body segment forces, the body segment accelerations generally have the same amplitudes. The pelvis again shows a higher dominant frequency than either the head or trunk, all of which appear to oscillate more than the force plate acceleration.

Showing acceleration instead of force, the body segment to force plate correlations in Figure 4.6(a) are 0.776 and 0.713 for the head and trunk respectively. Across the

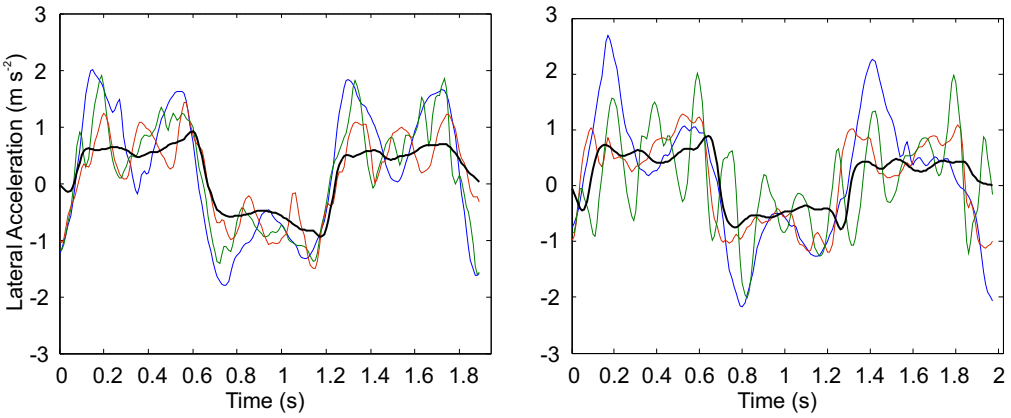

(a) (b)

Figure 4.6: (a) Body segment and force plate accelerations for the trial depicted in Figures 4.1 and 4.3. (b) Body segment and force plate accelerations for a different trial. Head (blue), trunk (green), pelvis (red), and force plate (black).

sample population, the correlation between the head and the force plate was again higher than that of the trunk or pelvis with 28 out of 38 samples indicating that the head exhibited a higher correlation. The trial in Figure 4.6(b) is the opposite, however; the head and trunk correlations are 0.829 and 0.843 respectively. In this case, the difference between the head and the trunk is likely to be caused by the lateral head acceleration near the heel-strike of each step. In both figures the frequency content of all three body segment accelerations is greater than that of the force plate. The body segment accelerations oscillate significantly more than the force plate acceleration; the force plate acceleration is typically stable compared to the markers – especially the pelvis.

Among the population, the mean correlations between the head markers and the force plate and the trunk markers and force plate are 0.724 and 0.645 respectively. These correlations are slightly better than the force-based comparisons, but are insufficient to show a strong linear relationship between the marker data and the force plate samples.

4.5 Discussion

When studying individuals moving within a crowd, there are few viable options beside optical methods. Isolating the motion of the test subject is essential yet the psychology and physiology of walking in a dense crowd on a bridge may be irreproducible in the lab. Accelerometers worn on the belt are one option for recording body motion, but they do not adequately define a local coordinate system in terms of the global coordinate system. Optimally, shear force transducers could be mounted onto or into a person's shoe, but they would restrict the flexibility of the foot and would also reference a floating local coordinate system (although one promising design has been explored by van den Noort *et al.* [147]). Alternatively force plates could be installed on the structure, but the researcher must ensure that only one subject touches the plate at a time, and with a perfectly clean step; difficult requirements to implement in the middle of a dense crowd.

So, therefore, optical measurement is less invasive, easier to control, and allows for better simultaneous capture of multiple targets compared to other options. The problem with optical tracking, however, is the accuracy of modelling lateral ground forces with the accelerations of reflective body-mounted markers. Three tests described in this chapter have attempted to find short-duration correlations between body segment motion and lateral ground forces. The fact that all three methods produced similar correlations shows that the correlations are relatively robust. With correlations varying from 0.707 to 0.797, the r^2 of 0.500 to 0.635 shows that more than half of the data in each method are represented by the force plate record.

The best overall correlation was obtained by optimising the mass coefficients provided by de Leva and summing the reconstructed head, trunk, and pelvis forces to simulate the ground force. This provided a mean correlation of 0.797 or an r^2 value of 0.635. While only a moderately high correlation, the results from this test could lead to an empirical lateral force model if further tests prove (1) that consistency exists in

Ψ_i across a larger population of trials and (2) how Ψ_i is physically represented in the body – be it energy consumption by muscles, isometric forces, internal restoring forces, or other reasons.

Overall, the three methods show that head motion is more strongly connected to lateral ground force than either trunk or pelvis motion. Even though the head contributes less than 10% of the total body mass, its higher correlation suggests that it plays an elevated role in lateral body control. One possibility is that the head (brain) mimics the ground force in order to minimize its lateral trajectory while still allowing the body to hinge [94]. Meanwhile, other body segments, such as the trunk and pelvis, exert local angular momentum to control the shift in body weight and affect overall balance. This is supported by the findings of Herr and Popović which show that segmental angular momentum is not only highly regulated, but also internally cancelled in order to enhance stability and manoeuvrability [102].

Carroll *et al.* show that a very good correlation can be obtained by comparing a reproduced head, trunk, and pelvis force from marker data to a 20 s ground force sample produced on an instrumented treadmill [48]. One reason for the discrepancy between their high correlations and the correlations produced in this experiment could be signal duration. The difference in signal durations indicates a significant difference in the number of samples that are used in the Pearson's r calculation. By analysing 10 times as many footsteps per test than in the NOC II tests, the correlation coefficients cited by Carroll *et al.* are less sensitive to outlying data than the tests described in this chapter.

One might suggest that the method of filtering could also play a role in the difference between the two studies. Carroll *et al.* utilised a fourth-order Butterworth filter after each derivation of the marker locations, while the present study only filters each data sample once. Using a Butterworth filter with the data presented here, the mean correlation for the sample population was only 0.774. This is in the same range

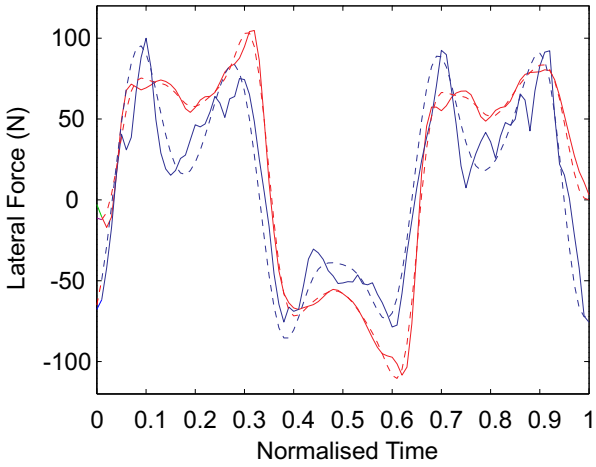

Figure 4.7: Comparison of signal filters. Force plate rectangular and Butterworth filters (solid and dashed red respectively); Reconstructed force rectangular and Butterworth filters (solid and dashed blue respectively).

as the three tests discussed above, so the filter appears to have a minimal effect on the correlation. Figure 4.7 shows a comparison of the two filtering methods for one trial. The correlations between the samples are similar, but the Butterworth filtering method smooths the data far more than the basic rectangular filter, so the basic filter was kept.

If a field test were devised such that subjects in a crowd were tracked by their head motion such as reported by Fujino *et al.* [27], the resulting lateral force estimates would therefore only be as accurate as the duration of the sample. Even assuming a stable walking surface without crowd interactions, the data of a person taking only a few footsteps would have marginal accuracy. That being said, a moderate correlation does exist between the reconstructed marker force and the lateral force plate force. This should not be neglected, especially considering that understanding lateral head motion could be immensely beneficial for the study of lateral ground forces and human structure interactions.

4.6 Conclusion

The purpose of this study was to use the acceleration of reflective markers mounted to the head, trunk, and pelvis to reconstruct the lateral ground force exerted by a healthy human walker. Three methods were utilized to analyse the acceleration data: direct reconstruction of the lateral force using Newtonian mechanics, optimisation of unbounded body segment coefficients Ψ_i, and a comparison of the segment accelerations to the mass-normalised 'force' in the force plate. All three methods produced Pearson's correlations between 0.7 and 0.8, indicating a moderate correlation between body movement and lateral ground force. Of the three methods, the optimised mass coefficient method produced the best correlations between individual segments and the ground force. All three tests suggest that the motion of the head is the best indicator of the lateral ground force. This is in spite of the fact that the trunk has the highest reconstructed force of the analysed body segments. Ultimately, with mean correlation coefficients up to 0.8, one can only confirm that a moderate correlation exists.

Chapter 5

Analysis and Modification of the Inverted Pendulum Model

The previous chapters have focused extensively on M-L ground force patterns: how they are characterised at the population, group, and individual levels; kinematic estimations of M-L ground force; and how the Inverted Pendulum Model compares to real ground forces. This chapter investigates the Inverted Pendulum Model in greater detail, beginning with its major assumptions. A kinematic analysis of the NOC II data show that the IPM produces a significantly different CoM trajectory than is observed in real walkers. A Modified Inverted Pendulum Model (MIPM) is proposed that eliminates small angle approximations made by previous versions of the IPM. Analysis also shows that the models are significantly more sensitive to M-L CoM-CoP separation than vertical separation, supporting the findings of Chapter 3. Finally, the MIPM and IPM models were applied to a single degree of freedom oscillator, showing that the assumption of a constant CoP location throughout a footstep can lead to significant over or under predictions of a hypothetical structure's response.

5.1 Key Assumptions

It has already been stated that the IPM makes seven assumptions about body movement during the gait cycle. The seven assumptions are worth deeper investigation in order to assess their validity and applicability to the IPM. The seven assumptions are:

1. The mass of a person can be estimated as a point mass acting at the person's CoM.

2. The legs are rigid; neither hip, knee, nor ankle motion/moments contribute to lateral ground force.

3. The upper body (specifically its angular momentum) does not contribute to lateral ground force.

4. There is no double stance phase; transition between feet is instantaneous and continuous.

5. The CoP remains fixed at a single point for each footstep.

6. The pendulum length L is assumed to equal $1.34h_t$, where h_t is the greater trochanter height [135, 126].

7. The angle between the pendulum and the vertical is approximately zero.

Assumptions one to three are concerned with the physical representation of the body. The first and third assumptions have been accounted for in the six-segment model of Townsend and are supported by the research of Herr and Popović, so are considered reasonable [122, 102]. The second assumption is more questionable since joint extension and flexion control the motion path of the Centre of Mass. Thus, omitting joints from the model implies a CoM motion path different from real gait. Even though the medial-lateral acceleration term of the IPM depends on CoM trajectory, neither Townsend's, nor more recent iterations of the model, address this physical deficiency.

Assumptions four and five address where the M-L ground force is felt by the individual. Townsend addresses the possibility of a moving CoP in the context of a tightrope walker or ice skater requiring instantaneous feedback; however he does not explore the case in detail, disregarding a moving CoP as a special case. The literature commonly reports (e.g. [148, 149, 150]) that up to 30% of the gait cycle is spent in double stance,

whereas the IPM assumes an instantaneous transition. An instantaneous transition between feet neglects the mechanics of contralateral weight shift, but the real mechanics of double stance are not well understood or modelled.

The final two assumptions are concerned with solving the mathematical model itself. The pendulum length represents the straight-line distance between the Centre of Mass and Centre of Pressure. This distance is approximately 1.2 m for most individuals but can vary by several hundred millimetres depending on the person's height [126, 67]. Making this or a similar assumption is practically unavoidable, however, because an individual's exact Centre of Mass is both variable and ambiguously located in the person's abdomen. Referring to Figure 1.7, the last assumption allows for the approximations $\ddot{\theta} \approx \ddot{y}/L$ and $L \sin\theta \approx L$, where y is the M-L displacement of the Centre of Mass. These result from small angle approximations of the angle complementary to θ.

The following analysis is primarily concerned with addressing assumptions two, four, five, and seven. Assumptions one and three will continue to be made based on the work of Townsend [122]. Assumption six will be discussed briefly but continue to be utilised for the practical reasons stated. In light of assumption five, the Centre of Pressure of the Inverted Pendulum Model is assumed to act at the second metatarsal marker (the 'toes') for the entire duration of the stance phase. The toe marker was selected for the CoP because the front of the foot spends a greater proportion of each stance phase in contact with the ground (approx. 80%) than the heel (approx. 50%), meaning it is less prone to M-L movement. Thus, the CoP was taken to be the mean lateral location of the second metatarsal marker across an entire stance phase.

5.2 Assumption Two and Model Configurations

The Inverted Pendulum Model's second assumption posits a rigid stick support between the Centre of Pressure and Centre of Mass. Therefore, the IPM precludes contributions from the hips, knees, or ankles to the ground force. A study of the applicability of the

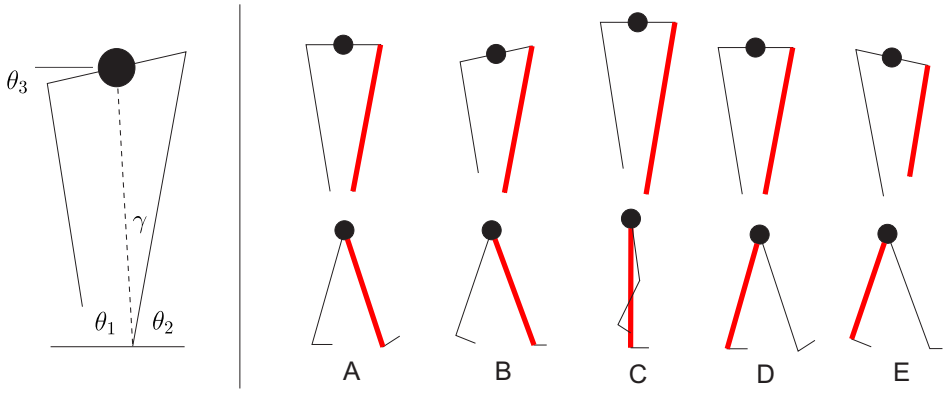

Figure 5.1: Left: Frontal plane anatomic angles based on experimental data; walker travelling out of the page. Right: The gait cycle in frontal (top row) and sagittal (bottom row) planes, with left leg red. (A) Left foot heel-strike, neutral hips. (B) Right foot toe-off, maximum pelvis angle. (C) Mid-stance, neutral hips (and highest CoM elevation). (D) Right foot heel-strike, neutral hips. (E) Left foot toe-off, maximum pelvis angle.

IPM's configuration suggests that geometric improvements might be possible, although at the expense of ease of implementation.

Consider the schematic of a pelvis and two legs in Figure 5.1. A point mass acts in the middle of the pelvis, which is assumed to be the total mass of the individual. The pelvis-leg joint is assumed to be a pin connection. This configuration of the legs and pelvis is promoted by Pandy *et al.*, who report that muscle activity in the hip abductor and adductor muscles promote double inverted pendulum motion rather than single inverted pendulum motion [94]. The angle θ_1 is the CoM-CoP-base angle, θ_2 is the base-CoP-hip angle, and θ_3 is the angle of pelvic tilt. The range of the angles for one footstep is typically between $80 - 90\,^\circ$ for θ_1 and θ_2 and $0 - 10\,^\circ$ for θ_3.

The three anatomic angles are plotted along with the M-L ground force over three successive steps (Figure 5.2). During double stance, the pelvic tilt (θ_3) progresses from neutral to maximum, peaking at toe-off or early single stance. This reveals a drop in the trailing (swing) hip relative to the standing hip. The hips regain their neutral angle before mid-stance, where they are at their highest elevation. The pelvic tilt remains neutral until the next heel-strike. This is shown in Figure 5.1 and is in agreement

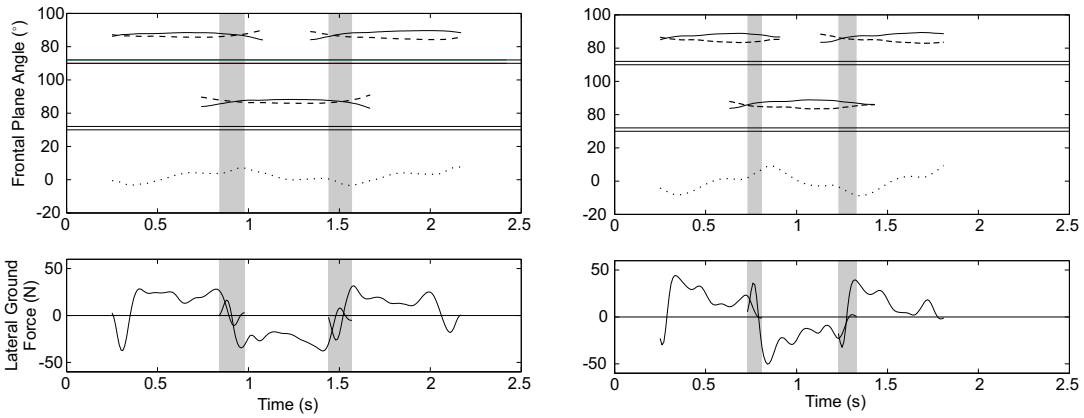

(a) (b)

Figure 5.2: Three-step trials for two subjects with shaded regions showing double stance. Top: Anatomic angles: CoM-CoP angle θ_1 (solid), and hip-CoP angle θ_2 (dashed). Pelvic tilt angle θ_3 (dotted) peaks at or just after toe-off, leveling out by mid-stance. Angles as shown in Figure 5.1. Bottom: The corresponding M-L ground force.

with MacKinnon and Winter [93]. The hip-CoP angle (θ_2) and the CoM-CoP angle (θ_1) exhibit a constant mean during stance. θ_1 increases from heel-strike to mid-stance before decreasing to the mean near toe-off. In contrast, θ_2 decreases from heel-strike to mid-stance before returning to the mean near toe-off. The sum $\theta_1 + \theta_2$ lies almost exclusively in the range $170 - 175°$. With a stance phase standard deviation less than $0.5°$, the CoM-CoP-hip angle (γ in Figure 5.2) remains constant throughout the stance phase. A constant γ implies that the pelvis and leg tandem moves as a rigid, inverted pendulum-like frame, but the alteration of the pelvis angle and the rise and fall of the hip due to motion in the sagittal plane make the motion of the CoM more nuanced.

Tesio *et al.* show that the frontal plane trajectory of the Centre of Mass may be described by a figure eight pattern [101]. Data collected by the present author corroborates these findings, as depicted in Figure 5.3. At heel-strike the CoM is located to one side of the anatomic centre line. The CoM then swings across the centre line and slightly upward before toe-off of the trailing foot. The lateral kinetic energy is converted to vertical kinetic energy, which carries the CoM upward to its maximum elevation (peak potential energy) at mid-stance. Then potential energy is converted

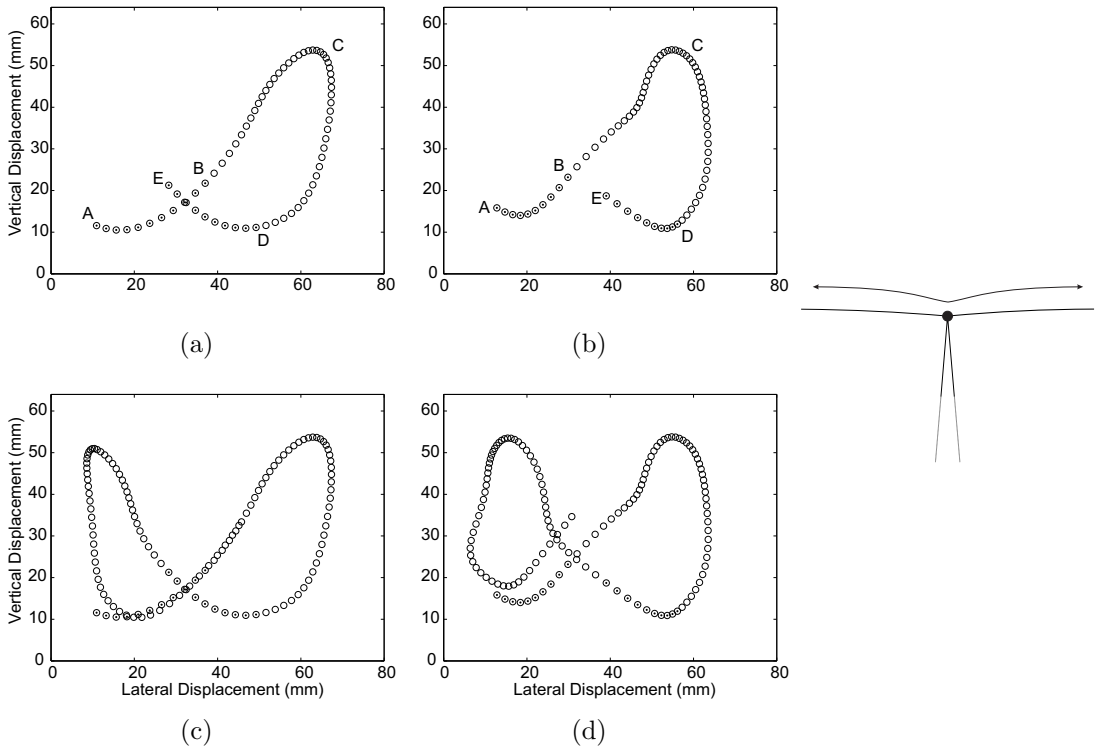

Figure 5.3: Frontal plane CoM trajectory as seen from behind. (a) and (b): CoM motion over one step with double stance periods represented by filled circles; (c) and (d): CoM motion over two steps; no data is available for double stance at the end of the second step. Gait cycle landmarks: (A) right heel-strike, (B) left toe-off, (C) mid-stance, (D) left heel-strike, and (E) right toe-off. Trajectory of the IPM shown at right.

back to kinetic energy as the CoM swings down and slightly towards the centre while the swinging leg extends forward for the next heel-strike. This is repeated for the second leg, developing the figure eight pattern.

For comparison, the Centre of Mass trajectory implied by the Inverted Pendulum Model is comprised of two concave downward arcs (Figure 5.3). Heel-strike occurs at the junction of the arcs with mid-stance occurring at the extreme left and right sides. By increasing θ_1 or decreasing the step width, the discontinuity between left and right support foot CoM trajectories may be minimised but not eliminated. This would produce a flat trajectory, parallel to the ground. Where the CoM trajectories presented in Figure 5.3 show a smooth transition from step to step, the Inverted Pendulum Model

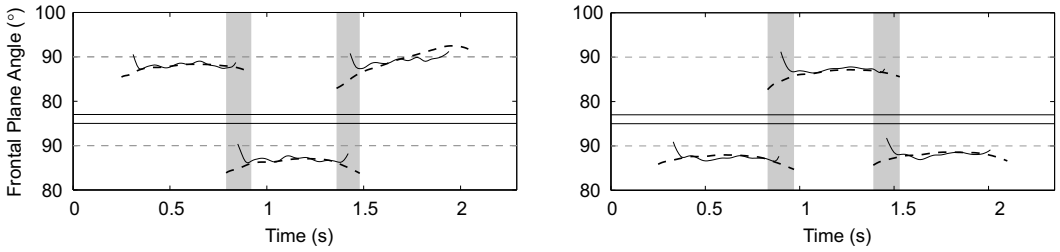

(a) (b)

Figure 5.4: Ground reaction force angle (solid) versus left and right CoM-CoP angles (dashed) for two trials. Left footsteps at top of plots. Gray bands show periods of double stance.

requires extra energy to overcome losses incurred by passing through double stance.

MacKinnon and Winter stated that pelvic tilt was an important function of maintaining lateral stability during walking [93]. Pelvic tilt corresponds to the activation of the hip abductor muscles, which provide the dominant frontal plane torque for stabilising and initiating medial-lateral CoM acceleration [93, 94, 96]. A double inverted pendulum in single stance, such as that discussed by Pandy *et al.*, or a four-bar linkage in double stance allow for the requisite kinematics shown in Figures 5.2 and 5.3, whereas the traditional single IPM does not [94]. Ultimately, however, implementing such a model(s) would be analytically and experimentally more complicated than using the single inverted pendulum, for which its simplicity is a major asset. In subsequent sections other assumptions will be addressed to improve the IPM without altering its geometry. That said, alternative geometries may yet prove useful in future work particularly as more is learned about double stance.

5.3 Assumption Seven and Angle Equivalence

Before addressing assumptions four and five, the CoM-CoP-ground angle (θ_1) is examined. Assumption seven requires this angle to be close enough to vertical that small angle approximations may be used. Figure 5.4 shows θ_1 for left and right feet along with the angle of the ground reaction force, $180 * \tan^{-1}(F_z/F_x)/(2\pi)$. A high correla-

tion is observed between the ground reaction force angle and the CoM-CoP angle. The maximum ground reaction force and CoM-CoP angles occur at mid-stance between $85 - 90\,^{\circ}$. Before and after mid-stance, the ground reaction force and CoM-CoP angle decreases to $80 - 85\,^{\circ}$. The biggest difference between the two angles occurs during double stance, when the angle of the ground reaction force exceeds $90\,^{\circ}$, indicating a change in support from one foot to the other.[1] The similarity of the angles throughout the stance suggests that the ground reaction force is always directed from the Centre of Pressure towards the Centre of Mass, agreeing with Zijlstra and Hof [125] and Hof [151]. This relationship can be exploited to eliminate the need to rely on θ_1, thereby avoiding the need to use small angle approximation as well.

5.3.1 Equal Angles Model

Based on Figure 5.4, the relationship between the ground reaction force angle and CoM-CoP angle is given by:

$$\tan^{-1}\left(\frac{F_z}{F_x}\right) = \tan^{-1}\left(\frac{z_{CoM} - z_{toe}}{x_{CoM} - x_{toe}}\right) \tag{5.1}$$

implying an equation for the M-L ground force, F_x:

$$F_x = F_z\left(\frac{x_{CoM} - x_{toe}}{z_{CoM} - z_{toe}}\right). \tag{5.2}$$

This is very similar to the relationship identified by Zijlstra and Hof [125], but Equation 5.2 is used for inverse dynamics rather than determination of CoM position. Note that by applying the assumptions of the Inverted Pendulum Model to Equation 5.2 we also obtain the IPM as derived by Macdonald [67]. Substituting $m_p g$ as an approximation of F_z, $(y - u)$ for the numerator, $L\sin\theta_1$ for z_{CoM}, zero for z_{toe} and $m_p(\ddot{x} + \ddot{y})$ for F_x, a right angle approximation of θ_1 yields the Inverted Pendulum Model,

$$m_p(\ddot{x} + \ddot{y}) = m_p g\left(\frac{y - u}{L\sin\theta_1}\right) \rightarrow \ddot{y} + \Omega_p^2(u - y) = -\ddot{x}. \tag{5.3}$$

[1] The curves start and end at different times due to the change of sign of M-L GRF, determined from the sum of the forces across both feet. The mid-double-stance discontinuity is thus when the total M-L force is zero. Even if the GRF had been depicted for each foot separately, the M-L GRF would be lateral at the beginning and end of stance, divergent from the CoM-CoP angle.

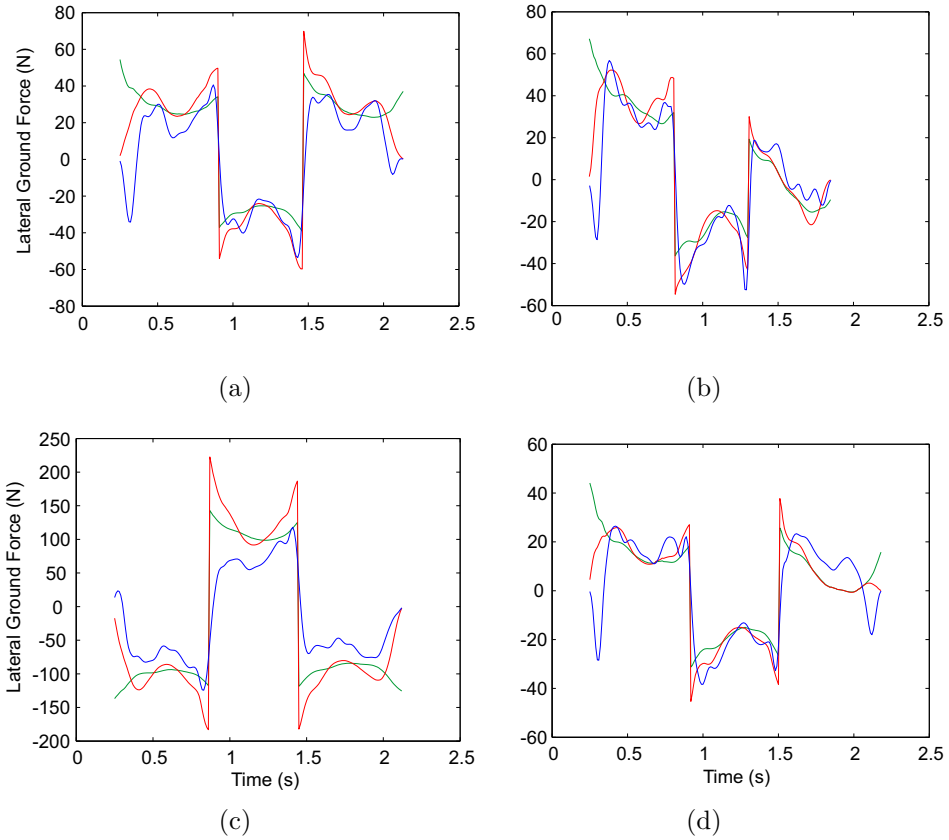

Figure 5.5: Trials showing real M-L force data (blue) versus EAM (red) and IPM (green). EAM calculated by assuming the CoP is fixed at the point of the second metatarsal.

The Inverted Pendulum Model *should* therefore produce an accurate reproduction of M-L ground forces yet the results of Claff *et al.* suggest that there is an error in the Inverted Pendulum [18]. If the model does not produce an accurate prediction, the error is most likely due to the assumptions made in developing the Inverted Pendulum. A validation of the results from Claff *et al.* and an investigation of the assumptions made by the Inverted Pendulum Model follows via a comparison of the parameters used in each model [18].

5.3.2 Comparison of Models

For the following discussion, Equation 5.2 will be referred to as the Equal Angles Model (EAM). Figure 5.5 presents four typical three-step trials. The blue curve represents

the sum of the M-L force data recorded by the force plates, while the red and green curves present the Equal Angles Model and the Inverted Pendulum (IPM) respectively. For both the EAM and the IPM, motion capture and vertical force data were plugged into the model to reproduce the M-L force recorded by the force plate. Since the EAM and IPM are both piecewise functions depending on which is the standing foot, the double stance phase is neglected.

The lateral position of the CoM and CoP are approximated in both models as the locations of the pelvic midpoint and the second metatarsal, respectively. The CoP approximation is appropriate for the IPM, which assumes the Centre of Pressure location remains fixed during each step (assumption five) [122, 126, 67].

The differences between the models are thus threefold:

1. For the vertical force component, the force plate data (ΣF_z) was used for the EAM. The constant $m_p g$ was used for the IPM.

2. The CoM height was assumed to be $1.34 h_t$ for the IPM [126, 67]; the mean height of the pelvic markers was used in the EAM [125].

3. θ_1 was approximated as $90\,^\circ$ for the IPM. The EAM does not rely on any angle measurements.

Confirming the NOC I tests, the Inverted Pendulum Model does not predict the real data precisely. The Model's smooth trajectories through the mid-stance phase do not capture the oscillations of the real M-L force. Moreover, the slope of the Inverted Pendulum Model during the instantaneous transition between steps is too steep; it does not account for any transitional behaviour that occurs during the double stance phase. The Equal Angles Model is closer to the real data, but also fails to accurately predict some behaviour. Like the Inverted Pendulum, the EAM produces smoother curves than the real M-L ground force data in mid-stance. The EAM tracks the real

data better than the IPM during double stance although it tends to over-predict the amplitude of the heel-strike, occasionally significantly.

Among 38 trials, the mean r^2 coefficient of determination between the Inverted Pendulum Model and the real data was 0.5537 while it was 0.6730 between the Equal Angles Model and the real data. In none of the 38 trials was the IPM correlation higher than the EAM correlation. This shows that the Equal Angles Model – with only the three differences identified above – is a superior model for recreating the real M-L ground force exerted by a walker. Nonetheless, the correlation between the EAM and the real data is only 0.6730. If the ground force angle and the CoM-CoP angle are indeed equal and predicted by Equation 5.1, the correlation between the EAM ground force and the real ground force should be much higher.

5.4 Assumption Five and Centre of Pressure Variation

In Equation 5.2 the most sensitive variable appears to be the change in CoM height in the denominator. Equation 5.1, however, shows that both the ground reaction force angle and the CoM-CoP angle are tangent functions. The denominator $(x_{CoM} - x_{toe})$ is thus very important. With $\theta_1 \approx 90\,^\circ$, $x_{CoM} - x_{toe} \approx 0$, so the equation is particularly sensitive to variations of the M-L CoM-CoP separation.

Figure 5.6 shows a range of left foot CoP tracks. Heel-strike occurs at the bottom of the panels and toe-off occurs at the top. As the subject travels forward (upward in each panel), the CoP moves forward as well. From left to right, the examples show an increase in the width through which the CoP tracks. In some cases it appears that the variation is due to lateral foot turn-out, whereas in others the trace of the CoP progresses in a backward question mark shape (i.e. panels 2, 4, 8, like those observed in Chapter 3. In the left-most case, the track is nearly straight, indicating that the individual did not vary their Centre of Pressure at all (laterally), but in the right

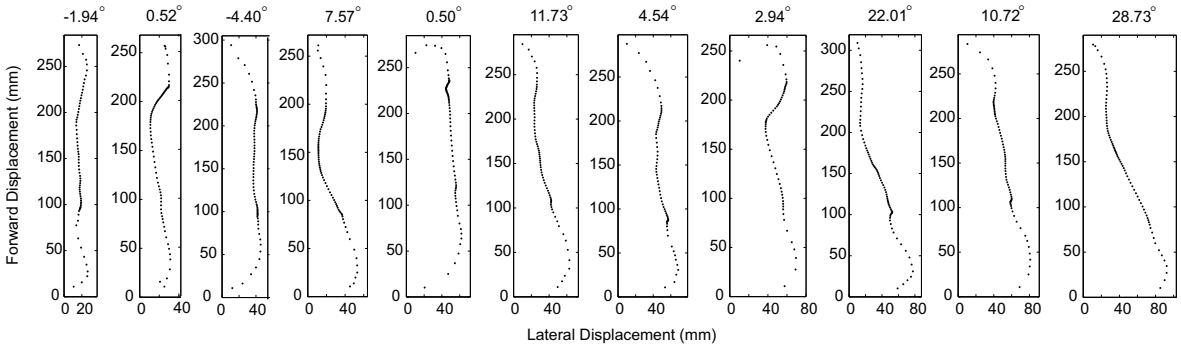

Figure 5.6: The CoP trajectory of 11 left footsteps arranged from least to most lateral displacement. Approximate angle of foot progression (lateral turn-out) given above each sample. The second and fifth trajectories were recorded by the same individual, as were the fourth and tenth trajectories, showing that while progression angle may not be prone to intra-subject variability, the lateral range of CoP trajectory is.

most case, the CoP exhibits a lateral range of 81.5 mm. Table 5.1 shows the mean and standard deviation of the M-L Centre of Pressure displacement for each of the participants' left and right feet. Left and right feet were treated separately because individuals could exhibit left-right bias in their walking. The total mean and standard deviation were calculated by taking the average of the participant means and standard deviations shown. Left feet show significantly higher range than right feet. This was possibly caused by the participants making a right turn around the figure eight track before crossing the force plates, even though approximately two metres of straight track preceded the force plates.

Table 5.1 also provides an estimation of the foot progression (lateral turn-out) angle for each of the participants. This estimate was obtained by taking the angle between the global reference frame – aligned with the force plates – and the line joining the second metatarsal marker and the heel marker at every time-step. These were then averaged over the duration of the stance phase. These angles are considered estimates for two reasons. First, both the toes and heel are simultaneously on the ground for at most $10 - 15\%$ (< 0.1s) of the stance phase per double stance. During the remainder of the step when the heel or toes are off the ground, the markers can move with respect to each other. Secondly, depending on the shoe and the participant's anthropometry,

Table 5.1: Means and Standard Deviations of CoP Displacement and Foot Progression (turn-out). Negative progression corresponds to turn-in.

	Left Foot				Right Foot			
	Range		Progression		Range		Progression	
Subject	Mean (mm)	St Dev (mm)	Mean (deg)	St Dev (deg)	Mean (mm)	St Dev (mm)	Mean (deg)	St Dev (deg)
$F1$	77.247	19.755	6.314	0.896	27.146	11.808	3.632	1.994
$F2^*$	116.354	9.879	14.783	0.464	32.526	-	10.097	-
$F3$	50.275	18.531	0.854	1.290	27.934	10.068	2.789	1.611
$F4$	52.232	14.593	1.931	0.601	23.391	0.472	2.259	1.992
$F5$	41.592	10.005	-1.573	2.116	20.014	2.106	-2.736	2.681
$F6$	39.641	8.931	9.037	1.832	24.449	8.068	3.976	1.571
$F7$	51.187	17.005	9.294	2.148	32.475	5.511	7.018	2.866
$F8^*$	38.297	28.318	1.841	3.816	15.227	-	3.655	-
$M1$	14.831	1.192	-1.967	0.045	49.134	10.166	-8.495	1.091
$M2$	79.586	4.274	28.590	0.145	31.522	6.352	13.191	2.016
$M3^*$	72.645	7.358	22.859	1.197	23.125	-	3.897	-
Mean	57.626	12.713	8.360	1.323	27.904	4.959	3.571	1.438

*Only one right foot strike was recorded.

the two markers may not have been aligned with the axis of the foot. The estimation is acceptable, however, because it is intended to provide only a general indication of the influence of foot progression on lateral CoP displacement. The table and Figure 5.6 suggest that CoP displacement may be affected both by foot progression and by the participant's unique gait.

Both assumptions five and seven can be tested by calculating the Equal Angles Model using the real Centre of Pressure data instead of the mean toe position. Since the force plates record an exact CoP location for each foot over time, an interpolation of CoP position needs to be taken during double stance. A linear interpolation was therefore assumed for the Centre of Pressure transition between successive steps.

Substituting the real CoP location for (x_{toe}, z_{toe}), Equation 5.2 may be written as:

$$F_x = F_z \left(\frac{x_{CoM} - x_{CoP}}{z_{CoM} - z_{CoP}} \right). \tag{5.4}$$

It is proposed that this variant of the Equal Angles Model be identified as the Modified Inverted Pendulum Model (MIPM).

Figure 5.7 depicts the same four trials as Figure 5.5 showing the MIPM instead of the EAM. The CoP trace of each force plate strike is shown along with the linear interpolation between the CoP traces. The Modified Inverted Pendulum comes very

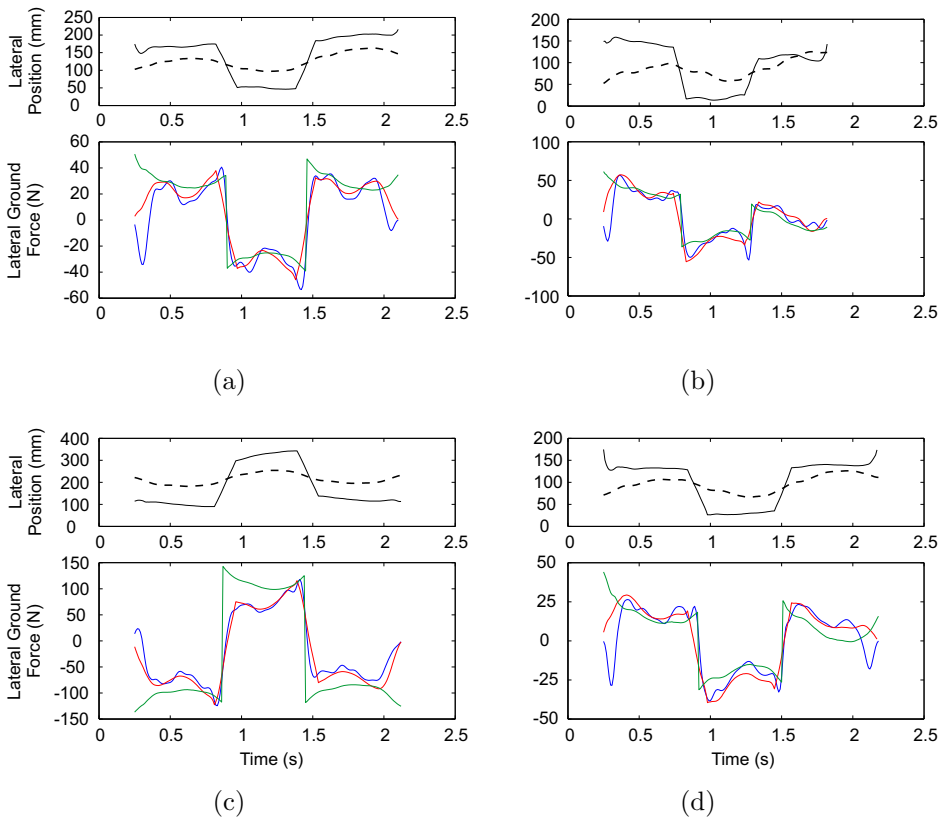

Figure 5.7: Top: Lateral location of CoP (solid) and CoM (dashed) over three steps. CoP position interpolated linearly during double stance to produce composite record. Bottom: Real M-L ground force data (blue) versus MIPM (red) and IPM (green). IPM to ground force r^2 coefficients: (a) 0.643, (b) 0.623, (c) 0.733, and (d) 0.506. MIPM to ground force r^2 coefficients: (a) 0.848, (b) 0.794, (c) 0.956, and (d) 0.758.

close to matching the real M-L force data. In every one of the 38 trials, the r^2 correlation between the MIPM and the real data was higher than that between the IPM and the data. The difference in r^2 correlation between the MIPM and IPM for the four samples in Figure 5.7 ranges from 0.171 to 0.252. The mean MIPM correlation to real data among the 38 trials is 0.7880, an increase of 0.115 compared to EAM correlation.

The trials used here do not portray the beginning nor end double stance phases correctly since data from the preceding and succeeding steps are unavailable. By omitting the first and last 0.1 s from each sample, the mean IPM correlation rises to 0.8062 and the mean MIPM correlation rises to 0.8957. This is an increase in both correlations, but shows that the MIPM matches the data much better than the IPM.

Table 5.2: Parameters required for IPM versus MIPM.

	IPM	MIPM
F_x	Output	Output
F_z		$\approx mg$
Mass (m_p)	Required	m_p or F_z
CoM location (x,y,z)	Output	Required
CoP location (x,y)	$\approx u$	Required
Margin of Stability (b_{min})	Required	
Leg length (L)	Required	
Gait cycle frequency (f_p)	Required	

5.5 Applications of the MIPM

This section investigates the broader applicability of the MIPM by developing a pair of simple models. The first model shows the potential future benefits of incorporating CoM and CoP kinematics into inverted pendulum models. The second model applies a forcing function based on a variable CoP trajectory to a SDOF oscillator, representing a bridge. The result is compared to the force produced by a static CoP, as per the IPM, in order to investigate the sensitivity of a hypothetical bridge model to CoP variation.

5.5.1 General Applications and Limitations

Important considerations when developing the MIPM are the model's applicability and limitations. Table 5.2 compares the parameters used for the IPM and the MIPM. The IPM requires the mass, leg length, and gait cycle frequency in addition to some estimate of u. Macdonald estimates u by using Hof's Extrapolated Centre of Mass, which further requires the margin of stability (b_{min}) and the initial velocity of each footstep. Even though the CoM location, and therefore velocity, can be predicted, b_{min} must be assumed.

In structural design applications using the IPM, the mass of the individuals, the leg lengths, and the gait cycle frequencies can be selected from a normal distribution. From these parameters and initial conditions for CoM position and velocity, the value of the constant u is determined. The CoM motion and ground force for the first footstep can then be calculated. The final CoM position and velocity then serve as the initial

conditions for the second footstep. Another prediction is made for u, and the process is repeated.

The IPM is useful because it requires just a few deterministic measurements. On the other hand, the incorrect kinematics cause errors in ground force prediction both directly and via the step width calculation. On a stationary base symmetrical gait produces a stable and reasonable outcome, but it has been shown that this is not representative of real ground forces.

Table 5.2 shows, in contrast, that the MIPM requires fewer inputs than the IPM. The deterministic values used for the IPM are exchanged for the real CoM and CoP positions. The resulting predictions – shown in the previous sections – are more accurate than the IPM because they are based on actual CoM-CoP separations rather than a constant leg length and CoP position. The main deficiency of the model is that it requires the user to have some knowledge about what the real CoM and CoP trajectories are.

In laboratory analysis, CoM and CoP motion can be tracked using motion tracking cameras and either force plates or pressure sensitive insoles, producing results like those shown above. Obtaining these data in the field, however, is more challenging because of logistic difficulties. The capture area on a real bridge is likely much greater than the range of normal laboratory motion tracking cameras. In addition, weather conditions need to be ideal in order to minimise glare in the cameras. The previous chapter discussed that optical tracking is also limited when it comes to recording an individual in a crowd.

But the improved accuracy of the MIPM compared to the IPM in a laboratory setting suggests that a more comprehensive understanding of CoM and CoP motion would be beneficial. The IPM is kinematically constrained, whereas the MIPM permits the possibility of introducing separate motion equations for the CoM and CoP. If models can be produced that describe the CoM and CoP trajecotries, then their insertion into

Table 5.3: Values used in parametric study.

A_1	20 mm	Φ_1	0 rad
A_2	10 mm	Φ_2	$2\pi/3$ rad
A_3	10 mm	Φ_3	π rad
A_4	10 mm	Φ_4	$-\pi/5$ rad
$\bar{h}_{CoM}$	1000 mm	v_p	1.2 m s^{-1}
m_p	70 kg	δ	100 mm

the MIPM should yield an improved prediction of ground force.

To illustrate the MIPM's potential, an exploratory set of parametric kinematic equations was developed. The equations describe motion of the CoM and CoP as sinusoidal functions of time:

$$x_{CoM} = A_1 \sin(\omega_p t + \Phi_{p1}) \tag{5.5a}$$

$$y_{CoM} = v_p t \tag{5.5b}$$

$$z_{CoM} = A_2 \cos(2\omega_p t + \Phi_{p2}) + A_3 \sin(2\omega_p t + \Phi_{p3}) + \bar{h}_{CoM} \tag{5.5c}$$

$$x_{CoP} = A_4 \sin(\omega_p t + \Phi_{p4}) \pm \delta/2. \tag{5.5d}$$

The parametric equations for CoM position are derived from equations describing the Cartesian position of a point moving on the surface of a cylinder oriented in the z-axis. ω_p is the gait cycle frequency; note that z_{CoM} oscillates at twice the gait cycle frequency. x_{CoM} is represented as a simple sinusoid of amplitude A_1. The A-P position of the CoM is the product of walking velocity v_p and time. Coefficients A_2 and A_3 describe the vertical amplitude of the CoM trajectory and $\bar{h}_{CoM}$ is the mean CoM height. The M-L position of the CoP is described by a sinusoid with amplitude A_4 and a step width offset, δ, that switches sign every footstep. Finally, the Φ_i values correspond to phase angles in radians. Note that each component may be out of phase from the other components. This allows the model to reproduce the characteristic figure eight trajectory of the CoM.

The M-L ground force can be predicted by inputting Equations 5.5a, 5.5c and 5.5d into the MIPM. Using the parameters in Table 5.3, a realistic combination of CoM trajectory, CoP trajectory, and M-L ground force are produced, as seen in Figure 5.8.

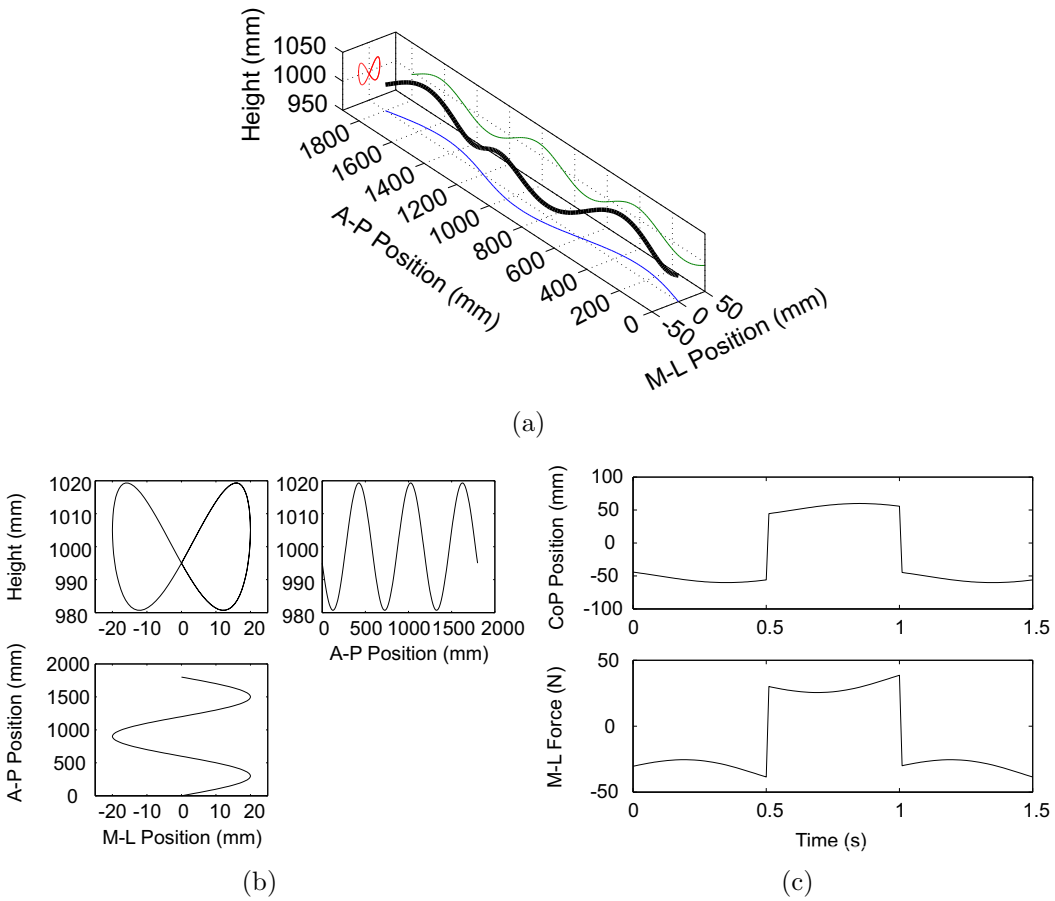

Figure 5.8: (a) and (b) Kinematics of CoM based on simple parametric equations. (c) Constructed CoP trajectory (top) and MIPM ground force (bottom) for three footsteps.

The frontal plane trajectory has a figure eight shape of approximately 40 mm vertical range and 40 mm lateral range. The bottom-left pane of Figure 5.8(b) shows that the M-L position of the CoM is sinusoidal with no phase lag. In comparison, Figure 5.8(c) shows that the M-L CoP position – though sinusoidal – has been phase shifted to reflect a quasi-question mark shape. The resulting M-L ground force is similar in shape and amplitude to the theoretical IPM (Figure 1.8). It is smooth because simple equations for the CoM and CoP have been used. If more appropriate equations can be found for the motion of the CoM and CoP, then the MIPM should prove to be a more accurate model than the IPM for design purposes.

5.5.2 Application to a SDOF Oscillator

To test the influence of Centre of Pressure location on M-L ground force and, more importantly, structural vibrations, the Inverted Pendulum Model and the Modified Inverted Pendulum Model were applied to a single degree-of-freedom (SDOF) oscillator, representing a structure such as a footbridge. The IPM and MIPM were both constructed from the left footstep and corresponding data record shown in Figure 5.6 panel eight, step L_1 (female, age 24, height 1.75 m, mass 65.6 kg). For this simple model, the IPM and MIPM do not receive feedback from the oscillation of the SDOF structure; nor do they contribute added damping or mass (Section 1.1.2).

A symmetric and periodic forcing function was constructed based on the MIPM of the data. To produce a symmetric forcing function, the CoP and CoM motion for L_1 should thus be mirrored about and translated along the y-axis to replicate a full gait cycle. Thus, instead of producing a sequence L_1, R_1, L_2, R_2, the sequence consists of steps $L_1, L_1', L_{1+T}, L_{1+T}'$ where L_1' is a mirror of L_1 and T denotes translation over one gait cycle period. From the original 3-step record, it was observed that L_1 overlapped with the subsequent right footstep (R_1) by five time steps, or 0.05 s. A mirror of the CoP data, L_1', was thus initiated at the start time of R_1. The location of the first CoP data point, $(x_{L_1'}, y_{L_1'})$ was set equal to the location of the first data point in (x_{R_1}, y_{R_1}). Following the same method, steps L_{1+T} and L_{1+T}' were also created. Having defined four footsteps with three double stance periods, the composite double stance location of the CoP was chosen to be a linear interpolation of the CoPs of the departing and arriving feet.

The Centre of Mass trajectory was developed in a similar manner. The three-dimensional CoM trajectory during L_1 was mirrored about the y-axis. Since the CoM trajectory for L_1 includes the double stance region phasing into R_1, the L_1' CoM trajectory was located such that $(x_{L_1,f}, y_{L_1,f}) = (x_{L_1',5}, y_{L_1',5})$: the last sample in L_1 was matched to the fifth sample in L_1'. As with the CoP data, the CoM trajectory was

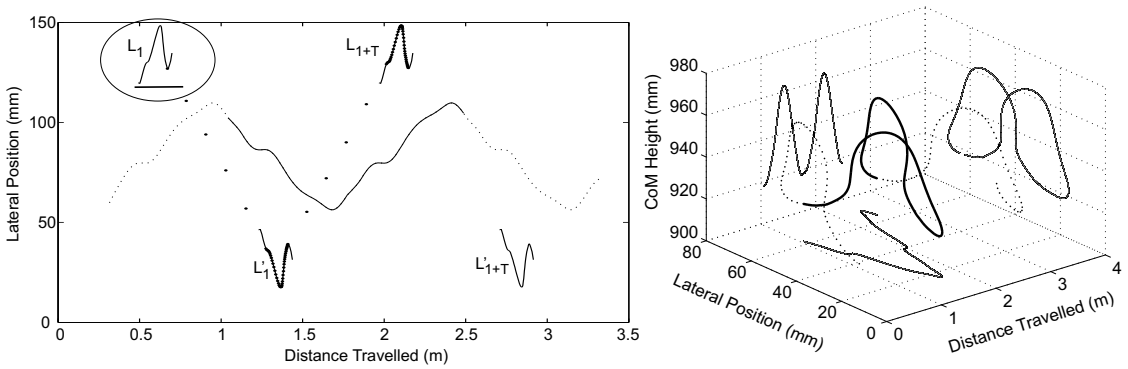

(a) (b)

Figure 5.9: (a) The composite four-step CoP (solid lines) and CoM trajectory (small dots) based on the original left foot CoP trajectory (circled) and its corresponding CoM trajectory. Sample trimmed to modular two-step sample (CoP, bold dots; CoM, bold line) for application to SDOF. Black bar shows mean lateral toe position used for IPM. (b) Constructed CoM trajectory in 3D.

repeated to create a periodic 4-step sample. Then the data in the double stance regions were linearly interpolated in three dimensions. To ensure symmetry in the M-L force record, the mean lateral position of the CoM trajectory was translated laterally to match the mean lateral position of the CoP record, an offset of 8.5 mm.

Since the MIPM also requires a vertical force record, the F_z force plate record of L_1 was reproduced for L'_1, etc, and the double stance regions summed. Finally, the composite data record – including the CoP, CoM, and vertical force – was trimmed from the heel-strike of L'_1 to the heel-strike of L'_{1+T}, resulting in a modular 2-step record complete with double stance regions. The finished record can be seen in Figure 5.9.

The forcing function for the IPM was developed from Equation 1.25. The parameters used in the model are identified in Table 5.4. The biometrics were measured at the time of the test, with the exception of the pendulum length. The trochanter height h_t was calculated from the measured ASI height (h_{ASI}) and the subject's total height (h_p), based on the anthropometric relations given by de Leva [92]. This was multiplied by 1.34 according to assumption six. δ was selected as the distance between the means of the toe marker position for L_1 and L'_1. The forcing frequency f_p was selected to

Table 5.4: Parameters Required for Application of the IPM and MIPM to an SDOF Oscillator. Based on data from footstep of one subject (see text). *FPs* corresponds to *Force Plates*.

	F_z	x_{CoP}	x_{CoM}	z_{CoM}	z_{CoP}	m_p
MIPM	From FPs	From FPs	From Markers	From Markers	0	65.6 kg
	δ	$u = \pm\delta/2$	$L^{\ddagger}$	$\Omega_p = \sqrt{g/L}$	f_p	m_p
IPM	73.6 mm	±36.8 mm	1.044 m	3.07 rad s^{-1}	1.0 Hz	65.6 kg
	m_b	K	ω_b	ξ_b		
SDOF	950 kg	Varies	1.26-13.8 rad s^{-1}	0.02		

$^{\ddagger}L = 1.34(h_{ASI} - R_{ASI}h_p)/(1 - R_{ASI})$ where $R_{ASI} = (h_{ASI} - h_t)/h_p$. [92]

match the record produced for the MIPM, which depends on the durations of the CoP sample and the double stance phase.

Since the IPM and MIPM have the same forcing frequency, both were extended to 50 cycles and applied to an SDOF oscillator with mass 950 kg and 2% damping. The oscillator's natural frequency f_b was incremented from 0.2 to 2.2 Hz, causing the frequency ratio $\beta = \omega_p/\omega_b$ to pass through resonance. The resulting oscillator displacement was solved using a numerical approach to Duhamel's Integral in MATLAB [152]:

$$\begin{aligned} x &= A\sin\omega_b t - B\cos\omega_b t \\ A &= \frac{1}{m_b\omega}\int_0^t p(\tau)\cos\omega\tau\,\mathrm{d}\tau \\ B &= \frac{1}{m_b\omega}\int_0^t p(\tau)\sin\omega\tau\,\mathrm{d}\tau \end{aligned} \tag{5.6}$$

where $p(\tau)\,\mathrm{d}\tau$ is an impulse function at $t = \tau$ to be represented by the (discretised) forcing function; m_b is the oscillator mass; and ω_b is its natural frequency (rad s^{-1}).

The forcing functions and peak structural response are shown in Figure 5.10. The IPM forcing function – with its characteristically smooth mid-stance region and instantaneous weight transfer – has a lower magnitude than the force exerted by the MIPM for most of each step. The MIPM forcing function, in contrast, has an early peak followed by a sharp decline down to the amplitude of the IPM. As a result the displacement response of the SDOF oscillator to the IPM has a maximum amplitude of approximately 60% of the MIPM regardless of frequency ratio. Figure 5.10(b) shows

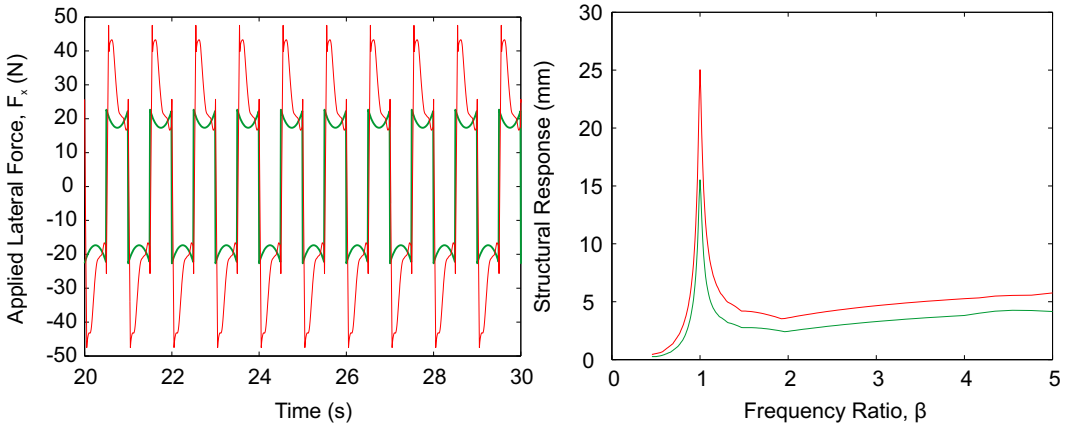

(a) (b)

Figure 5.10: Comparing IPM (green) and MIPM (red) as applied to an SDOF oscillator. (a) Forcing function excerpt; (b) Peak displacement response over a range of frequency ratios, $\beta = \omega_p/\omega_b$.

that the peak response at resonance is 25 mm for the MIPM compared to 15.5 mm for the IPM. Figure 5.11 compares the displacement response of the oscillator to each model at and away from resonance. The IPM produces a consistently lower amplitude response than the MIPM during both the transient and steady state regions. Figure 5.9 shows that the mean position of the toe marker was just medial of the first CoP point. Thus, it follows that the predicted force using the IPM should be less than that of the MIPM; ergo for the SDOF displacement as well.

The method was repeated for another left footstep, this time the subject with 21.47 degrees of foot progression (male, age 27, height 1.85 m, mass 98.8 kg). Notably, the mean position of the toe marker rested lateral of the CoP trajectory by 15.2 mm. The resulting forcing functions, peak displacement response, and the structural displacement at resonance are seen in Figure 5.12. Since the mean toe position lies outside the CoP trajectory, the IPM forcing function over-predicts the MIPM forcing function. The IPM structural response is also greater than the MIPM response. The peak lateral response at resonance is 89 mm for the IPM compared to 66.6 mm for the MIPM. The higher structural response reflects the fact that the IPM force is greater than the MIPM force.

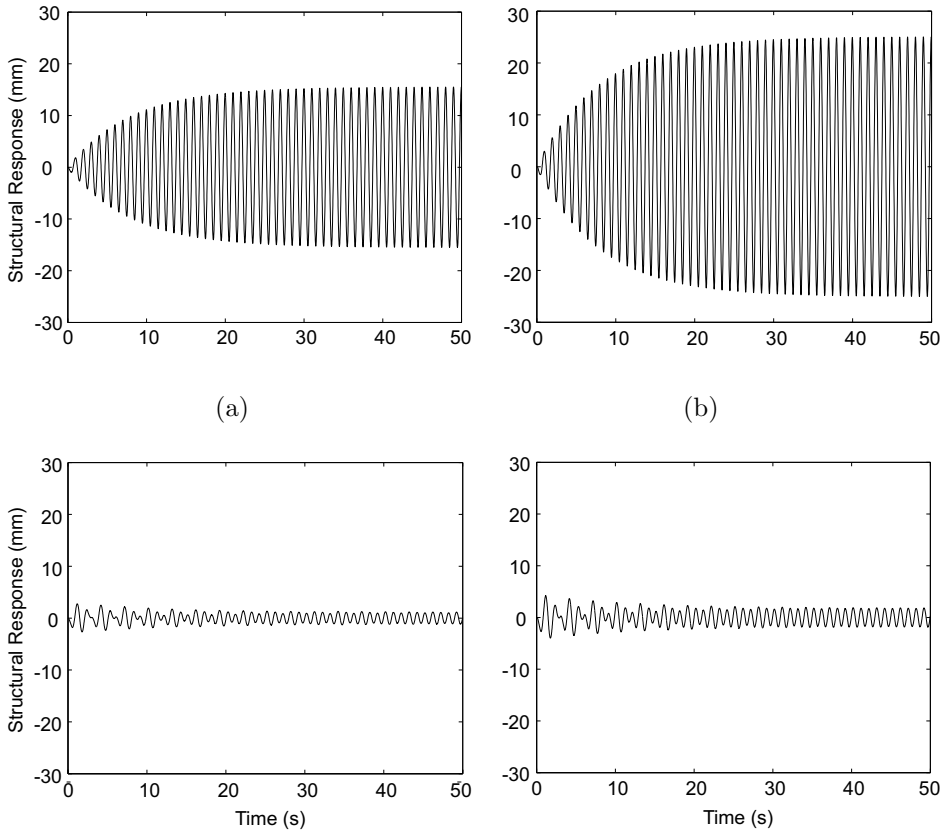

Figure 5.11: SDOF displacement responses shown for (a) IPM resonance, (b) MIPM resonance, (c) IPM at $\beta = 1.5$ and (d) MIPM at $\beta = 1.5$.

The lateral position of the Centre of Pressure thus makes a significant contribution to the IPM or MIPM, in agreement with Herr and Popović [102]. Due to the fact that an inverted pendulum-based model requires division by the narrow CoP-CoM distance, the location of the CoP should not be assumed to act at a single point without the admission of significant error, unless the mean of the CoP path can be determined precisely. Instead, it would be preferable to characterise lateral CoP position as a time-varying function. This merits further study as CoP motion is subject to a significant amount of both inter- and intra-subject variability, even for stable-ground walking (Figure 5.6).

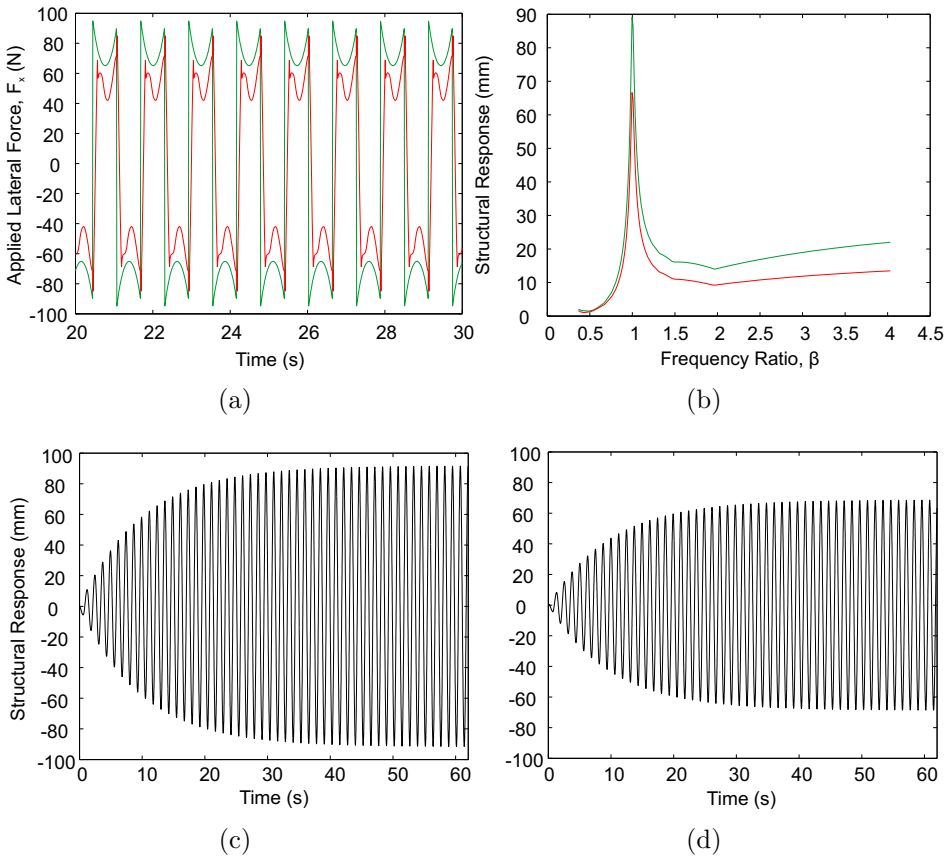

Figure 5.12: Comparing IPM (green) and MIPM (red) as applied to an SDOF oscillator. (a) Forcing function excerpt; (b) Peak displacement response over a range of frequency ratios, $\beta = \omega_p/\omega_b$. Oscillator displacement response at resonance for (c) IPM and (d) MIPM.

5.6 Discussion

Seven assumptions of the Inverted Pendulum Model have been identified. Of these, assumptions (1), (2), (3), and (6) are shown to be reasonable. The sixth assumption, stating that the height of the Centre of Mass is located at 1.34 times the leg length, was originally accepted because of the necessity of selecting an easily determinable CoM height. Hof states that this is the real pendulum length but technically the CoM is lower in the abdomen at approximately $1.11h_t$ [126]. Based on the MIPM, however, the assumption is reasonable because of the relative insensitivity of the vertical CoP-CoM separation compared to the horizontal separation. Figure 5.13 shows the Modified

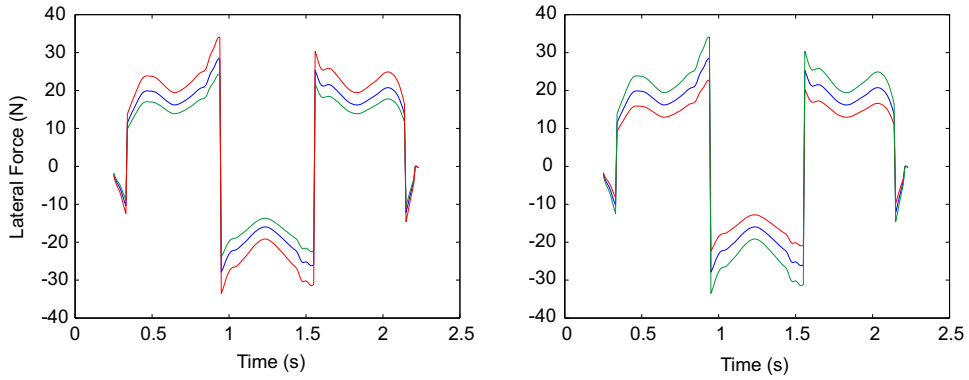

(a) (b)

Figure 5.13: (a) Model sensitivity of CoM height at 1000 (red), 1200 (blue), and 1400 mm (green) as compared to the (b) model sensitivity of the step half-width at 20 (red), 25 (blue), and 30 mm (green).

Inverted Pendulum calculated assuming a pendulum length of 1000 mm, 1200 mm, and 1400 mm for a fixed lateral displacement ($x_{CoP} - x_{CoM}$) of 25 mm. The figure also shows the MIPM calculated assuming a lateral separation of 20 mm, 25 mm, and 30 mm for fixed pendulum length of 1200 mm. The predicted variation caused by changing the height by 400 mm is similar to the variation caused by changing the CoM-CoP width by 10 mm. With the CoM trajectory typically varying by 20-50 mm vertically, the model is less sensitive to the height of the CoM than the medial-lateral separation between it and the CoP.

The remaining three assumptions, (4), (5), and (7), require additional consideration. It has been shown that the location of the Centre of Pressure relative to the Centre of Mass is of critical importance to the accuracy of the MIPM or IPM. Where θ_1 is greater than 85 degrees, the sensitivity of the model to the M-L CoP-CoM separation is high. The error caused by assuming the leg is perpendicular to the ground (i.e. $\theta_1 = 90\,^\circ$) is also high. Therefore a stationary Centre of Pressure (as utilised by the IPM) is an error-inducing over-simplification of CoP location. Data from the force plates showed that the CoP can translate over 100 mm laterally during a step, so accurate prediction of the CoP is essential for predicting M-L ground force.

Townsend only considered Centre of Pressure motion relevant in cases of foot movement, such as rope walking and skating; so-called 'moveable-ground-support gaits' [122]. He also identified the double stance phase as a case of moveable ground support, although he neglected any further discussion (and the other moveable ground support cases) in his analysis of walking. He states that in moveable ground support, 'feedback is effected by muscular activity shifting the relative location of the support foot relative to the system center of mass', acknowledging the importance of the M-L distance between the CoM and CoP. In spite of this, he does not go into further detail.

Hof states that the Base of Support (BoS) of an individual in single stance is roughly the perimeter of the individual's foot; in double stance, it is roughly the area between and including both feet [126]. A simple quiet standing test may be conducted to show the importance of CoP in maintaining stability, even in cases of moveable ground support. (Dozens of studies have also been conducted on single-leg quiet standing, as reported by King and Zatsiorsky [98].) Standing straight on one foot, an individual is perfectly balanced. The centreline of the body is directly aligned with his or her standing foot, $x_{CoM} - x_{CoP} = 0$. Shifting body weight towards the outside of the foot moves both the CoM and CoP. As the CoM reaches the extreme edge of the foot, the ankle will invert to maintain balance. Finally, when the foot cannot roll any farther, the individual will fall laterally or gyrate the hips, arms, or free leg so as to introduce angular momentum and move the CoM to the inside of the CoP. This makes sense because the CoM location cannot pass outside of the CoP lest the individual fall over [83, 126]. This test shows that static stability only occurs when the CoM is directly over the CoP (i.e. M-L force equals zero). Nonetheless, it shows that both the CoM and CoP have the capability of moving laterally *without* moving the foot in order to maintain balance. This is also true during double stance when the CoP moves rapidly from foot to foot to remain outside the CoM – a characteristic compliant with the margin of stability described by Hof *et al* [126].

In summary, dynamic stability is primarily maintained by the body altering the relative positions of the CoM and CoP throughout the gait cycle. Thus the assumption of a stationary Centre of Pressure during each step is fallible. Considering that the CoM-CoP angle (and, therefore, the ground reaction force angle) is near 90° and the tangent function places the M-L CoM-CoP separation in the denominator, measuring the CoM-CoP separation accurately is important. A comparison of the CoM trajectories produced by the IPM and kinematic data show that an inverted pendulum is not as kinematically accurate as, perhaps, a double inverted pendulum, four-bar linkage, or upright pendulum, but the approximation of the M-L ground force by the MIPM is still a significant improvement over the IPM.

A deficiency of the MIPM is the need to predict the location and displacement of the Centre of Pressure through each footstep. Representing the CoP as a static point is insufficient for predicting M-L force, but further research is needed to predict (1) where an individual places his/her foot for each step, and (2) how the Centre of Pressure moves within that footstep once the foot is placed.

5.7 Conclusion

This chapter has discussed the seven assumptions implied by the Inverted Pendulum Model. Based on the equivalence of the ground reaction force angle to the CoM-CoP angle, the Modified Inverted Pendulum Model was developed. This model – while similar to the IPM – is more accurate than the IPM, indicating that some of the assumptions used to develop the IPM were over-simplifying. The most important assumptions to reconsider pertain to the medial-lateral distance between the CoP and CoM. The model was sensitive to this distance, so a right angle approximation of the pendulum angle exaggerated predictions of the M-L ground force. Moreover, due to the sensitivity of the model to the M-L CoM-CoP separation, it is inaccurate to assume the CoP remains fixed when data show that it can translate even as much as 100 mm

laterally during single stance.

The development of the Modified Inverted Pendulum Model eliminates the need to approximate the CoP-CoM angle. In exchange, it requires the engineer to understand more about Centre of Pressure location, particularly how the CoP shifts with respect to the Centre of Mass, whether foot turn-out plays a role in lateral CoP trajectory, and the extent of inter/intra-subject variability. The nature of CoM shift and CoP transition from foot to foot during double stance also needs to be studied further. In spite of this, applying the IPM and MIPM to a single degree of freedom oscillator shows that the displacement responses due to the two models are significantly different and related to the location of the CoP.

Having concluded studies of walking on stable surfaces, the thesis turns its attention to the biomechanics of crossing a laterally moving footbridge. The MIPM can reproduce M-L ground forces with good accuracy, but is it as accurate when the walking surface is swaying laterally? How do pedestrians maintain balance when the ground moves, and to what extent does Centre of Pressure motion contribute to gait or structural (in)stability? To investigate this question, force plates were custom-designed for the Jenkin I and II tests. Their development is the topic of the next chapter.

Chapter 6

Integrating Force Plates into a Laterally Oscillating Footbridge

Having investigated the kinematics and kinetics of stable ground walking, attention must be turned to gait on a moving surface. It is pertinent to determine whether an individual alters their ground force patterns when he or she is no longer sure of his or her footing. To study the influence of base motion on gait, an experimental rig must be devised which can both apply motion to the test subject and record the consequent gait characteristics. Chapter 1 identified a variety of tests that have studied gait on both moving platforms and instrumented treadmills. Within each type of test set-up a number of configurations are possible. Unfortunately, no test can perfectly recreate field conditions and every test has its deficiencies. That said, each type of configuration allows the researcher to investigate a specific aspect of gait.

Treadmill tests have a significant advantage over platform tests in that the moving belt allows researchers to record a large number of consecutive footsteps. This is particularly beneficial for Fourier analyses, for which the frequency content of a longer sample is much less affected by any transient behaviour. Typically only one subject is tested at a time, but studies have occasionally used side-by-side treadmills to investigate synchronisation. To the author's knowledge, when treadmills are used to study gait in the presence structural motion, the oscillations are always applied externally (as opposed to naturally, from the test subjects). Of course this has advantages and dis-

advantages. External oscillations – applied either to the pedestrian or to the treadmill – can be applied either monotonically or at any frequency, permitting researchers to investigate the effects of frequency and amplitude on gait. The disadvantage, however, is that the oscillations cannot be affected by the test subject. The tests are action-reaction instead of feedback-based. Treadmill tests also have a disadvantage due to the inability of the subject to slow down or stop entirely if they feel unbalanced. Indeed, participants become comfortable with walking on the treadmill over time, but they are also consciously aware that they *will* fall if they stop suddenly, so they know they must continue walking if at all possible. This could have a significant influence on walking strategy.

Platform tests, naturally, are quite different to treadmill tests. Typical platform tests are either stationary with force plates and motion capture or oscillating with only motion capture; both of which are insufficient for the present study. A few researchers (e.g. [52, 41]) have recorded the force due to the motion of a platform subjected to pedestrian loading (with or without externally applied oscillations). However, these studies did not capture the ground forces of individual steps or examine M-L gait stability because they were focused on structural stability. Generally speaking, platform tests are limited to a relatively few number of footsteps, which make time-domain analyses preferential to frequency domain analyses. They inherently can not capture the steady state, but rather record a snap-shot of gait over several footsteps. From a practical standpoint, they also require significantly more laboratory space than treadmill tests. These difficulties may be major reasons why more treadmill tests have been conducted than platform tests.

That said, platform tests are still immensely beneficial because they are better at replicating field conditions than treadmill tests. Pimentel stated in his PhD thesis that pedestrians exert different ground forces on rigid structures versus flexible structures [35], so a flexible footbridge may be better represented by a platform test than

Figure 6.1: Solidworks rendering of the laboratory footbridge developed by Kaye, Mather, and Selley [140].

a treadmill test. Platform tests do not have the speed or cadence constraints of treadmills so test subjects can walk at their natural speed and react to bridge motion in a natural manner. Additionally, a well-designed platform will oscillate in response to pedestrian excitation rather than requiring external stimuli, allowing structural motion to feedback from participants' ground forces.

As described in Chapter 2, Kaye constructed a laterally oscillating footbridge in the Oxford University Department of Engineering Science [139]. The bridge was subsequently developed by Mather [140] and Selley [142] before the present doctoral work was undertaken. A Solidworks rendering produced by Mather can be seen in Figure 6.1.

In order to compare the ground forces from the NOC tests with walking on a laterally oscillating bridge, the bridge required a set of force plates and other instrumentation. This chapter describes the design and development of a force plate novel for its application in a laboratory footbridge. The force plate was conceptualised, constructed, and calibrated to record the medial-lateral forces produced by a walking individual while traversing the oscillating footbridge. Preliminary trials using a single force plate showed that the force plate data could be directly compared to the ground forces recorded in the NOC I tests. Then three additional force plates were installed in preparation for the Jenkin I and II tests.

6.1 Design and Configuration

6.1.1 Force Plate Requirements

A number of requirements were considered in the design of the force plates, starting with loading. The force plate needed to record the M-L ground force of a test subject with minimal cross-talk from loading in other directions. Since M-L forces are orthogonal to the dominant vertical force, they are more difficult to record accurately. The NOC I tests show that M-L ground forces can exceed 10% of body weight, but are usually under 5% for most of the force pattern. To encompass these extremes, the force plates must accurately record forces from at least zero to 100 N in both lateral directions, especially for low levels of force.

The next consideration was that of spatial limitations. The first spatial constraint was the depth of the existing superstructure. With girders only 150 mm deep, each force plate and mounting hardware needed to be shallow for the force plate to be flush with the deck. A beam was welded to the inside of the bridge girders upon which the force plates could rest, though this reduced the available depth for the force plates. The final force plate design was only 110 mm deep plus 18 mm decking on top.

The existing bridge configuration also presented constraints in the longitudinal direction. Based on the Oxford Gait Lab force plates, which were practically too small for adult walkers, the force plates for the bridge needed to be greater than 500 mm long. Unfortunately the existing structural joists are spaced at approximately 330 mm. To overcome this limitation, each force plate was designed to straddle a joist. The surrounding deck was raised from 18 mm to 28 mm to accommodate the force plate and the joist. In the transverse direction a 1 m clear span between girders did not pose significant limitations to the design. The final dimensions of the force plate, therefore, were 600 mm by 1220 mm (longitudinal by transverse), lifted 10 mm off of the superstructure.

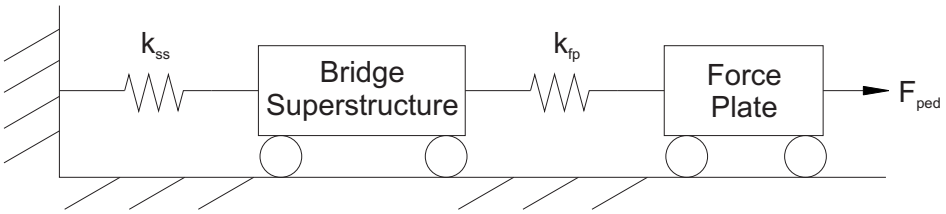

Figure 6.2: Bridge spring-mass system schematic. With stiff force transducers, k_{fp}, superstructure and force plate oscillate together. Despite the stiffness of the transducers, however, motion of the superstructure will always induce a force in the transducer.

Due to space limitations and the need to ensure accuracy, the force plate was not designed to record antero-posterior or vertical forces. Efforts were also taken to eliminate vertical and antero-posterior cross-talk in the lateral response given that vertical walking loads could reach 20 times peak lateral loads.

The final force plate requirement was to provide a walking surface as stable as the rest of the deck. By making the force plate stiff, M-L ground forces could be detected by a (stiff) custom-designed transducer. The spring-mass system in Figure 6.2 shows, however, that it is impossible to prevent bridge motion from inducing a force in the transducers. However, the error from this unwanted influence can be minimised.

6.1.2 Beam Theory

In the final force plate design the key components are four steel plates which act as beams in double bending. These 'spring elements' contain strain gauges in order to provide an estimate of the amount of lateral force exerted by the person onto the force plate. From Bernoulli-Euler Beam Theory and the method of superposition, a fixed-fixed beam with the configuration shown in Figure 6.3 has a maximum deflection of

$$\Delta = 2 * \frac{W\left(\frac{l}{2}\right)^3}{3EI} = \frac{Wl^3}{12EI} \tag{6.1}$$

where Δ is the displacement (mm), W is the load (N), l is the clear span (mm), I is the second moment of inertia of the cross section of the beam (mm^4), and E is Young's modulus of elasticity for the material (MPa). It can also be shown that the internal

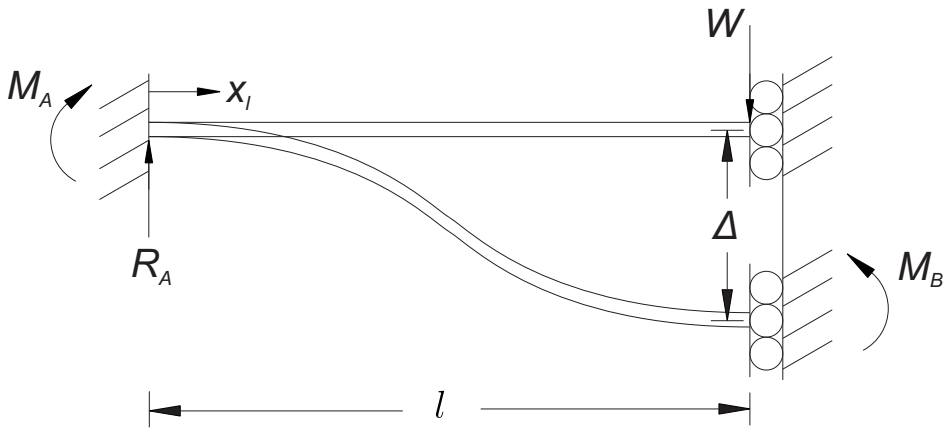

Figure 6.3: Deflection of a fixed-fixed beam with free translation of one end.

moment in the beam at any distance x from the left support is equal to

$$M = W\left(x - \tfrac{l}{2}\right) \qquad 0 < x < l. \tag{6.2}$$

Thus, substituting Hooke's Law and Equation 6.2 into the bending stress relationship $\sigma = My_{NA}/I$, the maximum strain experienced by the beam is

$$\varepsilon = \frac{Wy_{NA}(x - \frac{l}{2})}{EI} \qquad 0 < x < l \tag{6.3}$$

where y_{NA} is the distance from the neutral axis to the extreme fibre. A steel plate with a 50 mm clear span and a thickness of 2.38 mm (3/32 in) is assumed to act as a Bernoulli-Euler beam when a load is applied orthogonally to the plane of the plate. Thus, the peak deflection of the beam under a 10 N load would be 0.0088 mm; detectable yet sufficiently stiff that a test subject would not observe any difference between the force plate and the deck. At $x_l = l/8$, the theoretical bending strain would be $19\mu\varepsilon$.

6.1.3 Force Plate Configuration

Each force plate consists of the following main components, listed in order of load path: the deck, two outer beams, the four aforementioned spring element transducers, two inner beams, and the force plate support beam (Figure 6.4). The decking consists of 1220 x 600 x18 mm medium-density fibreboard (MDF). This is bolted to each of the

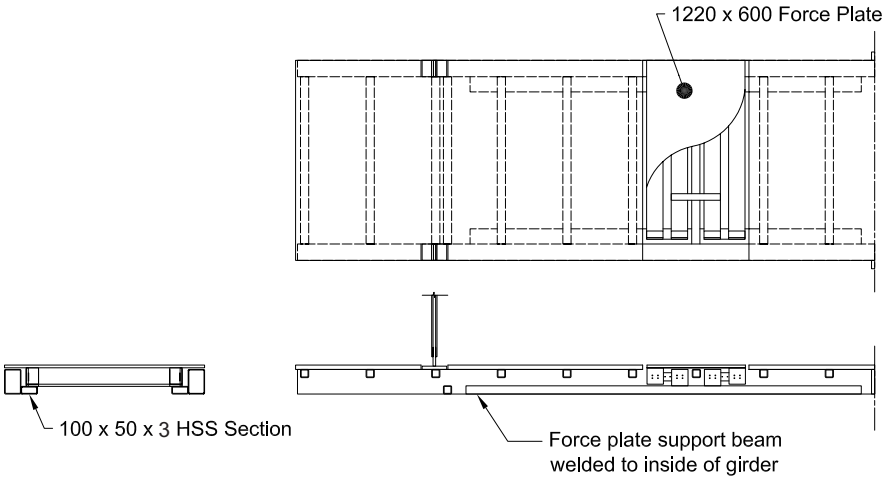

Figure 6.4: Modified bridge (compare with Figure 2.7) with one force plate and the force plate support beam installed.

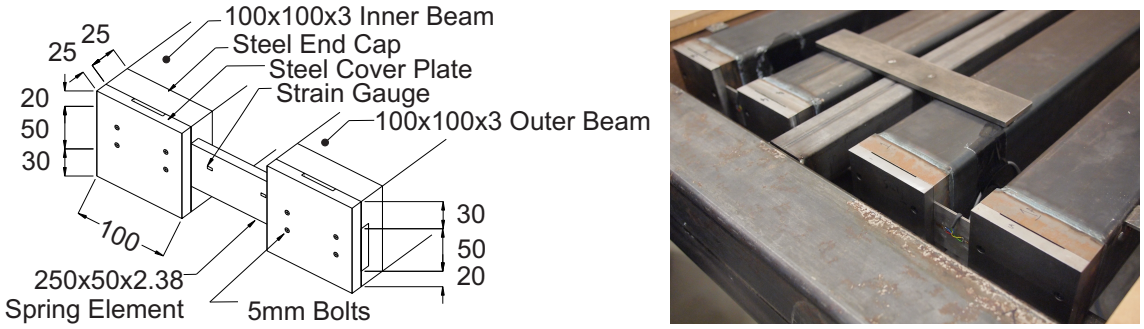

(a) (b)

Figure 6.5: Schematic of beam to spring element connections. All measurements in millimetres; not to scale. Photograph shows the four beams that make up the force plate.

two outer beams via angle brackets. Each beam is a 100 x 100 x 3 mm steel square hollow section of length 860 mm. A steel end cap, 100 x 100 x 25 mm, is welded to each end of the beam (Figure 6.5) to provide fixed ends for the spring elements. Each cap has a 100 x 50 x 2.38 mm groove, into which the spring element is fitted. The connection is secured by mounting a 100 x 100 x 12 mm cover plate to the spring element and the end cap, creating a fixed support. The beam's total length of 934 mm fits between the superstructure girders with approximately 43 mm clearance on each end.

The steel spring element consists of a 50 mm clear span (described in the previous

section) in addition to two 100 mm clamped regions for a total plate size of 250 x 50 x 2.38 mm (Figure 6.5(a)). The plane of the spring element is oriented in the bridge such that a vector orthogonal to the element is transverse to the bridge. Four RS Components 632-168 strain gauges (120Ω, 5 mm gauge length, 2.1 gauge factor) are affixed to each of the four spring elements. On both sides of the spring element a strain gauge is attached at a distance of $l/8$ or 6.25 mm from each fixed end. There are 16 total strain gauges in each force plate and each gauge is oriented parallel to the spring elements and to each other.

The spring element is mounted to the inner beam in the same configuration as the outer beam. Notice in Figure 6.5(a) that the groove in each end cap is vertically off-centre by 5 mm. With the groove below centre on the outer beam and above centre on the inner beam, a 10 mm gap is created between the tops of the two beams. This provides clearance between the joist and the deck for a brace that clamps the two inner beams to the superstructure (Figure 6.5(b)). The inner beams are also supported from below by two force plate support beams, which were welded to the superstructure girder (Figure 6.4).

When a person crosses the force plate, only lateral forces produce a signal. The M-L forces due to walking cause the outer beams to translate parallel to the fixed inner beams (Figure 6.6). This induces a deflection in the four spring elements and strain is recorded in the gauges. Vertical forces produce negligible bending or shear deflection due to the height to length ratio of the spring element and the fixity ensured by the end caps. Lateral torsional buckling of the spring element is prevented by the size and rigidity of the outer beam. Antero-posterior forces are transmitted axially through the spring elements.

Finally, P-delta effects are not a concern due to the symmetric orientation of the inner and outer beams. For any antero-posterior force, two spring elements are in tension, which stabilise the two in compression. Since the beams cannot rotate with

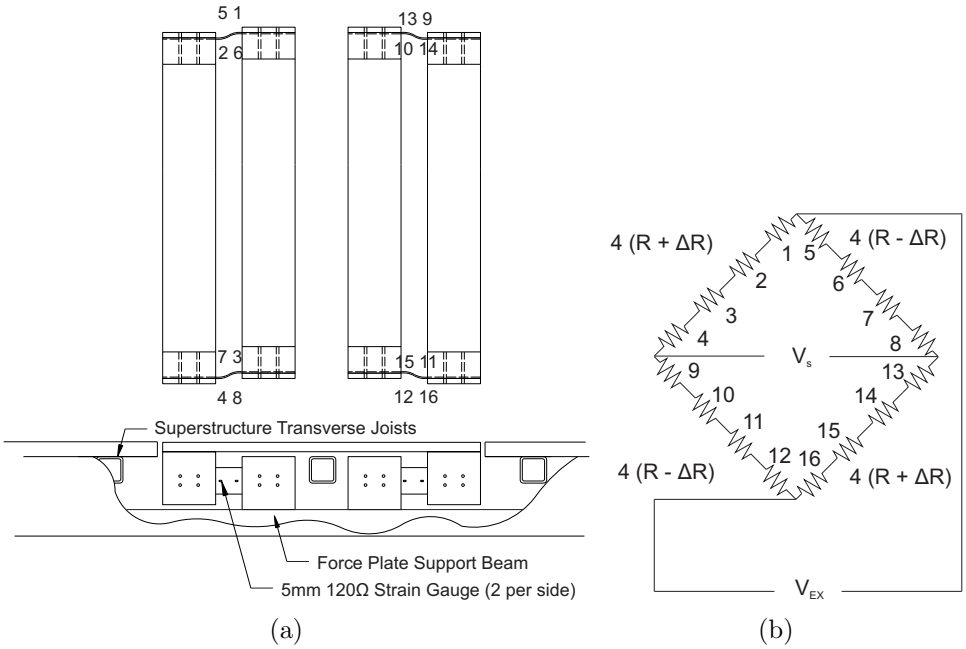

(a) (b)

Figure 6.6: Schematic showing the deformation of the spring elements with the location of 16 strain gauges. The circuit diagram shows how the Wheatstone bridge is wired. R is the resistance in any gauge and ΔR is the change in resistance in a gauge due to strain.

respect to each other, P-delta effects are avoided. Moreover, any uniform axial force experienced by the elements is cancelled out due to the arrangement of the strain gauges.

6.1.4 Wiring Configuration

The strain gauges for each force plate are wired into a modified Wheatstone bridge configuration. A typical full Wheatstone bridge consists of four variable resistors (strain gauges) arranged in two parallel branches. When excited by an excitation voltage V_{ex}, a balanced bridge (i.e. with no strain, $\Delta R = 0$) gives an output voltage differential $V_s = 0$. If a positive strain is applied to two opposite gauges and an equal but opposite strain is applied to the remaining two gauges, the voltage differential across the bridge becomes

$$V_s = -V_{ex} G F \varepsilon \tag{6.4}$$

where GF is the gauge factor of the strain gauge and ε is the strain experienced by a gauge. To minimise the influence of any differences in strain among the spring elements, 16 strain gauges (four per spring element) were wired into one Wheatstone bridge (Figure 6.6). In this configuration the positive and negative output signals are

$$V_{s^+} = \frac{4V_{ex}(R + \Delta R)}{4(R + \Delta R) + 4(R - \Delta R)} \tag{6.5a}$$

$$V_{s^-} = \frac{4V_{ex}(R - \Delta R)}{4(R + \Delta R) + 4(R - \Delta R)} \tag{6.5b}$$

where $R \pm \Delta R$ is the resistance of each gauge plus or minus the change in resistance of the gauge due to the application of tensile or compressive strain. Simplifying Equations 6.5 and substituting the relationship $\Delta R/R = GF\varepsilon$ yields

$$V_{s^+} = \frac{V_{ex}}{2}(1 + GF\varepsilon) \tag{6.6a}$$

$$V_{s^-} = \frac{V_{ex}}{2}(1 - GF\varepsilon). \tag{6.6b}$$

The total output is the voltage difference between the two branches, $V_s = V_{s^-} - V_{s^+}$, which results in Equation 6.4. Thus the use of 16 strain gauges averages out any errors across the Wheatstone bridge rather than amplifying them.

In summary, each force plate consists of 16 strain gauges which were wired together into one Wheatstone bridge. The strain gauges were wired together at a terminal, which was then connected to an RDP Electronics Ltd (Wolverhampton, UK, www.rdpe.com) S7DC transducer amplifier. The amplifier was connected to another terminal, which directed a ±10 V DC supply voltage into the system and diverted the output signal to a Data Translation DT9804 16-bit data acquisition system (DAQ). The channels were configured with differential inputs, meaning that interferences due to common mode voltage were reduced.

The DAQ was connected to a laptop via USB, where the data were recorded using QuickDAQ, a Data Translation software. The software allows the user to specify sampling frequency, circuit type (i.e. differential versus single-ended), and excitation

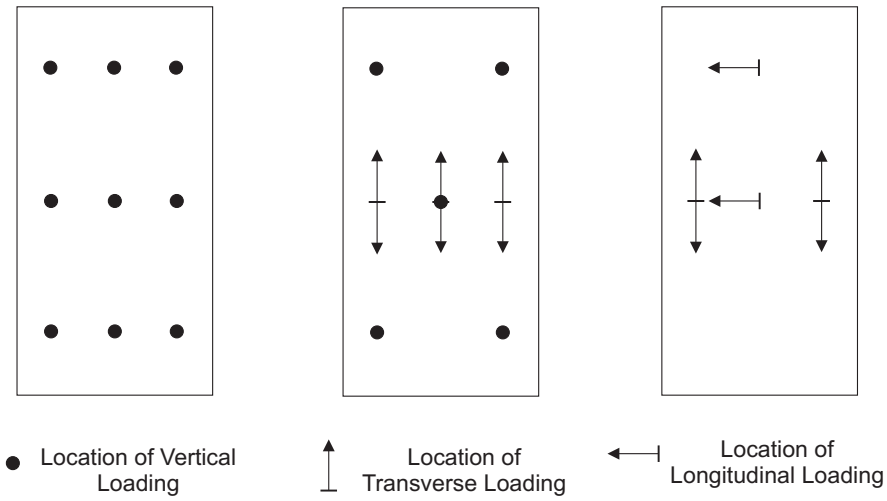

Figure 6.7: Schematics of force plate showing application of calibration loads. Three sets of calibration cases undertaken for each force plate. (Left) Vertical applied force only, (Centre) Vertical and Transverse force, and (Right) Transverse and Longitudinal force. In each set, all combinations of two load directions were tested for different levels of lateral (transverse) force.

voltage among other settings. For each channel, the user can also specify a calibration coefficient and offset for a wide variety of engineering units. Finally, the program also presents output signals in real-time with either digital or analogue read-outs.

6.2 Calibration

The force plate was calibrated against an RDP Electronics RLT0100 tension load cell. As with the force plate, the load cell was connected via S7DC amplifier to the DAQ. The load cell was first calibrated against known weights up to 158.8 N. The calibration constant and offset for the load cell were applied in QuickDAQ such that the signal recorded by QuickDAQ was in Newtons.

Calibration of the force plate consisted of three series of tests: applied vertical force only, applied vertical and transverse forces, and applied transverse and longitudinal forces (Figure 6.7). In the first set of tests, a known weight up to 981 N (100 kg) was placed in one of nine different locations around the force plate: one of the corners, one of the side mid-points, or the centre. QuickDAQ recorded the voltage output of

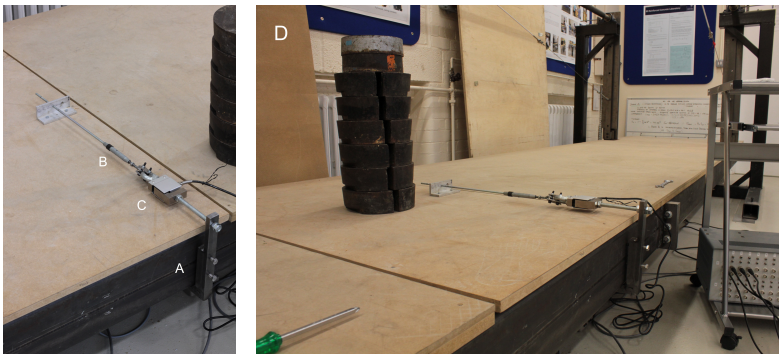

(a) (b)

Figure 6.8: Clamp (A) allows lateral force to be applied to the force plate. Force is aplied using a turnbuckle (B) and recorded by a load cell (C). A vertical-transverse calibration is conducted (D) using 686.7 N (70 kg) vertical force in the centre of the force plate while lateral force is applied to one edge.

the force plate at 100 Hz for 30 seconds, from which the mean value was recorded as the actual output. Two trials were recorded for each location-magnitude combination. The location and magnitude combinations of the vertical force were ordered randomly.

Ideally, the output voltage should be independent of the vertical force and thus the output should be constant for all magnitudes and locations of the vertical force. Based on this calibration, however, the magnitude and location of the force have a slight influence on the output voltage, with a range of 28 mV between the highest and lowest reading. While the 98.1 N (10 kg) vertical force always resulted in output values close to 110 mV, the 981 N (100 kg) force produced a graduated response from 102 mV in one corner of the plate to 130 mV in the opposite corner.

In the second series of tests, transverse loads in addition to vertical loads were applied to the force plate. These were undertaken to assess the level of vertical and lateral cross-talk. To achieve lateral loading, a special clamp was developed and applied to the bridge superstructure (Figure 6.8). The clamp functioned by pulling the force plate towards the superstructure, inducing a load in the spring elements. The clamp bolted into one end of the RLT load cell. The other end of the load cell was attached to a turnbuckle, which was in turn attached to a bracket screwed into the deck of the force

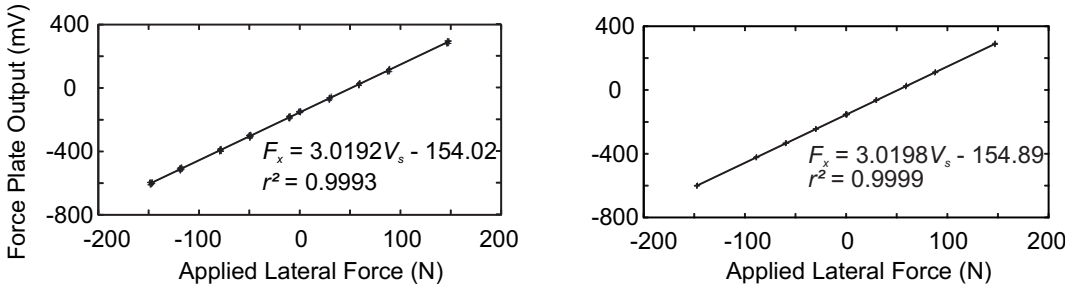

(a) (b)

Figure 6.9: Force plate output V_s (mV) versus applied lateral force F_x (N) during initial (a) transverse-vertical and (b) transverse-longitudinal calibration.

plate. Thus, the turnbuckle reduced the number of screw threads between the clamp and the bracket, which applied tension to both the load cell and the force plate. For most of the trials, a 686.7 N (70.00 kg) vertical load was applied in representation of an average person's static weight. The applied lateral loads varied from 0-147.2 N (0-15.00 kg). Vertical load was applied to the four corners and the centre of the force plate while lateral load was applied in both lateral directions from three locations along the force plate's longitudinal centreline. Figure 6.8 shows a vertical-transverse load test. For each calibration test, the lateral load was applied by tuning the turnbuckle while QuickDAQ was acquiring data. Once the target load was tuned, a 30-second sample recorded both the applied load and the force plate's output voltage.

The relationship between lateral force and output voltage for 152 calibration tests is shown in Figure 6.9(a), where the sign of the lateral force corresponds to the direction in which the force was applied. Even though the locations of the applied loads vary, the relationship between applied lateral force and output voltage is strongly linear. The maximum error between a data point and the linear model is 14.4 mV, an error of 4.7 N. The magnitude of the vertical load did not influence the output voltage, so the error is attributed to the location of the vertical load. Furthermore, the average standard deviation between the 152 trials and the regression line was 0.47 mV, so the strain gauges, wiring, and amplification act in a linear and repeatable manner.

In the final set of calibration tests, horizontal loading was applied in both the transverse and longitudinal directions. Longitudinal loading was achieved by suspending weights over a 'frictionless pulley'. A rounded steel plate attached to the end of the bridge served as the frictionless pulley. Another bracket was attached to the force plate, from which a steel cable ran the length of the bridge, over the rounded plate, and down to 394.2 N (40.18 kg) of suspended weight. The longitudinal loading was applied along the bridge centreline and from one edge of the force plate, while the transverse load was applied in the same manner as during the vertical-transverse tests. The transverse loading was again applied using the load cell and turnbuckle.

The calibration results from 42 transverse-longitudinal trials can be seen in Figure 6.9(b). The response of the force plate remains linear with approximately the same regression as the vertical-transverse tests. The improved r^2 value indicates that longitudinal loading does not influence the force plate reading.

Based on the vertical-transverse and transverse-longitudinal tests, a composite linear regression of all 194 trials produced a calibration curve for the force plate with a Coefficient of Determination $r^2 = 0.9995$. Using this regression, the output voltage from the force plate can be easily converted into lateral force.

6.3 Preliminary Results

The linear calibration was input into QuickDAQ so that the force plate output would be converted to force automatically. Two tests were conducted to examine the usefulness of the force plate. In the first test, the bridge was fixed in place such that no lateral oscillation could occur. This was intended to produce a stable-ground-style test which would produce similar results to trials conducted at the Oxford Gait Lab. A five minute trial was conducted, during which the author walked back and forth across the bridge, deliberately stepping in the middle of the force plate. After each crossing, he paused for a few seconds to allow any vibrations to dissipate. Figure 6.10 shows an unfiltered

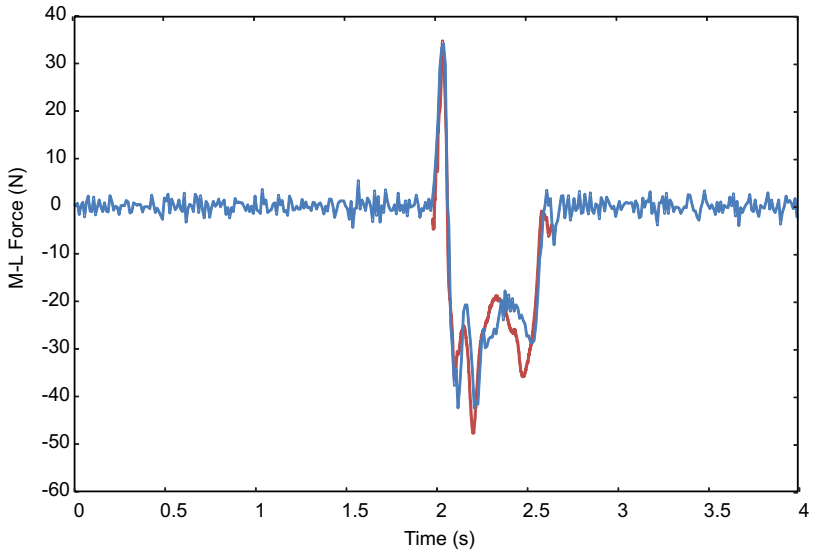

Figure 6.10: Ground force and ambient vibrations from walking across the fixed-in-place bridge (blue). Ground force recorded at the Oxford Gait Lab (red) matches the force plate sample very well.

force plate strike along with the internal vibrations induced in the force plate before and after the step. In spite of the high-frequency noise, the step is clearly discernible. The heel-strike begins at 1.9 s, changing from medial to lateral force at 2.1 s, before toe-off occurs at 2.6 s. Included for comparison, one can also see a sample from the same foot walking at the Oxford Gait Lab. The heel-strike region of the two steps is almost identical. Through the middle of the step, the same overall pattern exists although variation up to 10 N occurs throughout. This could reasonably be due to intra-subject variation. At the end of the step, the toe-off region is also very similar, with unloading occurring at the same rate in both steps.

For the second test, the bridge was released and allowed to oscillate freely. Another five-minute trial was conducted during which the author walked from end to end, allowing the bridge motion to dissipate between passes. The recorded motion during a typical pass is shown in Figure 6.11. Again, the force plate strike is clearly discernable among the ambient oscillations, from 2.0 to 2.7 s. The maximum force attributable to the bridge motion is approximately 8 N during normal walking with a frequency of 1.15 Hz.

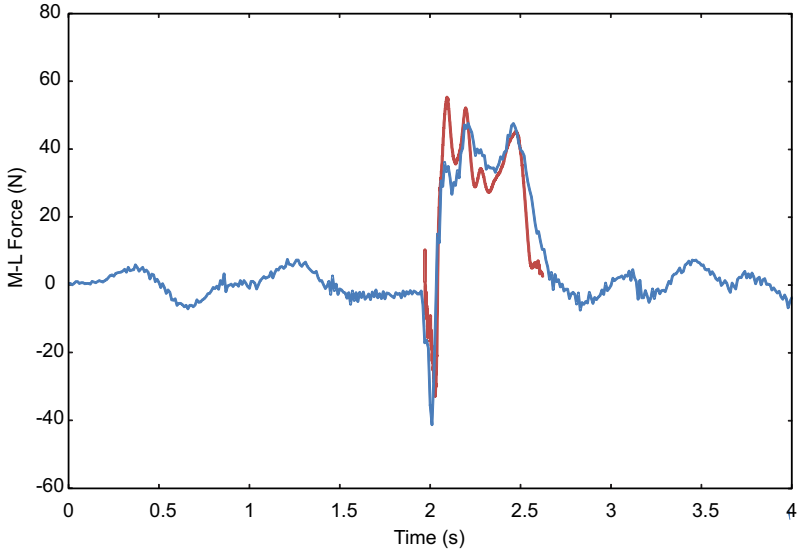

Figure 6.11: Ground force and peripheral vibrations from walking across the freely-oscillating bridge (blue). Ground force recorded at the Oxford Gait Lab (red) similar to the force plate sample.

This figure also shows a comparison between the force recorded on the bridge and a stable-ground Gait Lab sample. General agreement exists between the two samples, with similar heel-strike and mid-stance patterns. The similarity in these traces show, however, that the author did not feel significantly different to walking on stable ground. The major difference exists in the toe-off region, where the oscillating bridge step is slower to unload than its Gait Lab counterpart. The author anticipated seeing more distinctive differences between the stable and oscillating results during the Jenkin I tests when the bridge was to be continuously excited.

For one trial of the free-to-oscillate calibration test, the bridge was forced to resonate before the researcher crossed the force plate. This was achieved by standing on one end of the bridge and swaying from side to side in resonance with the bridge natural frequency. The result can be seen in Figure 6.12. The author swayed in resonance with the bridge from 3 s until approximately 14 s, when a peak ambient oscillation of 20 N was recorded. For the next 3 s while walking on the bridge, there was an immediate decline in the oscillations, marked by the halving of the force recorded in the plate. At 17 s, the author stepped on the force plate, recording the distinct footstep pattern.

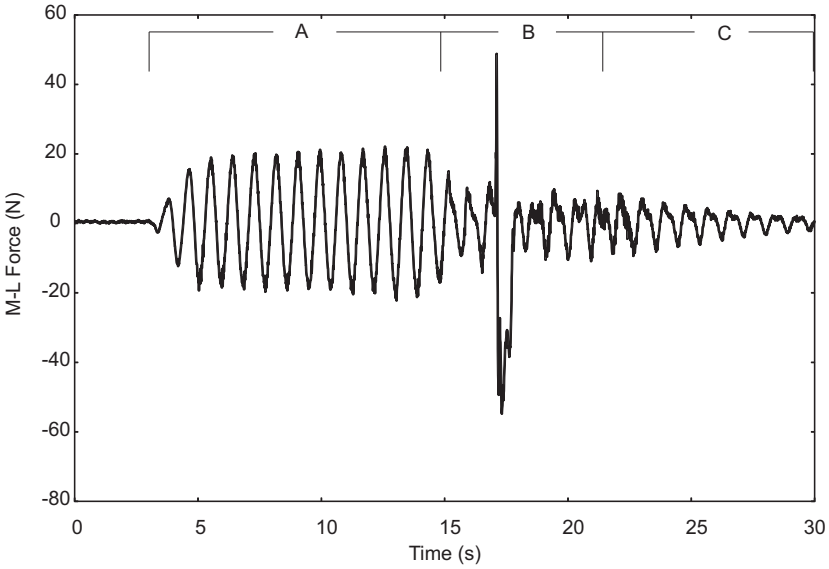

Figure 6.12: Ambient force recorded by force plate due to (A) resonance and (B) walking across the bridge. (C) Logarithmic decay after walking across the bridge.

For 3-4 s after toe-off, the author finished crossing the bridge, at which point he stood still. This final period is indicated by the region of logarithmic decay of the force from 22 s onward. The force recorded by the force plate is easily dominated by the step of a person, even when the bridge is swaying. Nonetheless, accelerometers and strain potentiometers were used in the Jenkin I tests and motion tracking markers in the Jenkin II tests to record the motion of the bridge. This allowed the ambient effect of the bridge motion to be subtracted from the force plate signal during post-processing.

6.4 Additional Force Plates

With the success of the first force plate, three additional force plates were added to the bridge (Figure 6.13). In an attempt to reduce ambient high-frequency vibrations recorded by the force plates, thin rubber bearing strips were inserted between the braces and the inner beam and between the inner beams and the force plate support beams. This isolated the force plates from any ambient high frequency vibrations in the bridge superstructure. Due to the installation of these rubber strips, the first force plate (FP1) needed to be recalibrated along with the additional force plates (FP2-4).

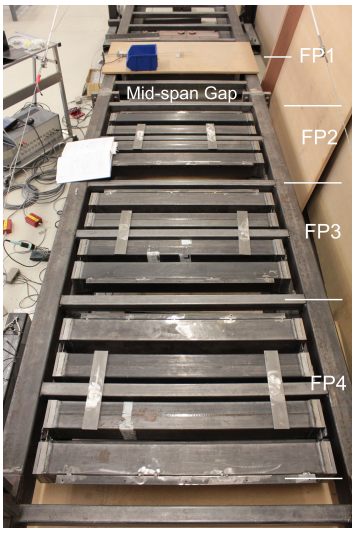

Figure 6.13: Installation of force plates two through four. Deck of FP1 can be seen at top of photo. The mid-span gap is too narrow for a force plate, so three force plates were installed on the near side of the bridge to only one on the far side. Steel counterweights were installed on the far side of FP1 to offset the weight imbalance in the bridge.

Table 6.1: Force Plate Calibration Equations. The force in Newtons (N) is a function of the output voltage in Volts (V).

	Calibration Trials	Calibration Equation	r^2
FP1	76	$N = 346.65V + 0.329$	0.9997
FP2	139	$N = 359.34V - 4.968$	0.9997
FP3	133	$N = 374.43V + 3.058$	0.9995
FP4	134	$N = 368.80V + 2.136$	0.9998

Table 6.1 presents a summary of the calibration tests and the calibration equations for each force plate.

The four force plates were installed asymmetrically along the length of the bridge, such that three force plates were on one side of mid-span to only one on the other side. An abnormally small gap is present between the joists at mid-span due to the fact that the bridge was originally constructed in two halves. This gap was too narrow to accommodate a force plate, yet it was wide enough for a person to take a clean step if force plates were located in adjacent gaps. Therefore, since only three force plates would fit on either side of the bridge and in hopes of recording three consecutive footsteps from each trial, the plates were installed in a three-one configuration about mid-span

rather than a symmetrical two-two configuration (Figure 6.13). Steel counterweights were installed on the side with the single force plate to compensate for the weight imbalance. Having a balanced bridge minimised the possibility that irregular rotational modes could develop.

6.5 Conclusion

Following the NOC tests, it is necessary to record subjects walking on a rig that would allow a participant to experience the full feedback loop inherent to human-structure interaction. Namely, the participant needed to (1) have the ability to influence the lateral motion of the walking surface and (2) be able to adjust his or her walking to the perceived structural motion. While some platform tests have been undertaken by previous researchers, no test had yet recorded individual footfall forces on a laterally oscillating surface.

Therefore, this chapter has presented the novel design of a force plate installed in an oscillating laboratory footbridge. The force plate was designed to fit within the spatial constraints of the laboratory footbridge and record the M-L ground forces exerted by walkers on the bridge. The configuration, mechanics, and wiring of the force plate were all custom-designed for the bridge. The calibration proves that the design is successful and only prone to minimal error.

Its successful calibration means that the rig can provide useful data showing how pedestrians are influenced by human-structure interactions. When combined with instrumented insoles, motion tracking sensors, video cameras, accelerometers, and strain potentiometers, the Jenkin footbridge becomes a powerful tool for understanding unstable human gait.

The novel force plate presented in this paper has the potential to reveal a wealth of new knowledge about human-structure interactions in the context of lateral bridge excitation. The plate's four structural beams provide rigidity and stability to the walker

while also conveying the load to four steel spring elements. The spring elements, which were designed to only deflect laterally, were calibrated to minimise the effects of cross-talk. Finally, two initial tests indicated that the bridge produces reasonable results, which are comparable to stable ground walking tests. The force plate was replicated, providing a series of four force plates from which multi-step trials could be recorded.

In the following chapters the results of the Jenkin I and II tests are analysed. These show that the mechanics of crossing an unstable surface are different to walking on stable ground, and that multiple methods are used to maintain balance. The results will also show that a three-dimensional inverted pendulum has the potential to predict lateral ground forces on unstable surfaces.

Chapter 7

Kinematics and Kinetics of Crossing a Swaying Bridge

Previous chapters have examined the components of the Inverted Pendulum Model in detail for walking on a stable base. The principle components of the IPM and MIPM are the Centre of Mass location, Centre of Pressure location, vertical force, and the step width. In Macdonald's and Hof's stable ground IPM, CoM movement towards the CoP leads to a decrease in the moment arm between the body's centre of gravity and the point of support [67, 126]. This causes the characteristic saddle shape in each step's M-L ground force. It has thus far been shown that real walkers exhibit much more nuanced M-L ground forces, largely due to the movement of the Centre of Pressure.

But what happens when a person walks across a moving base? The lateral oscillations of a structure surely influence how an individual walks, but the kinematic and kinetic implications of base motion on ground forces have not been studied at length. For inverted pendulum models to be upheld, data need to show that the relationships between the parameters hold the same as for stable ground walking, regardless of the characteristics of the base motion. Thus, the Jenkin II tests were conducted.

First, it may helpful to have an overview of observations made during the tests. In a typical test, there was zero or little bridge motion at the start of the test. Bridge amplitudes were typically low for the first couple crossings but increased to maximum by the fourth or fifth crossing. Most tests captured six crossings in approximately

115 s. Significant variation was observed for how pedestrians reacted to the structural oscillation. Some subjects crossed the bridge apparently unaffected by its motion, even at high amplitudes. During some trials subjects subtly slowed their step frequency for one to two footsteps or rotated about the vertical axis during single stance in order to adjust to the structural motion. The subjects of other trials had momentary stumbles, coming almost to a complete stop before continuing. This was particularly observed at midspan before crossing the force plates, especially when the author had pushed on the bridge mid-test, between passes. No subject needed to use the handrails, but most subjects spread their arms to assist with stability at higher bridge amplitudes. Unfortunately, when significant gait-altering corrections were made, subjects voided a clean three-step trial. The following analysis only examines three-step trials, for which the subjects typically only displayed subtle manoeuvers. Further study should examine the kinematics and kinetics of the more extreme corrections.

This chapter independently examines each parameter for walking across a swinging bridge during the Jenkin II tests. It is shown that patterns exist in each of the variables, although the patterns depend on base amplitude and phase. The first parameter considered is foot placement, or step width. So far it has been assumed that walking on a stable base results in walking with a symmetrical gait. This assumption means that the step width is constant, and therefore the lateral ground force alternates symmetrically about zero.

Now, however, with the addition of a moving base, it is unreasonable to assume that a person's gait is symmetric. In fact, the entire system is constantly in motion within the global reference frame. The bridge oscillates from side to side within the global reference. When a subject stands 'still' on the oscillating bridge, their feet move laterally with the bridge. When he or she walks, the CoP moves within the Base of Support both as a function of normal walking and as a function of the oscillating bridge – possibly with the further addition of corrective manoeuvres. Finally, the Centre of

Mass also moves as well. It follows then, that if the person feels unstable on the bridge, they are likely to stagger or to try to adapt to the motion of the bridge. In doing so, their 'erratic' steps are not symmetric, but irregular.

After looking at foot placement, the chapter discusses CoP motion, CoM motion, and CoM-CoP separation. Finally, the real ground forces are discussed in comparison with the MIPM. It is shown that while balance strategies may be irregular, they are generally predictable and dependent on the motion of the bridge during single stance.

7.1 Foot Placement

One of the most significant questions in human-structure interaction is how individuals know where to put their foot when the surface becomes unstable. In M-L gait stability then, the M-L placement of the foot from step to step is of critical importance. Before analysing the data from the bridge tests, however, a definition of step width must be elucidated.

Even in stable ground walking, measuring the step width is subject to some ambiguity. The step width is the M-L distance between two like landmarks on opposite feet at some instant during double stance. This presents a problem for the researcher. With both feet constantly in motion, there is not necessarily a point on both feet that is stably on the ground simultaneously. Measuring the heel separation would be ideal because the heel is the first part of the foot to contact the ground and one's chosen step width is possibly manifested through heel placement. Unfortunately the departing heel can be quite high off the ground when the arriving foot touches down, so any knee or foot rotation would cause the trailing heel to rotate inwards or outwards, distorting the step width. In Chapter 5 the metatarsal markers were used for the IPM because the toes are in contact with the ground for longer than the heel and briefly simultaneously with the heel. Natural foot progression (lateral turn-out) could cause the toe markers to be wider or narrower than the rest of the foot, though the measurements should be

consistent due to the small progression angle standard deviations in Table 5.1. Another similar method for measuring stable ground step width is to take the difference of the means of the heel and toe markers when each whole foot is on the ground. Of course this does not capture the step width at an instant in time, but it does provide a mid-foot placement less prone to marker movement errors. Finally, the most reasonable approximation for step width, especially if the MIPM is to be used in analyses, is the difference in the CoP locations at any given instant. This, however, requires extra instrumentation whereas the other aforementioned methods only need motion tracking cameras.

Whichever stable ground metric is used, an oscillating base adds a level of complication since the stance foot is always in lateral motion. On the one hand it would be valuable to assess what influence the structural motion has on the individual from step to step. On the other hand an instantaneous snapshot at heel-strike produces an easy-to-conceptualise picture of the relationship between departing and arriving footsteps. Thus two types of step width are here defined. The first type, *instantaneous step width* (ISW), is the M-L separation of the Centres of Pressure under each foot at the instant of heel strike. The second type, *net step width* (NSW), is the M-L separation between the global position of the first foot's heel-strike CoP and the global position of the second foot's heel-strike CoP, separated by some change in time.

Figure 7.1 shows a subject on the swaying bridge. Red (left) and dark blue (right) dots represent heel-strikes while pink (left) and light blue (right) dots show toe-off positions. Thus, net step width is the M-L separation between consecutive dark dots. Instantaneous step width is the M-L separation between a light dot and the next dark dot (i.e. the separation of the feet (CoPs) in each panel).

In the last panel of the figure the toe-offs and heel-strikes have been joined with dotted lines. Notice that the first two steps are fairly parallel to the bridge, suggesting a small ISW. The subsequent steps are more diagonal to the bridge, indicating larger

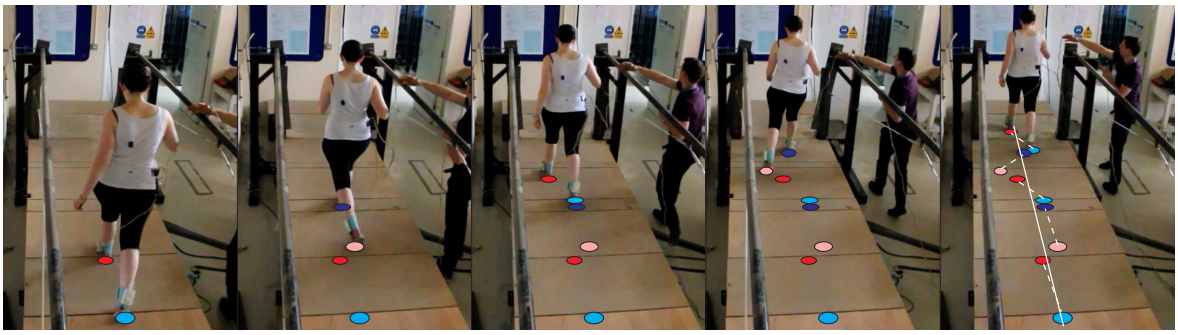

Figure 7.1: Sequence showing a participant crossing the bridge. Absolute position of heel-strikes indicated with red (left) and blue (right) dots. Corresponding toe-offs in pink (left) or light blue (right).

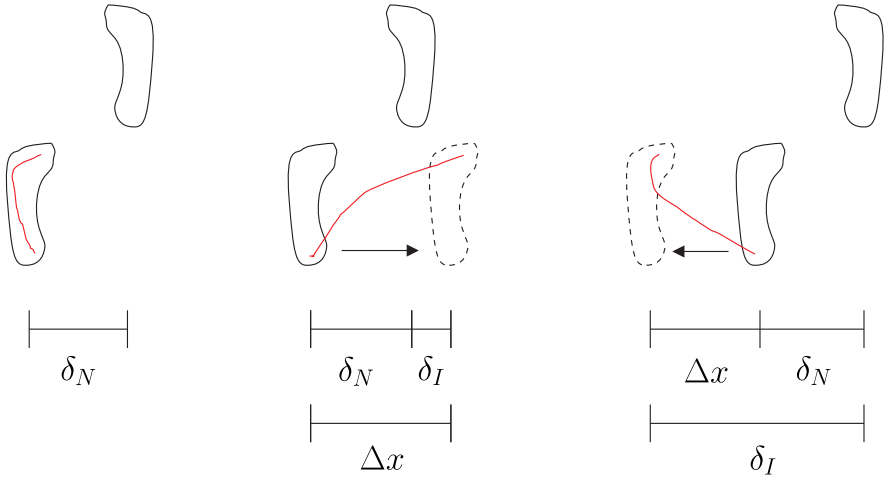

Figure 7.2: Step widths for different base motion. Stable ground walking in first panel shows NSW, δ_N. Even with base motion (Δx, middle and right panels), NSW remains nearly constant. ISW (δ_I) thus varies with base motion. Example CoP trajectories shown in red, indicating displacement from heel at heel-strike to toe at toe-off.

ISWs. In contrast, it appears that the heel-strikes are all generally equidistant from a centreline parallel to the bridge. This suggests minimal NSW variation from step to step. Thus, different behaviour is evident for net and instantaneous step widths.

The schematic in Figure 7.2 shows the different step configurations depending on base motion. The middle schematic is similar to the second panel of Figure 7.1 while the right schematic is representative of the fourth panel. From the 105 three-step samples in the Jenkin II tests, Figure 7.3 shows two histograms of the left and right ISWs. Though the histograms do not account for bridge displacement, the plots show that

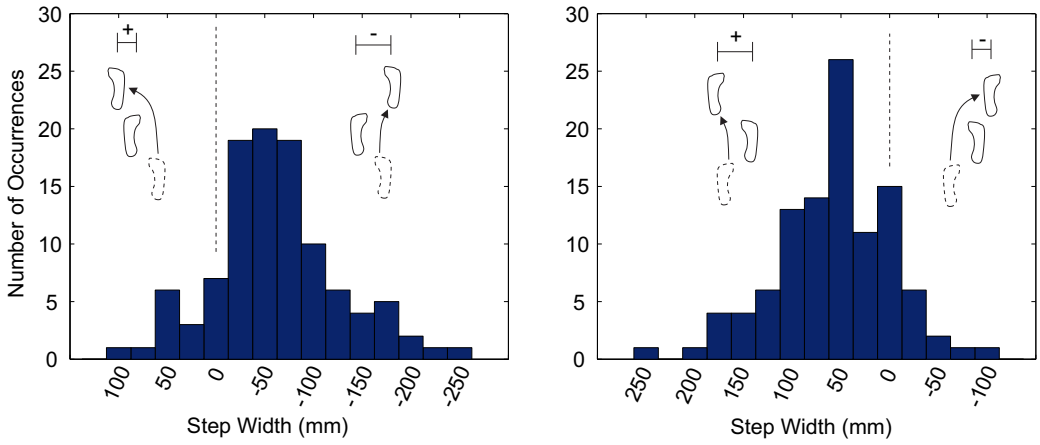

(a) (b)

Figure 7.3: Histograms of the instantaneous step widths of all three-step samples during the Jenkin II tests. Positive step width is displacement to the left; negative to the right. (a) Left-to-right steps and (b) Right-to-left steps. Bin ranges are the step width labels ± 12.5 mm.

a majority of the step widths are approximately 50 mm contralateral of the standing foot. Tails on the opposite side of zero from the mode exhibit crossed steps while the tails on the same side show wide steps.

Figure 7.4 shows how the ISW and NSW are correlated to the displacement of the bridge during single stance. The ISW plot supports the tests of Oddsson *et al.*; they and other researchers have suggested a proportionality between (instantaneous) step width and structural displacement [55]. Two regressions separately represent left and right foot stance. Most right-to-left steps have a positive (leftward) step width while most left-to-right steps exhibit a negative (rightward) step width.

The NSW, however, is approximately (because of CoP movement) equal to the displacement of the structure plus the instantaneous step width. Plotting the net step width against the bridge displacement, Figure 7.4(b) shows that foot placement is only slightly correlated to bridge displacement. The slope of the regressions is 0.178 for the left feet and 0.271 for the right. The intercept for each regression (−162.4 and 133.0 for left and right) is greater than the stable ground step width reported by Macdonald,

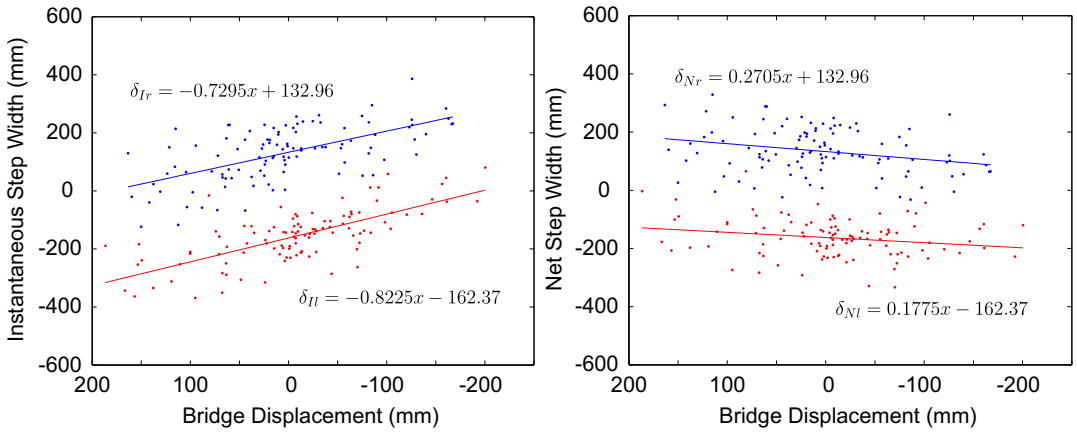

(a) (b)

Figure 7.4: The (a) instantaneous and (b) net step width at heel-strike versus bridge displacement over the previous stance phase. Right-to-left steps (blue) and left-to-right steps (red). Positive for leftward and negative for rightward position.

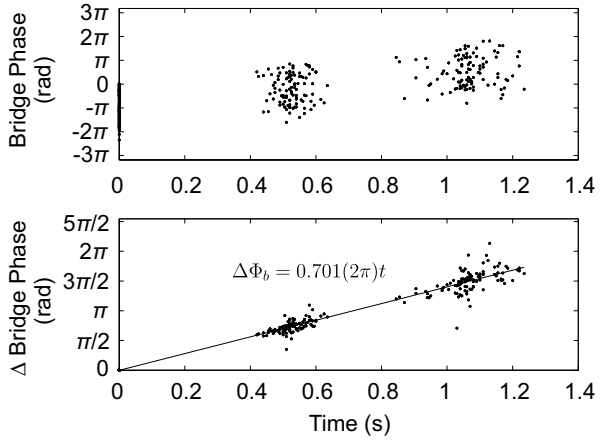

Figure 7.5: Bridge phase and change of phase over three consecutive steps. See text.

suggesting a slight widening of gait to maintain stability on the moving base [67].

Examining the influence of bridge phase during gait also helps to explain stepping behaviours. Previous treadmill studies have focused primarily on oscillation frequency or amplitude while platform studies have typically applied an impulse of known amplitude to the heel-strike of a step. The study presented here is novel for examining step width as a function of bridge phase and amplitude for free walkers. Figure 7.5 compares bridge phase to heel-strike time for all of the three-step trials. The three-step combinations have been aligned such that the first heel-strike occurs at $t = 0$. The

Table 7.1: Gait cycle period at different levels of bridge oscillation.

Amplitude, X (mm)	n_t	t_{mean} (s)	t_{sd} (s)
0-25	37	1.08	0.055
25-50	15	1.06	0.051
50-75	19	1.07	0.071
75-100	20	1.06	0.080
100-125	14	1.04	0.135
All Samples	105	1.07	0.077

groupings in the top plot show the timing and phase distribution of each successive heel-strike. The first heel-strike occurs across a distribution of bridge phases. The range of phases is approximately the same for the second heel-strike and the third heel-strike, although each grouping is offset by phase. The scatter of the heel-strike times increases with each step. The mean third heel-strike time – equal to the mean gait cycle period – occurs at 1.07 s. This is a good match with other reports in the literature (e.g. Macdonald [67]) that normal walking on stable ground has a period of approximately 1.11 s. Table 7.1 shows the mean gait cycle period and deviation for different amplitudes of bridge oscillation. The means are not statistically different than the overall mean based on Student two-tailed t-test, but the standard deviations increase as the bridge amplitude increases.

In the bottom plot of the same figure, all of the first heel-strikes have been offset to zero phase. This shows the change of bridge phase over one and two steps. The relationship is linear, showing that the subjects walked at a rate of 0.701 bridge cycles per second or 0.750 bridge cycles per gait cycle. Individuals did not lock their footsteps to the bridge motion and their footsteps occurred at random phases. This may be due to the fact that participants only took four to six steps on the bridge before reaching the force plates, therefore not having enough time to lock in with the bridge. Still, where some participants reported getting used to the motion of the bridge over time, it is surprising that none of the participants locked in.

The linearity of individual three-step samples indicates that while the walking speed varied from individual to individual, subjects maintained a near-constant walk-

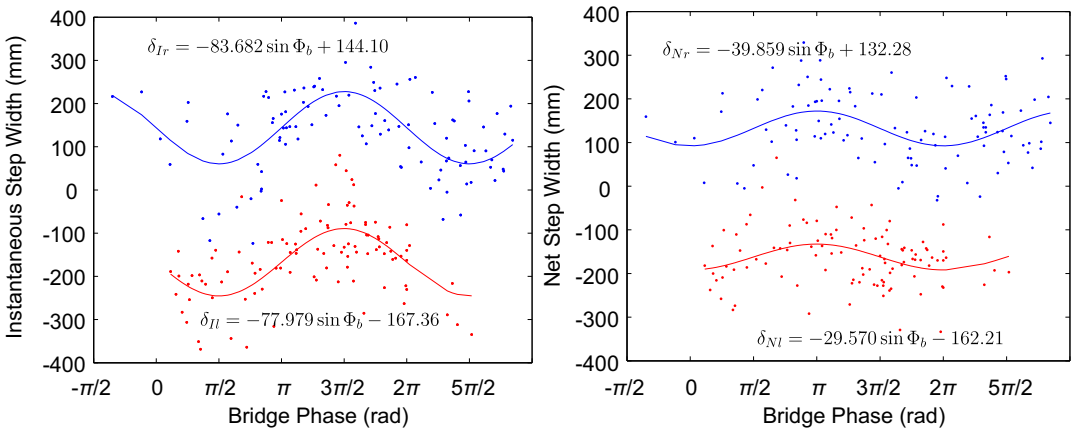

(a) (b)

Figure 7.6: The (a) instantaneous and (b) net step width versus bridge phase. Based on the phase of the bridge at one heel-strike, the subsequent step width can be predicted. Right-to-left steps (blue) and left-to-right steps (red). Positive step width constitutes a leftward step; negative corresponds to right steps.

ing speed. One reason for this trend is that the data here only show clean three-step trials, where subtle instability occurred. In many passes subjects stopped or stumbled, resulting in footsteps that straddled the edge of a force plate. Such cases of extreme gait alteration are not presented here, but the video and motion-tracking data for these cases would be interesting to study in the future.

The aforementioned regressions show that the step width is a function of bridge phase. The instantaneous step width, shown in Figure 7.6(a), is a sinusoidal function in phase with the bridge. Using MATLAB's `lsqnonlin` function, the amplitude and offset of the left and right foot curves were determined. The offsets (-167.4 and 144.1 mm respectively) are similar to but higher than the stable ground step width proposed by Macdonald, again suggesting a slight widening of the stance [67]. The amplitudes of the curves are -78.0 and -83.7 mm respectively. Curiously, the step width amplitudes do not seem to be related to bridge amplitude or its displacement during stance phase, so the magnitude of the step width amplitudes is unexplained.

For completeness, the net step width is shown as a function of bridge phase in Figure 7.6(b). Unsurprisingly, the net step width appears to be less affected by the

Table 7.2: Quadrants of HSI Based on Structural Characteristics and Heel-Strike Side

	Left Heel-Strike		Right Heel-Strike	
Quadrant	Bridge Position	Bridge Velocity	Bridge Position	Bridge Velocity
I	Right	Right	Left	Left
II	Right	Left	Left	Right
III	Left	Left	Right	Right
IV	Left	Right	Right	Left

phase of the bridge. The `lsqnonlin`-based optimisation yields sinusoids with less than half the amplitude, but a $\pi/2$ phase shift. The heel-strikes occur in a uniform distribution throughout the bridge cycle, so once again the data suggest that individuals locate each footstep as if the previous step were stationary.

Patterns of foot placement begin to emerge when the instantaneous step width is examined more closely. This requires a definition of the phases of the bridge for clarity. Here phase 0 corresponds to the bridge at central position, moving right. At $\pi/2$ the bridge is at its right-most extreme. At π, the bridge is once again central, but moving left. Finally, the bridge is at its left-most extent at $3\pi/2$.

Figure 7.7 shows left-to-right and right-to-left steps. The mean sinusoid has also been graphed. It has been divided into quadrants, corresponding to the bridge motion, to show different types of behaviour. The immediate explanation will discuss the quadrants in terms of a left heel-strike, but note that bridge motion would be opposite for a right heel-strike (Table 7.2). Quadrant I depicts left heel-strikes that occur while the bridge is on the right side of centre, moving to the right. In Quadrant II the heel-strikes occur while the bridge is right of centre with velocity towards the centre (leftward). Quadrant III depicts left heel-strikes occurring while the bridge is left of centre moving left, and Quadrant IV shows heel-strikes occurring while the bridge is left of centre moving rightward. Notice that Quadrant I for left steps corresponds to Quadrant III for right steps and vice versa.

Quadrants I and II depict wide steps. The the bridge is on the right side of centre, so a left heel-strike in this region is likely to be followed by a wide right step as the bridge

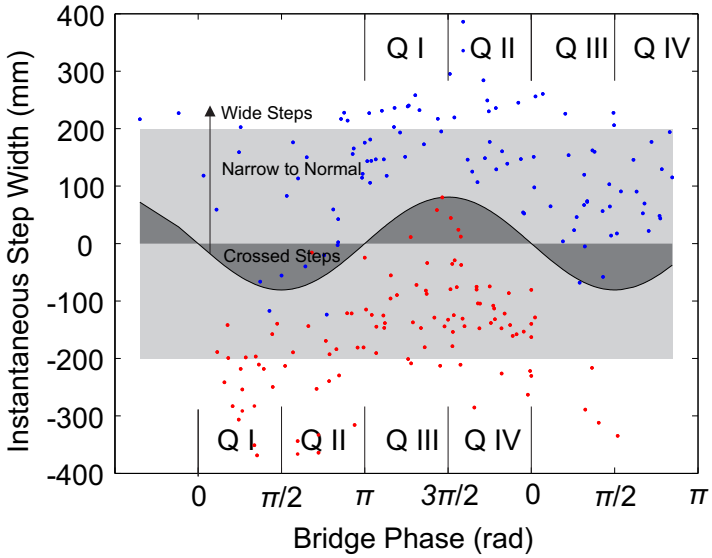

Figure 7.7: Step widths based on bridge phase at previous heel-strike. The mean of the two sinusoids in Figure 7.6(b) divides the left-to-right (red) and right-to-left (blue) footsteps. The sinusoid is divided into four quadrants, which are labelled according to the stance foot.

swings back to the left. The step width models (from Figure 7.6) peak at approximately ±250 mm, but some data far exceed that width. The widest steps occur in QII, where the bridge and stance foot move laterally away from the landing swing leg. Some step widths at the beginning of QI and the end of QII are quite narrow but they are never crossed.

In Quadrants III and IV participants take the narrowest steps. The bridge is left of centre, so a left heel-strike is most likely to be followed by a narrow or crossed right step. This occurs because the bridge ultimately moves to the right, carrying the standing (left) leg medially. Here, the step width models reach their minimum, around ±50 mm, but the variation in step widths show that some data take the opposite sign. Any data in Figure 7.7 that lie in the dark shaded regions show a heel-strike for which the next step crossed over (such as the second panel of Figure 7.1). This exclusively occurs in QIII and QIV. Notice, however, that it does *not* always occur; most of the steps in this period are narrow or normal, but not crossed over.

So far it has been shown that when walking on an oscillating surface, a subject's

net step width is similar to his or her stable ground step width. This is important because it describes the overall strategy employed by the subject – walk in a straight line towards a destination – even when lateral oscillations are present and their feet move beneath them. It has also been shown that the instantaneous step width is a function of the bridge phase at the previous heel-strike. This is important for the MIPM because the instantaneous step width is a parameter in Hof's Extrapolated Centre of Mass (XCoM), which Macdonald uses to determine the ground force offset from step to step [126, 67].

The reader should keep in mind that step width is not a continuous function but a constant for each footstep (if the duration of double stance is neglected). It is described here only for the instant heel-strike occurs. The instantaneous step width depends on the phase of the bridge at the previous heel-strike, but should not be confused as a time-dependent parameter. Before turning to an analysis of ground forces, CoP and CoM behaviour must also be examined for walking on a moving base. Both the CoP and CoM *are* time-dependent, and therefore can be expected to evolve with the motion of the bridge. If the Centre of Mass and Centre of Pressure motion – and their separation – can be related to the motion of the bridge, then it is possible the MIPM could be expressed simply in terms of structural motion in order to predict ground forces.

7.2 CoP Displacement

Characterisation of the step width is important for adapting a forcing model to a moving surface. Unfortunately, however, foot placement is only one piece of the puzzle, contributing the offset of the ground force from step to step. Predicting the ground force throughout the gait cycle requires an understanding of CoP and CoM movement as well.

The Centre of Pressure trajectory is difficult to predict. This is partly due to the asymmetry of standing in single stance. When a subject stands quietly on one foot,

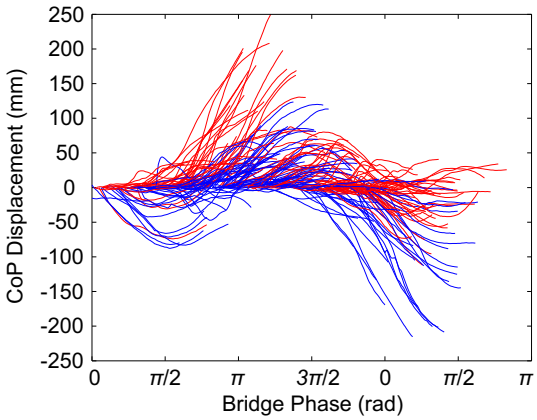

Figure 7.8: CoP displacements versus bridge phase during single stance for left (red) and right (blue) feet. Positive CoP displacement is to the left, negative to the right.

as discussed in Chapter 5, the structure of the ankle causes a different kinematic body reaction if the CoP moves medially versus laterally. This implies that the CoP moves differently depending whether the structure is moving medially or laterally to the foot.

Figure 7.8 shows 210 CoP displacements as a function of bridge phase. These curves show the lateral change in CoP location during single-stance. Again, left footsteps are red and right steps are blue. At first glance, the phase of the bridge is immediately apparent; the CoP displacement was generally in-phase with the bridge. When the bridge was at its maximum extents at phases $\pi/2$ and $3\pi/2$, the right or left CoPs respectively were dominated by the structure's motion. The structure's medial acceleration also caused a medial acceleration of the standing foot. This convergent behaviour could have been a source of positive damping to the structure because the CoM-CoP distance is compressed.

Around the inflection points, however, a surprising behaviour was observed. At π and 2π the left and right CoPs diverged respectively, rather than conforming to the structural phase. This divergence occurred when the bridge moved ipsilaterally to the stance foot, accelerating the stance foot away from the Centre of Mass. This could have resulted in a pedestrian providing negative damping to the structure, accompanied by a lateral push-off.

The previous figure was divided into groups to show how the CoP is affected by bridge amplitude. Figure 7.9 shows that CoP behaviour changed significantly as structural amplitude increased. Subplots (a) and (b) show that when the bridge amplitude was low, Centre of Pressure displacements were less than 50 mm and the trajectories often followed the typical question mark ('?') shape. In the first plot the samples were randomly distributed throughout the bridge cycle, but in the second grouping, some of the right and left footsteps were clustered. Plots (c) and (d) – depicting peak-to-peak bridge displacements of 50-100 mm and 100-150 mm – show that the CoP tracks began to align with the motion of the bridge. In the latter case, CoP displacements exceeded 100 mm in extreme cases. Finally plots (e) and (f) show CoP displacement for the greatest structural amplitudes. Most of the CoP displacement curves are sinusoidal like the motion of the structure, but these plots also show the most divergence around the inflection points.

Consider the curves in the 100-125 mm bridge amplitude case, Figure 7.9(f). Most of the curves are concentric about $\pi/2$ or $3\pi/2$. These sinusoidal CoP displacements indicate that the motion of the bridge controlled the motion of the CoP. This behaviour was exhibited in most samples across the bridge cycle. In contrast, notice the curves indicated with arrows. These two right feet and three left feet (all starting late in QIII) began with a period of zero CoP displacement. They then peaked in the lateral direction before concentrically following the other curves medially. In these situations, single stance started when the bridge velocity was almost zero. Thus, the zero CoP displacement suggests that the subject's CoP briefly acted in a stable base manner. As the bridge began to swing back towards the centre, the CoP swings laterally in an attempt to compensate for the motion of the structure. At the peak CoP displacement, the CoP reached the outside edge of the foot, the limit of the Base of Support. This was the extent of the CoP relative to the foot, so thus CoP displacement became controlled by the motion of the bridge. This condition also implies that in order to maintain gait

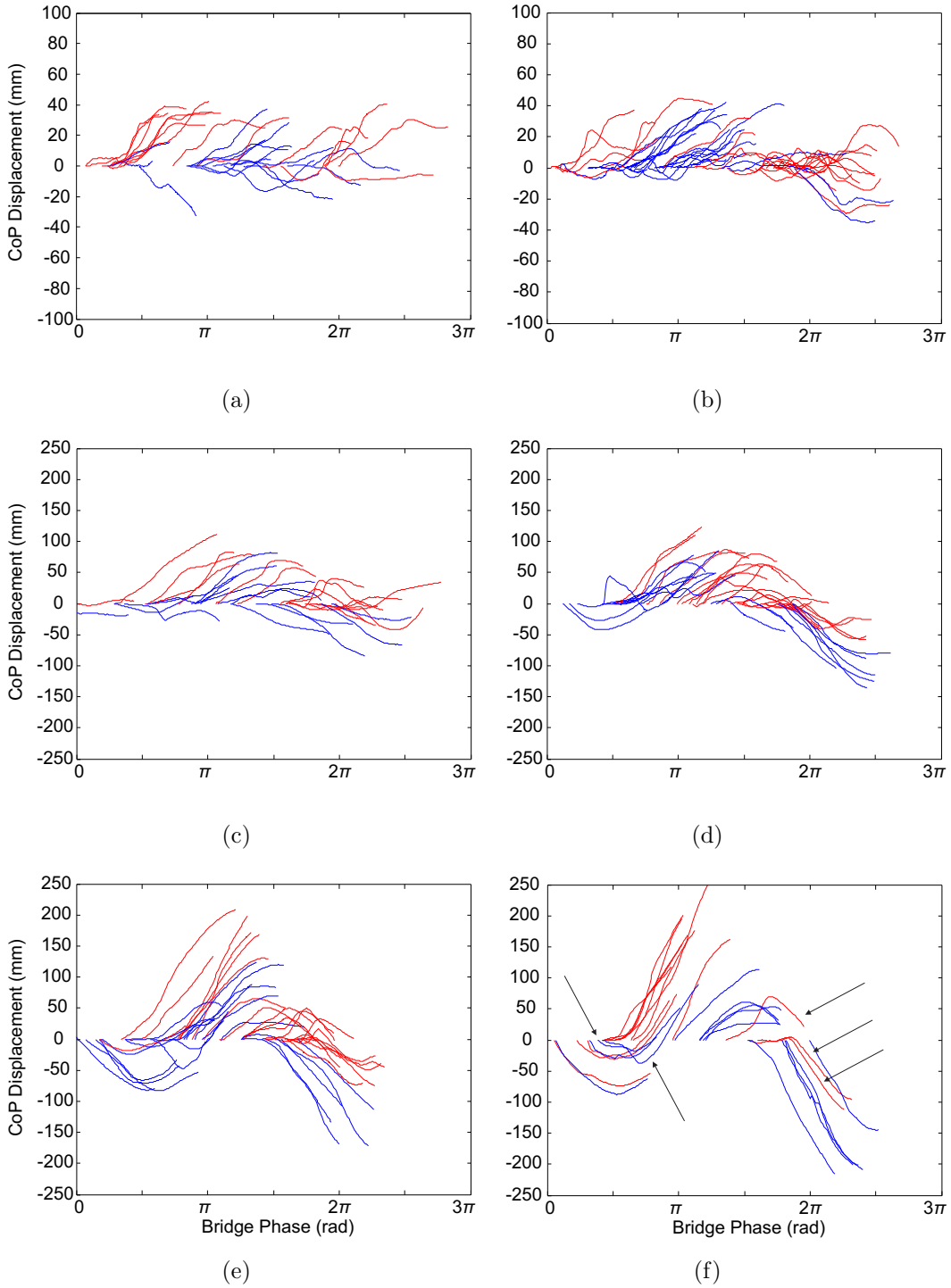

Figure 7.9: Centre of Pressure displacement during single stance versus bridge phase for different ranges of bridge amplitude. (a) Amplitude < 12.5 mm, (b) 12.5-25 mm, (c) 25-50 mm, (d) 50-75 mm, (e) 75-100 mm, and (f) 100-125 mm.

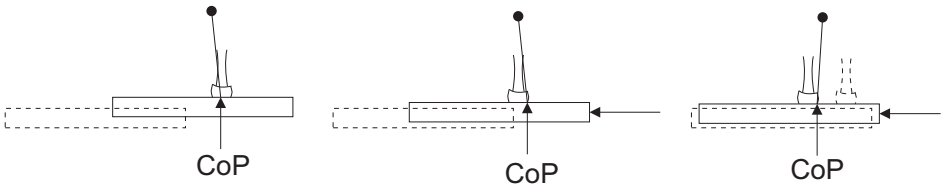

Figure 7.10: A right foot stance phase (frontal view from behind) with bridge at ipsilateral extent. As stance phase begins (left panel), bridge velocity zero; CoP normal. With bridge acceleration towards centre (middle panel), CoP moves to right extreme, where it becomes bridge-controlled. If the CoP displacement cannot compensate for CoM motion, the subsequent left step (dashed) is crossed (right panel).

stability, the subsequent foot crossed over to ensure that the CoM remained within the Base of Support, Figure 7.10.

In summary, four behaviours were exhibited by the Centre of Pressure when walking on a moving base. The first behaviour dominated when base motion was small, less than 25 mm amplitude. In such circumstances, CoP trajectories were largely unaffected by base motion, and subjects walked essentially the same as if the base were stable. The other three behaviours were observed for higher bridge amplitudes. Generally CoP motion was controlled by the sinusoidal oscillations of the bridge and thus reflected a sinusoidal shape. The two remaining behaviours were observed at bridge amplitudes over 50 mm. For steps taken during Quadrant II, the CoP displacement diverged from sinusoidal, resulting in a high instantaneous step width. In contrast, steps taken late in Quadrant III exhibited a moment of normal 'stable ground' gait before contralateral bridge motion controlled the CoP, causing a narrow or crossover step.

7.3 CoM Displacement

Data in the previous sections have shown that the Centre of Pressure location and instantaneous step width rely heavily on the amplitude and phase of bridge motion. These relationships are different for the Centre of Mass, which is *sometimes* affected by base motion. Brady *et al.* described that subjects on a laterally oscillating treadmill adopted one of two strategies, either keeping their CoM in phase with the base motion

Figure 7.11: Fixed-in-space (FIS, left) versus fixed-to-base (FTB, right) stability strategies for standing. In FIS standing, subject allows body to rotate about CoM as bridge moves. In FTB standing, whole body moves as a 'rigid' unit along with the bridge.

or fixing their CoM motion to the global reference and allowing their feet to oscillate like a pendulum beneath them [103]. In preliminary set-up of the Jenkin II tests, both types of CoM motion were informally observed during standing and walking (Figure 7.11).

In 'fixed-to-base' motion, the subject uses stiff joints and muscles to move monolithically with the bridge. In this sense, their pendulum length is infinite because the body does not rotate. Like a column or building in an earthquake, this method fails if the base acceleration causes the person to tip or if the foot slips/skids across the surface. Alternatively 'fixed-in-space' motion exhibits a pendulum length approximately equal to the CoM height, allowing the feet to oscillate in the fashion of a normal (i.e. non-inverted) pendulum beneath a stationary CoM. This method fails if the structure moves erratically, when an individual cannot tune their body pendulum to the oscillation of the structure. As inferred from Brady *et al.*, it is possible that individuals change between strategies depending on the motion of the structure and how stable the subjects feel.

Figure 7.12 shows a stacked histogram of CoM ranges. The CoM displacement refers to the lateral range through which the CoM traverses during one gait cycle while crossing the force plates. To determine the CoM range, the CoM values were adjusted

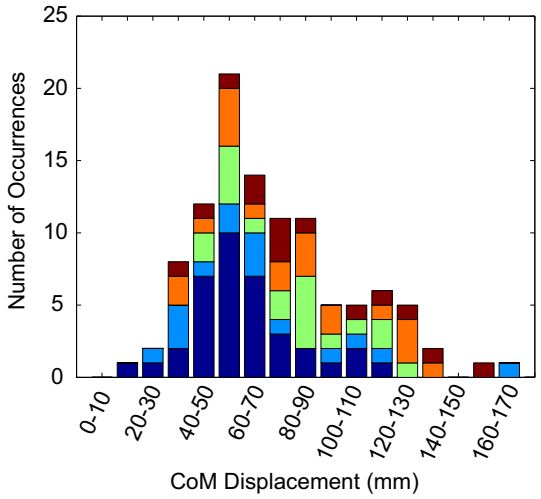

Figure 7.12: Stacked histogram of CoM ranges for varying bridge amplitudes. Dark blue, 0-25 mm bridge amplitude; light blue, 25-50 mm; green, 50-75 mm; orange, 75-100 mm; red, 100-125 mm.

Table 7.3: Mean and SD CoM Ranges for Different Bridge Amplitudes.

Bridge Amplitude (mm)	n	Mean CoM range (mm)	SD CoM range (mm)
0-25	37	61.27	21.45
25-50	15	68.91	37.44
50-75	19	79.81	24.28
75-100	20	80.69	32.38
100-125	14	85.36	33.84
All Samples	105	72.63	29.60

to account for subjects walking in a line skew to the coordinate plane. Then, the right-most CoM coordinate was subtracted from the left-most coordinate.

During the Jenkin II tests, the subjects overwhelmingly used the 'fixed-in-space' strategy during clean three-step trials. For the 0-25 mm bridge amplitude, all trials had a CoM range less than 120 mm, with the mode being 50-60 mm. The 25-50 mm bridge amplitude reflected this pattern, with all except one sample below 120 mm. For higher bridge amplitudes, the mean CoM range increased, Table 7.3. The histogram shows that variation is quite high however; a linear regression between CoM range and bridge amplitude (CoM range=0.289X+58.3) had a Pearson's r value of only 0.3249. The mode for 50-75 mm bridge amplitude was 80-90 mm CoM displacement, but the modes for higher bridge amplitudes were 50-60 mm and 70-80 mm. So while a weak trend exists, it would not necessarily be appropriate to consider CoM range to be a

function of bridge amplitude.

If the subjects had adopted a 'fixed-to-base' strategy, one would expect the CoM displacements to be more clustered by bridge amplitude, with the clusters clearly increasing in CoM range. The highest bridge amplitudes (100-125 mm) had a peak-to-peak displacement of up to 250 mm. Thus, the absence of CoM ranges – either outliers or clusters – over 170 mm suggests that the subjects did not fix their motion to that of the bridge. Several reasons could explain this behaviour. Foremost is the possibility that as subjects become accustomed to the structure's motion they all deemed fixed-in-space strategy to be more stable or comfortable. It is possible that a fixed-to-base strategy is only practicable for lower bridge amplitudes and lower accelerations. If so, it is possible that the effort required to maintain the appropriate body stiffness to move with the base is far greater than the flexibility allowed by adopting a fixed-in-space strategy.

Another possible reason for the predominance of fixed-in-space strategy is that forward walking requires a certain amount of joint flexibility prohibitive of the fixed-to-base strategy. When an individual starts to slip on an icy or gravelly surface, the temptation is to clench and stiffen one's muscles in an attempt to gain grip and stabilise. In essence, this is a fixed-to-base strategy. When Jenkin II participants stumbled due to unexpected bridge instability, they frequently stopped, stiffening up (and voiding a clean three-step trial). The author observed this behaviour when crossing the structure himself upon its original configuration. He also discovered – counter-intuitively – that by relaxing instead of stiffening his muscles, walking became much easier. This relaxation inherently required a fixed-in-space strategy that was subsequently observed in the participants.

Curiously the study by Brady *et al.* produced opposite results to the Jenkin II results [103]. Their laterally oscillating treadmill had a peak-to-peak displacement of 254 mm, comparable to the maximum bridge displacement in this study. They tested

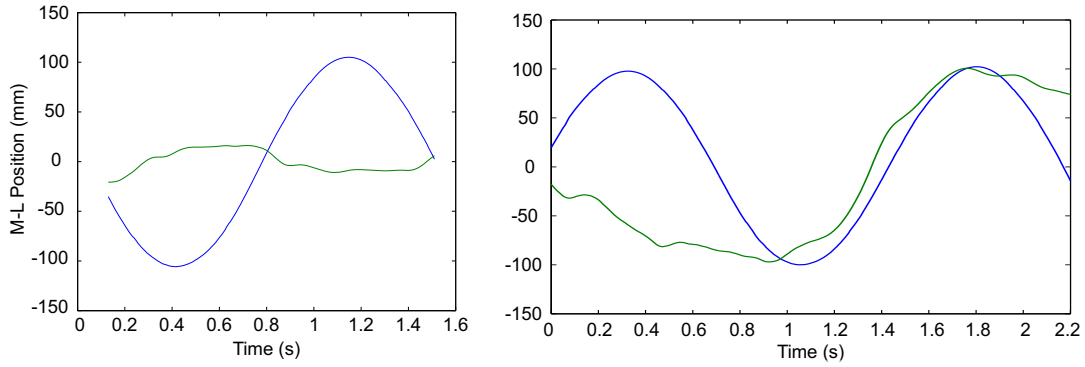

(a) (b)

Figure 7.13: Examples of (a) fixed-in-space CoM strategy versus (b) single step fixed-to-base strategy. CoM (green) and bridge position (blue) versus time.

two oscillation frequencies, 0.2 and 0.3 Hz, which were much lower than the natural frequency of the Jenkin bridge. They found that most participants adopted a fixed-to-base strategy over time; some even started with a fixed-in-space strategy before switching. The difference between the two studies could be due to the oscillation frequencies, for which a lower frequency imparts a lower lateral acceleration on the pedestrian. This, of course, would be easier to accommodate with a fixed-to-base strategy.

Finally, the fixed-to-base strategy is aided by a state of lock-in. Since the participants of the Jenkin II tests did not lock in to the motion of the bridge, fixed-to-base strategy was limited to transient, single-step balance control rather than prolonged balance strategy (Figure 7.13).

The main conclusion that can be drawn in this area from the Jenkin II tests is that bridge amplitudes over 50 mm cause a distribution of CoM ranges. For the three-step trials recorded, the subjects usually exhibited a fixed-in-space strategy, though during some transient motion the fixed-to-base strategy was evident.

Nonetheless, specific strategies were observed for CoM motion in the frontal plane. Unlike the conscious selecting of a fixed-to-base or fixed-in-space body motion, the subtle CoM strategies that follow appeared to be largely subconscious. Figure 7.14

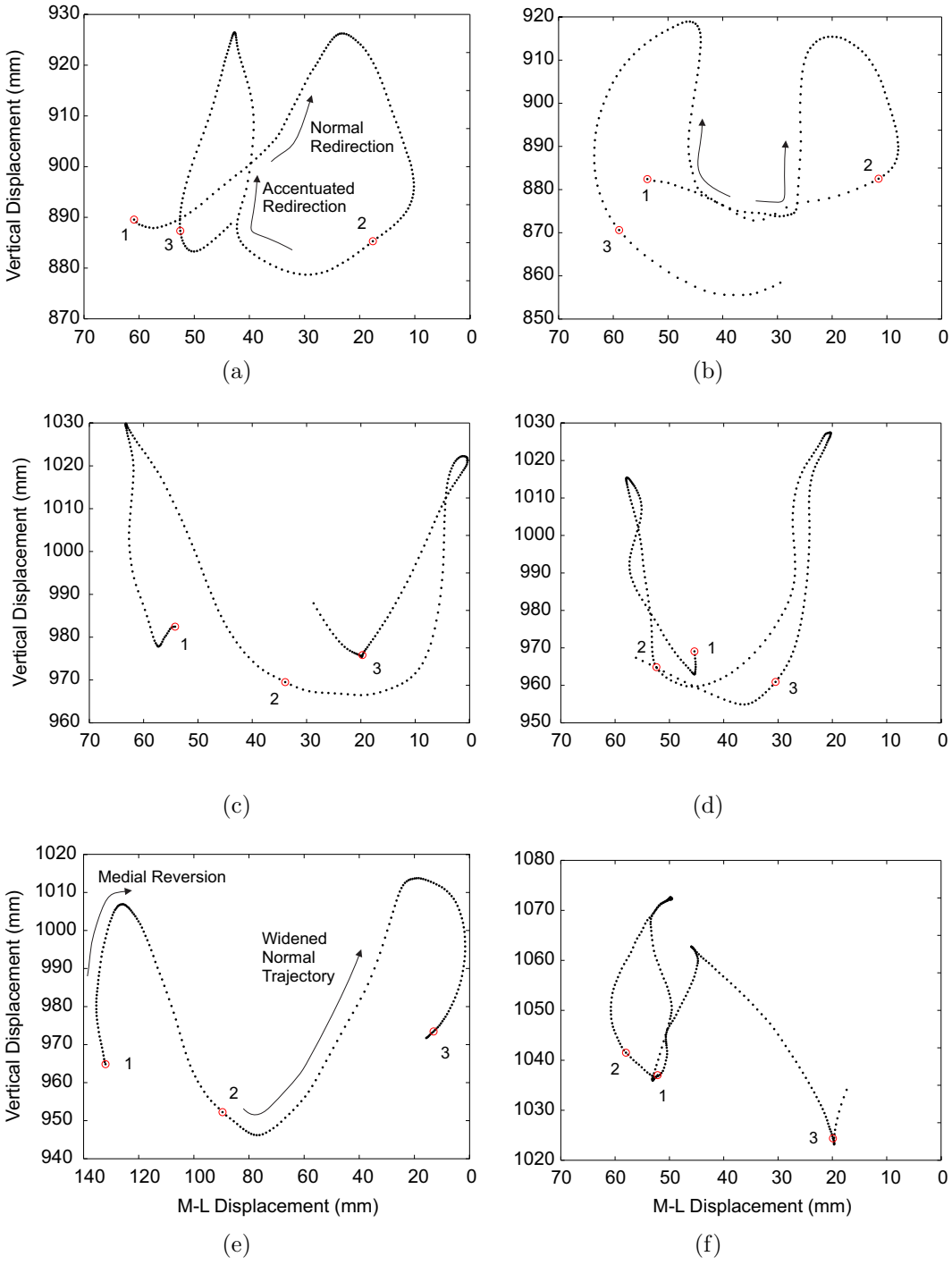

Figure 7.14: Various two-step CoM trajectories for coping with structural motion. Frontal plane projections from behind. Heel-strike points circled. See text.

shows a couple of the most commonly observed CoM patterns. The patterns shown here occurred on bridge amplitudes over 75 mm, again showing that the CoM range was usually tightly controlled.

Figure 7.14(a) shows an near-normal figure eight trajectory (compare to Figure 5.3), suggesting that a normal CoM trajectory is possible even for high bridge amplitudes. That said, it and Figure 7.14(b) exhibit sudden redirections of the CoM after heel-strike. During this behaviour the CoM changes from lateral to vertical motion at a near right angle. Figure 5.3 shows that a mild alteration of CoM trajectory can occur in normal walking, but the behaviour was more pronounced and more common in moving base trials. The change in CoM direction does not correspond to toe-off timing, so it is possibly due to an acute, corrective rise through the knee and/or ankle. This forces the pelvis upwards via the stance leg which in turn causes a torque about the CoM that opposes its lateral translation. Thus the CoM stabilises before continuing laterally as normal.

In many cases, subjects had a U-shaped CoM trajectory during the moving base tests, as observed in Figure 7.14(c) and 7.14(d). The total lateral CoM range in these cases remained small compared to the bridge amplitude, but the vertical range sometimes exceeded the M-L range, even by tens of millimetres. Most of the lateral motion occurs immediately after heel-strike, while most of the vertical motion transpires during single stance. Unlike the previously described behaviour, where the CoM continued laterally after the vertical redirection, these patterns show that the CoM retraces its trajectory, going vertically down. The patterns are similar to those observed by Tesio *et al.* who found that as gait speed increased from walking to running, CoM trajectory changed from a figure eight to a U-shape [101]. When M-L position is plotted against time, these U-shaped trajectories appear to be flattened sinusoids, as will be discussed later.

Though not the majority, there were cases of significant lateral displacement, such

as during transient fixed-to-base motion. Figure 7.14(e) shows an example where the CoM moves significantly. In the first step vertical motion – potentially due to the aforementioned knee and toe rise – causes a medial reversion of the CoM path. The subsequent step is corrected, but the medially directed motion of the first step causes the trajectory of the second step to be slightly wider than normal. In this case the medial reversion of the first step led to a stable second step, but medial reversion could cause the subsequent step to be unstable as well.

Finally, 7.14(f) shows an example of an irregular CoM trajectory. These could have been caused by body rotation about the vertical axis, sudden applications of upper body angular momentum, or other stabilising motions.

The variety of CoM trajectories presented here highlight the various ways individuals manage gait instability. Even though the lateral CoM motion is usually small for fixed-in-space walkers, patterns clearly vary depending on the individual. Given that the IPM and MIPM rely on CoM-CoP separation, the relationship of these two parameters will be investigated in the next section.

Even though the aforementioned trajectories are subtle, abrupt changes to CoM location play an important role in managing CoM velocity and acceleration. Various works by Hof *et al.* and supported by Macdonald *et al.* and Bruijn *et al.* among others used the so-called Extrapolated Centre of Mass (XCoM) as a measure of gait stability [126, 153, 67, 69, 127]. They state that for an inverted pendulum walker, the XCoM must remain within the Base of Support, where the XCoM position is defined in Equation 1.19. In theory, the Inverted Pendulum Model produces an alternating curved V-shaped XCoM, as seen in Figure 7.15. This requires a smooth, quasi-sinusoidal CoM displacement pattern and the sawtooth-like velocity pattern seen in the middle plot. In reality, however, the Jenkin II subjects rarely exhibited this ideal. The CoM patterns discussed above resulted in CoM patterns that did not vary quasi-sinusoidally in time, but were more eccentric or flattened. The abrupt redirection of the CoM position

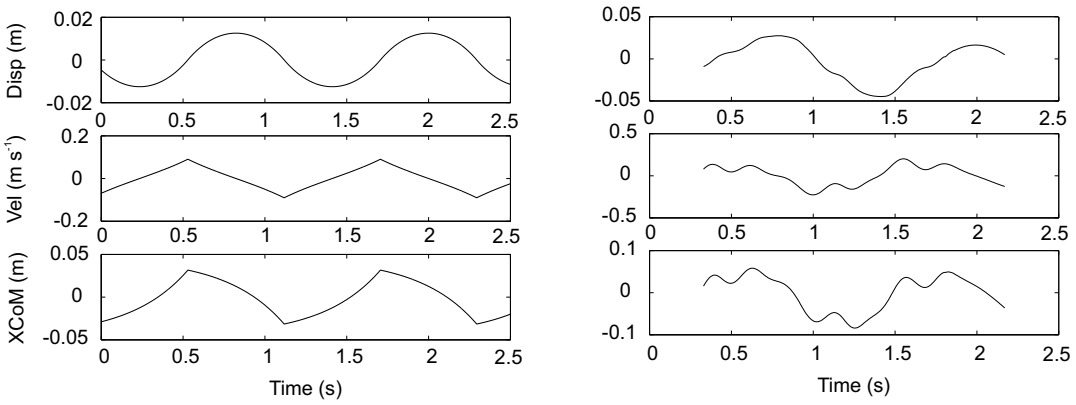

(a) (b)

Figure 7.15: A comparison of theoretical (left) and experimental (right) CoM displacement, velocity, and XCoM values versus time. The experimental results show values for three steps, left-right-left, with left positive and right negative.

resulted in a velocity pattern featuring doubled peaks.

Overall, the XCoM typically stayed within or at the Centre of Pressure, though Hof *et al.* state that the XCoM can be outside the CoP but within the Base of Support (or briefly even, in special circumstances, outside the BoS) for stability to be maintained. Given that the Jenkin II tests did not record the perimeter locations of the feet, it is not known for certain how close the XCoM and CoP were to the edge of the BoS. That said, the location of the XCoM at or within the CoP and the fact that no subjects fell over suggests that the XCoM values that were observed remained sufficiently within the Base of Support – even though they did not resemble the theoretical curve.

7.4 CoM-CoP Separation

Where the CoP trajectory depends on the phase and amplitude of the bridge and the CoM trajectory usually remains relatively stationary, the CoM-CoP separation can be expected to reflect the behaviour of the CoP. Figure 7.16 shows how the separation is affected by bridge phase and amplitude. At low bridge amplitudes the CoM-CoP separation is not visibly affected by the phase of the bridge. The CoM is always within 150 mm to the right of a left CoP and 150 mm to the left of a right CoP. The curves

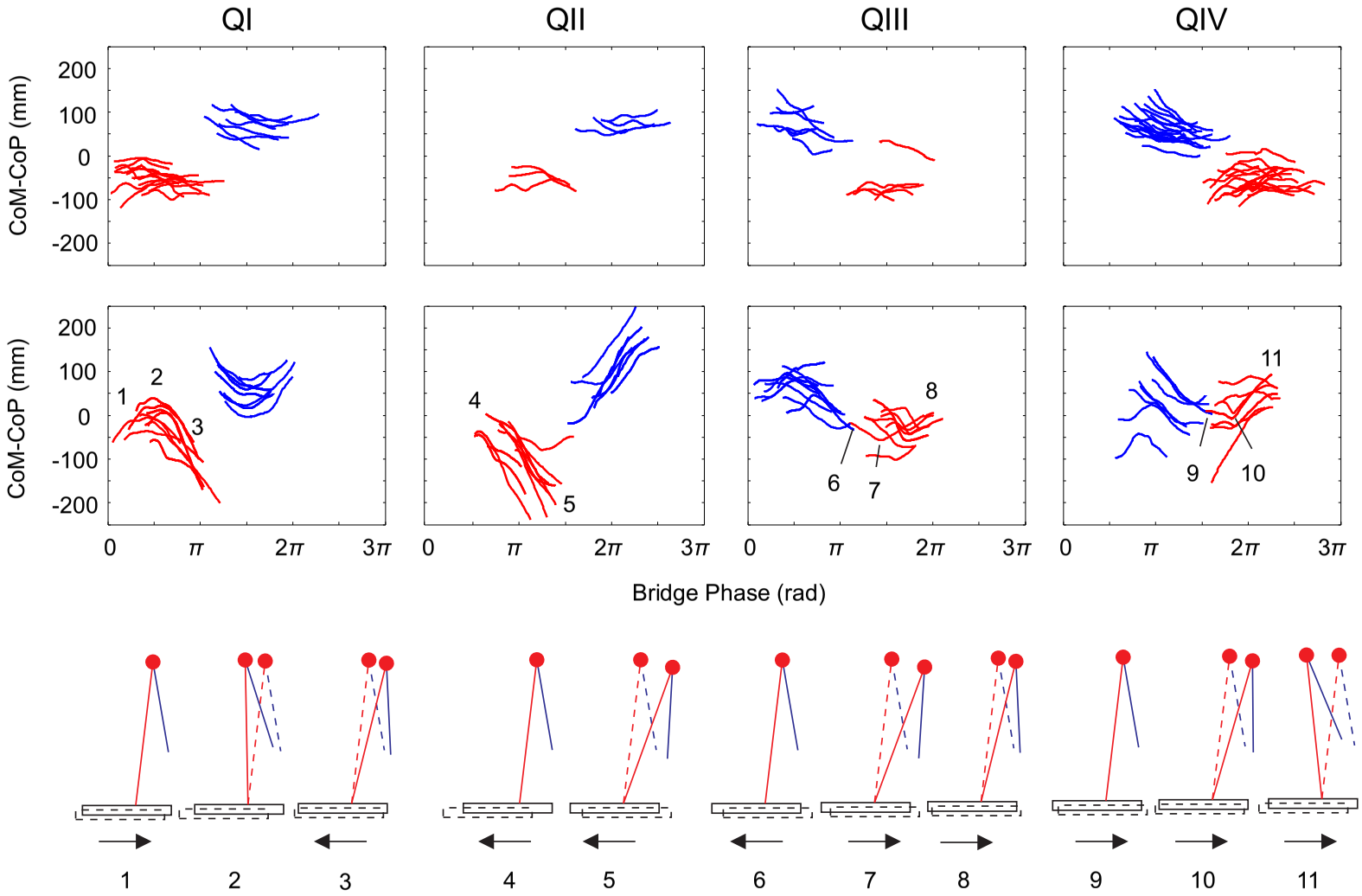

Figure 7.16: CoM-CoP separation for trials of bridge amplitude 0-25 mm (top) and 75-125 mm (bottom) based on phase at start of single stance. Left (red) and right (blue). IPM figures show relative CoM-CoP separation at key landmarks, arrows indicating base motion (dashed rectangles show bridge centre position).

are all relatively flat but most exhibit some oscillation in the early to middle portion of the step.

For the higher bridge amplitudes, phase dependence is observed. The CoM-CoP separation in QI is sinusoidal with the least separation occurring when the bridge was at its contralateral extent ($\pi/2$ for left feet, $3\pi/2$ for right). In some cases the CoM-CoP separation passed zero, suggesting that the CoM was outside the CoP (or, expressed another way the foot passed underneath the CoM). On a stationary-base, this would cause lateral gait instability, but the (ipsi-)lateral acceleration of the stance foot quickly reverts the CoP to the 'correct' side of the CoM. The corresponding lateral ground forces for these samples could be expected to reach or cross zero.

For stance phases beginning in Quadrant II, divergent CoM-CoP separation is observed, which corresponds to the CoP patterns discussed previously. The separation was maximised in this phase as the stance foot moved up to 250 mm away from the CoM. In the MIPM model these footsteps should cause the lateral forces to increase significantly over the course of the step.

Where the patterns in QI and QII were generally concentric, those of QIII and QIV are less so. Quadrant III reflects a similar behaviour to that mentioned for the CoP. In most cases the CoM-CoP separation increases slightly to a peak just after the bridge reaches its ipsilateral extent. The increase depends on the individual; some have a flat region followed by a steep increase (like the aforementioned CoP behaviour) while others increase consistently throughout. After the peak the CoM-CoP separation decreases, sometimes appearing to follow a sinusoidal trajectory.

Finally Quadrant IV reveals predominantly converging behaviour with the highest proportion of crossed footsteps. Most of the footsteps exhibit a decrease towards zero, indicating that the CoP is moving closer to the CoM. This is logical given that CoM and CoP are moving in opposite directions to each other at heel-strike (which also happens at the beginning of QI). Alternatively, some samples reveal a medial peak

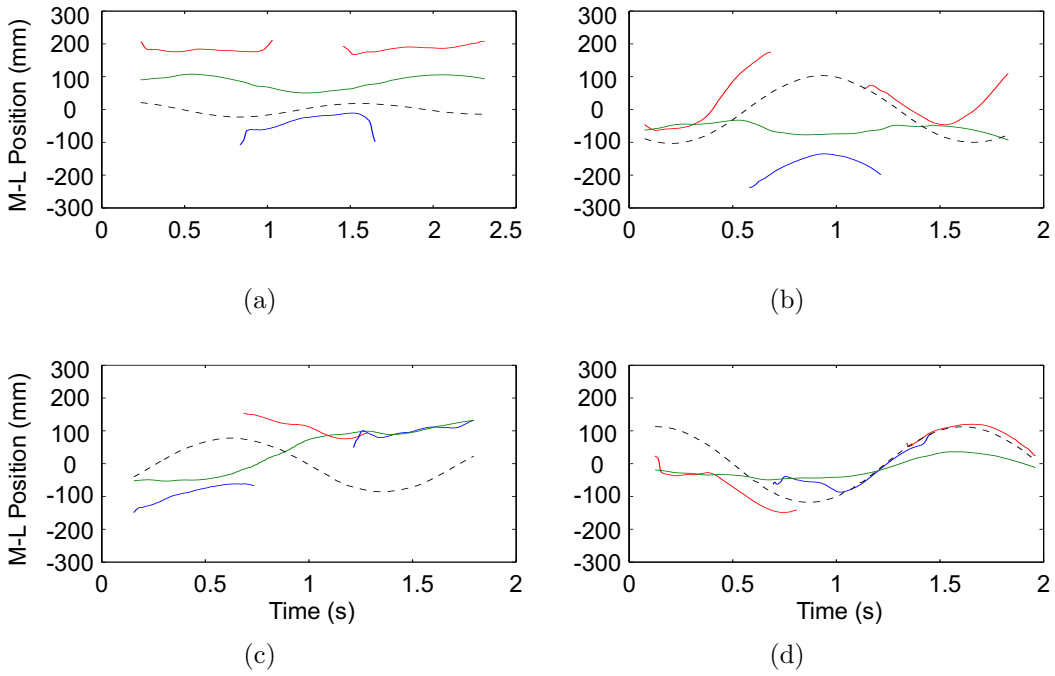

Figure 7.17: The relationship between CoM (green), CoP (red (left) or blue (right)), and base motion (black dashed) for different phases of the structure.

in early to mid-stance when the CoM is already at the edge or outside the Base of Support. This suggests that the CoM initially 'catches up' to the CoP before turning more lateral of the CoP. This inevitably leads to a crossed next footstep.

Putting together the CoM and CoP, it is necessary to examine how subjects connect their Centres of Pressure and locate their Centre of Mass from step to step. Figure 7.17 shows a number of three-step CoP traces with the bridge position and CoM location as a function of time. In Figure 7.17(a), where the bridge motion is small, the CoP traces are shaped normally and spaced evenly. The CoM oscillates in a sinusoidal manner, out of phase with the bridge. Figure 7.17(b) shows a subject walking nearly in anti-phase with the bridge. The first, left, step begins at the end of QI, resulting in divergent behaviour and a wide second step. The right step *also* begins in QI and leads to a wide next step. The final step begins in QIV and initially tracks the motion of the bridge. Meanwhile the CoM has a flattened trajectory compared to normal, clearly shifting from left to right and vice versa but remaining relatively linear during single stance.

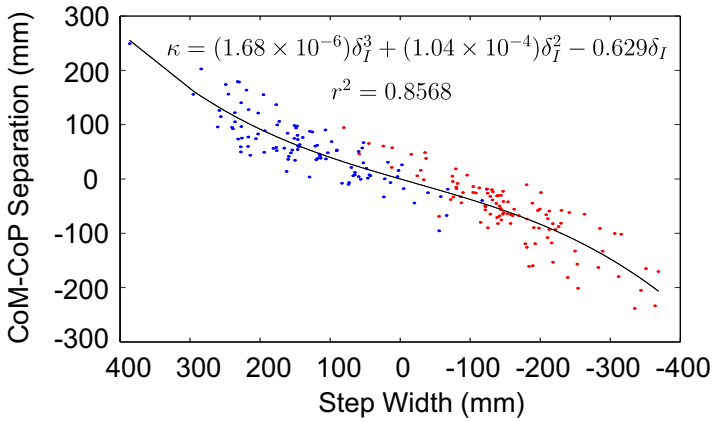

Figure 7.18: CoM-CoP separation as a cubic function of instantaneous step width. Left-to-right steps (red) and right-to-left steps (blue).

Figure 7.17(c) depicts a crossed step. With the first (right) single-stance beginning at the start of QI, the second step is a wide left step. This left step begins in QIV, so the subsequent right crosses over the previous step. The CoM is normal for the first step, but crosses the CoP in the second step and follows the CoP in the third. Here we could expect the MIPM to be zero for the last half of the trial. The final frame, Figure 7.17(d), shows a left and a right step beginning in QIV and QIII respectively. They have flat regions before conforming to the sinusoidal motion of the bridge. The second step is crossed and the final step is in-line with the second. The CoM is flat for the first two steps before adopting a wider trajectory for the third step. Where the CoM is almost constant and the CoP is sinusoidal, one might expect the M-L ground force to also be sinusoidal.

Recalling that instantaneous step width is directly related to the offset of the medial-lateral force from step to step, the step widths shown in Figure 7.17 become of importance to M-L ground force prediction. Thus, the CoM-CoP separation was plotted against the instantaneous step width to see if a relationship existed between the variables at heel-strike. Figure 7.18 shows that the CoM-CoP separation for both left-to-right and right-to-left is fitted well by a single cubic function, which can be used in the MIPM equation. It can also be shown that the CoM-CoP separation of the receiving

foot is best fitted by the equation $\kappa = (1.68 \times 10^{-6})\delta_I^3 + (1.04 \times 10^{-4})\delta_I^2 - 0.629\delta_I$ where κ is the CoM-CoP separation, which is approximately equal to Macdonald's $u - y$ [67].

7.5 Force Patterns & Modelling

Thus far a number of patterns have been identified in the placement of the foot, the CoP trajectory, the CoM trajectory, the XCoM, and CoM-CoP separation. These pertinent kinematic and kinetic data from eight representative trials are plotted in Figure 7.19. The plots include the adjusted frontal plane CoM trajectory; the time-variant M-L CoM position (unadjusted), CoP, XCoM, and bridge position; and the time-variant M-L ground force, IPM, and MIPM. For the IPM, the pendulum length was selected as the distance from the CoM to the CoP, though using a constant 1200 mm gave similar results. Also for the IPM, $u - y$ was chosen to be the difference in the lateral positions between the toe marker and the CoM during stance for the reasons discussed in Chapter 5. For the MIPM, the vertical force was assumed to be the body weight. In both models, the ground force was linearly interpolated from one foot to the other over the duration of double stance.

7.5.1 Force Plate Results

When examining the force plate records, the first aspect that stands out is that each pattern is unique. The eight patterns are not only produced by different individuals, but they occur at different bridge phases, leading to different characteristics. Nonetheless, some general patterns do emerge.

The amplitude of the M-L ground forces is generally correlated to the CoM-CoP separation. This is to be expected given the prior results in the thesis, but nonetheless bears mentioning. This trend is particularly evident in cases where the CoM-CoP separation is small. In Figure 7.19(a) steps one and three, the left CoPs touch the CoM trajectory, resulting in a lateral ground force close to or below zero. Similarly

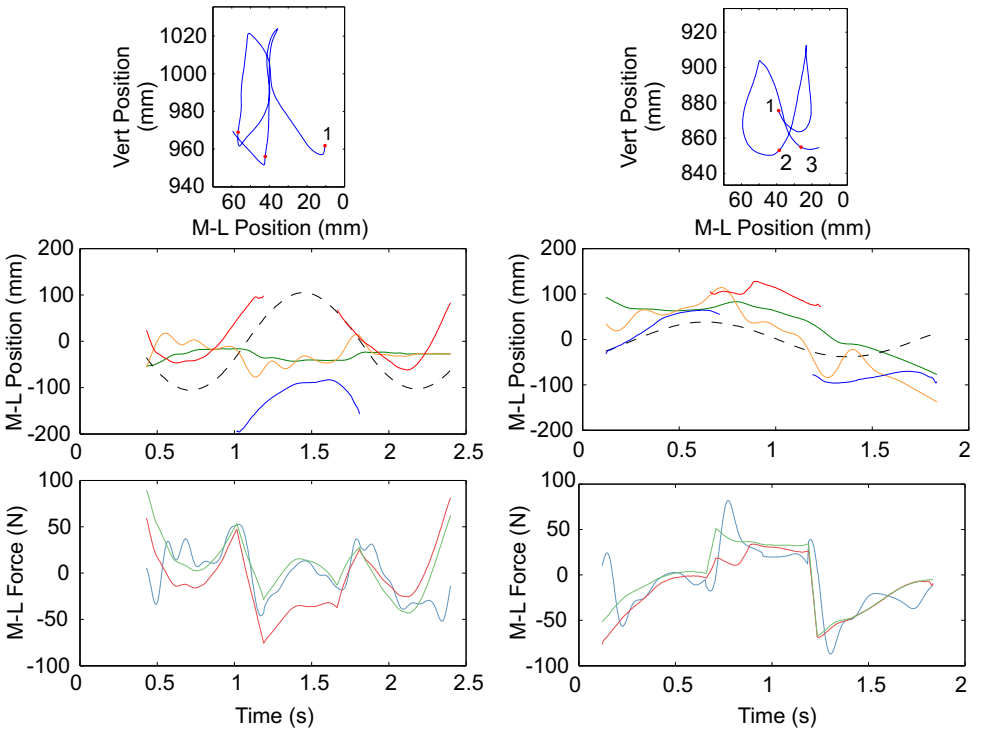

(a) (b)

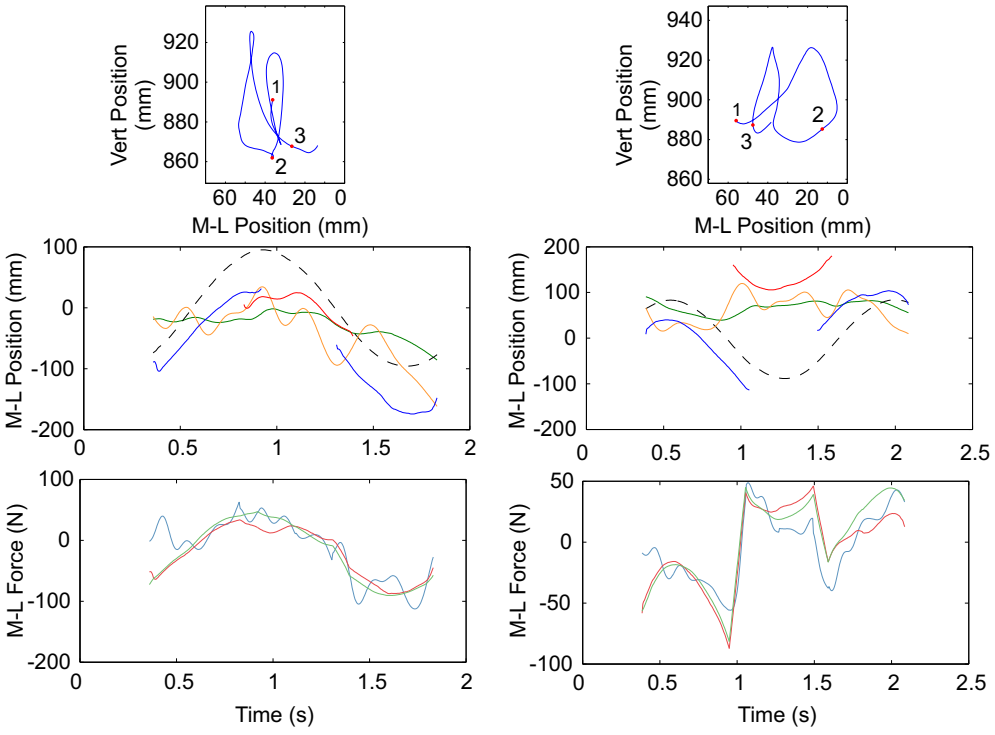

(c) (d)

Figure 7.19: (Continued next page)

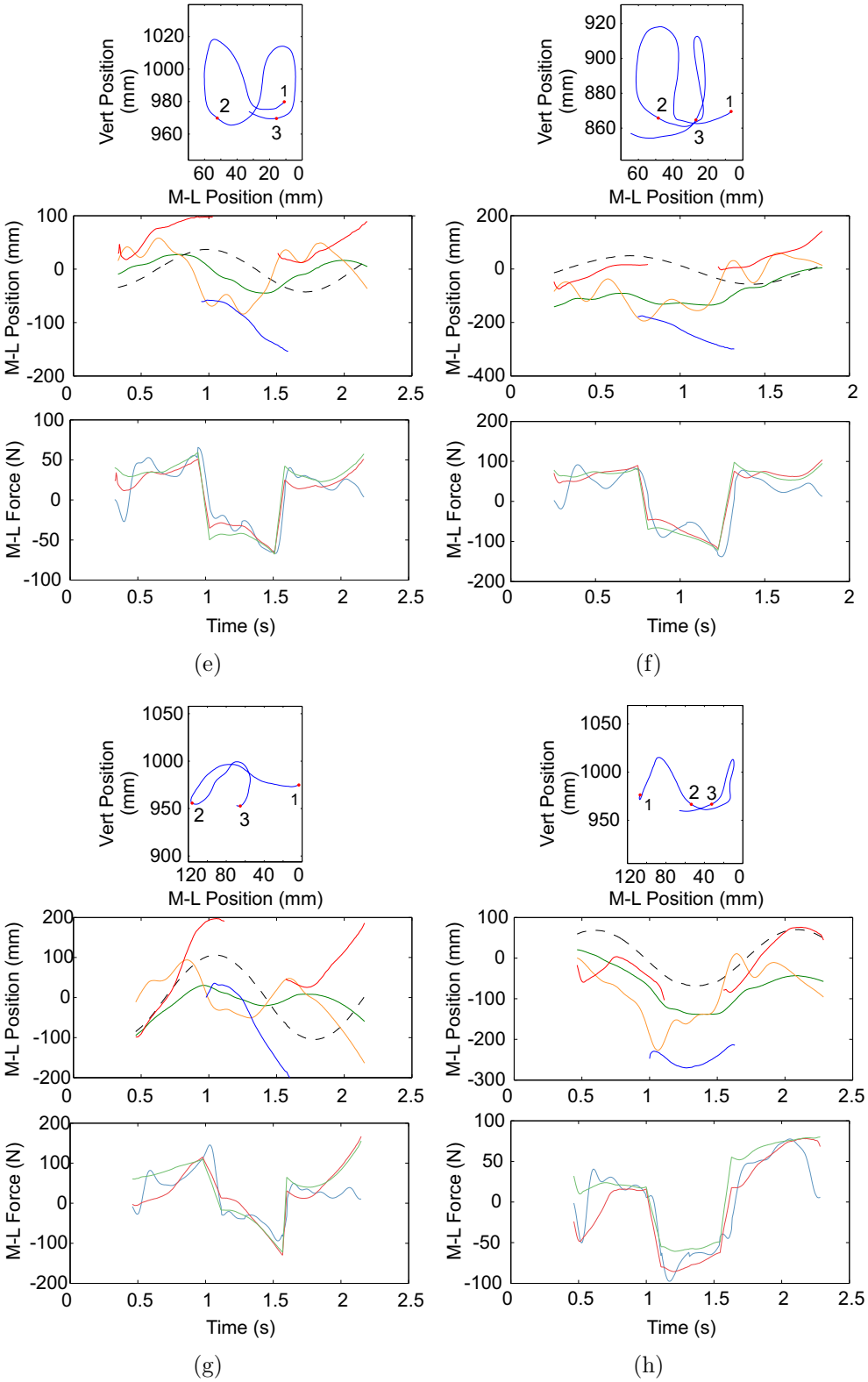

Figure 7.19: Top: Adjusted CoM trajectory (first two steps), heel-strikes red. Middle: Bridge position (black dash), CoPs (left red, right blue), XCoM (orange), CoM (green). Bottom: Sum of force plates (blue), IPM (green), and MIPM (red).

in Figure 7.19(b) the (right) CoPs approach the CoM, so M-L force decreases from (negative) 50 N to zero. In Figures 7.19(c) and (d) the first and last step respectively actually cross over the CoM. In these cases the M-L ground forces change from lateral to contralateral. Notice as well that all of these cases begin in Quadrant IV, indicative of the CoP moving medially under the CoM.

Whenever a subject took a wide step, he or she tended to push off with the trailing foot. At $t = 1$ s in Figure 7.19(d), the participant changes from right (originating in QI) to left feet. This wide step causes the trailing foot to push off laterally, reaching (negative) 50 N, a large increase over the course of the footstep. The same behaviour is seen at $t = 1.5$ s in Figure 7.19(e) and $t = 1.25$ s in Figure 7.19(f), where the wide step causes a lateral push-off much greater than the force over the rest of the step. Finally in Figure 7.19(g), the push-off forces are seen in consecutive wide steps. Rönnquist inferred in his doctoral thesis that the M-L ground force was correlated to bridge phase, but he suggested that the overall structural amplitude had to be increasing as well [41]. The results here clarify and support those of Rönnquist while also attributing the changes in ground force to the step width and CoP-CoM separation.

Concerning the step width, the figures also show that the offset in the M-L ground force from step to step is proportional to the width of the step. The participant in Figure 7.19(c) slightly crosses her second step over her first. As a result, no obvious offset occurs in the ground force, which incidentally is quasi-sinusoidal in phase with the structure. Figure 7.19(b) depicts a trial with a small and larger offset. The subject takes a small second step; even though a large transient peak in the ground force is evident, the level plane of the rest of the step is less than 30 N more than the force at the end of the previous step. The width of the third step is approximately 160 mm to the right of the second step. This large step is met with an approximately 90 N offset in the M-L force. Finally, the steps in Figure 7.19(e) are among the largest at about 160 and 170 mm. They correspond to force offsets of 70 and 90 N respectively. Assuming the

participants were walking at approximately the same speed (Figure 7.5) the correlations between bridge phase and step width can be extended to the relationship between phase and M-L ground force.

Finally, as an aside, most of the figures shown exhibit the flattening of the CoM trajectory indicative of a U-shaped and fixed-in-space strategy. Rather than the sinusoidal shape of the IPM CoM trajectory, Figures 7.19(a) to (c) and (f) all exhibit three flat (linear) phases separated by shallow offsets. These flat regions occur when the CoM is moving vertically, as seen in the accompanying frontal plane trajectories. Figure 7.19(h) is unique in that the CoM exhibits a 'wide' translation of the CoM in the first step, followed by almost zero lateral translation in the second step, followed by translation again in the third. Across the plots, the variations in the XCoM due to the redirection of the CoM are clearly visible. It is possible that the XCoM – and therefore the CoM velocity – relate to the high-frequency content of the M-L ground forces.

7.5.2 Fitting the IPM and MIPM Models

One of the major deficiencies of the Inverted Pendulum Model identified in Chapter 3 was that the model did not capture the higher frequency content of the real M-L ground forces. The plots of Figure 7.19 show a wide variety of acute oscillations in the forces recorded by the plates. The IPM and MIPM have also been plotted for comparison. As before, the Inverted Pendulum Model fails to account for these high-frequency oscillations. Now, however, the Modified Inverted Pendulum also fails in this regard. Ultimately, neither the CoP nor CoM exhibited the high-frequency content necessary to predict the frequency content of the ground forces, so these models are too simple to obtain a perfect match.

Nonetheless the amplitude of the models and the overall fit is good. In most cases the IPM matches the amplitude of the ground force well. The MIPM typically fares slightly better, though cases such as Figure 7.19(a) show that sometimes the MIPM

was incorrect. It should be noted that since the CoP trajectory for the motion-tracking insoles was aligned to the global coordinate system using the toe marker as a reference, and since the IPM was based on the toe marker exclusively, many of the IPM and MIPM forces converge during the latter half of the step. It was also observed that using the heel marker instead of the toe marker for the IPM did not make an overall improvement to the predictions, but improved some heel-strike predictions and worsened some other toe-off predictions.

One further deficiency was observed for the MIPM predictions. In many cases, the MIPM failed to predict transient behaviour in heel-strikes. In samples beginning in QIII-IV, such as the middle step ($t = 0.8$ s) of Figure 7.19(b) or the first step of Figure 7.19(h), the flat part of the CoP trajectory before the lateral peak causes the MIPM to decrease instead of increase. In other cases as well (Figure 7.19(g) first step), the MIPM dramatically under-predicts the real ground force.

The MIPM relies on an accurate reproduction of the CoP trajectory using the insoles. The toe marker was easy to locate in the insole coordinate system, and provided the rotational reference point for transforming the local coordinates to global. Since it was harder to locate the heel marker to the insole coordinate system (due to the structure of the shoe, etc.), it is likely that some error could have been introduced to the CoP trajectory. Since the local coordinate system was rotated about the toe, CoP positions nearer to the toe were less prone to error. The error at the heel could be ± 20 mm before rotation.

In spite of the deficiencies, both models not only reproduced the amplitudes of the M-L ground forces, but did so regardless of foot placement. Whether the steps were wide or crossed, the inverted pendulum models were reasonably close to correct. This shows that even with deficiencies, the motion of a human on a moving surface is similar to an inverted pendulum with base motion.

7.6 Discussion

This chapter has provided a variety of interesting results from the Jenkin II tests. These tests involved asking participants to cross a naturally swinging bridge most closely related to the oscillating platform tests conducted by previous authors. The advantages to these tests were that the structure was allowed to swing completely in response to forces imparted by the test subjects and that the subjects could freely select their walking speed. This meant the structure could react to the sudden movements of individuals and individuals could react to the instability of their gait. Having only one pedestrian on the structure at a time meant that the mass ratio was below 10% and sudden inertial changes to the structure were very subtle. Even still, participants did occasionally have to pause to catch their balance, although these cases typically caused the subject to double-step or step off of a force plate. The video and motion capture from these tests is worth future analysis.

A wide variety of M-L ground force patterns were depicted which exhibited a strong correlation with the CoM-CoP separation, whether during crossed, narrow, normal, or wide steps. The instantaneous step width was found to be correlated to the displacement of the bridge and its phase at the previous heel-strike. The phase of the bridge at heel-strike was a major determinant of CoP displacement over the course of the subsequent stance phase. The net step width was minorly correlated to bridge motion, suggesting that a person will usually aim to put their next step in a 'normal' (i.e. stable ground) position relative to their first step.

In addition to these revelations, the offset of the ground forces between steps was found to be proportional to the instantaneous step width. With the CoM-CoP separation – which is related to M-L ground force via the MIPM – also proportional to the step width, the possibility arises for the development of a model that describes M-L ground force solely in terms of structural motion and a few anatomic measurements.

Unfortunately, while the motion of the CoP is highly correlated to the motion of the structure, the CoM is not. The IPM describes the frontal plane trajectory of the CoM as two intersecting circular arcs while the MIPM allows the CoM to be in any position relative to the CoP. In stable ground symmetric gait, the M-L CoM position (i.e. versus time) is nearly sinusoidal, but this is not the case on a moving base. While previous research has suggested that individuals fix their CoM motion to the structure, the Jenkin II results suggest a fixed-in-space strategy. Even for a fixed-in-space strategy, however, M-L CoM motion can be either sinusoidal or flattened versus time and the variation of CoM trajectories in the frontal plane makes modelling difficult. Given that the MIPM requires knowledge of the CoM-CoP separation (not just at heel-strike, as shown above), more research is required if M-L ground forces are to be modelled in terms of structural motion. Still, most of the component relationships are present; future study of CoM motion could provide the link to make a structurally-based ground force model possible.

7.7 Conclusion

Having examined many facets of walking on a moving base, the MIPM is found to be a good model for predicting the amplitude of M-L ground forces. The model fails to reflect the high-frequency content of the force plate-recorded ground forces, but the amplitude match should be sufficient for most modelling purposes. Most importantly, the behaviour of the MIPM during wide and crossed steps shows that an inverted pendulum-style model is indeed appropriate for predicting ground forces in an oscillating base condition. The results therefore verify that IPM-based simulations can be appropriate for designing and analysing structures with similar parameters.

Chapter 8

Gait Analysis in Spherical Coordinates

Thus far the Inverted Pendulum Model has been examined from a variety of perspectives. One of the main deficiencies of the IPM is that it cannot reproduce the figure eight trajectory of the Centre of Mass. This is due primarily to the fact that the IPM consists of a rigid stick support so in the frontal plane the CoM remains at a constant distance from the Centre of Pressure.

If an inverted pendulum oscillates in the frontal plane, the pendulum length remains constant and the CoM traces a circular arc. If, however, an inverted pendulum is permitted to sweep through three dimensions along the surface of a sphere, the pendulum length remains constant and the frontal plane trajectory can produce a figure eight shape.

In this final chapter, the kinematics of gait in spherical coordinates are explored. A preliminary theoretical spherical MIPM is presented and its motion is compared with experimental data from both the stable ground and moving bridge tests.

8.1 Theory

Consider the coordinate system defined in Figure 8.1. The Inverted Pendulum Model of gait has been converted to three dimensions using spherical coordinates. As with the 2D case the base of the pendulum is a pinned joint representing the Centre of

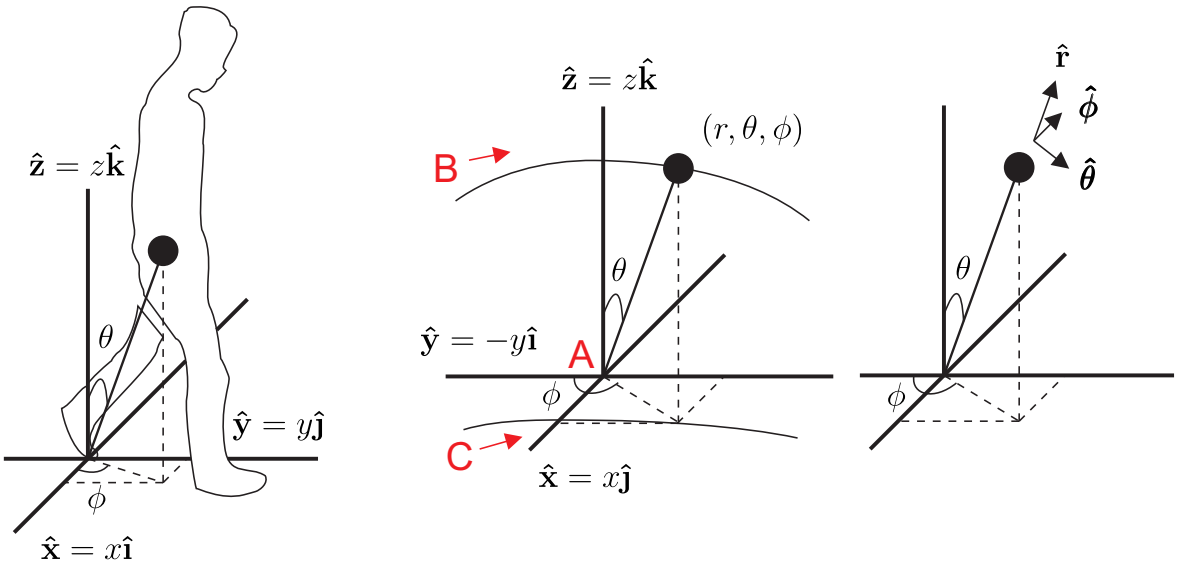

Figure 8.1: Depiction of an inverted pendulum in spherical coordinates. (Left) Typical coordinate system for deriving kinematic equations. (Centre) Coordinate system used for this study. As the subject's Centre of Mass moves parallel to the y-axis it pivots about the (A) Centre of Pressure. Approximate 3D CoM motion path shown by curve (B) with its projection on the ground shown by (C). (Right) Spherical coordinate system.

Pressure and the free end consists of a point mass representing the Centre of Mass. The configuration shown represents the MIPM of a left footstep (after mid-stance): the mass moves in a spherical path more or less parallel to the y-axis (the A-P direction) with x (the M-L direction) always positive for normal, stable walking. The 2D inverted pendulum would be represented by the projection in the $x - z$ plane.

The vector (r, θ, ϕ) defines a point on a sphere where $\mathbf{r}$ is a vector from the origin to the point, θ is the angle between the positive z-axis and $\mathbf{r}$, and ϕ is the angle between the negative y-axis and the projection of $\mathbf{r}$ in the $x - y$ plane with anti-clockwise being positive. The resulting unit vectors $(\hat{\mathbf{r}}, \hat{\boldsymbol{\theta}}, \hat{\boldsymbol{\phi}})$ constitute an orthogonal coordinate system superimposed in a cartesian coordinate system.

The derivation that follows is based on a typical derivation of spherical motion (e.g. Kasdin and Paley [154]) where Cartesian unit vectors $(\hat{\mathbf{i}}, \hat{\mathbf{j}}, \hat{\mathbf{k}})$ would correspond to $(\hat{\mathbf{x}}, \hat{\mathbf{y}}, \hat{\mathbf{z}})$. Generally such a derivation is taken with ϕ from the positive x-axis. In the following derivation, however, the end application makes it desirable for the sign

of ϕ to vary from zero to π for left footsteps and zero to $-\pi$ for right steps. Therefore ϕ is measured from the negative y-axis – the axis of walking progression – as seen in the figure. This leads to the subsequent derivation of spherical motion with $(\hat{\mathbf{i}}, \hat{\mathbf{j}}, \hat{\mathbf{k}})$ corresponding to $(-\hat{\mathbf{y}}, \hat{\mathbf{x}}, \hat{\mathbf{z}})$.

In spherical coordinates the unit vectors may be defined as:

$$\hat{\mathbf{r}} = \sin\theta(\cos\phi\hat{\mathbf{i}} + \sin\phi\hat{\mathbf{j}}) + \cos\theta\hat{\mathbf{k}} \tag{8.1a}$$

$$\hat{\boldsymbol{\theta}} = \cos\theta(\cos\phi\hat{\mathbf{i}} + \sin\phi\hat{\mathbf{j}}) - \sin\theta\hat{\mathbf{k}} \tag{8.1b}$$

$$\hat{\boldsymbol{\phi}} = -\sin\phi\hat{\mathbf{i}} + \cos\phi\hat{\mathbf{j}}. \tag{8.1c}$$

Some simplifying relationships are also observed:

$$\hat{\mathbf{l}} = -\sin\phi\hat{\mathbf{i}} + \cos\phi\hat{\mathbf{j}} \qquad \hat{\mathbf{m}} = \cos\phi\hat{\mathbf{i}} + \sin\phi\hat{\mathbf{j}} \tag{8.2a}$$

$$\frac{\mathrm{d}\hat{\mathbf{l}}}{\mathrm{d}t} = -\dot{\phi}\hat{\mathbf{m}} \qquad \frac{\mathrm{d}\hat{\mathbf{m}}}{\mathrm{d}t} = \dot{\phi}\hat{\mathbf{l}}. \tag{8.2b}$$

Using these relationships, the first derivatives of Equation 8.1 are

$$\frac{\mathrm{d}\hat{\mathbf{r}}}{\mathrm{d}t} = \dot{\theta}(\cos\theta\hat{\mathbf{m}} - \sin\theta\hat{\mathbf{k}}) + \dot{\phi}\sin\theta\hat{\mathbf{l}} \tag{8.3a}$$

$$\frac{\mathrm{d}\hat{\boldsymbol{\theta}}}{\mathrm{d}t} = -\dot{\theta}(\sin\theta\hat{\mathbf{m}} + \cos\theta\hat{\mathbf{k}}) + \dot{\phi}\cos\theta\hat{\mathbf{l}} \tag{8.3b}$$

$$\frac{\mathrm{d}\hat{\boldsymbol{\phi}}}{\mathrm{d}t} = -\dot{\phi}\hat{\mathbf{m}}. \tag{8.3c}$$

With the aim of expressing the velocity of a point on the sphere as a function of only $\mathbf{r}, \theta$, and ϕ, a further relationship is observed from Equations 8.1a and 8.1b. This uses the Jacobian matrix and its property of orthonormality:

$$\begin{bmatrix}\hat{\boldsymbol{\theta}}\\ \hat{\mathbf{r}}\end{bmatrix} = \begin{bmatrix}\cos\theta & -\sin\theta\\ \sin\theta & \cos\theta\end{bmatrix}\begin{bmatrix}\hat{\mathbf{m}}\\ \hat{\mathbf{k}}\end{bmatrix}$$

$$\begin{bmatrix}\hat{\mathbf{m}}\\ \hat{\mathbf{k}}\end{bmatrix} = \begin{bmatrix}\cos\theta & \sin\theta\\ -\sin\theta & \cos\theta\end{bmatrix}\begin{bmatrix}\hat{\boldsymbol{\theta}}\\ \hat{\mathbf{r}}\end{bmatrix}. \tag{8.4}$$

Finally, substituting Equation 8.4 into Equation 8.3 provides the required unit velocity

vectors:

$$\frac{\mathrm{d}\hat{\mathbf{r}}}{\mathrm{d}t} = \dot{\theta}\hat{\boldsymbol{\theta}} + \dot{\phi}\sin\theta\hat{\boldsymbol{\phi}} \tag{8.5a}$$

$$\frac{\mathrm{d}\hat{\boldsymbol{\theta}}}{\mathrm{d}t} = -\dot{\theta}\hat{\mathbf{r}} + \dot{\phi}\cos\theta\hat{\boldsymbol{\phi}} \tag{8.5b}$$

$$\frac{\mathrm{d}\hat{\boldsymbol{\phi}}}{\mathrm{d}t} = -\dot{\phi}(\sin\theta\hat{\mathbf{r}} + \cos\theta\hat{\boldsymbol{\theta}}). \tag{8.5c}$$

The position, velocity, and acceleration of a point on a spherical surface may now be obtained by identifying the spherical position vector, taking its derivatives, and reorganising the terms. ρ represents the magnitude of the position vector, the pendulum length.

$$\vec{\mathbf{d}}_{\mathbf{s}} = \rho\hat{\mathbf{r}} \tag{8.6}$$

$$\vec{\mathbf{v}}_{\mathbf{s}} = \frac{\mathrm{d}\vec{\mathbf{d}}}{\mathrm{d}t} = \dot{\rho}\hat{\mathbf{r}} + \rho\dot{\theta}\hat{\boldsymbol{\theta}} + \rho\dot{\phi}\sin\theta\hat{\boldsymbol{\phi}} \tag{8.7}$$

$$\begin{aligned}\vec{\mathbf{a}}_{\mathbf{s}} = \frac{\mathrm{d}\vec{\mathbf{v}}}{\mathrm{d}t} &= (\ddot{\rho} - \rho\dot{\theta}^2 - \rho\dot{\phi}^2\sin^2\theta)\hat{\mathbf{r}} \\ &+ (\rho\ddot{\theta} - \rho\dot{\phi}^2\sin\theta\cos\theta + 2\dot{\rho}\dot{\theta})\hat{\boldsymbol{\theta}} \\ &+ (\rho\ddot{\phi}\sin\theta + 2\dot{\rho}\dot{\phi}\sin\theta + 2\rho\dot{\theta}\dot{\phi}\cos\theta)\hat{\boldsymbol{\phi}}\end{aligned} \tag{8.8}$$

Considering the inverted pendulum presented in Figure 8.1, the equations of motion for the system can be determined by equating the sum of the moments about the origin to the rate of change of system angular momentum,

$$\sum M_o = \frac{\mathrm{d}\vec{\mathbf{H}}}{\mathrm{d}t}. \tag{8.9}$$

This of course assumes that the angular momentum of a real person is dominated by the pendulum angular momentum. For the left side of the equation the sum of the moments about the origin provides

$$\sum M_o = \rho\hat{\mathbf{r}} \times -m_p g\hat{\mathbf{k}} + \rho\hat{\mathbf{r}} \times \vec{\mathbf{F}} \tag{8.10}$$

where $m_p g$ is the force due to gravity and $\vec{\mathbf{F}} = m_p\vec{\mathbf{a}}$ is the external force due to ground motion acting on the pendulum's Centre of Mass, as in the $m\ddot{x}$ term of Figure 1.7. By

assuming that only lateral force is applied to the pendulum, $\vec{\mathbf{a}} = a_x\hat{\mathbf{x}}$ and (neglecting the $\hat{\mathbf{r}}$ term, which develops zero moment) $\hat{\mathbf{x}} = \cos\theta\sin\phi\hat{\boldsymbol{\theta}} - \cos\phi\hat{\boldsymbol{\phi}}$. Resolving the forces of Equation 8.10 into spherical components while recognising that $\hat{\mathbf{r}} \times \hat{\mathbf{r}} = 0$ and assuming the derivatives of ρ are zero yields

$$\begin{aligned}\sum M_o &= \rho\hat{\mathbf{r}} \times (m_p g\sin\theta\hat{\boldsymbol{\theta}} + m_p a_x\cos\theta\sin\phi\hat{\boldsymbol{\theta}} - m_p a_x\cos\phi\hat{\boldsymbol{\phi}}) \\ &= m_p\rho(a_x\cos\phi\hat{\boldsymbol{\theta}} + g\sin\theta\hat{\boldsymbol{\phi}} + a_x\cos\theta\sin\phi\hat{\boldsymbol{\phi}}).\end{aligned} \tag{8.11}$$

Next the angular momentum of the system is obtained. As with the two-dimensional inverted pendulum, the mass of a pedestrian is assumed to act entirely at a point at the free end of the three-dimensional inverted pendulum. Using Equation 8.7 and again omitting the $\hat{\mathbf{r}} \times \hat{\mathbf{r}}$ term,

$$\begin{aligned}\vec{\mathbf{H}} &= \vec{\mathbf{r}} \times m_p\vec{\mathbf{v}_\mathbf{s}} \\ &= \rho\hat{\mathbf{r}} \times m_p(\rho\dot{\theta}\hat{\boldsymbol{\theta}} + \rho\dot{\phi}\sin\theta\hat{\boldsymbol{\phi}}) \\ &= m_p\rho^2(-\dot{\phi}\sin\theta\hat{\boldsymbol{\theta}} + \dot{\theta}\hat{\boldsymbol{\phi}}).\end{aligned} \tag{8.12}$$

The derivative of the angular momentum is then

$$\frac{\mathrm{d}\vec{\mathbf{H}}}{\mathrm{d}t} = m_p\rho^2(-\ddot{\phi}\sin\theta\hat{\boldsymbol{\theta}} - 2\dot{\theta}\dot{\phi}\cos\theta\hat{\boldsymbol{\theta}} + \ddot{\theta}\hat{\boldsymbol{\phi}} - \dot{\phi}^2\sin\theta\cos\theta\hat{\boldsymbol{\phi}}). \tag{8.13}$$

Substituting Equations 8.11 and 8.13 into Equation 8.9, the equations of motion are obtained by equating like-terms and rearranging.

$$\begin{cases}\hat{\boldsymbol{\theta}}: & \ddot{\phi} = -\dfrac{1}{\sin\theta}(2\dot{\theta}\dot{\phi}\cos\theta + \dfrac{a_x}{\rho}\cos\phi) \\ \hat{\boldsymbol{\phi}}: & \ddot{\theta} = \dot{\phi}^2\sin\theta\cos\theta + \dfrac{g}{\rho}\sin\theta + \dfrac{a_x}{\rho}\cos\theta\sin\phi\end{cases} \tag{8.14}$$

At this point it is beneficial to examine the terms to ensure they make sense logically. First the $\hat{\boldsymbol{\phi}}$ equation describes rotation about $\hat{\boldsymbol{\phi}}$ or in other words rotation in the $\hat{\mathbf{r}}$-$\hat{\boldsymbol{\theta}}$ plane. In addition to the acceleration term, there is a velocity squared term, indicative of centripetal acceleration. The remaining terms pertain to the applied forces, gravity, and applied lateral (bridge-induced) force. The $\hat{\boldsymbol{\theta}}$ equation has only three terms. Again,

there is an angular acceleration term as well as a lateral forcing term. The remaining term, with the product $\dot{\theta}\dot{\phi}$, appears as a result of the coriolis effect. This effect occurs as a result of motion relative to a moving reference frame. In a normal two dimensional inverted pendulum model the term does not influence the lateral force, but where the true motion of the CoM about the CoP is nearly on a spherical surface, this should be taken into account.

Before continuing it should be observed that for practical purposes the acceleration of the point in space must be resolved back into cartesian coordinates. The cartesian location of the point is given by Equation 8.15. Note that these equations pertain to the coordinate system in Figure 8.1, with ϕ measured from the negative y-axis.

$$x = \rho \sin\theta \sin\phi \tag{8.15a}$$

$$-y = \rho \sin\theta \cos\phi \tag{8.15b}$$

$$z = \rho \cos\theta \tag{8.15c}$$

The accelerations are obtained by double differentiating Equation 8.15 and recalling that derivatives of ρ are zero:

$$\begin{aligned} \ddot{x} =& \ddot{\theta}\rho\cos\theta\sin\phi + \ddot{\phi}\rho\sin\theta\cos\phi - \dot{\theta}^2\rho\sin\theta\sin\phi \\ & - \dot{\phi}^2\rho\sin\theta\sin\phi + 2\dot{\theta}\dot{\phi}\rho\cos\theta\cos\phi \end{aligned} \tag{8.16a}$$

$$\begin{aligned} -\ddot{y} =& \ddot{\theta}\rho\cos\theta\cos\phi - \ddot{\phi}\rho\sin\theta\sin\phi - \dot{\theta}^2\rho\sin\theta\cos\phi \\ & - \dot{\phi}^2\rho\sin\theta\cos\phi - 2\dot{\theta}\dot{\phi}\rho\cos\theta\sin\phi \end{aligned} \tag{8.16b}$$

$$\ddot{z} = -\ddot{\theta}\rho\sin\theta - \dot{\theta}^2\rho\cos\theta \tag{8.16c}$$

The Cartesian kinematics of a spherical inverted pendulum have been solved in an unconventional reference frame. First, spherical unit vectors were defined and differentiated. These were then used to determine the spherical velocity and acceleration of a point. Next, a three-dimensional summation of moments was equated to the derivative of angular momentum in order to develop spherical equations of motion. Finally,

transformation functions were identified in order to convert spherical motion back into Cartesian motion.

8.2 Theoretical Results

The equations of motion presented in Equation 8.14 were solved using a Modified Euler Method time-stepping algorithm in MATLAB (e.g. [155]). In this method, values for θ, ϕ, and their derivatives are calculated at discrete time steps over the duration of one simulated footstep. For the purposes of this simulation a time step of $\Delta t = 0.01$ s was used.

The algorithm begins by establishing initial conditions for position and velocity. Values were selected from experimental data and corresponded to the spherical position and velocity of the Centre of Mass at heel-strike. The initial values of angular acceleration, $\ddot{\theta}_0$ and $\ddot{\phi}_0$ were determined by applying the initial positions and velocities to Equation 8.14 and solving for acceleration.

Using these initial values, a state space was established.

$$\left[T\right] = \begin{bmatrix}\theta_0 \\ \dot{\theta}_0\end{bmatrix} \qquad \left[P\right] = \begin{bmatrix}\phi_0 \\ \dot{\phi}_0\end{bmatrix} \tag{8.17a}$$

$$\left[\dot{T}\right] = \begin{bmatrix}\dot{\theta}_0 \\ \ddot{\theta}_0\end{bmatrix} \qquad \left[\dot{P}\right] = \begin{bmatrix}\dot{\phi}_0 \\ \ddot{\phi}_0\end{bmatrix} \tag{8.17b}$$

The new values for position and velocity were then predicted:

$$\begin{aligned} T^* &= T + \dot{T}\Delta t \\ P^* &= P + \dot{P}\Delta t \end{aligned} \tag{8.18a}$$

These values are input into 8.14 to obtain predictions for the new values of acceleration, leading to a prediction of the updated state space:

$$\left[T^*\right] = \begin{bmatrix}\theta^* \\ \dot{\theta}^*\end{bmatrix} \qquad \left[P^*\right] = \begin{bmatrix}\phi^* \\ \dot{\phi}^*\end{bmatrix} \tag{8.19a}$$

$$\left[\dot{T}^*\right] = \begin{bmatrix}\dot{\theta}^* \\ \ddot{\theta}^*\end{bmatrix} \qquad \left[\dot{P}^*\right] = \begin{bmatrix}\dot{\phi}^* \\ \ddot{\phi}^*\end{bmatrix} \tag{8.19b}$$

Finally, the 'corrected' version of the new point is determined by adding the initial condition to the average of the initial and predicted derivatives multiplied by the time increment.

$$T_1 = T + \frac{\Delta t}{2}(\dot{T} + \dot{T}^*)$$
$$P_1 = P + \frac{\Delta t}{2}(\dot{P} + \dot{P}^*) \tag{8.20a}$$

This algorithm is repeated for every time step over the duration of a footstep. Six time vectors are obtained from the algorithm corresponding to the position, velocity, and acceleration of the Centre of Mass in both θ and ϕ. For practical purposes, these vectors can be converted into Cartesian coordinates using Equations 8.15 and 8.16.

To verify the model reasonable initial conditions are selected and tuned by trial and error and the lateral acceleration is set to zero. A right footstep is examined by selecting $\theta_0 = 15$ degrees, $\dot{\theta}_0 = -60$ degrees s^{-1}, $\phi_0 = -15$ degrees, and $\dot{\phi}_0 = -20$ degrees s^{-1}. If one imagines a normal right footstep, the CoM is quite far behind and slightly to the left of the CoP at heel-strike. Thus it follows that ϕ is negative but small and θ is (always) positive. As a person steps, their CoM progresses forward, almost over the CoP. Since positive θ is measured away from the vertical axis, the large negative $\dot{\theta}$ value makes sense: the initial velocity is towards the vertical – negative – direction and its magnitude is indicative of the speed of forward walking. $\dot{\phi}$ is harder to visualise, but the sign follows from the fact that the CoM should always remain to the left of the CoP during right foot stance. It is also assumed that $g = 9.81$ m s^{-2}, the pendulum length $\rho = 1$ m, the stance duration is 0.75 s and the time step is 0.01 s.

The CoM trajectories are plotted in the frontal plane and in three dimensions in Figure 8.2. In the frontal plane projection the typical butterfly shape of the CoM trajectory is observed (Figure 5.3). The CoM starts at the left-most point of the trajectory, moving up and to the right. At mid-stance the CoM crests the peak of its trajectory before losing elevation with only a slight leftward motion. The maximum

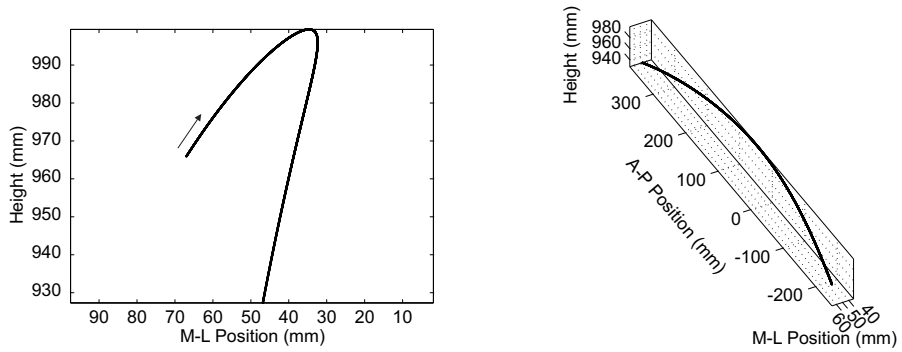

(a) (b)

Figure 8.2: Frontal plane projection and three-dimensional view of the CoM trajectory from a spherical inverted pendulum model.

lateral excursion is just under 40 mm and the vertical excursion is approximately 70 mm. Both of these values are quite reasonable, though slightly larger than suggested by data of real walkers. Both of these results can be tuned with the selection of different initial conditions.

In the three dimensional plot the Centre of Mass trajectory is dominated by a long, sweeping arc in the sagittal plane. The peak of the arc occurs between 30 and 40% of its length, where the CoM remains to the medial side of the CoP (i.e. the left side of vertical). The length of the arc is approximately 0.5 m, which is a typical step length for a normal walker.

Figure 8.3 shows typical curves for θ, ϕ, and their derivatives over the single right step. When comparing the θ and ϕ (and derivative) plots, notice that the scales are dramatically different for the two angles. θ is a positive concave-up parabola-like shape with values up to 0.5 rad, indicative of the CoM remaining close to the CoP. At 0.33 s, θ_{min} is 0.035 rad or 2.0 degrees. The velocity plot consists of two parallel nearly linear regions separated by a short transition region around θ_{min}. This is reflected in the acceleration plot where a peak during the transition region dominates over the relatively flat portions on each side.

The plots for ϕ and its derivatives exhibit much greater range than θ. ϕ itself ranges

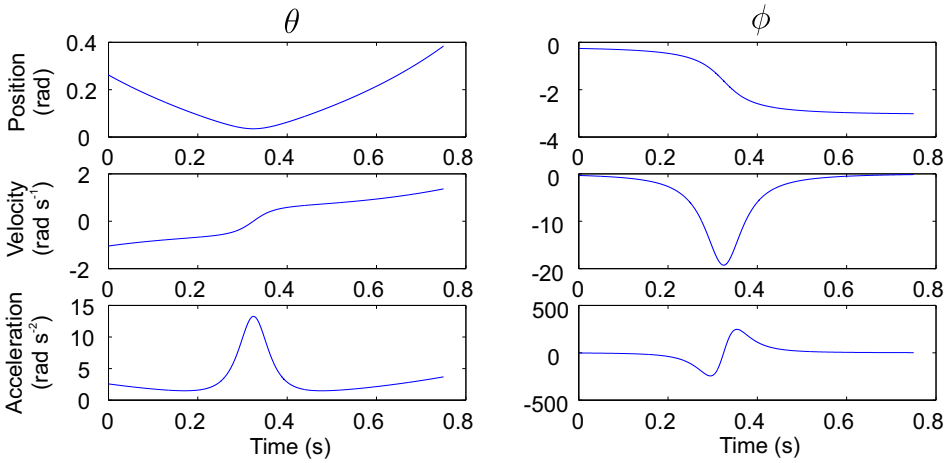

Figure 8.3: θ, ϕ and their derivatives over one right step.

from approximately -0.3 to -3.0 rad, or -17 to -172 degrees. Early in the footstep, the ϕ is nearly constant, decreasing slightly. At approximately 0.25 s, the angle rapidly changes by almost 180 degrees, corresponding to the CoM moving at close proximity past the CoP. The time of θ_{min} corresponds to the inflection point of ϕ. After this rapid change in ϕ, the angle again remains nearly constant for the remainder of the footstep. As for the derivatives of ϕ, the peak magnitudes of both functions are very high. The magnitude of the velocity is small through much of the footstep, except for in the region of the ϕ inflection point. The acceleration is similarly small for most of the step with a sign changing asymptote during the transition region.

8.3 Experimental Results

In order to verify the theoretical results, a spherical coordinate analysis was conducted on experimental data as well. Data for these results came from the NOC II and Jenkin II tests. One important assumption made in this analysis is that the pendulum length remains constant throughout each step. This is important because it allows the radial velocity and acceleration terms to go to zero, as in the theoretical analysis. In practice the height of the Centre of Mass varies by around 50 mm during stable ground walking. Swept through a spherical path, however, this variation corresponds

to a change in pendulum length of around 70 mm. Ultimately 70 mm out of 1 m is a negligible change; this will be seen in the verification below.

First the Cartesian data points from the experimental records were converted to spherical coordinates. The MIPM is based on the separation between the CoM and CoP in the x, y, and z directions, $x = x_{CoM} - x_{CoP}$, etc. at every time step. The projection of the pendulum length in the $x - y$ plane, r_{xy} is therefore the magnitude of the hypotenuse of x and y. The spherical reference angles can then be determined:

$$\theta = tan^{-1}\frac{r_{xy}}{z}$$
$$\phi = \begin{cases} tan^{-1}\dfrac{y}{x} + \dfrac{\pi}{2}, & \text{for left footsteps} \\ -\left(tan^{-1}\dfrac{y}{-x} + \dfrac{\pi}{2}\right), & \text{for right footsteps.} \end{cases} \tag{8.21}$$

The time series for θ and ϕ are then differentiated twice using the central difference method (Equation 4.1) to obtain their velocity and acceleration values. Once again six time series vectors were obtained describing the position, velocity, and acceleration of a point (the CoM relative to the CoP) in θ and ϕ coordinates. These values can be converted back to Cartesian coordinates using Equations 8.15 and 8.16.

Figure 8.4 shows typical curves for θ, ϕ, and their derivatives over one left-right-left step sequence from the NOC II tests. The shaded areas in the position plots indicate the periods of double stance and a black line marks the time of θ_{min}. One immediately recognises a striking similarity between these plots and the theoretical results. θ, $\dot{\theta}$, and ϕ exhibit the same shape and nearly identical values in both the theoretical and experimental results, while the remaining plots differ by sign, depending on the footstep.

The experimental results over a three-step trial show that θ has a period half the duration of ϕ. Each of the plots in θ depicts three very repeatable steps. The ϕ plots, however, clearly exhibit an alternating footstep pattern with left feet producing positive angles and velocities and right feet producing negative angles. This is particularly

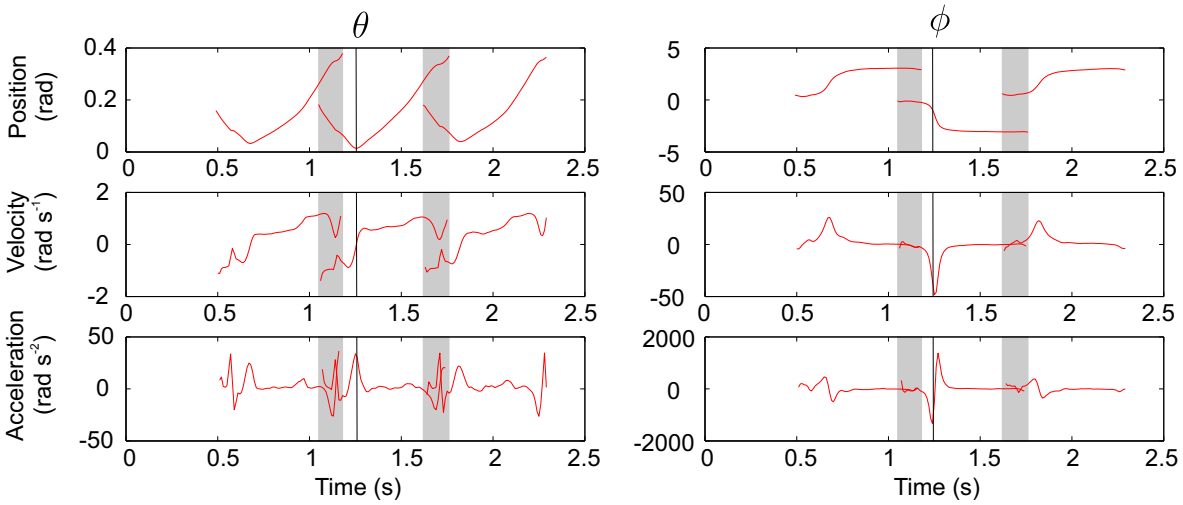

Figure 8.4: Experimental plots for θ and ϕ with their derivatives over three steps. Shaded areas correspond to double stance period. Time of θ_{min} for the second footstep indicated with a black line.

interesting because motion (and ground forces) in the vertical and A-P directions have half the period of motion in the M-L direction. Consideration of the walking subject in a spherical context helps to elucidate the reason for this behaviour.

Curiously, the plots of ϕ reveal a seamless transition from footstep to footstep. The velocity and acceleration plots overlap during double stance phases with similar slopes, indicating that there is no jarring rotation in the transverse plane at or after heel-strike. This is because gait is nearly symmetric, so the final ϕ at toe-off is similar to the initial ϕ of the subsequent heel-strike. In the θ plots, no such smooth transition occurs. The two feet are far apart in the sagittal plane but fairly close together in the frontal plane, so θ is dependent on the sagittal plane leg configuration at heel strike. Since the CoM is past the mid-point between the feet in the sagittal plane (Figure 8.5), the departing θ is greater than the arriving θ.

One prominent difference between the experimental and theoretical results is in the double stance regions of $\dot{\theta}$ where the experimental toe-off and heel-strike sections vary from their theoretical counterparts. The variations exhibited in the experimental results appear to show that the toe-off and heel-strike velocities are co-linear, suggesting

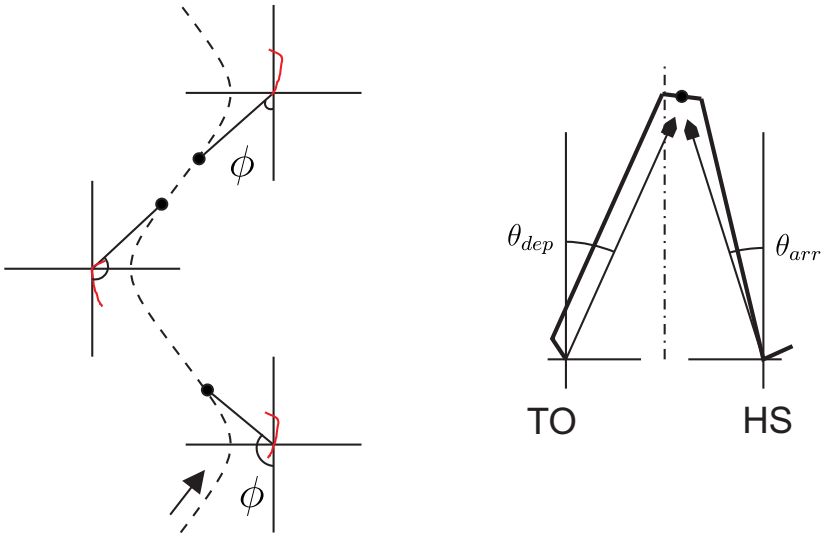

Figure 8.5: (Left) Horizontal plane projection of MIPM over consecutive steps, walking up the page. As each coordinate system moves along the CoP trajectory (red), ϕ sweeps through an angle from 0 to $\pm\pi$. (Right) Sagittal plane projection of double stance. CoM forward of centre at mid-stance causing $\theta_{dep} > \theta_{arr}$.

that a weighted average of the two curves might produce a smooth transition curve from foot to foot.

The patterns indicated here were observed across all 38 stable ground three-step samples. Given that the inflection point of ϕ corresponded to θ_{min}, there appears to be a strong correlation between the two variables. In this trial the middle step θ_{min} occurs at 29.6% of the stance phase duration. Across all 38 middle steps, θ_{min} occurred at a mean time of 31.8% with a standard deviation of 2.75% and a range of 27.1 to 37.7%.

8.3.1 NOC II Results

The MATLAB code was expanded for use with the three-step trials recorded at the Nuffield Orthopaedic Centre. The base of the MIPM translates with the Centre of Pressure, so the theoretical pendulum location was made to translate along the CoP trajectory instead of remaining at a fixed point. The initial conditions for each footstep of the theoretical model were the initial θ and ϕ calculated from the experimental data. Since the numerically determined derivatives of the experimental θ and ϕ were noisy

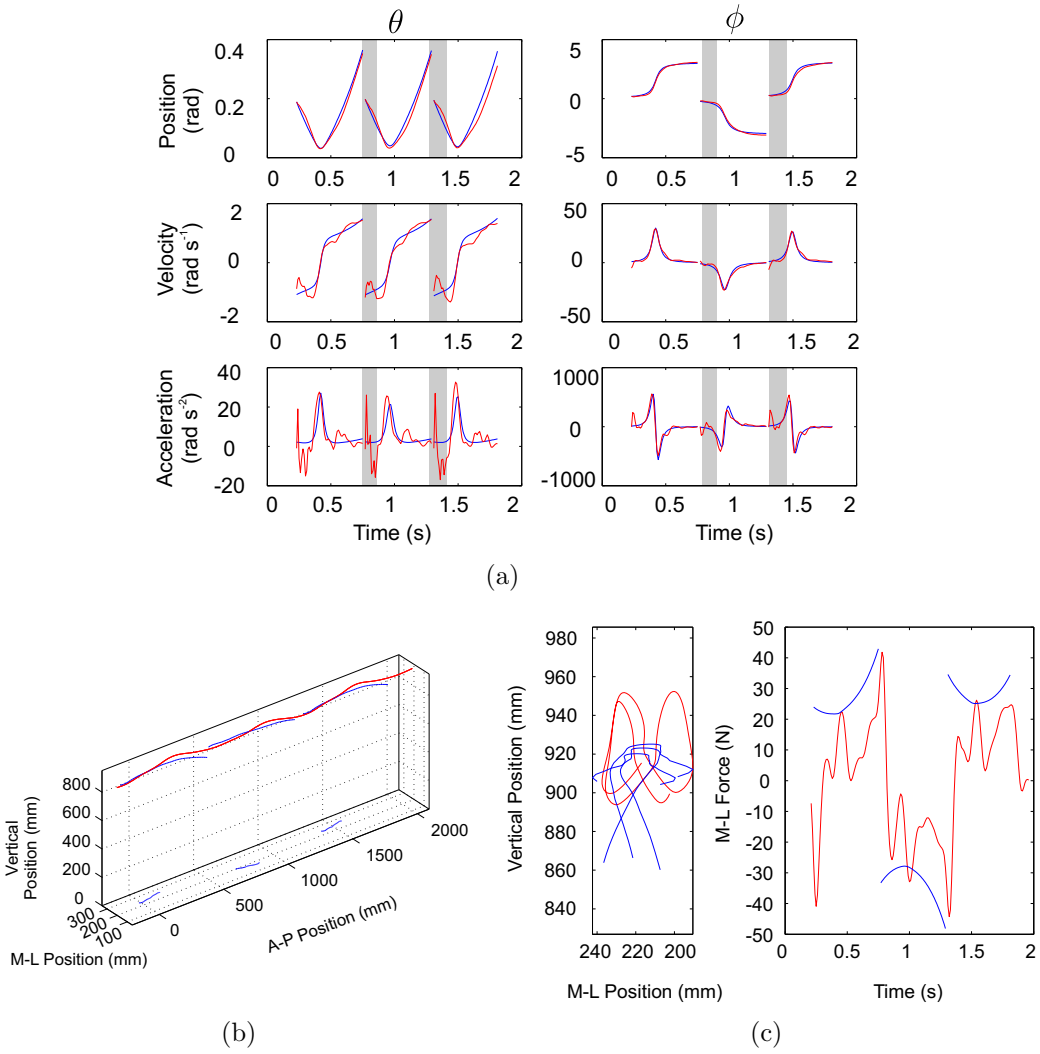

Figure 8.6: Comparison between experimental (red) and theoretical (blue) results for data from NOC II tests.

around heel-strike, the initial values of the velocities $\dot{\theta}$ and $\dot{\phi}$ were found by optimisation, using the `lsqnonlin` function. Finally, the theoretical results were calculated from heel-strike to heel-strike and do not include any interpolation or correction for double stance.

Figure 8.6 shows the theoretical and experimental results from a typical three-step NOC II trial. A close match exists between the theoretical and experimental θ and ϕ plots. Typically – as shown here – noise in the $\dot{\theta}$ profile is exacerbated upon differentiation to acceleration. The theoretical acceleration appears to fit one peak

of the experimental data for each footstep well. The experimental data do, however, portray a negative peak during each double stance and a small positive peak during late single stance that is not recreated by the theoretical model. Noise was not a significant problem in the ϕ derivatives, which exhibited a very good match between experimental and theoretical data. Figure 8.6(b) shows that the heel-strike regions are typically modelled better than the toe-off regions, where the experimental CoM trajectory is greater than its experimental counterpart. This is reflected in Figure 8.6(c) where the height of the theoretical trajectories does not match the experimental CoM trajectories well. Each blue curve should match one of the red loops; the plot suggests the theoretical model does not progress through sufficient vertical range. Finally, the reproduced M-L ground forces suggest that the model is inadequate for predicting the experimentally recorded force. The MIPM over-predicts the real force though the overall trend during each step is reasonable.

In an attempt to compensate for the height difference between the theoretical CoM trajectory and the experimental data, the experimentally recorded pendulum length was used in the theoretical model instead of a constant. The distance from CoM to CoP was used for ρ even though the theoretical model neglects velocity ($\dot{\rho}$) and acceleration ($\ddot{\rho}$) in the $\hat{\mathbf{r}}$ direction. Allowing the pendulum length to vary results in Figure 8.7. The plots show that the change in pendulum length did indeed increase the range of the theoretical CoM, which fitted slightly better to the experimental data. The change made no significant difference to the θ or ϕ plots however – nor any change to the M-L ground force.

8.3.2 Jenkin II Results

In the previous section the stable base condition required that a_x from Equation 8.14 was zero. On a moving base, however, the lateral acceleration is a function of the structure's position, period, and phase at any given time. These were all determined from the motion tracking marker on the bridge, and input into the equations.

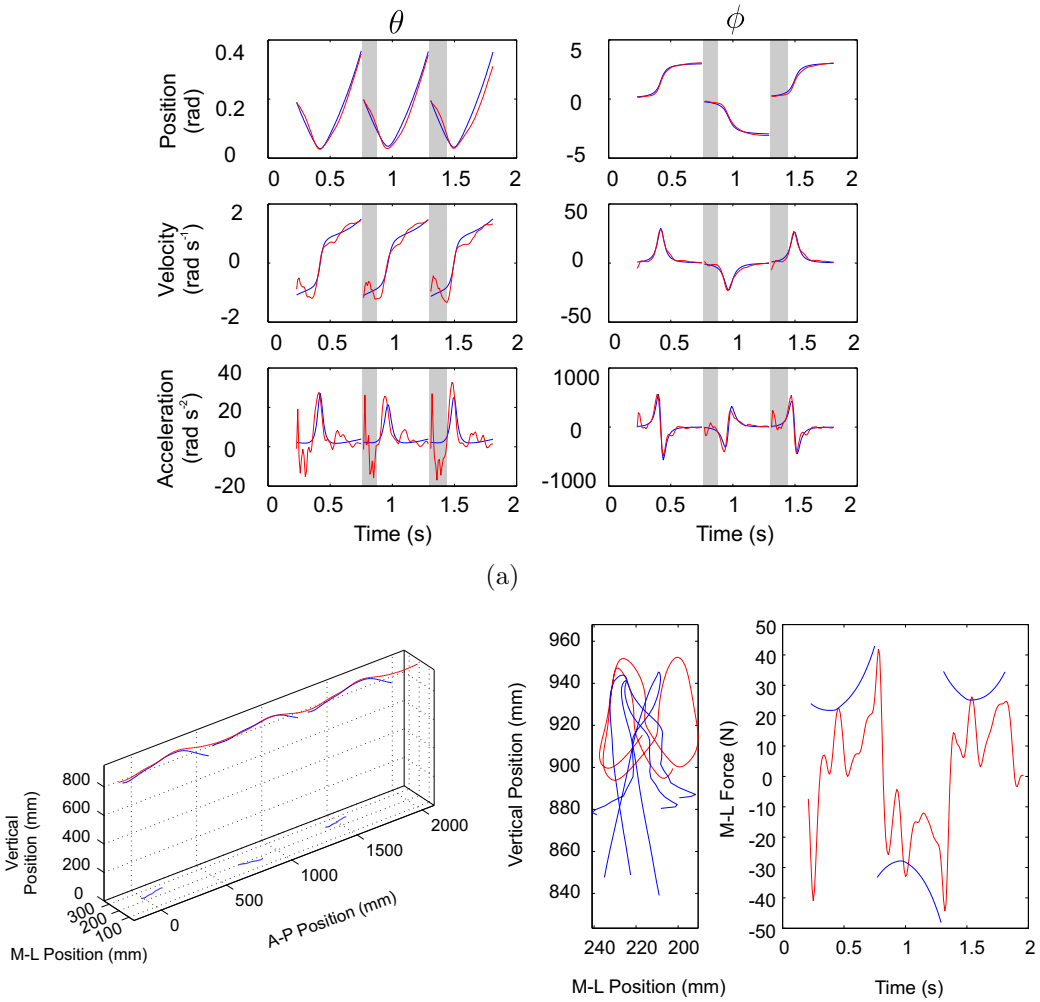

Figure 8.7: Comparison between experimental (red) and theoretical (blue) results for data from NOC II tests, using variable instead of fixed pendulum length.

Overall, the kinematic matching between the model and the experimental CoM trajectory was reasonable but not perfect. Figure 8.8(a) shows the spherical variables from a Jenkin trial conducted by the same participant as in the previous section. Generally the theoretical model predicted θ, ϕ, and their first derivatives very well before the inflection point. After the inflection, however, the match was worse. As seen in the first panel, the model over-predicted θ in the last two-thirds of the first two steps. This was common throughout the tests. Here ϕ was predicted well throughout each step, but this was not typical. In addition, the acceleration terms for both variables

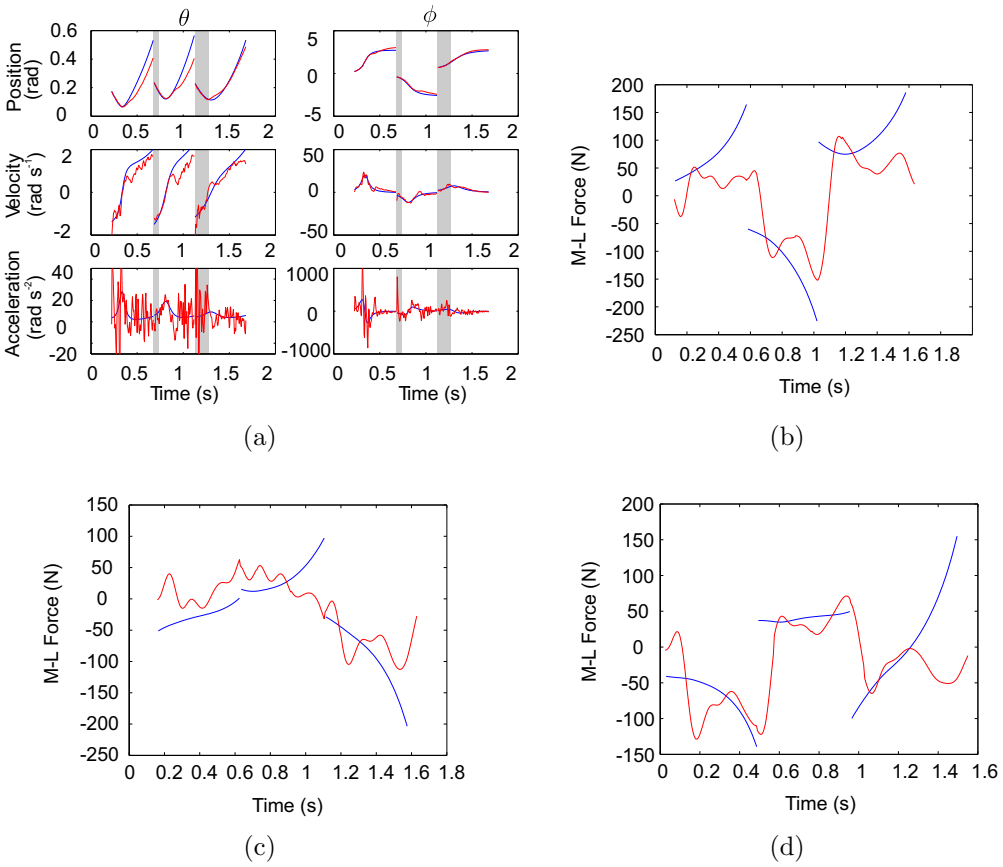

Figure 8.8: Comparison between experimental (red) and theoretical (blue) results for data from Jenkin II tests. All trials by same participant as in Figure 8.6.

were subject to considerable noise, though it appears that the theoretical result could match the underlying trend in the experimental data.

Figures 8.8(b) to (d) show force reconstructions for several trials by the same participant. The spherical MIPM does not usually predict the real ground force well. As with the NOC II results, the model is a simplistic estimate because it does not portray high frequency components exhibited by the experimental data. The amplitude of the model around heel-strike and the first half of each footstep is typically reasonable. Often, however, the model diverges from the experimental force over the course of the footstep. The concave nature of the model reflects the concavity of the traditional IPM, but as seen in (c) and the previous chapter such concavity is not always reflected in the real ground force.

8.4 Discussion & Conclusions

Ultimately using spherical coordinates for predicting M-L ground forces is appealing because of the physical representation of the pendulum moving through space. It would allow for the assumption of a rigid stick support of constant length while permitting – at least in principle – a better representation of frontal plane CoM trajectory. This could be very useful in tandem with a CoP model as proposed in the previous chapter.

There is a strong resemblance between the experimentally recorded data and the theoretical spherical MIPM. On stable ground the experimental kinematic data match the theoretical data well, though the reproduced frontal plane CoM trajectories are rather crude. On a moving base, however, the theoretically determined values for θ and ϕ tended to over-predict the experimental data late in the step. This meant that the CoM reconstruction was a poorer match than for stable ground.

The predicted M-L ground forces for both stable and moving base cases did not typically reproduce the real ground force well. For the stable ground predictions, the theoretical force amplitude was typically reasonable, but exhibited no high frequency oscillations. On a moving base the amplitude of the model was inconsistent compared to the real ground forces, suggesting that the model does not truly represent motion on a moving base.

In late 2015 Goldsztein undertook a different spherical analysis of inverted pendulum motion from a purely theoretical (and predominantly kinetic) perspective [156]. It showed the potential for using spherical coordinates to describe CoM motion, keeping a constant pendulum length. It was limited for the context of this thesis because it neither predicted ground forces nor compared its results to kinematic experimental data, so only general conclusions could be drawn from it. Nonetheless the future combination of his analysis and the work presented here could lead to a useful three-dimensional inverse dynamic model.

This chapter has shown that a spherical model has potential to be utilised for predicting CoM motion and M-L ground forces, but the model presented here is too primitive to attain a high level of accuracy. Future work should update the model to include more sources of variation, possibly including velocity and acceleration terms in $\hat{\mathbf{r}}$, compliant leg behaviour to account for stabilisation on a moving base, and account for double stance and step width.

Chapter 9

Conclusion

This thesis has examined medial-lateral (M-L) ground forces from a variety of perspectives in the context of the Inverted Pendulum Model (IPM). The research was conducted for two reasons. First, it sought to gain new insights on how individuals walk over stable ground and adapt their gait for crossing an unstable surface such as a footbridge. Secondly, the research was aimed at testing the applicability of the IPM, particularly on an oscillating bridge. Four experimental test regimes were carried out – two in the Nuffield Orthopaedic Centre's gait laboratory and two in the Oxford University Department of Engineering Science on a swinging bridge.

The first portion of the thesis was dedicated to an analysis of walking on stable ground. The M-L ground forces of a population of individual samples were normalised and compared:

1. The population of samples followed a 'w' shape with a maximum post-heel-strike amplitude of approximately 10% of body weight. Group subsets were similar to each other and the population. Individuals exhibited a high degree of inter-subject variability with a moderately low degree of intra-subject variability.

2. Aiming to reproduce M-L ground forces solely by kinematic means, three methods were used to fit combinations of head, trunk, and pelvis motion to M-L ground force records. Overall, motion of the head was best correlated to M-L ground force

and pelvis motion had a higher frequency content than either of the other body segments. Unfortunately, the reproduced M-L forces only exhibited a moderate correlation to experimental data.

3. IPM predictions were found to be significantly different than both the subsets and individual subjects' ground force samples. The IPM often over-predicted the M-L ground force, and failed to predict any of the acute unique oscillations exhibited by individual subjects.

4. An investigation of the seven major assumptions made by the IPM revealed that some assumptions were inappropriate. Observing that the ground reaction force is aimed through the Centre of Mass (CoM), a relationship was developed that avoided several of the assumptions of the IPM, called the Modified Inverted Pendulum Model (MIPM). The MIPM always correlated to force plate data better than the IPM for stable ground walking.

5. A pair of exploratory models were produced to investigate the applicability of the MIPM. A parametric model showed that kinematic CoM and Centre of Pressure (CoP) models could be input into the MIPM, producing a more accurate model than the IPM. A synthetic ground force model was applied to a single degree of freedom oscillator to show how differences in CoP prediction make a difference to simulated structural response. The IPM was shown to significantly over-predict or under-predict the MIPM depending whether the toe or heel was used as the static CoP point.

A novel set of experiments was prepared in the Jenkin Engineering Science building. Their results constitute the second portion of the thesis. Force plates were added to a 7 m laboratory footbridge constructed by prior research students. The bespoke force plates were designed to record M-L ground forces exerted on the structure's deck while the suspension bridge was oscillating. For the Jenkin II tests, the force plates were

used in concert with Tekscan pressure-sensing insoles and a CODA motion-tracking system. This provided kinematic CoM, CoP, and structural motion data in addition to the ground forces.

6. A subject's net step width proved to be correlated to bridge motion with a shallow slope, suggesting that subjects try to take 'normal' steps as if they were walking on a stable base. The instantaneous step width at heel-strike was found to be strongly correlated to the displacement of the bridge and its phase.

7. Participants crossing the bridge tended to adopt a fixed-in-space CoM strategy. The CoM trajectory often exhibited a U-shape in the frontal plane, showing that lifting the CoM early in single stance was a common technique for maintaining gait stability.

8. The CoP location was found to vary according to bridge amplitude and phase, adopting one of four general strategies. The phase and amplitude of the structure thus made it possible to predict whether a pedestrian exerted positive or negative damping on the structure.

9. CoM-CoP separation mimicked CoP displacement and was found to be strongly correlated to instantaneous step width.

10. Ground forces recorded on the bridge were typically correlated to CoM-CoP separation. As the separation decreased or the CoM crossed the CoP, the M-L ground force did as well. When the CoP followed a quasi-sinusoidal trajectory in phase with the bridge – even over successive crossed steps – the M-L ground force was also quasi-sinusoidal.

11. The offset of the ground force from step to step was generally proportional to instantaneous step width. Crossed and in-line steps caused no change in M-L force while large steps produced a large offset and a push-off.

12. The MIPM was found to correlate to the recorded forces slightly better than the IPM, although both models produced similar results. Neither model reflected high-frequency oscillations of the recorded forces, but both were usually close in amplitude.

13. A spherical MIPM was explored in order to assess whether a three-dimensional model could reproduce a real CoM trajectory and M-L ground force with a rigid stick support. The kinematics of the spherical angles matched well on stable ground, but CoM trajectories and M-L ground forces were less accurately reproduced. For the moving base data, the medial-lateral force results again showed discrepancies between the model and measurements despite a good kinematic correlation in spherical coordinates.

Modelling human-structure interaction (HSI) requires the researcher to have an accurate pedestrian load model in addition to a structural model. Significant research has been conducted through the years to learn about how structures respond to dynamic loads, but it has only been in the last two decades that HSI has gained significant scientific attention. Humans, naturally, are more complex than other ambient loads. Humans react to their surroundings, and take corrective manoeuvres to maintain gait stability. Some of these may include intentional or incidental synchronisation or lock-in. In conducting this research, a model was sought that was simple enough to be used in the prediction of crowd loading, but correctly represents the intricacies of inter- and intra-subject variability. Moreover, the model needed to reproduce the kinematics and kinetics of walking on a laterally oscillating surface in addition to a stable surface.

Research has previously been undertaken to address this issue, but all studies have deficiencies. Most previous tests were taken on instrumented treadmills, allowing the researchers to record long sequences of steps. For the present research, it was believed that treadmill walking does not allow sufficient freedom for pedestrians to react to the structure, or for the structure to vibrate according solely to pedestrian input.

These treadmill tests have typically yielded frequency domain models utilising dynamic load factors. While frequency models are excellent for capturing a long-term picture of a structure's state, they do not reflect the immediate state of a system in response to transient behaviour. Because of this, the present research developed a database of three-step trials in both stable and moving base situations in order to model transient responses.

Another deficiency of frequency domain models is that they are not derived from the kinematics of gait. They merely reflect kinetic excitation. A number of time-domain models address this issue, the simplest of which was the IPM. The major benefit of the model is that it predicts M-L ground forces with very few input parameters. Its simplicity is a computational boon, but not without a trade-off. Its simplicity is also detrimental to accurate predictions of forces on stable and moving structures.

The present thesis investigates the IPM in great detail, asking participants to conduct walking trials both in a gait lab and on an oscillating bridge. To the author's knowledge, no previous study has combined force plates, pressure-tracking insoles, and kinematic motion capture on an oscillating platform. This has provided an unprecedented look at how individuals alter their gait to affect balance on a swinging bridge. Furthermore, it has produced a wealth of data supporting the theory that the IPM and MIPM are generally valid for walking on a moving base, which has not previously been shown in such detail experimentally.

This thesis opens the door for a variety of future studies. Foremost is the challenge of describing the kinematics of the CoM when walking on a moving base. Future studies should assess what conditions cause the trajectory to narrow (or, conversely, become fixed-to-base), and whether these patterns are systematically applied by walkers. With this addressed, it might become plausible to develop a M-L ground force equation based solely on the phase of the bridge, the height of the CoM, and an individual's cadence. The tests conducted for this thesis suggest that such a relationship is possible,

but further studies would need to show that the relationship is applicable for other structural conditions such as varying natural frequencies and/or amplitudes.

Another course of future study would be to continue refining the spherical model. Whether in spherical or normal coordinates, the MIPM can also be adapted for a compliant-legged walker. Adding springs and dampers to the IPM has been shown to increase model complexity significantly, even on a stable base. Nonetheless, the moving base tests have shown that the rigid-leg inverted pendulum models rarely exhibit higher-frequency components. Thus, a compliant-leg model might allow for additional oscillatory behaviour in the M-L ground force.

Finally, the NOC II and Jenkin II tests produced a large number of trials where the subject stepped on two or fewer force plates. Particularly for the moving base tests, which produced over 550 passes, the data and video can still yield a great deal of knowledge about major corrective strategies for maintaining balance.

In closing, the study of HSI is interesting and unique because it examines in a scientific context the intersection of humans' ancient necessity to cross spans and the prehistoric development of gait. Walking has evolved over millions of years, so it is unsurprising that balance and posture are difficult to comprehend. This thesis has taken the next step towards understanding human-structure interaction by advancing a simple model and investigating strategies of lateral gait stability. Yet the future demands that researchers continue the study of HSI. Humans will continue to test the limits of construction, both out of the necessity of access and the aesthetics of design. Thus, understanding HSI is not simply a question of looking into the past, but expanding peoples' possibilities in the future.

Glossary

abduction Rotation of a body segment away from the sagittal plane of the body.

adduction Rotation of a body segment towards the sagittal plane of the body.

anterior superior iliac spine (left LASI; right RASI) Prominent left and right bony crests located at the top of the front of the pelvis.

antero-posterior (A-P) An anatomic axis; forces or motion parallel to the ground in the sagittal plane, forward or backward for a pedestrian.

autoparametric excitation In a multi-modal dynamic structure, the excitation of one component (such as an automobile suspension) due to the resonant excitation of a quasi-independent second component (such as an automobile engine). Intermediary components (such as framing) need not be excited. Often the components exhibit a 2:1 natural frequency ratio.

base of support (BoS) The area of the standing foot during single stance or the area encompassed by both feet plus the space in between the feet during double stance.

cadence The step frequency of a pedestrian.

centre of mass (CoM) The location in space where the mass of a person is concentrated such that if hypothetically supported at that point no net torques would occur. Theoretically located within the body, in front of the base of the spine. In

reality located in a different place for every individual; also changing according to the relative positioning of a person's head, trunk, arms, and legs.

centre of pressure (CoP) The location on the ground, within the base of support, representing the centroid of a walker's vertical pressure into the ground. The ground reaction force originates from this point.

compass gait A gait model (e.g. sagittal inverted pendulum model) that limits motion of the Centre of Mass in the sagittal plane to a circular path about the Centre of Pressure.

contralateral Describing a feature on the 'opposite' lateral side of the body, e.g. the left arm is contralateral to the right foot.

coronal plane See Frontal Plane.

critical number In theoretical models of structural stability, the number of pedestrians needed to induce sudden non-linear divergent bridge motion. In some models, the number of pedestrians causing the system damping to become negative.

determinants of gait Originally developed by Saunders *et al.* [118], the 'six determinants' defined gait kinematics based on energy efficiency as opposed to mechanical efficiency [128]. They are pelvic rotation, pelvic tilt, knee flexion (mid-stance), foot and ankle motion, knee motion, and lateral pelvic motion.

deterministic model A model in which the parameters are prescribed arbitrarily, empirically, or from statistical mean values. The parameters are fixed in time, as opposed to models in which the parameters are allowed to vary within a statistical distribution or randomly over time.

distal The part of a body segment most distant from the centre of the body.

dorsiflexion Rotation of the ankle in the sagittal plane marked by the toes moving upwards towards the shank.

double stance The portion of the gait cycle when both feet are in contact with the ground. Double stance duration typically decreases as walking speed increases. Running is defined as a gait with zero double stance.

dynamic load factor (DLF) For an individual pedestrian or a generalised walking model, the amplitude of the Fourier-domain ground force divided by body weight.

equivalent added damping Damping of a structure due to pedestrians; pedestrian force in phase with bridge velocity. When negative, the amplitude of structural vibration diverges rapidly.

equivalent added mass Mass added to structure due to pedestrians; pedestrian force in phase with acceleration.

extrapolated centre of mass (XCoM) Devised by Hof *et al.*, the effective dynamic location of the Centre of Mass due to its real position, velocity, and the individual's effective pendulum length.

foot progression angle The angle of rotation in the horizontal plane of the foot measured from the antero-posterior axis. Lateral positive, medial negative.

force plate An instrument consisting of several (usually four) force transducers installed level with the ground that measures forces, moments, and/or Centre of Pressure of a walker on the ground.

frontal plane An anatomic plane described by the vertical and medial-lateral axes or the cross sectioning of an individual into front and back 'halves'.

gait cycle Usually defined as the period from the heel-strike of one foot to the subsequent heel-strike of the same foot.

ground force Force exerted by an individual on the ground, located at the Centre of Pressure.

ground reaction force From Newton's Third Law of Motion, the force exerted by the ground on an individual's foot (feet), located at the Centre of Pressure.

head, arms, trunk (HAT) A model assuming that the upper body acts as a single rigid element consisting of the head, arms, and trunk.

heel-strike The instant during the gait cycle in normal non-pathological gait when the foot initially contacts the walking surface following swing phase.

hip abductors/adductors A collection of muscles in the thighs and abdomen generating rotation of the swing leg and/or the pelvis in the frontal plane.

horizontal plane Anatomic plane described by medial-lateral and antero-posterior axes or the cross sectioning of an individual into top and bottom 'halves'.

insole (instrumented) A foot-shaped polyester film containing a piezoresistive ink grid. A current passing through the grid is affected by the location and intensity of pressure applied to the film. This results in a pressure map that can record vertical force or Centre of Pressure location.

instantaneous step width (ISW) The medial-lateral separation of the two foot Centres of Pressure at the instant of heel-strike.

inter-subject variability Differences in gait (and therefore kinetics) across individuals in a population.

interrupted light technique Motion tracking method whereby subjects wear small blinking lights in a darkened room. A camera with a long shutter time records the light, which appears as a series of dots across the frame. Continuous light

technique requires subjects to wear steady lights while crossing in front of a camera.

intra-subject variability Differences in gait (and therefore kinetics) across a series of steps for one individual.

inverse dynamics The prediction of ground forces using known kinematics.

inverted pendulum model An inverse dynamics model that resolves gait into a series of alternating inverted pendulum motions. The mass of the body is represented as a point mass, which moves in a circular path about a fixed point representing the foot-ground interface.

ipsilateral Describing a feature on the 'same' lateral side of the body, e.g. the right arm is ipsilateral to the right foot.

isometric force Force applied by muscles in the body when the angle of the joint crossed by the muscle is constant, resulting in zero work done, e.g. pulling on an immobile object.

kinematics A branch of mechanics relating to the motion of objects in space without consideration of the forces applied to them.

kinetics A branch of mechanics relating the motion of objects to the forces applied to them.

lateral In structures (and generally), motion in a sideways or transverse direction. In biomechanics, a part of the body away from the centreline of the body in the frontal plane.

lock-in Occurs when a pedestrian adjusts his/her gait cycle period to match the oscillation period of a structure, regardless of the phase difference between them.

malleolus Lateral malleolus is a bony protrusion on the distal end of the fibula; medial malleolus is a bony protrusion on the distal end of the tibia.

margin of stability Parameter developed by Hof describing the necessary distance between the Extrapolated Centre of Mass and the Centre of Pressure such that a pedestrian does not fall.

medial In biomechanics, a part of the body closer to the centreline of the body in the frontal plane.

medial-lateral (M-L) An anatomic axis; forces or motion parallel to the ground in the frontal plane, left or right for a pedestrian.

metatarsal Five parallel foot bones numbered from medial to lateral, joining the tarsals (under the malleoli) to the phalanges (toes).

mid-stance The instant during the normal gait cycle when the swing leg is even with the stance leg and the pelvis is level to the ground. (Note that other works may alternatively define mid-stance as 50% of the duration of stance, regardless of limb position).

motion capture system Either active (e.g. CODA) or passive (e.g. Vicon), a set of camera sensors which use pulsating infrared light to track the motion of a marker through space.

narrow band random process A quasi-periodic function. A power spectral density plot is only non-zero at a central frequency and a surrounding narrow distribution of frequencies.

net step width (NSW) The medial-lateral separation between the two foot Centres of Pressure at consecutive heel-strikes.

parametric excitation In a dynamic system, resonant excitation without the application of external forces. This occurs if a component of the system – such as walking pedestrians – oscillates in resonance with the rest of the structure.

pedestrian Scruton number A non-dimensional index calculated as the product of modal damping ratio and structure-to-pedestrian mass ratio. Based on structural design for vortex shedding, higher values indicate more stable structures.

plantarflexion Rotation of the ankle in the sagittal plane marked by the toes moving downwards away from the shank.

proximal The part of a body segment closest to the centre of the body.

sacrum A large bone at the base of the spine consisting of five (fused) vertebrae, essentially providing the structural link between the spine and the hips.

sagittal plane An anatomic plane described by the vertical and antero-posterior axes or the cross sectioning of an individual into left and right sides.

self-excited force The additional force applied to a system switching repeatedly between multiple nearby resonant modes or stable states.

single degree of freedom system (SDOF) A dynamic mechanical system, which may be described as a mass attached to an ideal linear spring and optionally an ideal linear damper. An external force applied to the mass is equal to the sum of the forces contributed by the mass (inertial), the spring, and the damper.

social force The mathematical relationships used to ascribe quantitative value to a pedestrian's attraction to or repulsion from their destination, other pedestrians, obstacles, railings, and so on while walking in a confined area such as a footbridge.

stability criterion (gait) A kinematic or kinetic rule used to determine when a pedestrian is off-balance, falling over, or feeling unstable.

stability criterion (structure) Any of several types of mathematical relationships that describe a condition whereby a structure (e.g. bridge) oscillates at an abnormal or uncomfortable level, often as a function of synchronous lateral excitation.

stance phase The portion of the gait cycle when a foot is in contact with the walking surface. Single and double stance refer to the portions of the stance phase when one or two feet are in contact with the ground.

stochastic model A model in which one or more of the parameters is determined via random sampling from some probability distribution.

subtalar joint The articulation between the talus bone and the calcaneous and navicular bones which allows the foot to invert (rolling the ankle laterally) or evert (rolling the ankle medially).

swing phase The portion of the gait cycle when a foot is not in contact with the walking surface. For walking this is the same as single-leg stance for the contralateral leg.

synchronisation When a group of pedestrians tune their cadence to match the gait cycle period and phase of each other.

synchronous lateral excitation (SLE) A phenomenon whereby the oscillation of a structure (i.e. bridge) suddenly increases rapidly with the attainment of a critical number of (possibly synchronised) pedestrians.

toe-off An instant during the gait cycle when the foot is no longer in contact with the walking surface, initiating swing phase.

treadmill (instrumented) A device used to record long, continuous records of pedestrians walking or running at a constant speed in a laboratory environment. For

human-structure interaction research, treadmills are often equipped to oscillate laterally at a predefined frequency and amplitude.

trochanter (greater) A bony protrusion on the lateral side of the proximal end of the femur. Often an anatomic landmark used for the estimation of body Centre of Mass height and/or pendulum length.

vertical An anatomic axis; forces or motion perpendicular to the ground.

Bibliography

[1] S. Strogatz, D. Abrams, A. McRobie, B. Eckhardt, and E. Ott, "Crowd synchrony on the Millennium Bridge," *Nature Communications*, vol. 438, no. 3, pp. 43–44, 2005.

[2] K. Rötzel, https://commons.wikimedia.org/wiki/File:Akashi_Bridge.JPG, 2006, online; accessed 2016-01-10.

[3] R. Niewiroski Jr, http://www.projectrich.com/gallery, 2007, online; accessed Wikimedia Commons 2016-01-10.

[4] Viaduc de Millau, http://www.leviaducdemillau.com/en_index.php#/phototheque/, 2016, online; accessed 2016-01-10.

[5] Glabb, https://commons.wikimedia.org/wiki/File:Sutong_Yangtze_River_Bridge.JPG, 2012, online; accessed 2016-01-10.

[6] Shakeelgilgity, https://commons.wikimedia.org/wiki/File:Bridge_Astore.jpg, 2008, online; accessed 2016-01-10.

[7] K. Pomakis, https://commons.wikimedia.org/wiki/File:Brooklyn_Bridge_2004-01-11.jpg?uselang=en-gb, 2004, online; accessed 2016-01-10.

[8] "Bridges to Prosperity," http://www.bridgestoprosperity.org, 2015, online; accessed 2015-10-02.

[9] "Bridging the Gap Africa," http://www.bridgingthegapafrica.org, 2015, online; accessed 2015-10-02.

[10] "Rolling Bridge," http://www.heatherwick.com/rolling-bridge, 2015, online; accessed 2015-10-02.

[11] M. Kawaguchi, Z. Chen, and X. Wang, "Yong-Le Bridge, Tianjin, China: An integrated foot- and vehicle bridge," in *Footbridges: Past, present, and future*, London, July 2014, proceedings of Footbridge 2014: 5th International Conference.

[12] J. Harrison, https://commons.wikimedia.org/wiki/File:Sydney_Harbour_Bridge_from_Circular_Quay.jpg, 2010, online; accessed 2016-01-10.

[13] E. Pessoa, http://structurae.net/photos/209653-tianjin-eye, 2010, online; accessed Structurae 2016-01-10.

[14] British Standards Institution, "UK National Annex to Eurocode 1. Actions on structures. Part 2: Traffic loads on bridges," BSI, Tech. Rep. BS NA EN 1991-2, 2003.

[15] International Organization for Standardization (ISO), "Bases for design of structures - Serviceability of buildings and walkways against vibrations," ISO, Tech. Rep. ISO 10137, 2007.

[16] The British Standards Institution, "BS 5400-2," BSI, Tech. Rep., 2006, withdrawn.

[17] S. Živanović, A. Pavic, and P. Reynolds, "Vibration serviceability of footbridges under human-induced excitation: a literature review," *J Sound Vib*, vol. 279, no. 1, pp. 1–74, 2005.

[18] D. Claff, M. Williams, A. Blakeborough, and J. Stebbins, "Medial-lateral gait patterns of healthy adult walkers," in *Conference Proceedings of the Society for Experimental Mechanics Series*, vol. 39, 2013, pp. 337–348.

[19] D. Claff, M. Williams, and A. Blakeborough, "Using infrared motion-tracking markers to model lateral ground forces," in *Proceedings of the 9th International Conference on Structural Dynamics, EURODYN 2014*, 2014, pp. 999–1006.

[20] ——, "Integrating force plates into a laterally oscillating footbridge," in *Footbridges: Past, present, and future*, London, July 2014, pp. 174–175, proceedings of Footbridge 2014: 5th International Conference.

[21] V. Racic, A. Pavic, and J. Brownjohn, "Experimental identification and analytical modelling of human walking forces: Literature review," *J Sound Vib*, vol. 326, no. 1–2, pp. 1–49, 2009.

[22] E. Ingólfsson, C. Georgakis, and J. Jönsson, "Pedestrian-induced lateral vibrations of footbridges: A literature review," *Eng Struct*, vol. 45, pp. 21–52, 2012.

[23] F. Fromonot, *Marc Mimram–Minimal Design: Solferino Bridge in Paris.* Basel: Birkhuser, 2001.

[24] P. Dziuba, G. Grillaud, O. Flamand, S. Sanquier, and Y. Tetard, "La passerelle Solférino comportement dynamique (dynamic behaviour of the Solferino bridge)," *Bull Ouvrages Metalliques*, vol. 1, pp. 34–57, 2001, [In French].

[25] P. Dallard, T. Fitzpatrick, A. Flint, A. Low, R. Smith, M. Willford, and M. Roche, "London Millennium Footbridge: Pedestrian-induced lateral vibration," *J Bridge Eng*, vol. 6, no. 6, pp. 412–417, 2001.

[26] P. Dallard, A. Fitzpatrick, A. Flint, S. L. Bourva, A. Low, R. R. Smith, and M. Willford, "The London Millennium Footbridge," *The Structural Engineer*, vol. 79, no. 22, pp. 17–33, 2001.

[27] Y. Fujino, B. Pacheco, S.-I. Nakamura, and P. Wamitchai, "Synchronization of human walking observed during lateral vibration of a congested pedestrian bridge," *Earthq Eng Struct D*, vol. 22, no. 9, pp. 741–758, 1993.

[28] S. Nakamura, "Field measurements of lateral vibration on a pedestrian bridge," *Struct Eng*, vol. 81, no. 22, pp. 22–26, 2003.

[29] S. Nakamura and H. Nakamura, "Interactive lateral dynamic behaviours of girder and pedestrians," in *Footbridges: Past, present, and future*, London, July 2014, proceedings of Footbridge 2014: 5th International Conference.

[30] J. Macdonald, "Pedestrian-induced vibrations of the Clifton Suspension Bridge, UK," *Proceedings of the Institution of Civil Engineers: Bridge Engineering*, vol. 161, no. 2, pp. 69–77, 2008.

[31] J. Brownjohn, P. Fok, M. Roche, and P. Moyo, "Long span steel pedestrian bridge at Singapore Changi Airport - part 1: Prediction of vibration serviceability," *Struct Eng*, vol. 82, no. 16, pp. 21–27, 2004.

[32] ——, "Long span steel pedestrian bridge at Singapore Changi Airport - part 2: Crowd loading tests and vibration mitigation measures," *Struct Eng*, vol. 82, no. 16, pp. 28–34, 2004.

[33] E. Caetano, Á. Cunha, F. Magalhães, and C. Moutinho, "Studies for controlling human-induced vibration of the Pedro e Inês footbridge, Portugal. Part 1: Assessment of dynamic behaviour," *Eng Struct*, vol. 32, no. 4, pp. 1069–1081, 2010.

[34] K. Van Nimmen, G. Lombaert, I. Jonkers, G. De Rock, and P. Van den Broeck, "Characterisation of walking loads by 3d inertial motion tracking," *J Sound Vib*, vol. 333, no. 20, pp. 5212–5226, 2014.

[35] R. Pimentel, "Vibrational performance of pedestrian bridges due to human-induced loads," Ph.D. dissertation, University of Sheffield, September 1997.

[36] S. Živanović, A. Pavic, and P. Reynolds, "Dynamic analysis of lively footbridge under everyday pedestrian traffic," in *Proceedings of the 6th International Conference on Structural Dynamics, EURODYN 2005*, 2005.

[37] J. Brownjohn, S. Živanović, and A. Pavic, "Crowd dynamic loading on footbridges," in *Footbridges for Urban Renewal*, Porto, July 2008, proceedings of Footbridge 2008: 3rd International Conference.

[38] T. Fitzpatrick, P. Dallard, S. Le Bourva, A. Low, R. Smith, and M. Willford, *Linking London: The Millennium Bridge.* London: The Royal Academy of Engineering, 2001.

[39] A. Blekherman, "Swaying of pedestrian bridges," *J Bridge Eng*, vol. 10, no. 2, pp. 142–150, 2005.

[40] "Swaying causes running wariness over bosphorus bridge," http://www.hurriyetdailynews.com/default.aspx?pageid=438&n=swinging-bosporus-bridge-alerts-experts-2010-10-18, 2010, online; accessed 2015-10-14.

[41] A. Rönnquist, "Pedestrian induced lateral vibrations of slender footbridges," Ph.D. dissertation, Norwegian University of Science and Technology, 2005.

[42] W. Strobl, I. Kovacs, H. Andrä, and U. Häberle, "Eine fußgängerbrücke mit einer spannweite von 230 m (a footbridge with a span length of 230 m)," *J Biomech*, vol. 16, no. 8, pp. 591–601, 1983, [In German].

[43] S. Pollalis and C. Otto, "The Golden Gate Bridge: The 50th Anniversary Celebration," http://goldengatebridge.org/research/documents/researchpaper_50th.pdf, 1988, online; accessed 2015-10-14.

[44] K. Pedersen, "Golden Gate Bridge - 50th Fiasco Firsthand(1987)," https://youtu.be/aotjC9YfPfE, 2014, online; accessed 2015-10-14.

[45] E. Ingólfsson, C. Georgakis, F. Ricciardelli, and J. Jönsson, "Experimental identification of pedestrian-induced lateral forces on footbridges," *J Sound Vib*, vol. 330, no. 6, pp. 1265–1284, 2011.

[46] B. Peters, R. Brady, and J. Bloomberg, "Walking on an oscillating treadmill: Strategies of stride-time adaptation," *Ecological Psycology*, vol. 24, no. 4, pp. 265–278, 2012.

[47] F. Ricciardelli, M. Mafrici, and E. Ingólfsson, "Lateral pedestrian-induced vibrations of footbridges: Characteristics of walking forces," *J Bridge Eng*, vol. 19, no. 9, 2014.

[48] S. Carroll, J. Owen, and M. Hussein, "Reproduction of lateral ground reaction forces from visual marker data and analysis of balance response while walking on a laterally oscillating deck," *Eng Struct*, vol. 49, pp. 1034–1047, 2013.

[49] ——, "Experimental identification of the lateral human-structure interaction mechanism and assessment of the inverted-pendulum biomechanical model," *J Sound Vib*, vol. 333, no. 22, pp. 5865–5884, 2014.

[50] V. Racic and J. Brownjohn, "Stochastic model of near-periodic vertical loads due to humans walking," *Adv Eng Inform*, vol. 25, no. 2, pp. 259–275, 2011.

[51] R. Hobbs, "Test on lateral forces induced by pedestrians crossing a platform driven laterally." Imperial College London, London, Tech. Rep., August 2000, Tech Rep for Ove Arup and Partners.

[52] A. McRobie, G. Morgenthal, J. Lasenby, and M. Ringer, "Section model tests on human-structure lock-in," *Bridge Eng*, vol. 156, no. 2, pp. 71–79, 2003.

[53] P. Charles and V. Bui, "Transversal dynamic actions of pedestrians," in *Footbridge Conference*, Venice, July 2005, proceedings of Footbridge 2005: 2nd International Conference.

[54] A. Rönnquist and E. Strømmen, "Pedestrian induced lateral vibrations of slender footbridges," in *Conference Proceedings of the Society for Experimental Mechanics Series*, 2007.

[55] L. Oddsson, C. Wall III, M. McPartland, D. Krebs, and C. Tucker, "Recovery from perturbations during paced walking," *Gait & Posture*, vol. 19, no. 1, pp. 24–34, 2004.

[56] F. Venuti and L. Bruno, "Crowd-structure interaction in lively footbridges under synchronous lateral excitation: A literature review," *Phys Life Rev*, vol. 6, no. 3, pp. 176–206, 2009.

[57] G. Piccardo and F. Tubino, "Parametric resonance of flexible footbridges under crowd-induced lateral excitation," *J Sound Vib*, vol. 311, no. 1–2, pp. 353–371, 2008.

[58] F. Ricciardelli, "Lateral stability of footbridges subjected to crowd loading," in *Proceedings of the 9th International Conference on Structural Dynamics, EURODYN 2014*, 2014.

[59] D. Newland, "Pedestrian excitation of bridges – recent results," in *Proceedings of the Tenth International Congress on Sound and Vibration*, Stockholm, July 2003.

[60] S. Carroll, J. Owen, and M. Hussein, "A coupled biomechanical/discrete element crowd model of crowd-bridge dynamic interaction and application to the Clifton Suspension Bridge," *Eng Struct*, vol. 49, pp. 58–75, 2013.

[61] F. Ricciardelli and A. Pizzimenti, "Lateral walking-induced forces on footbridges," *J Bridge Eng*, vol. 330, no. 6, pp. 1265–1284, 2007.

[62] T. Roberts, "Lateral pedestrian excitation of footbridges," *J Bridge Eng*, vol. 10, no. 1, pp. 107–112, 2005.

[63] ——, "Probabilistic pedestrian lateral excitation of bridges," *P I Civil Eng – Bridge Eng*, vol. 158, no. 2, pp. 53–61, 2005.

[64] A. Blekherman, "Autoparametric resonance in a pedestrian steel arch bridge: Solferino Bridge, Paris," *J Bridge Eng*, vol. 12, no. 6, pp. 669–676, 2007.

[65] D. Newland, "Pedestrian excitation of bridges," *P I Mech Eng C–J Mec*, vol. 218, no. 5, pp. 477–492, 2004.

[66] A. Champneys, "Dynamics of parametric excitation," in *Encyclopedia of Complexity and Systems Science*, R. Meyers, Ed. New York: Springer, April 2014, pp. 1–31. [Online]. Available: http://dx.doi.org/10.1007/978-3-642-27737-5_144-3

[67] J. Macdonald, "Lateral excitation of bridges by balancing pedestrians," *Proceedings of the Royal Society A: Mathematical, Physical, and Engineering Sciences*, vol. 465, no. 2104, pp. 1055–1073, 2009.

[68] E. Ingólfsson and C. Georgakis, "A stochastic load model for pedestrian-induced lateral forces on footbridges," *Eng Struct*, vol. 33, no. 12, pp. 3454–3470, 2011.

[69] M. Bocian, J. Macdonald, and J. Burn, "Biomechanically inspired modelling of pedestrian-induced forces on laterally oscillating structures," *J Sound Vib*, vol. 331, no. 16, pp. 3914–3929, 2012.

[70] ——, "Probabilistic criteria for lateral dynamic stability of bridges under crowd loading," *Computers and Structures*, vol. 136, pp. 108–119, 2014.

[71] F. McRobie, "Long-term solutions of Macdonald's model for pedestrian-induced lateral forces," *J Sound Vib*, vol. 332, no. 11, pp. 2846–2855, 2013.

[72] S. Erlicher, A. Trovato, and P. Argoul, "A modified hybrid Van der Pol/Rayleigh model for the lateral pedestrian force on a periodically moving floor," *Mech Syst Signal Pr*, vol. 41, no. 1–2, pp. 485–501, 2013.

[73] J. Qin, S. Law, Q. Yang, and N. Yang, "Pedestrian-bridge dynamic interaction, including human participation," *J Sound Vib*, vol. 332, no. 4, pp. 1107–1124, 2013.

[74] T. Morbiato, R. Vitaliani, and A. Saetta, "Numerical analysis of a synchronization phenomenon: Pedestrian-structure interaction," *Computers and Structures*, vol. 89, no. 17–18, pp. 1649–1663, 2011.

[75] F. Venuti, L. Bruno, and P. Napoli, "Pedestrian lateral action on lively footbridges: A new load model," *Structural Engineering International*, vol. 17, no. 3, pp. 236–241, 2007.

[76] C. Caprani, "Vibration response from a pedestrian with arbitrary ground reaction force spectrum," in *Proceedings of the 9th International Conference on Structural Dynamics, EURODYN 2014*, 2014.

[77] V. Inman, H. Ralston, and F. Todd, *Human Walking*. Baltimore: Williams and Wilkins, 1981.

[78] D. Levine, J. Richards, and M. Whittle, *Whittle's Gait Analysis*, 5th ed. London: Churchill Livingstone, 2012.

[79] P. Archbold and B. Mullarney, "A review of gait parameters pertinent to pedestrian loading," in *The 5th Joint Symposium Proceedings of Bridge & Infrastructure Research in Ireland: Concrete Research in Ireland*, N. Ni Nuallain, D. Walsh, and R. West, Eds., Cork, September 2010.

[80] M. Murray, "Gait as a total pattern of movement," *Amer J Physical Med*, vol. 46, no. 1, pp. 290–333, 1967.

[81] F. Galbraith and M. Barton, "Ground loading from footsteps," *J Acoust Soc Am*, vol. 48, no. 5 (Part 2), pp. 1288–1292, 1970.

[82] A. Ebrahimpour, A. Hamam, R. Sack, and W. Patten, "Measuring and modeling dynamic loads imposed by moving crowds," *J Struct Eng*, vol. 122, no. 12, pp. 1468–1474, 1996.

[83] D. Winter, *Biomechanics and Motor Control of Human Movement*, 3rd ed. Hoboken, NJ: Wiley, 2005.

[84] H. Elftman, "Forces and energy changes in the leg during walking," *Am J Physiol*, vol. 125, pp. 339–356, 1939.

[85] E. Schneider and E. Chao, "Fourier analysis of ground reaction forces in normals and patients with knee joint disease," *J Biomech*, vol. 16, no. 8, pp. 591–601, 1983.

[86] G. Giakas and V. Baltzopoulos, "Time and frequency domain analysis of ground reaction forces during walking: an investigation of variability and symmetry," *Gait & Posture*, vol. 5, no. 3, pp. 189–197, 1997.

[87] H. Stolze, J. Kuhtz-Buschbeck, C. Mondwurf, A. Boczek-Funcke, K. Jöhnk, G. Deuschl, and M. Illert, "Gait analysis during treadmill and overground locomotion in children and adults," *Electroen Clin Neuro*, vol. 105, no. 6, pp. 490–497, 1997.

[88] N. Rosenblatt and M. Grabiner, "Measures of frontal plane stability during treadmill and overground walking," *Gait & Posture*, vol. 31, no. 3, pp. 380–384, 2010.

[89] P. Archbold and B. Mullarney, "The influence of selected gait parameters on vertical pedestrian loading," in *Attractive Structures at Reasonable Costs*, J. Biliszczuk, J. Bien, P. Hawryszkow, and T. Kaminski, Eds., Wroclaw, July 2011, proceedings of the 4th International Footbridge Conference: Footbridge 2011.

[90] H. Dang and S. Živanović, "Experimental characterisation of walking locomotion on rigid level surfaces using motion capture system," *Eng Struct*, vol. 91, pp. 141–154, 2015.

[91] V. Zatsiorsky and V. Seluyanov, "Mass and inertia characteristics of the main segments of the human body," *International Series on Biomechanics*, vol. 4, pp. 1152–1159, 1983.

[92] P. de Leva, "Adjustments to Zatsiorsky-Seluyanov's segment inertia parameters," *J Biomech*, vol. 9, no. 9, pp. 337–348, 1996.

[93] C. MacKinnon and D. Winter, "Control of whole body balance in the frontal plane during human walking," *J Biomech*, vol. 26, no. 6, pp. 633–644, 1993.

[94] M. Pandy, Y.-C. Lin, and H. Kim, "Muscle coordination of mediolateral balance in normal walking," *J Biomech*, vol. 43, no. 11, pp. 2055–2064, 2010.

[95] K. Jansen, F. De Groote, J. Duysens, and I. Jonkers, "How gravity and muscle action control mediolateral center of mass excursion during slow walking: A simulation study," *Gait & Posture*, vol. 39, no. 1, pp. 91–97, 2014.

[96] C. John, A. Seth, M. Schwartz, and S. Delp, "Contributions of muscles to mediolateral ground reaction force over a range of walking speeds," *J Biomech*, vol. 45, no. 14, pp. 2438–2443, 2012.

[97] P. Hoogvliet, W. van Duyl, J. de Bakker, P. Mulder, and H. Stam, "A model for the relation between the displacement of the ankle and the center of pressure in

the frontal plane during one-leg stance," *Gait & Posture*, vol. 6, no. 1, pp. 39–49, 1997.

[98] D. King and V. Zatsiorsky, "Periods of extreme ankle displacement during one-legged standing," *Gait & Posture*, vol. 15, no. 2, pp. 172–179, 2002.

[99] A. Hof, R. van Bockel, T. Schoppen, and K. Postema, "Control of lateral balance in walking. experimental findings in normal subjects and above-knee amputees," *Gait & Posture*, vol. 25, no. 2, pp. 250–258, 2007.

[100] S. Bruijn, O. Meijer, J. van Dieën, I. Kingma, and C. Lamoth, "Coordination of leg swing, thorax rotations, and pelvis rotations during gait: The organisation of total body angular momentum," *Gait & Posture*, vol. 27, no. 3, pp. 455–462, 2008.

[101] L. Tesio, V. Rota, C. Chessa, and L. Perucca, "The 3d path of body centre of mass during adult human walking on force treadmill," *J Biomech*, vol. 43, no. 5, pp. 938–944, 2010.

[102] H. Herr and M. Popović, "Angular momentum in human walking," *J Exp Bio*, vol. 211, no. 4, pp. 467–481, 2008.

[103] R. Brady, B. Peters, and J. Bloomberg, "Strategies of healthy adults walking on a laterally oscillating treadmill," *Gait & Posture*, vol. 29, no. 4, pp. 645–649, 2009.

[104] S. Rietdyk, A. Patla, D. Winter, M. Ishac, and C. Little, "Balance recovery from medio-lateral perturbations of the upper body during standing," *J Biomech*, vol. 32, no. 11, pp. 1149–1158, 1999.

[105] M. Sari and M. Griffin, "Postural stability when walking: Effect of the frequency and magnitude of lateral oscillatory motion," *Appl Ergon*, vol. 45, no. 2 PB, pp. 293–299, 2014.

[106] A. Hof, S. Vermerris, and W. Gjaltema, "Balance responses to lateral perturbations in human treadmill walking," *J Exp Bio*, vol. 213, no. 15, pp. 2655–2664, 2010.

[107] A. Zivotofsky and J. Hausdorff, "Modelling spatially unrestricted pedestrian traffic on footbridges," *J Neuroeng Rehabil*, vol. 4, no. 28, 2010.

[108] J. Nessler and S. Gilliland, "Interpersonal synchronization during side by side treadmill walking is influenced by leg length differential and altered sensory feedback," *Hum Movement Sci*, vol. 28, no. 6, pp. 772–785, 2009.

[109] ——, "Kinematic analysis of side-by-side stepping with intentional and unintentional synchronization," *Gait & Posture*, vol. 31, no. 4, pp. 527–527, 2010.

[110] J. Nessler, T. Gonzales, E. Rhoden, M. Steinbrick, and C. De Leone, "Stride interval dynamics are altered when two individuals walk side by side," *Motor Control*, vol. 15, no. 3, pp. 390–404, 2011.

[111] D. Helbing and P. Molnár, "Social force model for pedestrian dynamics," *Phys Rev E*, vol. 51, no. 5, pp. 4282–4286, 1995.

[112] M. Moussaïd, N. Perozo, S. Garnier, D. Helbing, and G. Theraulaz, "The walking behaviour of pedestrian social groups and its impact on crowd dynamics," *PLoS One*, vol. 5, no. 4, pp. 1–7, 2010.

[113] H. Bachmann and W. Ammann, *Vibrations in Structures: Induced by Man and Machines*, 3rd ed. Zürich: International Association for Bridge and Structural Engineering, 1987.

[114] E. Ingolfsson, "Pedestrian-induced lateral vibrations of footbridges," Ph.D. dissertation, Technical University of Denmark, January 2011.

[115] D. Newland, *An Introduction to Random Vibrations, Spectral & Wavelet Analysis*, 3rd ed. Harlow, Essex, England: Longman, 1993.

[116] S. Živanović, A. Pavic, and P. Reynolds, "Probability-based prediction of multimode vibration response to walking excitation," *Eng Struct*, vol. 29, no. 6, pp. 942–954, 2007.

[117] V. Racic and J. Brownjohn, "Mathematical modelling of random narrow band lateral excitation of footbridges due to pedestrians walking," *Computers and Structures*, vol. 90–91, pp. 116–130, 2012.

[118] M. Saunders, V. Inman, and H. Eberhart, "The major determinants in normal and pathological gait," *J Bone Joint Surg*, vol. 35-A, no. 3, pp. 543–558, 1953.

[119] "OpenSim Community," www.opensim.stanford.edu, 2016, online; accessed 2016-04-05.

[120] "AnyBody Modelling System," www.anybodytech.com, 2016, online; accessed 2016-04-05.

[121] M. Townsend, "Dynamics and coordination of torso motions in human locomotion," *J Biomech*, vol. 14, no. 11, pp. 727–738, 1981.

[122] ——, "Biped gait stabilization via foot placement," *J Biomech*, vol. 18, no. 1, pp. 21–38, 1985.

[123] D. Winter, "Human balance and posture control during standing and walking," *Gait & Posture*, vol. 3, no. 4, pp. 193–214, 1995.

[124] D. Winter, A. Patla, F. Prince, M. Ishac, and K. Gielo-Perczak, "Stiffness control of balance in quiet standing," *J Neurophysiol*, vol. 80, no. 3, pp. 1211–1221, 1998.

[125] W. Zijlstra and A. Hof, "Displacement of the pelvis during human walking: experimental data and model predictions," *Gait & Posture*, vol. 6, no. 3, pp. 249–262, 1997.

[126] A. Hof, M. Gazendam, and W. Sinke, "The condition for dynamic stability," *J Biomech*, vol. 38, no. 1, pp. 1–8, 2005.

[127] S. Bruijn, O. Meijer, P. Beek, and J. van Dieën, "Assessing the stability of human locomotion: a review of current measures," *J R Soc Interface*, vol. 10, no. 83, pp. 1–23, 2013.

[128] A. Kuo, "The six determinants of gait and the inverted pendulum analogy: A dynamic walking perspective," *Hum Movement Sci*, vol. 26, no. 4, pp. 617–656, 2007.

[129] R. Alexander, "A model of bipedal locomotion on compliant legs," *Phil Trans R Soc Lond B*, vol. 338, no. 1284, pp. 189–198, 1992.

[130] H. Geyer, A. Seyfarth, and R. Blickhan, "Compliant leg behaviour explains basic dynamics of walking and running," *Proc R Soc B*, vol. 273, no. 1603, pp. 2861–2867, 2006.

[131] H. Hong, S. Kim, C. Kim, S. Lee, and S. Park, "Spring-like gait mechanics observed during walking in both young and older adults," *J Biomech*, vol. 46, no. 1, pp. 77–82, 2013.

[132] Q. Yang, J. Qin, and S. Law, "A three-dimensional human walking model," *J Sound Vib*, vol. 357, pp. 437–456, 2015.

[133] K.-Y. Lee, N. O'Dwyer, M. Halaki, and R. Smith, "A new paradigm for human stick balancing: a suspended not an inverted pendulum," *Experimental Brain Research*, vol. 221, no. 3, pp. 309–328, 2012.

[134] J. Milton, J. Cabrera, T. Ohira, S. Tajima, Y.Tonosaki, C. Eurich, and S. Campbell, "The time-delayed inverted pendulum: Implications for human balance control," *Chaos*, vol. 19, no. 2, 2009.

[135] C. Massen and L. Kodde, "A model for the description of left-right stabilograms," *Agressologie*, vol. 20, no. B, pp. 107–108, 1979.

[136] N. Shubin, E. Daeschler, and M. Coates, "The early evolution of the tetrapod humerus," *Science*, vol. 304, no. 5667, pp. 90–93, 2004.

[137] S. Pierce, J. Clack, and J. Hutchinson, "Three-dimensional limb joint mobility in the early tetrapod Ichthyostega," *Nature*, vol. 486, no. 7404, pp. 523–526, 2012.

[138] T. Pozzo, A. Berthoz, and L. Lefort, "Head stabilization during various locomotor tasks in humans," *Exp Brain Res*, vol. 82, no. 1, pp. 97–106, 1990.

[139] A. Kaye, "Human induced sway of footbridges: A model testing approach," Master's thesis, Oxford University, 2010.

[140] A. Mather, "Human induced sway of footbridges," Master's thesis, Oxford University, 2011.

[141] S. Nhleko, "Human-induced lateral excitation of assembly structures," Ph.D. dissertation, University of Oxford, Trinity Term 2011.

[142] G. Selley, "Human induced sway of footbridges," Master's thesis, Oxford University, 2012.

[143] A. Ebrahimpour and L. Fitts, "Measuring coherency of human-induced rhythmic loads using force plates," *J Struct Eng*, vol. 122, no. 7, pp. 829–831, 1996.

[144] Tekscan, "Comparison of Interface Pressure Measurement Options," Tekscan, Inc., South Boston, Massachusetts, Tech. Rep., August 2008.

[145] R. Mann and J. Hagy, "Biomechanics of walking, running, and sprinting," *American J of Sports Med*, vol. 8, no. 5, pp. 345–350, 1980.

[146] E. Lohman III, K. Sackiriyas, and R. Swen, "A comparison of the spatiotemporal parameters, kinematics, and biomechanics between shod, unshod, and minimally supported running as compared to walking," *Physical Therapy in Sport*, vol. 12, no. 4, pp. 151–163, 2011.

[147] J. van den Noort, M. van der Esch, M. Steultjens, J. Dekker, M. Schepers, P. Veltink, and J. Harlaar, "Influence of the instrumented force shoe on gait pattern in patients with osteoarthritis of the knee," *Med Biol Eng Comput*, vol. 49, no. 12, pp. 1381–1392, 2011.

[148] C. Mummolo and J. Kim, "Passive and dynamic gait measures for biped mechanism: formulation and simulation analysis," *Robotica*, vol. 31, no. 4, pp. 555–572, 2013.

[149] S.-B. Joo, S. Oh, T. Sim, H. Kim, C. Choi, H. Koo, and J. Mun, "Prediction of gait speed from plantar pressure using artificial neural networks," *Expert Systems with Applications*, vol. 41, no. 16, pp. 7398–7405, 2014.

[150] M. Pau, B. Leban, G. Collu, and G. Migliaccio, "Effect of light and vigorous physical activity on balance and gait of older adults," *Archives of Gerontology and Geriatrics*, vol. 59, no. 3, pp. 568–573, 2014.

[151] A. Hof, "The equations of motion for a standing human reveal three mechanisms for balance," *J Biomech*, vol. 40, no. 2, pp. 451–457, 2007.

[152] J. Humar, *Dynamics of Structures*, 2nd ed. Leiden, Netherlands: Balkema, 2002.

[153] A. Hof, "The 'extrapolated center of mass' concept suggests a simple control of balance in walking," *Hum Movement Sci*, vol. 27, no. 1, pp. 112–125, 2008.

[154] N. Kasdin and D. Paley, *Engineering Dynamics*, 1st ed. Oxford: Princeton University Press, 2011.

[155] G. James, *Advanced Modern Engineering Mathematics*, 3rd ed. Harlow, England: Pearson, 2004.

[156] G. Goldsztein, "Lateral oscillations of the center of mass of bipeds as they walk. Inverted pendulum model with two degrees of freedom," *AIP Adv*, vol. 5, no. 10, p. 107208, 2015.